UTILISATION OF SINGLE TOOTH PROCEDURES TO ESTABLISH THE CUTTING MECHANICS OF WOODWORKING HAND-SAW TEETH

ANDREW NAYLOR

PhD

2012

UTILISATION OF SINGLE TOOTH PROCEDURES TO ESTABLISH THE CUTTING MECHANICS OF WOODWORKING HAND-SAW TEETH

ANDREW NAYLOR BEng (Hons)

A thesis submitted in partial fulfilment
of the requirements of the
University of Northumbria at Newcastle
for the degree of
Doctor of Philosophy

Research undertaken in the
School of Computing, Engineering and
Information Sciences
and in collaboration with
SNA Europe, R&D Centre for Woodworking

October 2012

ABSTRACT

The work reported in this thesis details the original research undertaken by the author into the cutting mechanics of wood-working handsaw tooth geometries. The research can be separated into three distinctive sections. The first section is a review of both fundamental and recent literature regarding wood characteristics and machining processes. The second section documents the findings of a cutting process in which a variety of ***work-piece parameters*** were evaluated whilst limiting the parameters associated with ***tooth geometry***. The third and final section documents the findings of a cutting process in which a variety of ***tooth geometry*** parameters were evaluated whilst limiting ***work-piece*** variation.

Two separate experimental procedures were developed to carry out the work for sections two and three respectively: The first of these procedures utilised a CNC router machine to perform the controlled cutting action. A single "rip" tooth was attached to the tool holder. The work-piece was constrained to a tri-axis dynamometer which was used to measure the resultant tool forces in the relative X, Y and Z axes. At the same time a universal testing machine was employed to perform mechanical test procedures on a variety of wood species. A predictive cutting force model was developed using the obtained mechanical properties as categorical predictors.

The second procedure utilised a shaper machine to perform the controlled cutting action. Three different saw tooth geometries were evaluated for only one variety of wood species. A tri-axis dynamometer was again used to measure the resultant tool forces. The geometric parameters of each tooth were carefully evaluated at using SEM micrographs. A predictive cutting force model using the geometric parameters as categorical predictors was developed.

Chip and surface formation was carefully evaluated. For procedure one this involved observation of the chip/surfaces under an optical microscope. For procedure two this involved capturing footage of the cutting process using a high speed camera.

The findings of the research show that un-bevelled teeth with orthogonal edges generally yield high cutting forces. However, these teeth are very effective at removing material along the wood grain in a "chisel like" cutting action. Bevelled teeth with sharp lateral edges generally yield low cutting forces. These teeth are well suited to severing the wood fibres perpendicular to the grain in a "knife like" cutting action.

ACKNOWLEDGMENTS

I would like to thank Dr. Philip Hackney, Dr. Noel Perera and Professor Mohammed Sarwar for their attentive supervision throughout the duration of the programme....

I would like to express my gratitude to Professor Håkan Hellberg and Mr. Emil Clahr of SNA Europe for their continual industrial support....

I would also like to thank Mr. Philip Donnelly, Mr. Sam Hutchinson and Mr. Simon Neville for their technical support....

Finally, I would like to thank my wife Laura for her support and patience over the past three years.

AUTHOR DECLARATION

I hereby declare that the work presented in this thesis is credited to the author alone and has not been submitted for any other award.

Andrew Naylor

.....

TABLE OF CONTENTS

LIST OF FIGURES

LIST OF TABLES

NOMENCLATURE

Fv	Major Cutting Force (N)
Fp	Thrust Force (N)
Fr	Side Force (N)
Fsp	Specific Cutting Force (N/mm)
γ	Rake Angle (°)
α	Flank Angle (°)
β	Wedge Angle (°)
λ	Bevel Angle (°)
k	Cutting Edge Angle (°)
δ	Depth of Cut (mm)
L	Major Cutting Edge Contact Length (mm)
L'	Lateral Cutting Edge Contact Length (mm)
P	Constrained Cutting Perimeter (mm)
A	Un-deformed Cutting Area (mm^2)
t_c	Measured Chip Thickness (mm)
t_u	Un-deformed Chip Thickness (mm)
r_c	Chip Ratio
φ	Shear Plane Angle (°)
σ	Plane Stress (MPa)
ε	Plane Strain (GPa)
MOR	Modulus of Rupture in Bending (MPa)
MOE	Modulus of Elasticity in Bending (GPa)

τ	Shear Stress (MPa)
G	Modulus of Rigidity/Elasticity in Shear (MPa)
Ub	Bending Toughness (J/m^2)
Us	Shear Toughness (J/m^2)
ρ	Density (kg/m^3)
MC	Moisture Content (%)
WPC	Work-piece Coefficient
$ANOVA$	Abbreviation of "Analysis of Variance"
DF	Degrees of Freedom
SS	Sum of Squares
MS	Mean Squared
R^2	Coefficient of Determination for Regression Fit (%)
F	F value / Ratio of Variance
P	P value / Significance Probability
$_{REG}$	Suffix - Abbreviation of "Regression"
$_{RES}$	Suffix - Abbreviation of "Residual"
$_{TOT}$	Suffix - Abbreviation of "Total"

CHAPTER 1
INTRODUCTION

1.1 A Background to Hand-sawing

Throughout history the handsaw has proven to be one of the most widely used hand tools. This dates back to the first flint saws used during the Neolithic revolution circa 9500 BC [1]. Throughout the ages technology advanced past the bronze and iron ages and the applications of the hand saws widened through the Roman era and the middle ages being used more in construction and even as a method of execution [2]. The closed handle handsaw that we recognise today (figure 1.2) has its origins at the turn of the 18th century. Prior to this, saws with an open handle or "pistol grip" were the norm (figure 1.1). The teeth were manually filed and set using a small hammer and anvil. In the developing world, where carpenters see their tools as an investment rather than a replaceable good, this method is still widely used. The saw teeth are re-set and filed when the edges become too worn for functional use thus increasing the life of the saw. Since the latter part of the 20th century the developed world has opted for hardened saw teeth. This is achieved by inducing an electromagnetic field at the edge of the blade heating the steel and hence forcing martensitic transformation. This makes the saw teeth extremely resilient to tool wear removing the need to re-sharpen. Additionally, grinding and setting are fully automated processes.

The major companies that manufacture hand tools have a combined annual turnover of nearly 14 billion USD worldwide (figure 1.4). These are "Stanley – Black and Decker" who are responsible for the "Stanley" brand of hand-saws, "Newell – Rubbermaid" who manufacture "Irwin" handsaws and "Snap – On" who produce the "Bahco" range of handsaws. Although these major manufacturers also produce a range of machine driven alternatives to manual

sawing, the hand-saw is still considered a viable product. This is primarily because there will always be a market for handsaw users as it can be used absolutely anywhere regardless of power supply. It is also used as an important test of innovation through research and development improving aesthetic design, ergonomics (figure 1.3) and most importantly tooth geometry.

Each manufacturer claims that their patented tooth geometry requires less effort from the end user during manual sawing (appendix 2), but what is it that actually influences the cutting mechanics? Traditionally there are two types of tooth geometry for wood-cutting handsaws (figure 1.5):

- Rip teeth – These are widely understood to act as orthogonal cutting tools and are used to remove material along the wood grain.
- Cross cutting teeth – These teeth have bevelled edges and are used to machine the wood across the grain.

More recently saws with compound teeth have been developed. These tooth geometries consist of three bevel ground edges. These saws are marketed for universal use, i.e. they can be used to machine both along and across the wood grain (appendix 2).

Contrary to wood machining, a significant volume of research has been performed in the area of metal cutting, the most fundamental of which describe it as a plastic deformation process of an isotropic material [3, 4]. Wood is a material which is both heterogeneous and anisotropic, making it very unpredictable during any machining process. Wood gains its heterogeneity from its concentric annual growth rings composed of earlywood fibres formed in the warmer months of the year and the denser latewood fibres which form during the colder months (figure 1.6). These fibres grow longitudinally through the trunk of the tree. Additionally wood contains knots where limbs grow out from the trunk; these weaken wood as a material as they

are poorly bonded to the surface which surrounds them. It is these characteristics that make wood anisotropic, attributing different mechanical properties to its three separate orthogonal planes of symmetry.

1.2 Research Aim and Objectives

1.2.1 Aim

The aim of the research is to establish the cutting mechanics of wood-working hand-saw tooth geometries. The cutting mechanics will be described both quantitatively (through measured tool forces) and qualitatively (through captured images/footage of chip formation). The research aim will be facilitated through achievement of the following objectives:

1.2.2 Objectives

1.2.2.1 Review of wood properties

A review of wood characteristics will be carried out to determine what the scientific community considered the most important attributes/properties associated with wood as a material. Although it is important to consider the structure of wood at a cellular (microscopic) level, the emphasis of this review will focus on features visible to the naked eye (macroscopic level). Mechanical test procedures and wood grading methods from a wide range of published literature and standards will be considered

1.2.2.2 Review of wood machining processes

The extensive body of wood machining research will also be reviewed. This will start with the fundamental cutting processes (orthogonal cutting) and will progresses onto areas such as oblique cutting and tool wear. The review on wood machining will continue with sawing, detailing standards on tooth geometry, setting patterns and touching upon cutting mechanics.

1.2.2.3 Evaluation of the influence of work-piece variations on the cutting mechanics

This experimental work will be conducted to determine the effects of wood properties on the cutting mechanics (chip formation and tool forces) for simplified cutting conditions. Eight different wood species have been selected (including both hardwoods and softwoods) at four moisture levels ranging from dry to saturated. Each work-piece variation will be machined in a single tooth test rig using a simple orthogonal (rip) tooth, both across and along the wood grain. Tool forces will be recorded using a piezoelectric dynamometer. Optical microscope images of the chip and surface formation were taken.

In addition to this, a series of mechanical tests will be conducted to determine the bending properties across the wood grain and the shear properties along the wood grain. These tests will be performed for the same species and moisture levels as used for the cutting tests. Multiple regression analyses will be performed using strength, elasticity, toughness, moisture content and depth of cut as parameters to determine the relationship between work-piece properties and the major cutting force.

1.2.2.4 Evaluation of the influence of tooth geometry on cutting mechanics

Three tooth geometries have been selected; an un-bevelled (orthogonal) tooth, a bevel ground cross cutting tooth and a thrice bevelled compound tooth. Only one wood species (Douglas fir) will be used with two moisture variations (dry and saturated) machining both along and across the grain.

Tool forces will again be measured using a piezoelectric dynamometer. Furthermore, a high speed camera will be used to capture footage of the chip formation process at one thousand frames per second. This footage, along with optical microscope images, will be used to describe the chip formation modes.

1.3 Original Contribution to the Body of Knowledge

1.3.1 Novel aspects of the PhD research

The fundamental literature in this research area has provided a detailed explanation of the cutting mechanics for large orthogonal plaining tools cutting in the three wood machining directions. This is based upon measurement of tool forces and images of chip formation. Additionally, the available literature related to wood sawing focuses only on high speed industrial processes such as band sawing and circular sawing.

Previous attempts at constructing multiple regression models, for single band-saw teeth, used only a limited amount of work-piece parameters for only a small variety of wood species. Namely; machining direction, density and moisture content [5-7]. The experimental work detailed in this thesis used obtained work-piece properties from a series of mechanical tests as parameters for multiple regression modelling for eight wood species (consisting of both hardwoods and softwoods). These consist of; material strength, elastic modulus, toughness for bending across the grain and for shearing along the grain. Moisture content, density and depth of cut were also used as parameters for predicting the major cutting force. This yielded linear models with R^2 values of 0.8 and 0.9 along and across the grain respectively. As no coefficients of species were included as parameters the models stand to be species independent, i.e. the effects of wood species are insignificant when mechanical properties are used as predictors instead.

Regression modelling was also used for multiple tooth geometry parameters with limited work-piece variations. For this scenario work-piece coefficients were used to normalise the empirical data obtained from different work-piece variations. This allowed the focus of the

model to be purely on tooth geometry parameters. In total, three different tooth geometries with different bevel orientations were used. The interaction of these three different teeth with the un-deformed work-piece provided a multitude of geometric parameters used as predictors in the model. Additional statistical analysis allowed for the most significant geometric parameters to be identified.

The original aspects of this author's thesis builds upon the previous published literature, but also contributes entirely novel findings to the body of work. Although the single saw-tooth cutting test has been used previously for metal cutting and for high speed, industrial wood sawing processes, there is no evidence found showing that it has been used to evaluate handsaw teeth. Tool forces have been measured for band-saw and circular saw teeth [8, 9] and high speed video footage has previously been recorded for circular saw teeth, machining along the wood grain [10]. Nominal depths of cut per tooth are significantly smaller for handsaw teeth (ranging between 0.05 and 0.15 mm) with narrower cutting edge width (0.85 mm). As a result, the tool forces documented in this thesis were much smaller than any values from the previously mentioned comparable studies.

1.3.2 Published Work (appendix 1)

1.3.2.1 Conference Papers

1. Naylor A, Hackney P and Clahr E. *"Machining of Wood using a Rip Tooth: Effects of Work-piece Variations on Cutting Mechanics"* 20th International Wood Machining Seminar June 7-10, 2011. Skellefteå, Sweden.
2. Naylor A, Hackney P, Perera N and Clahr E, *"Determination of wood strength properties through standard test procedures"* International Conference on Manufacturing Research. September 11-13, 2012. Aston, UK

3. Naylor A, Hackney P, Perera N and Clahr E, *"Evaluation of handsaw tooth performance through the development of a controlled cutting test rig"* International Conference on Manufacturing Research. September 11-13, 2012. Aston, UK

1.3.2.2 Journal Articles

1. Naylor A, Hackney P, Perera N and Clahr E, (2012). *"A predictive model for the cutting force in wood machining developed using mechanical properties,"* BioResources 7(3) 2883-2894

1.3.3 Prizes and Awards

The high quality of the research presented in this thesis was recognised by the ***Institution of Mechanical Engineers*** educational awards committee. As a result this author won the ***Thomas Andrew Common Grant*** which was used to attend the ***International Conference on Manufacturing Research*** held at Aston University.

An award for best doctoral paper submitted to the ***International Conference on Manufacturing Research*** was given to the author for the paper entitled; *"Determination of wood strength properties through standard test procedures"* (appendix 1).

1.3.4 Industrial Impact

The findings of this research will be used by industrial collaborators SNA Europe to aid the development of new high performance tooth geometries for the BAHCO brand of hand-saws.

1.4 Structure of the Thesis

This thesis is divided into five chapters, two of which detail separate experimental pieces of research carried out. Each of these two chapters separately covers experimental methodology, results, discussion and a summary of findings:

- Chapter one provides the background to the subject area, rationale for the research carried out and the research aim and objectives.
- Chapter two consists of a review of published literature. Important wood material characteristics were considered from a range of publications including standards for grading and mechanical testing. The wood machining process was also evaluated starting with the fundamental research carried out using simple orthogonal cutting tools, progressing on towards a review of more relevant publications concerning sawing mechanics.
- Chapter three (experimental) investigates the effects of work-piece properties on tool forces. Eight different wood species (consisting of both hardwoods and softwoods) at four moisture levels were fully evaluated by means of mechanical tests; 1) Bending tests to evaluate the strength properties across the grain, 2) Shear tests to evaluate the strength properties along the grain. Each of these evaluated wood work-pieces was machined along and across the grain using a single, orthogonal (rip) tooth within a CNC router machine. Tool forces were recorded using a force dynamometer data acquisition system. Collected chip was observed using images taken from an optical microscope. Regression analysis was performed to determine the relationship between work-piece properties and the major force in the direction of cutting.
- Chapter four (experimental) evaluates the cutting of different handsaw tooth geometries. One wood species (Douglas fir) at two moisture levels (dry and saturated)

was machined along and across the grain using a variety of tooth variations. The tooth forms evaluated were; 1) Un-bevelled “orthogonal” teeth, 2) Bevelled cross cutting teeth, 3) Thrice bevelled compound teeth. Tool forces were once again recorded using a force dynamometer data acquisition system. The chip formation process was observed by high speed video recordings and optical microscope images of collected chip. Regression analysis was performed to determine the relationship between the tooth geometric parameters and the major force.

- Chapter five, “Overall Discussion”, summarises the novel findings of the research. Key observations from both chapters three and four are unified here building illustrated descriptions of the different cutting scenarios.
- Chapter six presents the original findings in the form of concise, bulleted conclusions. Further work also suggested in this chapter, finalising the thesis.

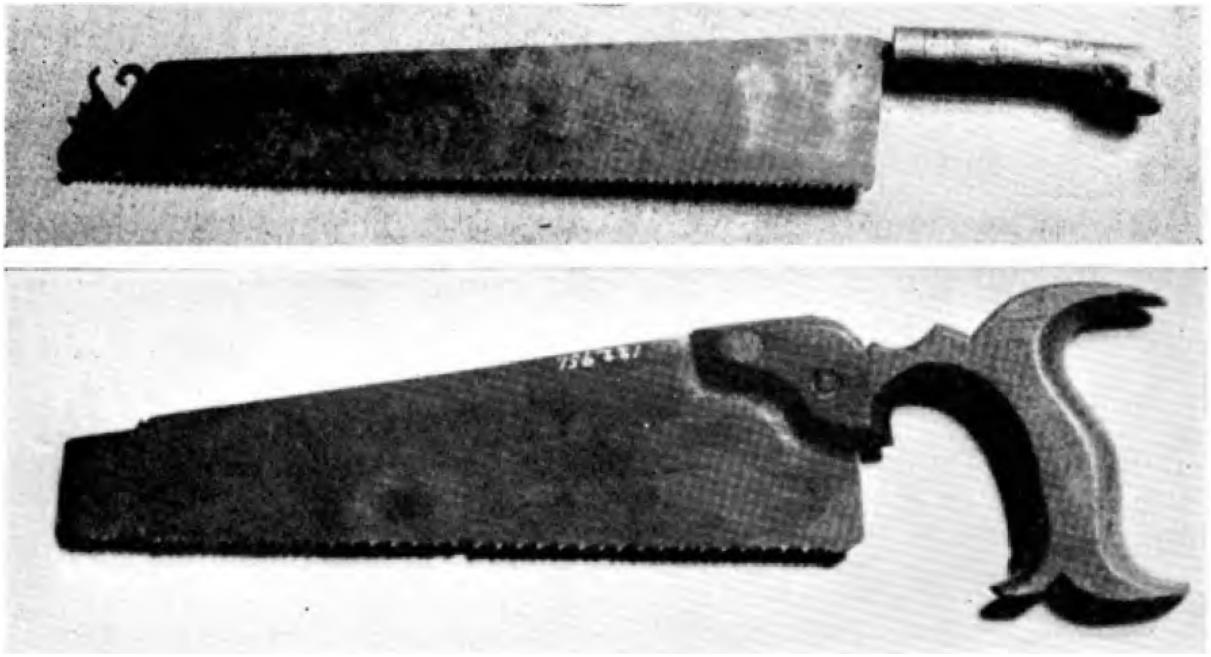

Figure 1.1 – Open handled saws circa 1800 [1]

Figure 1.2 – Spear and Jackson cross cutting saw circa 1960 [1]

Figure 1.3 – Bahco ergonomic handsaw blades and handle

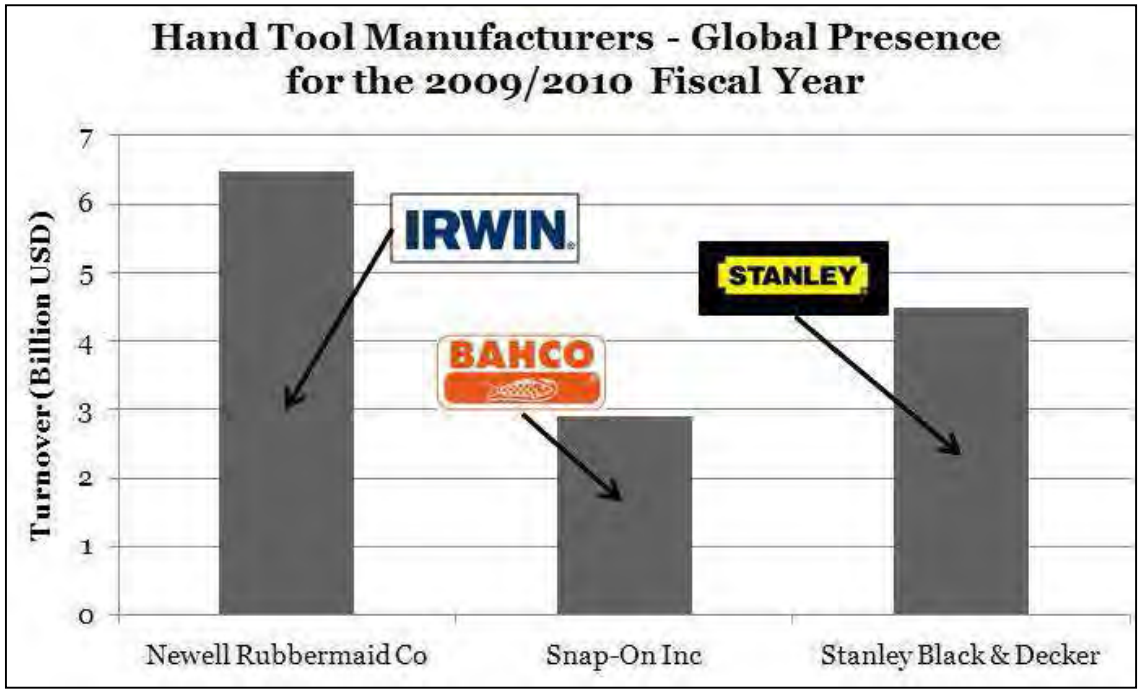

Figure 1.4 - The Global Hand Tool Market {S&P 500 Consumer Discretionary Index (accessed July 2011)}

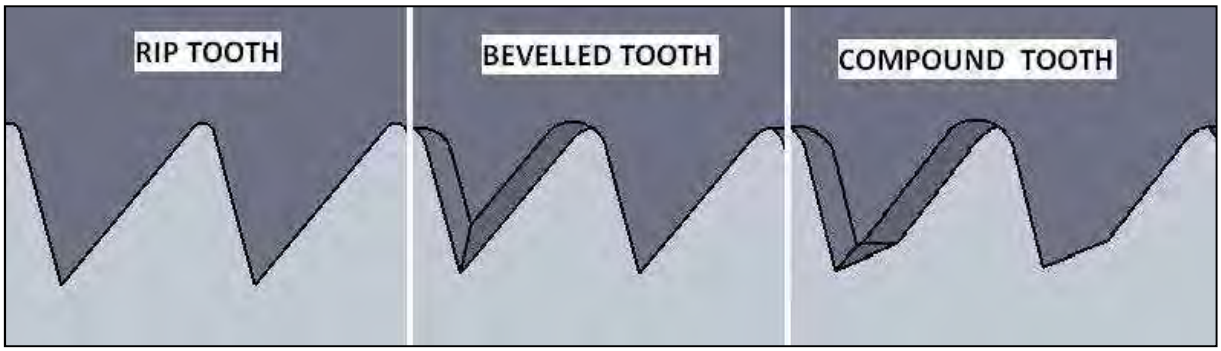

Figure 1.5 – Handsaw Tooth Geometries

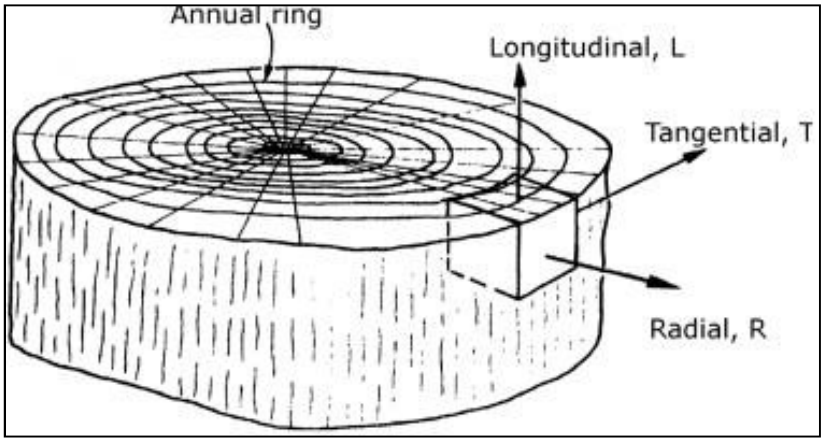

Figure 1.6 – Wood Planes of Symmetry [11]

CHAPTER 2
LITERATURE REVIEW

2.1 Classification and Characteristics of Wood

2.1.1 General Characteristics of Wood

Wood is a heterogeneous material with an intricate grain structure and imperfections in the form of knots and mineral entrapments. Any section of wood is perceived to have three planes of symmetry; the radial, the tangential and the axial planes. These planes of symmetry are relative to the major machining directions described in section 2.2.1. It is widely understood that the wood cell is composed of 3 organic polymers; Cellulose (40-44% of total cell biomass), Hemicelluloses (20-32%) and Lignin (25-35%) [12]. The function of Cellulose is to provide large structural fibres, Hemicelluloses surrounds cellulose providing smaller structural microfibers to fill in the gaps and Lignin binds and provides rigidity. The cell wall itself has a tubular structure. The cells are aligned in the axial direction creating the wood fibres visible to the human eye.

Scanning electron microscope (SEM) images of wood at a cellular level shows the cells to have a strong anisotropic honeycomb structure [13]. SEM images combined with computer aided tomography techniques have been able to assess the surface geometry (roughness) of woods [14] and even the deformation of the cell structure under mechanical stresses [15, 16].

In the trunk there are three main sections; 1) the heartwood, which is physiologically inactive 2) the sapwood, where all conduction and storage occurs 3) the bark, which protects the interior of the tree trunk [17]. The heartwood consists of a series of growth rings surrounding the pith. The growth rings form the grain structure observed in cuts of timber sawn from the

trunk of the tree. The inner part of the growth ring formed first in the growing season is called earlywood and the outer part formed later in the growing season, latewood. Earlywood is characterized by cells with relatively large cavities and thin walls. Latewood cells have smaller cavities and thicker walls. This means that the latewood cells are denser than the earlywood.

Knots are present where branches have grown out from the main body of the tree trunk and are considered as defects. They are much denser than the rest of the wood, the grain around a knot is distorted and the knot itself may be poorly bonded to the rest of the wood [11].

2.1.2 Hardwood and Softwood

When considering different woods from a biological perspective, there are two distinct phyla: The *Magnoloiphyta* and the *Coniferoliophyta*. *Magnoliophyta* are flowering plants and reproduce via seed dispersal. This method of reproduction can often lead to plant growth in random locations far away from the parent plant. All hardwoods fall under this category. *Coniferoliophyta* are cone-bearing plants. The genetic trends and physical functions of cone-bearing plants are well documented [18]. The seeds of these plants reside in the female cone and when fertilised by pollen from the male cone, drop locally to the parent plant. In addition to this most cone-bearing plants have pine needles surrounding the cone; this is to deter animals from eating the seeds and hence prevents seed dispersal. All softwoods are cone-bearing plants. It is often misunderstood that all cone-bearing plants are evergreen and that all flowering plants are *deciduous* (sheds leaves in winter). Although this is the case for most trees there are some exceptions to the rule. Holly for instance is a flowering plant that stays green all year and Larch is a cone-bearing tree that sheds its needles in the winter months.

As well as genetically, hardwoods and softwoods also differ physiologically. Hardwoods have a more complex structure than softwoods. SEM imaging shows hardwoods to have a presence

of larger transport vessels within the grain of the structure [19]. These vessels called *xylem* increase the porosity of the wood and when inactive creates micro-cavities for mineral entrapments or even a space for micro-organisms to spread and cause rot.

The growth patterns and location of softwoods have been investigated heavily in Scandinavia [20-22] but also in mainland Europe [23, 24] and the United Kingdom [25, 26]. The trends show that by their very nature, softwoods tend to grow locally to their parent plants. This makes it very easy for timber manufacturers to cultivate and harvest trees as they naturally grow in self-sustained forests.

2.1.3 Grading of Woods

The physical and chemical characteristics of wood dictate the strength properties and longevity of the timber produced from it. British Standards dictate the mechanical properties for different structural grades [27] and how these grades should be labelled with respect to different wood species [28]. Grading can be performed visually taking manual measurements such as knot content and grain pitch, or it can be machine graded in a log scanner where all the quantities are calculated automatically [29].

The moisture contained in the wood of felled trees can range from 30 – 200% of the woods dry mass. There is free water that is stored in the empty space within and around the cells, and water stored in the fibres of the cell wall. It is important to remove the free water during seasoning as it can be the dwelling place for fungi which cause decay. When the overall moisture content of the wood increases to a level where the fibres of the wood cells can no longer contain any more moisture, the wood is referred to having reached the *fibre saturation point*. Findings from prior research [30] concludes that the cross sectional area of sawn timber varies with respect to moisture content . It is hence important to install timber at the

same moisture content as its final atmospheric conditions for end use; this is known as *equilibrium moisture content.*

Standards on moisture content for structural timber [31] dictates the appropriate moisture content for dry graded structural timber (table 2.0). There are two standard ways of measuring the moisture content. The first is the oven dying method [32] where the loss of water mass during the drying process is expressed as a ratio of the dry mass (equation 2.1). The second method is the electrical resistance method [33] where a *protimeter* (moisture probe) is calibrated to the same sensitivity of the dielectric constant for water. This allows for accurate estimation of the presence of water.

$$MC = \frac{m_{wet} - m_{dry}}{m_{dry}} \qquad (2.1)$$

Table 2.1 – Moisture grading for structural timber [31] *

Service Class	Conditions for end use	Moisture Content (%)
3	External uses, fully exposed	20+
2	Covered and generally unheated	18
2	Covered and generally heated	15
1	Internal uses, in a continuously heated building	12

Wood can experience mineral deposition due to the transport of nutrients. Previous research covers the effects mineral salt entrapments [34] and the crystallisation of minerals during the freezing and thawing processes [35]. Generally the strength of the timber is not compromised

*

a) Service class 1 is characterized by a moisture content in the materials corresponding to a temperature of 20 °C and the relative humidity of the surrounding air only exceeding 65 % for a few weeks per year. In such moisture conditions most timber will attain an average moisture content not exceeding 12 %.
b) Service class 2 is characterized by a moisture content in the materials corresponding to a temperature of 20 °C and the relative humidity of the surrounding air only exceeding 85 % for a few weeks per year. In such moisture conditions most timber will attain an average moisture content not exceeding 20 %.
c) Service class 3, due to climatic conditions, is characterized by higher moisture contents than service class 2

the presence of minerals; however complications arise when machining timber, as a heavy presence of minerals can cause tool wear.

Imaging techniques for lumber grading have become increasingly popular as it is a non-destructive form of grading. Traditionally the use of x-ray log scanners has been used to machine grade lumber. Research into the traditional x-ray method [36-38] reveals that a significant proportion of logs scanned (20 -30%) are incorrectly graded. More recently the applications of scanning computerised tomography (CT) have been widely investigated. Use of this technology for detecting physiological boundaries has been investigated [39, 40] where the heartwood – sapwood boundary and pith has been detected. Arguably the most useful application of this method for lumber grading is in the detection of defects [41-44]. This is extremely useful for the timber industry as operators know where the defects lie in the lumber before it passes into the saw-mill.

Research has been performed exclusively on the detection of knots using imaging techniques. The conventional CT scan method has been adopted to detect internal knots for lumber [45]. A unique approach using grey-scale imaging has been used to identify knots in wood veneer an timber [46]. Pixels from the grey-scale image are used to detect and quantify the knots.

It has been previously mentioned that knots are poorly bonded to the wood and the grain surrounding them is distorted [11]. A valid statistical model was developed to estimate the amount of distorted wood grain surrounding a knot [47]. Dimensional measurements such as diameter, volume and distance from pith were used as predictors in the model. The findings prove accurate prediction of the propagation of the distorted grain surrounding knots leading to optimum utilisation of lumber when sawing it into sections of timber.

Statistical methods of predicting lumber grades based on measurements of the tree taken at felling have been investigated [48, 49]. These methods are effective at categorising lumber

into correct grades; however, they cannot determine any information of the internal structure of the wood.

2.1.4 Obtaining Properties through Mechanical Testing

Wood is anisotropic and hence some mechanical test procedures are often performed both along and across the grain. Tension and compression tests have been successfully performed both along and across the grain. Compression tests show that wood has much larger strength and modulus of elasticity values along the grain rather than across [50-52]. The trend for tensile tests is the same as compressive [51, 53, 54] (larger values along the grain) however the magnitude of the compressive strengths is significantly larger than tensile, typically ten times larger. Due to the nature of the test procedure, static bending test procedures are mainly implemented to characterise wood strength across the wood grain. Shear test procedures have been implemented in all three wood machining directions [55] revealing that only a true shear failure mode occurs along the wood grain. Bending and Shear test procedures are discussed further within this section.

2.1.4.1 Static Bending

Four point bending is recommended by British Standards for wood as failure occurs at the point of maximum displacement between the two loaded anvils [56]. This eliminates the excessive compressive forces that would occur with the use of a single anvil and reduces the possibility of shear along the grain. American Standards for three point bending specifies a span to depth ratio of 1:14 [57]. Once again this ensures that the failure mode is bending with no shear along the grain or compressive deformation caused by the loaded anvil.

Previous research into the properties of Finnish birch [58] has evaluated both test procedures. The findings reveal an average modulus of elasticity (MOE) of 11.2 GPa for three point bending compared to 14.9 GPa for four point bending, an increase of approximately 25%.

Records [59] reveal an MOE value of 13 GPa in static bending which resides between these two values, showing that results from both test procedures are within an appropriate range. The modulus of rupture (MOR) or bending strength is calculated to be the same regardless of the testing procedure.

Despite the discrepancy between the two procedures for determination of MOE, evidence from literature shows that MOE has been accurately determined using the three point method. The three point method was specifically used to evaluate the bending properties of Green wood [60] and some wood plastic composites [61].

$$MOR = \frac{3FL}{2bd^2} \qquad \textbf{At point of fracture} \qquad (2.2)$$

$$MOE = \frac{FL^3}{4bd^3\omega} \qquad \textbf{At elastic limit} \qquad (2.3)$$

2.1.4.2 Shear

Shear occurs most commonly along the grain direction; hence values in this direction are referred to as longitudinal shear. French standards for longitudinal shear incorporate a test specimen with three separate shear zone where failure can occur [62]. This standard has been used previously to determine the modulus of rigidity for a predictive cutting force model where a tool machines wood along the grain [63].

Alternatively, American standards have developed a method for accurately measuring the shear strength ($\boldsymbol{\tau}$) and modulus of rigidity (G) [57]. The set-up consists of a test piece that can fail along only one zone of shear. This makes it significantly easier to determine the properties using convention theory for strength of materials. A non-liner, anisotropic, finite

element model has been developed to simulate this method [64]. Force extension plots were produced through mechanical tests generating enough data to develop the model.

$$\tau = \frac{F}{A} \qquad \textbf{At point of fracture} \qquad (2.4)$$

$$G = \frac{\tau}{\gamma} = \frac{FL}{Ax} \qquad \textbf{At elastic limit} \qquad (2.5)$$

A previous study on wood shear [55] using spruce, applied the same shear methodology using the same apparatus in all three orthogonal planes of symmetry with respect to the wood grain direction. The results indicate that the wood is much stronger in the 90°-0° direction than in either 90°-90° or 0°-90°, this is exhibited by larger values for $\boldsymbol{\tau}$ and G (table 2.2).

Furthermore, only true shear is observed in the 90°-0° direction. This is demonstrated by a uniform fault line along the grain direction (figure 2.1). Other failure modes were observed: Buckling of the annual growth rings (90°-90°) and bending of the fibres across the grain (0°-90°) which are both referred to as rolling shear.

Table 2.2 – Shear properties in the three wood machining directions [55]

Direction	τ (Mpa)	G (Gpa)
90°-0°	9.1011	0.9515
90°-90°	1.7099	0.0229
0°-90°	1.7651	0.0251

2.2 Fundamental Wood Machining Research

2.2.1 Introduction

Research performed into optimum wood machining conditions [63, 65] states that there are three significant factors that affect the cutting mechanics:

1. Factors attributed to the machining process
2. The species of the wood
3. The moisture content of the wood

Analysis of the wood cutting process in published literature [66-69] examines all of these three effects, with publications investigating defects in the wood grain such as knots [70].

As previously discussed in this chapter, wood has three planes of symmetry; axial, radial and tangential. Corresponding these planes of symmetry are the cutting directions by which machining processes can be described (figure 2.2). When referring to a machining direction the nomenclature states a labelling system consisting of two number separated by a hyphen. The first number denotes the orientation of the cutting edge to the wood grain direction; the second number denotes the movement of the tool with respect to the grain direction. To illustrate this, the three main cutting directions are listed:

- 90°-90° - The axial plane or the wood end grain. Both the cutting edge and tool movement are perpendicular to the grain.
- 0°-90° - The radial and tangential planes, cutting across the grain. The cutting edge is parallel to the grain but the tool movement is perpendicular.
- 90°-0° - The longitudinal plane, cutting along the grain. The cutting edge is perpendicular to the grain but the tool movement is parallel.

Previous research into wood-cutting mechanics investigates machining parallel and perpendicular to the grain [66, 68-74]. Additionally, more recent studies have investigated the effects of cutting across the grain at various angles with and against the annual growth rings [75-79].

Evidence from fundamental literature suggests that cutting velocity has negligible effect on the forces acting on the tool. This is for the ranges of 0.2 m/s – 6.3 m/s along the grain [69] and 2.5 m/s – 50 m/s across the grain [67].

2.2.2 The Plaining Process

Plaining is a process by which a knife edge removes a layer of material on the top surface of a work-piece. As there is clearly material removal in the form of chip or swarf, analysis of the chip formation is often used to characterize the process. Early research into the metal-cutting process by Ernst [3], Merchant [4], Lee and Shaffer [80] has established relationships between the cutting conditions and the deformed chip. These relationships have successfully explained the process as *plastic deformation* of an *isotropic* material. As wood is an *anisotropic* material chip formation changes with respect to the machining direction.

2.2.2.1 Orthogonal Planing

The first comprehensive investigation into wood machining [67] investigated the effects of varying tool geometry and species factors for plaining operations. In experimental work evaluating the cutting action of the tool, the work-piece properties were not varied standardising on Finish birch as the sole species. It was found that the main cutting force was inversely proportional to the sharpness of the tool, i.e. the sharper the tool, the lower the force. It is also stated at this point that the thrust force is caused by contact between the rake face and the chip. The larger the rake angle the thicker the chip and hence the lower the thrust force. This is because the chip is not being compressed. Although it is observed that there is

no significant effect of cutting velocity on the major cutting force, the orientation of the tool with respect to the grain does have a significant effect on the cutting forces. The highest cutting forces are observed to be in the 90°-90° direction (wood end grain) with the lowest cutting forces in the 90°-0° direction (cutting along the grain).

In other experimental work the tool sharpness and rake angle remain constant for the testing of 21 different species of wood. Analysis of data found a linear trend between the density of the wood and the major cutting force. From this empirical data a predictive model for cutting force was created.

For orthogonal wood cutting, extensive work into the chip formation produced through varied cutting conditions has been carried out by Franz [66, 74], McKenzie [69], Woodson and Koch [68, 71]. The cutting tools used in the experiments represent a planning tool that removes material across the entire width of the work-piece. This set up typically consists of the tool being attached to a force dynamometer consisting of two strain gauges (measuring cutting and thrust force components). Cutting along the grain gives three types of characterised chip (figure 2.3):

- Type I chip is caused by a large rake angle producing a negative thrust forces (acting in a positive vertical direction relative to the work-piece). The wood fibres split ahead of the tool and finally fail due to bending. This type of chip is beneficial where quick removal of material is required.
- Type II chip is formed by a very sharp tool edge and a diagonal plane of shear. Excellent surface finish is achieved due to the continuous chip formation.
- Type III chip is caused by dull tool edges, and very small or negative rake angles. It is also suggested that very large depths of cut may form this chip where there is too

much contact with the blade surface. This type of chip causes a raised *fuzzy grain* where wood fibres become protrudes, hence a poor surface finish.

Further work done cutting across the grain by Woodson and Koch [71] demonstrates that higher moisture contents increases the length of chip type II before failure. The forces observed in the latewood cells are approximately double that of the earlywood cells with a positive correlation between cutting force and moisture content. The same publication documents the effects of cutting across the grain in what is described as the *veneer peeling* process. This process uses high rake angles (approximately 70°) and small depth of cut (less than 1 mm) with a *nosebar* used to compress the cells before cutting to ensure that the veneer remains a single unbroken sheet. The chip is formed by an initial compaction of the wood fibres (3) followed by an ongoing shearing process (2) with some tensile failure also observed (1) (figure 2.4). This form of cutting results in higher forces and discontinuous chip compared to veneer peeling. Cutting forces for ealywood and latewood in this direction are the same.

McKenzie [69] investigated the effects of cutting across the grain and discovered two distinct chip types (figure 2.5). Type I is typical for cutting wood with a very high moisture content and type II for low moisture content. The cutting mechanics for both conditions specify a tensile failure mode causing parallel gaps to propagate between the fibres; however these gaps become larger with decreased moisture content. Cutting forces in this direction are strongly affected by cell type, moisture content, depth of cut, and rake angle where the values of the cutting force for latewood are approximately three times the value for earlywood.

Further research conducted by Goli et al [75, 76, 78, 79, 81, 82] delves into the change in cutting mechanics when machining at different angles to the annual growth rings. The grain orientation that provides the highest forces and leaving behind the most protruded fuzzy grain is cutting in the 90°-90° direction, against the annual growth rings at 45° [75]. As previously

discovered by Kivimaa [67] cutting parallel to the grain provides the lowest cutting force values [77] with chip formation characteristic of the Franz type 1 chip. Furthermore cutting at angles with the annual growth rings produces smaller cutting forces and less fuzzy grain compared to cutting against the growth rings [76].

Analysis of the formation of the surface finish is also investigated [81-84]. Surface roughness measurements using a perthometer (optical 3D roughness measurement) and a profileometer (surface roughness stylus) were taken to quantify the surface finish of the woods. Machining in the standard machine directions (90°-0°, 0°-90°, 90°-90°) provides results concurrent to the respective chip formation types of Franz, McKenzie and Koch. Typically cutting along the grain provides a better surface finish than cutting across the grain, where the effects of moisture content, rake angle, depth of cut and edge sharpness all affect the surface finish in the same way as previously investigated in the fundamental studies [66, 68, 69]. When investigating the new area, cutting at angles with and against the annual growth rings, it is established that the surface roughens is significantly larger when cutting at angles against the growth rings as opposed to with the growth rings. This is verified by both surface roughness measurement techniques.

2.2.2.2 Oblique Planing

In orthogonal cutting, it has been known for tools with large rake angles (>25°) to produce a negative thrust forces (acting in a positive vertical direction relative to the work-piece), although this observation is usually attributed to larger depth of cut [66, 71]. For oblique cutting parallel to the grain, the cutting and thrust forces decrease as the oblique edge angle increases [85, 86]. As observed with orthogonal cutting, it is also recognised that negative thrust forces can also occur when wood is machined using oblique tools [86]. This occurs for the same cutting conditions as with oblique cutting (large rake angles and depths of cut) for oblique edge angles over 30°. It is recognized that the negative thrust forces cause the

propagation of longitudinal cracks in front of the knife edge during cutting [66, 87, 88]. By decreasing the rake angle and depth of cut the magnitude of the negative thrust force becomes lower, and eventually changing from negative to positive. This reduces the roughness of the surface caused by the chip splitting ahead of the tool, instead leaving behind a slight fuzzy grain [89].

Cutting perpendicular to the grain it has been observed that fibres have been pulled out or up-rooted from the work-piece [90]. After investigation this phenomenon is explained to be caused by lateral forces exerted on the work-piece by the oblique tool [89], causing an increased in surface roughness compared to that of surfaces that have been machined using orthogonal tools. Furthermore an increase in the oblique edge angle causes more fibres to be pulled out and hence an increase in the surface roughness of the work-piece.

A study investigating cutting using extreme oblique angles [91] states that cutting with very large oblique angles (45° to normal and above) provides a much better surface finish when compared with orthogonal cutting. This is a result of the time delayed edge engagement and an increased cutting edge contact with the work-piece. This effect also results in lower forces acting on the tool, which in turn, reduces tool wear.

2.2.3 Effects of Worn Edges on Cutting Mechanics

2.2.3.1 Causes of wear in wood-cutting tools

In a comprehensive review on wood cutting tool wear [92] it is concluded that the abrasive wear plays the largest role is edge recession of tools. From recent studies [93-97] it is evident that cemented carbide tools are extremely sensitive to corrosive wear suggesting that high speed steel is a better corrosion resistant alternative. Having said this, it has been known for corrosive wear to significantly affect high speed steel when cutting green wood [96, 98]. This

is due to much higher moisture content values as well as naturally occurring acids and phenolic compounds.

The presence of silica and other mineral entrapments is known to play a role in corrosive wear [99], however further study has showed that the silica residue found within the wood cell walls plays a very small role. Instead contamination with coarse silica during the harvesting and storage of timber/lumber is seen to contribute in a larger way to corrosion. It is also suggested that the mechanical properties of tool material at the tip, or even coating materials, can be altered by corrosive wear [100]. This can allow the effects of abrasive wear to become more prominent or even result in brittle failure.

2.2.3.2 Effects of tool wear on cutting mechanics

Kivimaa was the first to notice an increase in cutting forces due to the dulling of the cutting edge [67]. It has been documented that all of the tool forces (cutting, thrust and side force) are sensitive to tool wear [101] with side force said to be the most affected by wear.

Further research documents a rise in the cutting force with respect to continuous length of cut [102]. Cutting force vs. length of cut has a similar trend to edge recession vs. length of cut [103]; both exhibit a rapid exponential rise which then levels off. A more detailed study offers an explanation of how tool forces increase due to wear [104] describing the wear and cutting force increase over a continuous length of cut in three stages.

1. An exponential increase in cutting force which levels off – This is caused by the initial blunting of the tool.
2. A linear increase with small gradient – The tool is now blunt and this trend is caused by edge rounding where the radius gradually increases
3. An exponential increase and then failure – When critical edge radius has been reached the clearance face starts to wear, eventually causing the failure of the tooth.

Using this knowledge, research into a predictive model for tool wear was conducted [105] revealing a linear relationship between the main cutting force and the square root of the edge radius. It is also noted that the relationship between the main cutting force and wear on the clearance face is approximately linear.

Compared to machining using sharp tools, it is widely accepted that worn edges generally lead to a more compressed chip formation and the work-piece is left with a fuzzier, protruded grain [66-69, 71] . This is for all of the major machining directions.

2.3 Mechanics of Wood Sawing

2.3.1 Tooth and Blade Geometry

Nomenclature for tooth geometry is detailed by British Standards [106]. The geometry of the saw teeth can be varied to suit the end use of the saw (appendix 3). Rip saws have un-bevelled cutting edges and small rake angles to remove material parallel to the grain. Cross cutting saws however need negative rake angles and sharp bevelled edges to sever the wood fibres perpendicular to the grain. Compound saw teeth have more than one cutting edge so can generally perform well cutting both parallel and perpendicular to the grain. Fleam teeth are usually seen on bow-saws for cutting green wood, the rake and flank angles are the same to allow cutting in both directions.

The thicknesses for the blade raw material is also specified [106] with the prospective user in mind (appendix 3). The teeth should be alternately set on either side of the blade. Approximately two-thirds of each tooth measured from the tip shall be set and the method of setting shall be such that the remainder of the tooth will remain un-deformed. The set width of the left and right set teeth should be equal and shall be expressed as a ratio of the thickness of the blade. For cross cutting and general use saws not less than one-fifth and not more than

two-fifths the thickness of the blade on each side. For rip saws no less than one-quarter and no more than one-half the thickness of the blade on each side. Saw blades use a variety of different set patterns depending upon the wood grain direction and the driving method (either manual or machine driven). Hands saws use a variation of the raker set.

During rip sawing the wood fibres are initially compressed and then sheared [107]. Post shearing the compressed fibres adjacent to the shearing edge spring back nearly to their original position. For this reason, the set of the saw must be large enough to prevent the sprung back fibres from making contact with the body of the saw. Softwoods produce fuzzy grain leaving the kerf not as cleanly cut as hardwoods, hence sawmills processing mainly softwoods apply greater set widths to the saw teeth.

Increased gullet size limits the number of teeth per unit of length of blade (i.e. decreases pitch). The feed velocity during sawing must be reduced for decreased pitch saws to prevent an excessive depth of cut per tooth known as over-biting. Conversely small gullet sizes tend to increase the tooth pitch [107]. In band sawing the cutting velocity needs to be reduced as sawdust can become compressed within the reduced gullet. The reciprocating cutting stroke does not provide enough of a respite for the sawdust to be removed from the kerf. In order to overcome these problems it is recommended that the area of the gullet should be approximately the same as the area of the tooth. Furthermore the bite of the tooth should be approximately one third of set width. This is to ensure that the smallest of the sawdust particles will not be any larger than the set width and hence will be completely swept out of the machined groove by the set teeth reducing lateral cutting forces.

Using a blade with uniform tooth pitch results in the set and unset teeth having the same bite profile and hence the same principle cutting and thrust forces [108]. Using a differential pitch i.e. the gullet size of the set teeth is smaller than that of the neutral teeth, means that the set

teeth have only a fraction of the bite of the neutral teeth. This results in the role of the set teeth to be that of removing swarf from the kerf rather than actually performing any of the cutting action. Reduced lateral cutting forces and wear are observed for the set teeth.

Bevelling the outer lateral edge of the set teeth reduces the bite profile and improves the surface quality through less damage to the fibres (creating cleaner cuts) [109]. Bevelling the inner lateral edge of the set teeth can as much as double the bite increasing the bite profile, cutting forces and reduces the surface quality. Overall bevelled teeth reduce cutting forces hence improving cutting performance. Uniform tooth pitch and geometry results in high surface quality and accurate sawn dimensions. The number of teeth/points per 25 mm shall be in accordance British Standards [106]. The teeth shall be evenly formed as shown by geometrical nomenclature (appendix 3).

2.3.2 Tool Forces

2.3.2.1 Recording Tool Forces

Cutting forces for single saw tooth tests are generally measured and recorded using one or more piezoelectric transducers. A piezoelectric transducer is a quartz crystal that generates an electric charge in response to an applied load. They can be calibrated to measure exact forces with very small margins of error. The simplest of data acquisition systems consist of a single transducer connected to a single saw tooth, aligned to measure the force in the direction of cutting [110]. Where three transducers are simultaneously used to measure forces in the X, Y, and Z directions, they are collectively referred to as a force dynamometer. Dynamometers are generally set up to constrain the work-piece (wood) and thus record the resultant forces applied by the single tooth. The transducers aligned in the X, Y and Z directions are set up to record cutting, lateral and thrust forces. Usually the X, and Y directions record cutting or later forces and the Z direction records the thrust force, although this is completely depended on

orientation of the tool path with respect to the work-piece. This method has also been used for a constrained tooth with the work-piece attached to a moving feed bed [111]. As far as wood cutting mechanics are concerned, the tool forces are the most important measured response attributed to the tooth for a repeatable work-piece (i.e. if the work-piece stays the same but the tooth changes). This can either be in the pure, unaltered force form [5-7, 9, 70, 72], or as a specific force value with respect to depth of cut or volume of material removed [8, 112-114].

2.3.2.2 Tool Force Trends

For band-sawing operations machining across the wood fibre direction positive rake angles of 15°-30° are used for high power driven processes [107]. The tooth is allowed to "hook" or "barb" onto the work-piece to allow for quick machining. These rake angles would be far too large hand sawing operations as the forces required for cutting would be too large to perform manually. Clearance angles are varied (between 6°-16°) for varying feed velocities. This is to prevent the flank of the tooth from making unnecessary contact with the work-piece during sawing. This will decrease the overall friction hence reducing thrust forces. Research into the effects of changing the rake angle of band-saw teeth when machining the wood end grain (the 90°-90° direction), has yielded interesting results with regard to the force in the direction of cutting [115]. Three teeth with 25°, 30° and 35° rake angles were examined. It was found that the largest rake angle produced the lowest cutting forces and the smallest rake angle produced the largest cutting forces.

A comparison of the performance between individually set teeth and swaged teeth show a reduction in lateral forces for the swaged teeth [116]. Furthermore a quadratic relationship has been established between the variation (standard deviation) of lateral forces and side clearance. Through analysis of the cutting, thrust and side forces a mechanistic cutting force model could be developed evaluating the individual roles of the set and neutral teeth [112]. It

was found that the unset teeth contribute to the majority of the cutting and thrust forces and the set teeth cause the majority of the lateral forces measured.

A numerical model using the un-deformed chip of the set and neutral teeth has been developed to estimate the cutting resistance and principle cutting force [117]. This information has been used to aid design of the set band-saw teeth for reduced wear. The bite of an individual tooth, or depth of cut, is often used to approximate the un-deformed chip thickness (figure 2.6).

$$b_{1s} = b_{1n}\left(1 - \frac{1}{2\cos k_s}\right) \tag{2.6}$$

$$b_{10} = \left(\frac{b_{1n}+2\delta}{2\cos k_s}\right) - b_{1n} \tag{2.7}$$

$$C_r = \frac{F_H}{(n_s+1).h_{1n}.b_{1i}} \tag{2.8}$$

Where:

b_{10} approximate un-deformed width of chip for neutral teeth, mm

b_{1s} approximate un-deformed width of chip for right- and left-set teeth, mm

b_{1i} total un-deformed width of chip, mm

b_{1n} nominal width of chip, mm

C_{ri} cutting resistance, mm

F_{Hi} main cutting force, N

h_{1n} nominal un-deformed chip thickness, mm

n_s number of teeth between two subsequent equally set teeth

k_s setting angle, degrees

Specific cutting pressure, *Ks*, is used to rate the performance of the bite of a single tooth using the un-deformed area, A, the force acting along the x axis, *Fx* [112]. *Ky* and *Kz* are the coefficients in the y and z axes respectively.

$$Ks = \frac{\overline{Fx}}{A} \tag{2.9}$$

$$Ky = \frac{\overline{Fy}}{A} \tag{2.10}$$

$$Kz = \frac{\overline{Fz}}{A} \tag{2.11}$$

Regression analysis has been frequently used to develop predictive cutting force models for simple rip tooth geometries [5-7, 72] were a linear decrease in the cutting force for an increased positive rake angle (10° – 30°) has been observed [72]. At the same time a linear increase in cutting forces is observed for increased edge radii (5 – 20 μm). This shows that in the ripping scenario sharp teeth with small rake angles provide the lowest cutting forces. Factors that are considered to have a significant effect of the major cutting force are depth of cut, rake angle, and edge radius. Cutting force increases with depth of cut, increases with edge radius and decreases with rake angle. Furthermore cutting the wood end grain yields the largest cutting forces with the lowest cutting forces observed machining along the fibre direction. Work-piece parameters have been used as predictors in statistical modelling to describe force trends. The most often used parameters are density, moisture content and grain direction although coefficients of have previously been determined to discretely quantify wood species [7]. Adding additional moisture to a piece of timber leads to swelling, likewise removing moisture from timber leads to shrinking. As a result of this change in volume, the

density did not dramatically change with respect to moisture content. Higher tool forces are observed when cutting wood species of greater density [5, 6]. It is generally accepted that tool forces decrease with increased work-piece moisture content, an exception to this rule is for frozen wood specimen [7]. Increased moisture content for frozen wood leads to an increase in tool forces. Furthermore, it is observed work-pieces at decreasing sub zero temperatures lead to a significantly higher tool forces.

An investigation into lateral tool forces was conducted for sharp bevelled tooth geometries [9]. Very sharp teeth yielded in-significant lateral forces in all machining directions. Lateral forces only became noticeable when the teeth became worn or damaged. In this instance high lateral forces were observed machining both the wood end grain (90°-90° direction) and across the fibre direction (0°-90° direction) with lower lateral forces machining along the grain (90°-0° direction).

2.3.3 Chip and Surface Formation

Research into the effects of varied rake angle band-saw teeth on the on surface formation was conducted [115]. This was performed machining in the 90°-90° direction (wood end grain). Three teeth with 25°, 30° and 35° rake angles were examined. Initially, it appeared that the 25° and 35° rake angles produced a smooth work-piece finish after machining, whilst the 30° rake angle produced a rough finish with fuzzy grain. Microscope images showed that the 25° rake angle only appeared smooth when in fact the machining caused fuzzy grain which was then compressed due to the comparably lower rake angle of the tooth.

A high speed camera has been previously utilised to capture footage of the cutting process for single circular saw teeth [10]. The camera was set up to record 40,000 frames per second for a circular saw rotating at a speed of 3250 RPM. Green, dry and frozen wood was machined in the 90°-0° direction (along the grain) using single rip teeth with rake angles of 0°, 10°, 20°

and 30°. The only observed continuous chip formation was for green wood, with the dry and frozen work-pieces yielded smaller broken wood particles. Furthermore the footage was able to evaluate the action of the gullet. Reduced rake angle leads to a reduction in gullet volume, still images from this footage show a build up of wood particles for the larger rake angles (lower gullet volume), as the wood chips/particles are prevented from curling past the much smaller root radii. This results in an impaction of wood particles in the gullet impeding the material removal from the kerf.

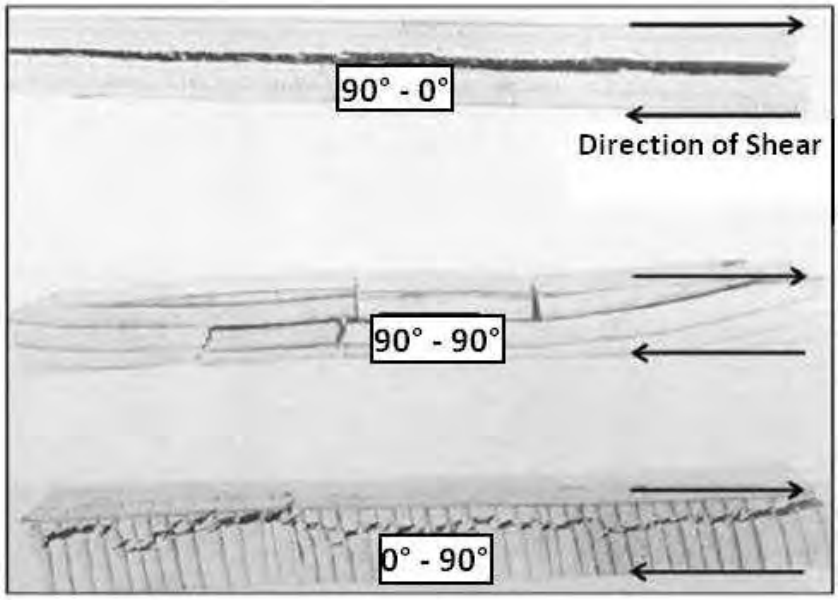

Figure 2.1 – Shear Failure Modes [55]

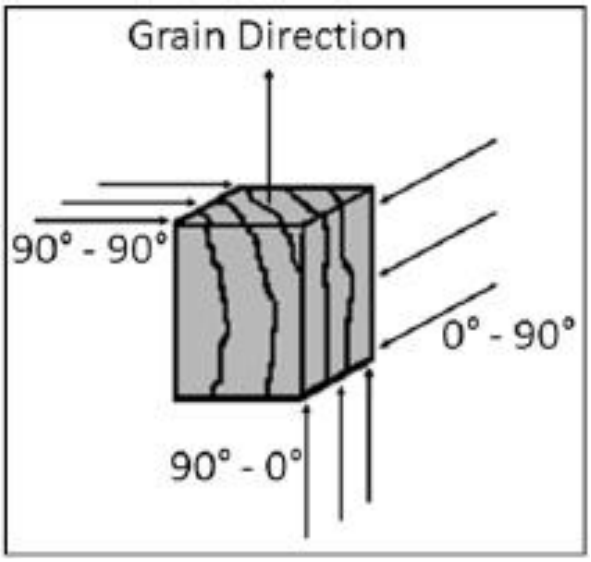

Figure 2.2 – Wood Machining Directions

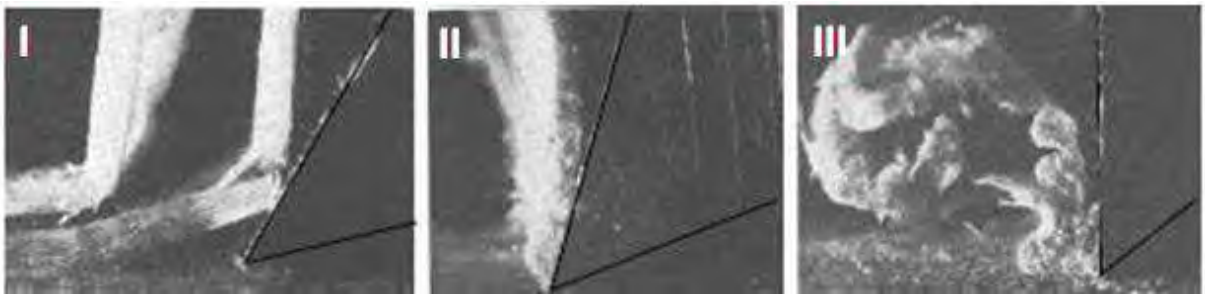

Figure 2.3 – McKenzie Chip Types (Along the Grain) [69]

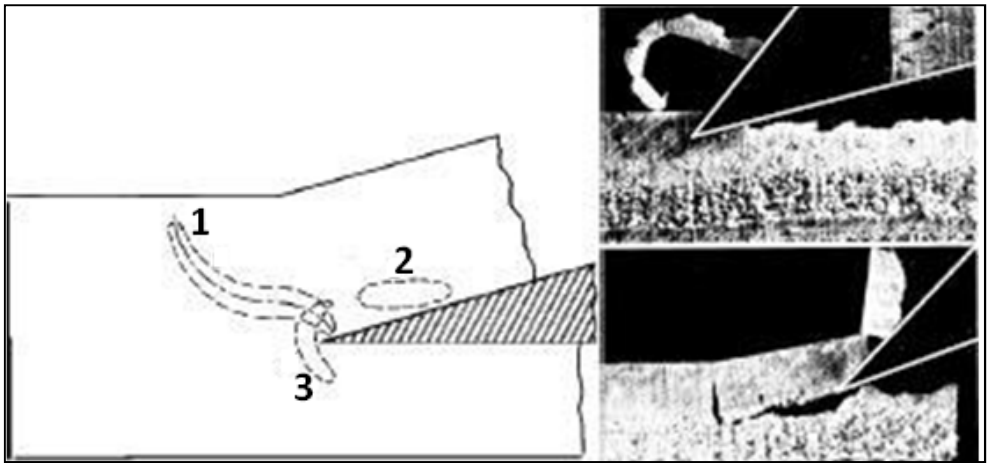

Figure 2.4 – Veneer Peeling (Across the Grain) [71]

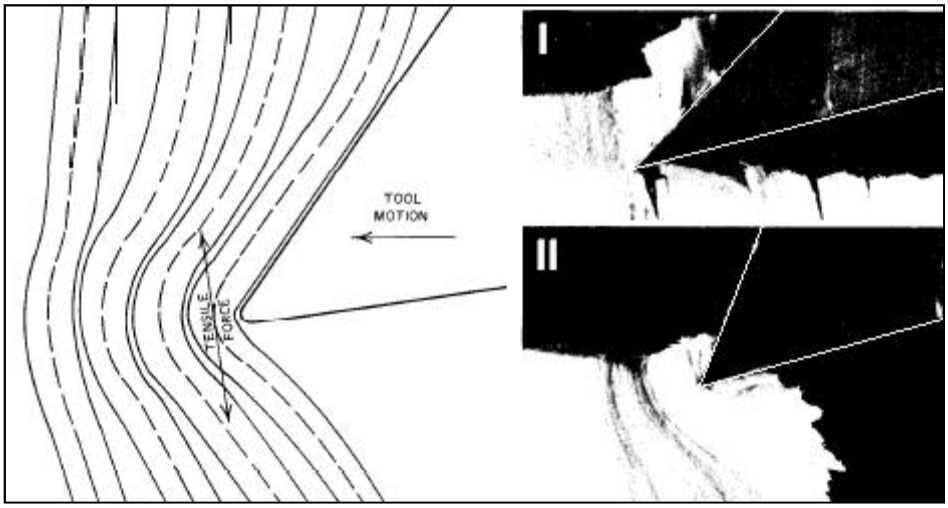

Figure 2.5 – Machining the Wood End Grain [71]

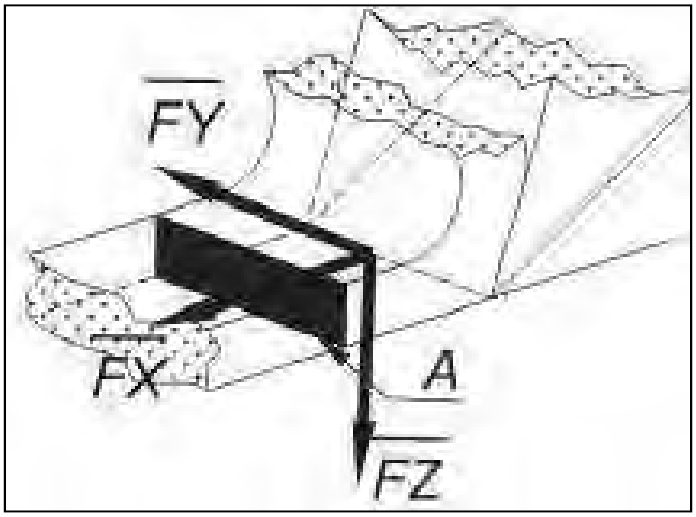

Figure 2.6 – Specific Cutting Pressure Model [112]

CHAPTER 3
INFLUENCE OF WORK-PIECE FACTORS ON THE CUTTING MECHANICS

3.1 Introduction

The influence of wood characteristics on the cutting mechanics has been considered before [5-7, 63, 70, 72, 111, 113, 114], with emphasis of the effect on tool forces. The previous studies in this area are either not relevant to handsaw tooth geometries [7, 63, 70, 72, 113, 114] or simply do not consider a wide enough range of wood properties to evaluate [5, 6, 111].

The aim of experimental work discussed in this chapter was to develop a predictive cutting force model using wood work-piece properties as predictors. This aim was facilitated by the following objectives:

- The determination of a variety of wood properties through standard mechanical test procedures
- Controlled cutting tests measuring the cutting (Fv), thrust (Fp) and side (Fr) forces using a piezo-electric dynamometer

A simple, orthogonal, rip tooth geometry was selected for the cutting tests to limit the number of tooth geometry parameters maintain the focus on the wood work-piece properties instead. This rip tooth geometry was machined from high speed steel.

3.2 Methodology

3.2.1 Router Machine Test Rig

The experimental test rig comprised of a rip tooth geometry driven by a 3 axis CNC router machine (figure 3.1). The tool was mounted to the router arm using a specially designed clamp. The tool path could be accurately assigned using the CNC software that accompanied the router machine. The wood work-piece was attached via a clamp to a force dynamometer equipped with three piezoelectric load cells measuring the cutting, thrust and side force components acting on the tool. The router machine arm could be driven in the X, Y and Z directions. The velocity in the X and Y directions could be varied between 1 – 100 mm/s and in the Z direction 1-50 mm/s.

3.2.2 Force measurement instrumentation

The simplified test rig schematic (figure 3.2) shows how the tool forces were measured during cutting. The cutting tool (1) passed through the work-piece clamped to the dynamometer. The dynamometer platform fed into the cutting tool in even increments for each stroke (2). The forces applied to the work-piece stimulated a charge output from the transducers which then channelled through to the charge amplifiers (3). These amplified values were converted from analogue to digital (4) and finally were recorded on the PC (5).

To elaborate, the Kistler type 9377C dynamometer consisted of three piezoelectric transducers measuring forces in the x, y and z directions (appendix 6). The x and y axes transducers had a sensitivity of 3.9 pC/N and could measure up to 75 kN of force. The z axis had a sensitivity of 1.95 pC/N and could measure up to 150 kN of force. The signal output from each transducer was channelled into an analogue charge amplifier (one amplifier per transducer). The input sensitivity was calibrated to match the transducer sensitivity (in pC) and the output range was set to 100 N = 1 V up to a maximum output of 10 V (1 kN). The

output from the charge amplifier was then channelled to a data acquisition PLC, converting the analogue signal to digital allowing the forces to be recorded on a PC using LabView signal express.

To verify that the data acquisition set up was accurately measuring the forces; loads were applied to each axis using the Instron universal testing machine. This was performed within the loaded range of 1 – 5 kN measuring not only the force in the direction of the load but also the cross interference in the other two directions. For all three axes the measurement of the forces started to lose accuracy beyond the 2 kN region. This was not seen as significant cause for concern, as the highest of the recorded forces for single tooth tests fell below 1 kN. When loading the X and Y axes cross interference in the other two un-loaded axis was observed to be more prominent than when loading the Z axis alone. However, these measured values were less than 10% of the force measured in the loaded axis.

3.2.3 Error Evaluation (appendix 6)

Before the commencement of controlled cutting test runs, the test rig was carefully evaluated. This consisted of calibration of the data acquisition (performed routinely) and estimation of the systematic errors involved in cutting using the router. The two key parameters investigated were depth of cut and unwanted forces (noise) induced by machine vibration. Obomodulan^{TM} tooling board was used to investigate all of the parameters. This is because it is approximately the same density as wood (470 kg/m^3) but it is homogenous and isotropic, hence defects in the material are minimised.

3.2.3.1 Machine noise forces

The magnitude of vibration forces of the router were determined to be negligible compared to the magnitude of the tool forces. As the machine forces threshold was determined, any forces

that that registered below this threshold were removed during analysis, leaving only data acquired during at the time of cutting.

3.2.3.2 Depth of Cut

Maintaining a level surface and constant depth of cut carried a degree of difficulty. The most effective solution to this was to machine a groove in the work-piece using an end mill attached to the router arm. This process ensured that the tool axis of the router was parallel to the work-piece. The work-piece was not disturbed until the single tooth passes through the machined groove. The depth of cut is the most critical machining parameter as it is the hardest to control. The values of depth of cut typical in sawing (0.05-0.2 mm) were investigated increasing to much larger depths (up to 1.2 mm). The error 0.1 and 0.2 mm was calculated to be (+/-) 70% and (+/-) 30% respectively, which is considerably large for controlled testing . The smallest value with an acceptable error limit was 0.4 mm with (+/-) 12.5% error. Hence it was decided at this point to perform the experiment with depth increments no smaller than 0.4 mm.

3.2.4 Work-Piece

The annual growth rings, along with other defects, give all wood species anisotropic properties. In order to evaluate the error caused by this, cylindrical samples of dry Scots pine (<6% moisture content) were machined along and across the grain in various machining directions as well as cutting through knots. All cuts were taken at 1 mm depth of cut using a rip tool with 1 mm edge width. Similarities can be drawn between the method for this error measurement and the research performed by Costes [77]. The key difference being that in this case the orientation of the tool changes with respect to the annual growth rings rather than the wood grain direction. The results show that the machining across the grain with and against the inclination of the growth rings result in an insignificant difference in the major cutting

force (Fv), with no significant error in all of the major machining directions. The error cutting through knots was found to be significantly large and hence was avoided during controlled tests.

3.2.4.1Moisture Content

Regulation of moisture content is an important variable to consider for machining and hence was controlled within a certain range. During the seasoning process timber manufactures use a specialist kiln to dry wood. In the absence of a kiln, a fan assisted oven was used instead. Results from initial tests showed that moisture content varied throughout the work-piece and took a certain amount of time to reach equilibrium. There were four methods of treatment employed to obtain the desired moisture levels. Spruce was selected to evaluate the moisture regulation; work-piece samples prepared had dimensions of 50x25x100 mm. A protimeter was used to measure work-piece moisture content probing the radial plane at a depth of 10 mm and the tangential plane at a depth of 5 mm.

1. The wood as it arrives from the supplier is usually in the range of 9-11% moisture content. This is due to the seasoning treatment performed at the saw mill. No additional processes were applied to the wood to achieve the desired moisture content (approximately 10%).
2. To achieve a dry work-piece (<6% moisture content) the seasoned wood as it arrived from the supplier was dried for 20 - 30 minutes at 100°C.
3. To reach the fibre saturation point, the wood was submerged under water for 48 hours with no additional treatment.
4. To achieve approximately 20% moisture content the wood was submerged under water and then dried for 20-30 minutes at 100°C.

After the woods were treated for the individual moisture levels, they were stored in vacuum sealed containers for a minimum of 120 hours to allow for redistribution of moisture (appendix 5).

3.2.5 Tool Force Measurement

Recorded tool force data for wood samples along the grain displays cutting (Fv) and thrust forces (Fp) at a steady state for uniform chip formation. It must be noted that the grove machined by the tool exhibits little disturbance, i.e. it is a clean cut with no chip break off points. Cutting across the grain, is an entirely different scenario. Cutting and thrust forces fluctuate significantly; this is due to the tool machining through the earlywood fibres (lower density) and then latewood fibres (higher density).

3.2.6 Cutting Velocity vs. Cutting Forces

Evidence from fundamental literature suggests that cutting velocity has negligible effect on the forces acting on the tool. This is for the ranges of 0.2 m/s – 6.3 m/s [1] along the grain and 2.5 m/s – 50 m/s across the grain [2]. This has been investigated further by a velocity experiment performed in a lathe (appendix 4). The tool dynamometer platform holding a band saw rip-tooth of 2 mm thickness was fed into the rotating work-piece at intervals of 0.5 mm depth per cut. Twelve cuts were taken at each velocity for each work-piece variation (along and across the grain). The first two cuts were not used to calculate the average as these operations were used to make the work-piece parallel to the tool path arc. The following 10 cuts were used to calculate the average cutting and thrust forces.

The findings show that cutting velocity has no significant effect on the major tool forces for a velocity range of 0.5 and 2.5 m/s. Examination of collected chip formation and kerf, using an

optical microscope, show no significant changes in the formation of chip in this velocity range.

3.2.7 Mechanical Test Procedures

A further programme of work was completed providing complimentary data to the cutting force data obtained through the single tooth tests. ASTM D143-09 standard test procedures for three point bending and longitudinal shear was implemented to characterize wood strength across and along the grain respectively. ASTM standards were selected over British standards as they could be more easily performed in the Instron universal testing machine.

3.2.7.1 Three point Bending

All tests were performed using the ASTM standard methodology described in the literature review chapter 2 of this report (2.1.4). The span (L) of all of test specimens was kept at 300mm with a 20mm depth (d); this is in keeping with the specified 14:1 minimum span to depth ratio. An additional criterion that was also specified by the standard was a 1.3 mm/min crosshead maintained throughout testing until failure. The wood is placed into experimental set-up in the Instron machine (figure 3.3) where the apparatus is placed between a loaded anvil and a 10 kN load cell.

3.2.7.2 Determination of Modulus of Rupture and Modulus of Elasticity

In order to calculate these values a force displacement must be obtained using the Instron data acquisition system. The linear region where Force is directly proportional to Displacement is taken to be the elastic region where no permanent deformation occurs. Force and Displacement measurements from this region are used to calculate MOE (equation 3.2). The Force measurement at the point of fracture is the subsequently used to calculate MOR (equation 3.1).

$$MOR = \frac{3FL}{2bd^2} \qquad \textit{At point of fracture} \qquad (3.1)$$

$$MOE = \frac{FL^3}{4bd^3\omega} \qquad \textit{At elastic limit} \qquad (3.2)$$

3.2.7.3 Longitudinal Shear

As with the three point bending tests, all tests were performed using the ASTM standard methodology. The experimental set up (figure 3.4) also uses the 10 kN load cell. All proportions for the test piece used in experimentation are detailed below. A 0.6 mm/min crosshead maintained throughout testing until failure.

3.2.7.4 Determination of Modulus of Rigidity (G) and Shear Strength (τ)

As the shear zone is square, both the length and width are taken to be *a.* Equations 3.3 and 3.4 can be modified to accommodate the standard test specimen. Once again a Force Displacement plot was acquired to determine the elastic region and the point of fracture $\boldsymbol{\tau}$ and G are calculated using equations 3.2 and 3.3 respectively.

$$\tau = \frac{F}{A} \qquad \textit{At point of fracture} \qquad (3.3)$$

$$\therefore \tau = \frac{F}{a^2}$$

$$G = \frac{\tau}{\gamma} = \frac{FL}{Ax} \qquad \textit{At elastic limit} \qquad (3.4)$$

$$\therefore G = \frac{Fa}{a^2x} = \frac{F}{ax}$$

3.2.7.5 Toughness (U)

Toughness was calculated from the stress strain curves (figure 3.5) generated from the Instron machine force extension plots. The stress strain curve was in the form of a quadratic polynomial. Toughness (U) was obtained by taking the definite integral of the quadratic function between zero and the point of facture (n) (equation 3.5).

$$U = \int_n^0 f(\varepsilon) = \int_n^0 (a\varepsilon^2+b\varepsilon+c) \tag{3.5}$$

3.2.8 Statistical Treatment of Data

3.2.8.1 Simple Least Squares

Regression models with only one variable and one measured response use simple, linear least squares method to determine the equation of a straight line for *n* number of data plots. This can be expressed in the form of equation 3.6:

$$y = \beta x+\alpha \tag{3.6}$$

Where β and α are the unknown coefficients. β is calculated using least squares and then substituted into equation 3.7 using the average values of the x and y values to calculate α. Now both the β and α coefficients are known, they can be substituted into equation 3.8 defining the equation of the fitted line which can be superimposed over the plotted values.

$$\beta = \frac{\sum_{i=1}^{n} (x_i-\bar{x})(y_i-\bar{y})}{\sum_{i=1}^{n} (x_i-\bar{x})^2} \tag{3.7}$$

$$\alpha = \bar{y}-\beta\bar{x} \tag{3.8}$$

3.2.8.2Multiple least squares

Multiple least squares can be used to determine a linear relationship between a measured response and multiple variables. The multiple variables are expressed by means of a design matrix (equation 3.9), allowing the regression equation to be expressed in the form of equation 3.10.

$$X = \begin{pmatrix} x_{11} & \cdots & x_{1p} \\ x_{21} & \cdots & x_{2p} \\ \vdots & \ddots & \vdots \\ x_{n1} & \cdots & x_{np} \end{pmatrix} \tag{3.9}$$

$$y = \beta_0 + \beta_1 x_{i,1} + \ldots + \beta_p x_{i,p} + \alpha \quad \{i=1,\ldots,n\} \tag{3.10}$$

In order to determine the coefficients of each x variable [$\hat{\beta} = \{\beta_0, \beta_1, \beta_p\}$] least squares is used (equation 3.11).

$$f(\hat{\beta}) = \sum_{i=1}^{n} (y_i - X\hat{\beta})^2 = (y - X\hat{\beta})'(y - X\hat{\beta}) \tag{3.11}$$

The derivative of the beta function provides the normal equation 3.12.

$$f'(\hat{\beta}) = -2X'(y - X\hat{\beta}) = 0 \tag{3.12}$$

$$\therefore (X'X)\hat{\beta} = X'y$$

The inverse of the X'X product matrix is applied to both sides providing the coefficient for the specific *x* variable (equation 3.13).

$$\hat{\beta} = (X'X)^{-1}X'y \tag{3.13}$$

3.2.8.3 Analysis of Variance (ANOVA)

ANOVA is used to determine the statistical validity of regression models. The first stage of this analysis involves the partitioning of the degree of freedom (DF) terms (equation 3.14). Where K is the number of terms in the study and N is the total number of obtained data points (equations 3.15, 3.16).

$$DF_{TOT} = DF_{REG} - DF_{RES} \tag{3.14}$$

$$DF_{REG} = K - 1 \tag{3.15}$$

$$DF_{RES} = N - K \tag{3.16}$$

This is followed by the partitioning of the sum of squares (SS) terms (equation 3.17). Where $y_{i....n}$ are the predicted response values, $\hat{y}_{i....n}$ are the actual responses and $\bar{y}$ is the average of all plotted response values (equations 3.18, 3.19).

$$SS_{TOT} = SS_{REG} - SS_{RES} \tag{3.17}$$

$$SS_{REG} = \sum_{i=1}^{n} (\hat{y}_i - \bar{y})^2 \tag{3.18}$$

$$SS_{RES} = \sum_{i=1}^{n} (y_i - \hat{y}_i)^2 \tag{3.19}$$

The R^2 value acts as a ratio determining how well the fitted regression line can predict the outcome of the individual data points (equation 3.20).

$$R^2 = 1 - \frac{SS_{RES}}{SS_{TOT}} \tag{3.20}$$

F testing is used to compare different regression models and is calculated using mean squared (MS) values (equations 3.21, 3.22). It is used to compare the variability between and within the data group's analyzed (equation 3.23).

$$MS_{REG} = \frac{SS_{REG}}{DF_{REG}} \tag{3.21}$$

$$MS_{RES} = \frac{SS_{RES}}{DF_{RES}} \tag{3.22}$$

$$\text{F VALUE} = \frac{\text{Between Group Variability}}{\text{Within Group Variability}} = \frac{MS_{REG}}{MS_{RES}} \tag{3.23}$$

The P value is used to test the statistical significance of the obtained test data. It uses the cumulative probability function [f(y)] for the data set, where $P(y_i \geq X)$ is the probability distribution of the response value y_i with respect to the random variable X. Any "P value" of less than 0.05 (within 95% confidence interval) shows that its respective model is statistically significant.

$$f(y) = \sum_{i=1}^{n} P(y_i \geq X) \tag{3.24}$$

$$\text{P VALUE} = 1\text{-}f(y) \tag{3.25}$$

3.2.9 Experimental design

The tool used in the experiment has geometry similar to rip tooth formations (figure 3.6). The tool has an orthogonal cutting edge with a width of 1 mm and a rake angle (γ) of zero. To ensure that the cutting edge was sharp the tool was sharpened using precision grinding equipment at regular intervals. Although it was assumed that no edge recession occurred during the cutting tests, the test runs were randomised to counteract any systematic error related to the sharpness of the cutting edge. The two machining directions selected for the experiment were 90°-0° (across the grain) and 0°-90° (along the grain) as these are deemed to be the most common directions for manual wood-sawing.

Eight species of wood were evaluated in the experiment, five softwoods (Scots Pine, Yellow Pine, Siberian Larch, Douglas Fir and Western Red Cedar) and three hardwoods (Ash, Beech and Sapele). Each of these wood species had four nominal moisture levels; Dry (<6%), 10%, 20% and Saturated (>30%). Including the two machining directions this amounts to sixty-four work-piece variables. The wood was machined both along and across the radial plane, this was because the ratio of earlywood to latewood bands in this plane are approximately 1:1. Each of the sixty-four work-piece variations was machined at three depths of cut; 0.4, 0.8 and 1.2 mm, providing a total of one hundred and ninety-two cutting thrust and side force values for analysis.

Table 3.1 – Randomised sequence of test runs to eliminate systematic error

Direction	**Species**	**Scots Pine**	**Yellow Pine**	**Siberian Larch**	**Douglas Fir**	**Western RedCedar**	**Ash**	**Beech**	**Sapele**
Parallel	**DRY**	60	2	24	14	41	6	26	16
	10%	53	13	43	9	45	48	61	39
	20%	37	42	23	34	46	40	27	19
	SAT	32	17	21	59	58	3	62	11
Perpendicular	**DRY**	33	10	55	22	63	18	54	8
	10%	64	18	1	5	29	51	31	30
	20%	44	20	12	35	57	4	7	15
	SAT	49	36	52	25	47	56	50	38

3.3 Results

3.3.1 Mechanical Properties

In general the average strength of the wood species tested across the grain obtained through the three point bending tests (denoted by MOR) was measured to be over 50 times greater than the strength along the grain obtained through the longitudinal shear tests (denoted by τ). The average elasticity of the wood across the grain (denoted by MOE) was measured to be nearly 400 times greater than along the grain (denoted by G).

3.3.1.1Shear

The average shear strengths recorded (τ) range from 5 – 12 MPa (figure 3.7). The highest values represent the three hardwoods tested which have values approximately 45 % greater than the softwoods. Furthermore a linear decrease in strength is observed with an increase in moisture content. The elastic modulus in shear (G) of the wood species evaluated range from 15 – 230 MPa with the larger values once again representing the hardwoods. These values are approximately 50 % greater than the softwoods. The elastic modulus exhibits a negative linear trend with respect to moisture content.

3.3.1.2 Bending

For all moisture levels evaluated, values for mean modulus of rupture in bending (MOR) for the wood species evaluated range from 50 - 90 MPa (figure 3.8). A linear decrease is observed for increased moisture content with the highest values yielded by the three hardwood species tested, on average 70% greater than the softwood values. The values for mean modulus of elasticity in bending (MOE) of the wood species evaluated ranges from 40000 – 80000 MPa with a linear decrease in elasticity also observed for increased moisture content. The results from the force extension plots show there is no discernable pattern to suggest that the hardwoods yield higher MOE values than the softwoods.

3.3.1.3 Toughness

The average response plots for toughness i.e. the energy absorbed by the wood up to the point of fracture, shows that the magnitudes were not as significantly affected by the grain direction as the materials strength (MOR and τ) or elasticity (MOE and G). The mean toughness obtained from the three point bending stress vs. strain plots (Ub) yielded approximate values of only 10% greater than the mean toughness obtained from the longitudinal shear stress vs. strain plots (Us). This holds true for the relationships with respect to moisture content and for the individual wood species evaluated.

Table 3.2 – Obtained Mechanical Properties

	Species	MOE (GPa)	MOR (MPa)	Ub (J/m^2)	G (MPa)	τ (MPa)	Us (J/m^2)	ρ (kg/m^3)	MC (%)
DRY (NOMINAL)	Scots Pine *(SW)*	6.28	79.21	33250	151.47	9.53	26650	576.64	6.00
	Yellow Pine *(SW)*	5.08	47.72	24910	286.27	6.28	17100	484.80	6.00
	Douglas Fir *(SW)*	6.92	72.01	49000	236.51	7.58	34080	496.62	8.00
	Western Red Cedar *(SW)*	9.15	99.28	40600	52.78	8.62	31730	671.57	6.00
	Siberian Larch *(SW)*	7.33	65.24	49020	260.16	9.31	54000	638.46	8.00
	Ash *(HW)*	5.75	105.57	84000	277.03	17.06	94300	912.87	6.00
	Beech *(HW)*	8.89	127.44	61750	363.83	15.55	86400	669.00	6.00
	Sapele *(HW)*	7.80	92.73	58050	219.11	18.17	57200	819.08	6.00
	AVERAGE	**7.15**	**86.15**	**50070**	**230.90**	**11.51**	**50180**	**658.63**	**6.50**
	RANGE	**4.07**	**79.72**	**59090**	**311.05**	**11.89**	**77200**	**428.07**	**2.00**
	STANDARD DEVIATION	**1.44**	**25.24**	**18350**	**94.06**	**4.65**	**28200**	**148.44**	**0.93**
10% (NOMINAL)	Scots Pine *(SW)*	5.83	61.99	21000	152.64	7.97	25200	559.04	14.00
	Yellow Pine *(SW)*	4.03	47.62	19200	91.30	5.69	16120	436.15	11.00
	Douglas Fir *(SW)*	6.14	58.57	24750	43.32	3.97	26850	478.93	14.00
	Western Red Cedar *(SW)*	3.95	54.60	22100	268.98	4.76	26250	460.96	11.00
	Siberian Larch *(SW)*	6.70	88.62	28840	208.32	10.34	27280	615.38	11.00
	Ash *(HW)*	8.23	119.09	61740	123.21	14.20	84000	850.73	10.00
	Beech *(HW)*	11.36	95.04	47250	211.37	14.15	60750	696.65	11.00
	Sapele *(HW)*	9.11	113.05	45500	691.02	14.31	28600	759.75	8.00
	AVERAGE	**6.92**	**79.82**	**33790**	**223.77**	**9.42**	**36880**	**607.20**	**11.25**
	RANGE	**7.41**	**71.47**	**42540**	**647.70**	**10.34**	**67880**	**414.58**	**6.00**
	STANDARD DEVIATION	**2.54**	**27.77**	**15670**	**202.15**	**4.43**	**23080**	**151.22**	**1.98**
20% (NOMINAL)	Scots Pine *(SW)*	6.49	53.85	8750	128.55	10.85	15260	546.36	20.00
	Yellow Pine *(SW)*	3.24	30.57	3840	46.22	2.22	11700	416.88	25.00
	Douglas Fir *(SW)*	4.47	40.92	20470	152.23	4.85	21000	462.60	25.00
	Western Red Cedar *(SW)*	4.69	56.63	10330	138.98	3.74	16640	434.53	25.00
	Siberian Larch *(SW)*	4.08	48.80	22500	136.96	5.76	24080	604.35	20.00
	Ash *(HW)*	7.76	103.94	42750	84.88	7.32	70950	714.17	24.00
	Beech *(HW)*	5.11	78.47	42000	209.07	7.17	35500	737.15	27.00
	Sapele *(HW)*	3.15	62.47	38740	195.14	10.64	28250	632.64	23.00
	AVERAGE	**4.87**	**59.46**	**23670**	**136.50**	**6.57**	**27920**	**568.59**	**23.63**
	RANGE	**4.61**	**73.37**	**38910**	**162.85**	**8.63**	**59250**	**320.27**	**7.00**
	STANDARD DEVIATION	**1.58**	**22.93**	**15730**	**53.23**	**3.08**	**18980**	**124.04**	**2.50**
SAT (NOMINAL)	Scots Pine *(SW)*	4.41	47.00	15400	6.21	5.70	9100	530.23	32.00
	Yellow Pine *(SW)*	2.49	26.65	10200	7.75	2.31	7100	407.70	35.00
	Douglas Fir *(SW)*	3.66	29.69	22000	25.20	4.42	11600	448.67	35.00
	Western Red Cedar *(SW)*	4.33	43.84	21930	19.91	3.49	11000	354.88	30.00
	Siberian Larch *(SW)*	4.45	40.83	22800	7.71	4.71	14200	575.65	32.00
	Ash *(HW)*	5.62	73.15	45990	18.45	6.34	40000	708.26	45.00
	Beech *(HW)*	5.84	76.76	45600	16.20	8.35	31200	787.75	40.00
	Sapele *(HW)*	4.78	69.15	45000	19.54	11.39	21000	595.21	31.00
	AVERAGE	**4.45**	**50.88**	**28610**	**15.12**	**5.84**	**18150**	**551.04**	**35.00**
	RANGE	**3.35**	**50.11**	**35790**	**18.99**	**9.08**	**32900**	**432.87**	**15.00**
	STANDARD DEVIATION	**1.06**	**19.64**	**14610**	**7.02**	**2.89**	**11760**	**147.96**	**5.13**

3.3.2 Tool Force Average Responses

In general the highest average force values are observed to be in the direction of cutting (50 – 160 N) followed by the values in the direction of thrust (15 – 40 N). The lateral tool forces are observed to be the lowest recorded (2 – 6.5 N). The trends for cutting, thrust and side forces are dealt with separately within this section.

3.3.2.1 Cutting Force (Fv)

The major cutting force was noticeably affected by two parameters; the wood grain direction and the moisture content (figure 3.10). Cutting force vs. Depth of cut shows that the cutting forces exhibit a linear increase with respect to depth of cut (figure 3.9). Furthermore, recorded forces display a more exaggerated effect across the grain illustrated by the larger gradient. These recorded force values across the grain range from 6% greater than along the grain at 0.4 mm depth of cut to 40% greater at 1.2 mm depth of cut. Cutting force vs. Moisture content exhibits a linear decrease in cutting forces for increased moisture content. The difference between force values across and along the grain becomes significantly more prominent with reduced moisture content. These recorded cutting forces across the grain range from 7% greater than along the grain for dry (<6% moisture content) wood to 88% greater for saturated (>30% moisture content). When looking at the values for individual wood species it is clear that the softwood species yielded lower cutting forces than the hardwood species. The only exception to this is Siberian Larch which yielded an average cutting force value of 100 N, which is 40% greater than the other softwoods tested.

3.3.2.2 Thrust Force

Unlike the major cutting force, the thrust force was not significantly affected by the wood grain direction. Similar to the recorded cutting force values, for thrust force vs. Depth of cut the trend shows an increase in force for increased cutting depth. Cutting across the wood grain at 1.2 mm depth yielded a force only 4% greater than along the grain, being the largest difference between the two trends. Likewise, Thrust force vs. Moisture content still has a

negative linear trend with respect to moisture content, however this time at its highest. The mean recorded thrust force across the grain is only 10% greater than along the grain at a moisture content of 20. Softwood species yield much lower thrust forces than hardwoods however grain direction still has no noticeable influence on these force values.

3.3.2.3 Side Force (Fr)

Wood grain direction and moisture content both prove to have a significant effect on the side force however there is no noticeable difference between the mean side force values observed for hardwoods and softwoods respectively. Side force has a non-linear relationship with respect to depth of cut with more exaggerated mean side forces observed machining along the grain with values of 40%, 160% and 200% greater than across the grain (at depths of cut of 0.4 mm, 0.8 mm and 1.2 mm respectively). As with the mean cutting and thrust forces, side force has a negative correlation with respect to moisture content. In this instance side force values along the grain are measured to be approximately 4N greater than across the grain.

3.3.3 Chip Formation

3.3.3.1 Along the grain

Discontinuous (broken) chips were observed for dry work-pieces of all wood species at all three depths of cut (figure 3.11). The finish quality of the affected part of the work-piece surface appeared poor due to several break-off points of the chip.

Continuous chip formation occurred for work-pieces at 10-20% moisture content for 0.4 - 0.8 mm depth of cut as well as for saturated work-pieces at 0.4 mm depth of cut (figure 3.12). The surface formation left behind by this type of chip appeared to have high quality surface finish on account of the reduced amount of chip break off points.

Fuzzy chip formation occurred mainly for saturated work-pieces (with some occurring at 20% moisture content) at the larger depths of cut of 0.8 and 1.2 mm (figure 3.13). The surface finish of the work-piece displayed up-rooted wood fibres left behind in the groove. It was apparent from the microscope images (appendix 7) that this type of formation occurred more frequently for softwoods than hardwoods.

3.3.3.2 Across the grain

Bending was observed to be the primary failure mode for all depths of cut machining across the grain. However, the depths of cut that provide better visibility are 0.8 – 1.2 mm (figure 3.14). The work-piece surface formation was greatly affected by moisture content. For dry wood a sever degree of work-piece deformation was observed, with a visible channel down the centre of the tool path. At 10-20% moisture content it is visible that the fibres have been ploughed through, however the channel down the centre of the affected area is less visible on account of the wood fibres springing back towards the tool path. For saturated it appeared that even less of the ploughed area was deformed, in some instances it is even hard to see visible evidence that a tool has passed through it. This suggests one thing. Higher moisture content causes an increase in the elasticity of the wood fibres. For higher moisture content the fibres break and then attempt to spring back towards the initial position, for dry wood the fibres simply split and remain in that position due to the lack of fibre elasticity.

3.3.4 ANOVA

ANOVA (analysis of variance) tables were constructed (tables 3.2 – 3.9) using the simple least squares method. These tables display R^2, F values and p values as described in the methodology (equations 3.12 – 3.23). Specific cutting force (Fsp), defined as force over depth of cut was used as the response value for the selected categorical predictors. Across the grain these predictors are: modulus of elasticity (MOE), modulus of rupture (MOR), density (ρ) and

bending toughness (U_b). Along the grain the predictors are; shear modulus (G), shear strength (τ), density (ρ) and shear toughness (U_s). Moisture content (MC) was not selected for these trials in order to keep an emphasis on the properties obtained through mechanical testing. The spread of the residual Fsp values had data a range of 159 N/mm across the grain and 168 N/mm along the grain. Standard deviation was also calculated with values of 34 across the grain and 33.5 along the grain.

All tables returned p values of zero showing that all of the simple linear models are statistically valid. The ultimate material strength values yielded the highest R^2 and F values with F=131, R^2=58% for MOR across the grain and F=127 R^2=57% for τ along the grain. The toughness followed the same pattern as the strength properties with F=162, R^2=63% for Ub across the grain and F=125, R^2=67% for Us along the grain. The elastic properties yielded the lowest values with F=42, R^2=31% for MOE across the grain and F=37, R^2=28% for G along the grain. Density (ρ) returned relatively large values across the grain F=149, R^2=61% compared to along the grain F=60, R^2=39%.

Table 3.3 – Fsp vs. MOE across the grain

Fsp vs. MOE
Analysis of Variance

Source	DF	SS	MS	F	P	R^2
Regression	1	33135	33135.4	42.40	0.000	33.1
Error	94	73463	781.5			
Total	95	106599				

Regression Equation Fsp = 38.51 + 0.0009183 MOE

RANGE = 167.9
SD = 33.48

Table 3.4 – Fsp vs. MOR across the grain

Fsp vs. MOR
Analysis of Variance

Source	DF	SS	MS	F	P	R^2
Regression	1	62051	62050.7	130.93	0.000	57.8
Error	94	44548	473.9			
Total	95	106599				

Regression Equation Fsp = 26.54 + 0.9507 MOR

RANGE = 167.9
SD = 33.48

Table 3.5 – Fsp vs. ρ across the grain

Fsp vs. ρ
Analysis of Variance

Source	DF	SS	MS	F	P	R^2
Regression	1	65338	65338.0	148.85	0.000	60.9
Error	94	41261	438.9			
Total	95	106599				

Regression Equation Fsp = - 18.68 + 0.1860 ρ

RANGE = 167.9
SD = 33.48

Table 3.6 – Fsp vs. Ub across the grain

Fsp vs. Ub
Analysis of Variance

Source	DF	SS	MS	F	P	R^2
Regression	1	67407	67407.2	161.67	0.000	63.2
Error	94	39192	416.9			
Total	95	106599				

Regression Equation Fsp = 42.32 + 0.00001466 Ub

RANGE = 167.9
SD = 33.48

Table 3.7 – Fsp vs. G along the grain

Fsp vs. G
Analysis of Variance

Source	DF	SS	MS	F	P	R^2
Regression	1	30294	30294.1	37.07	0.000	28.3
Error	94	76818	817.2			
Total	95	107112				

Regression Equation Fsp = 55.16 + 0.1286 G

Range = 159.3
SD = 33.58

Table 3.8 – Fsp vs. τ along the grain

Fsp vs. τ
Analysis of Variance

Source	DF	SS	MS	F	P	R^2
Regression	1	61517	61517.4	126.83	0.000	57.4
Error	94	45594	485.0			
Total	95	107112				

Regression Equation Fsp = 25.04 + 5.951 τ

Range = 159.3
SD = 33.58

Table 3.9 – Fsp vs. ρ along the grain

Fsp vs. ρ
Analysis of Variance

Source	DF	SS	MS	F	P	R^2
Regression	1	41553	41552.6	59.58	0.000	38.8
Error	94	65559	697.4			
Total	95	107112				

Regression Equation Fsp = - 13.79 + 0.1483 ρ

Range = 159.3
SD = 33.58

Table 3.10 – Fsp vs. Us along the grain

Fsp vs. Us
Analysis of Variance

Source	DF	SS	MS	F	P	R^2
Regression	1	61149	61148.7	125.06	0.000	57.1
Error	94	45963	489.0			
Total	95	107112				

Regression Equation PSC = 38.46 + 0.00001087 Us

Range = 159.3
SD = 33.58

3.3.5 Regression Models

General linear models were created using the multiple linear regression method using all of the categorical predictors. In both cases the major cutting force, Fv, was the measured response with MOE, MOR, ρ, Ub, MC and δ as predictors for the model across the grain (table 3.11) and G, τ, ρ, Us, MC and δ as predictors for the model along the grain (table 3.12). The regression plots (figure 3.15) are shown with 95% prediction intervals along with the histograms (figures 3.16) display the distribution of the residual plots with respect to the regression line. The models exhibit R^2 values of 80% and 90% along and across the grain respectively. Additionally, the ratio of range to standard deviation is considered (R/SD). These values evaluate the spread of the data and the variance. They are 4.54 and 4.66 along and across the grain respectively.

Models excluding selected categorical predictors were also developed. Predicting Fv along the grain by negating G returned an R^2 value of 78.9% (table 3.14). By negating ρ along the grain returned an R^2 value of 79.1% (table 3.15). By negating both G and ρ along the grain returned an R^2 value of 78.6% (table 3.16). These only differ by a very small amount from the R^2 value of 80% when all categorical predictors are used. Predicting Fv across the grain by negating MOE returns and R^2 value of 85.9% compared to the slightly larger value of 90 when using all categorical predictors (table 3.13).

It is also noticed that the F values from the ANOVA tables vary when using different combinations of categorical predictors. Along the grain these vary from 59.33 using all of the categorical predictors, 67 excluding G, 68 excluding ρ and 84 excluding both G and ρ. Across the grain yields and F value of 90.54 using all of the categorical predictors and a value of 110 excluding MOE.

Table 3.11 – ANOVA table, model 1 across the grain

MODEL 1 – ACROSS GRAIN

Fv_p = - 72.7 - 0.000093 MOE + 0.235 MOR + 0.0594 ρ + 108 δ -0.129 MC +0.0000526 Ub
R-FV = 210.4 SD-FV = 45.12

Analysis of Variance

Source	DF	SS	MS	F	P	R^2
Regression	6	166247	27707	90.54	0.000	90
Residual Error	89	19924	306			
Total	95	193443				

Table 3.12 – ANOVA table, model 2 across the grain

MODEL 2 – ACROSS GRAIN (NO MOE)

FV_p = - 75.2 + 0.0000171 MOR + 0.0596 ρ + 108 δ - 0.093 MC + 0.0000549 Ub
R-FV = 210.4 SD-FV = 45.12

Analysis of Variance

Source	DF	SS	MS	F	P	R^2
Regression	5	166149	33230	109.58	0.000	85.9
Residual Error	90	27293	303			
Total	95	193443				

Table 3.13 – ANOVA table, model 1 along the grain

MODEL 1 – ALONG GRAIN

FV_p = - 15.3 + 0.0243 G + 2.54 τ - 0.0246 ρ + 65.4 δ - 0.301 MC + 0.0000492 Us
R-FV = 155.7 SD-FV = 34.29

Analysis of Variance

Source	DF	SS	MS	F	P	R^2
Regression	6	89347	14891	59.33	0.000	80
Residual Error	89	22337	251			
Total	95	111684				

Table 3.14 – ANOVA table, model 2 along the grain

MODEL 2 – ALONG GRAIN(NO G)

FV = - 11.0 + 2.89 τ - 0.0234 ρ + 65.4 δ - 0.486 MC + 0.0000454 Us
R-FV = 155.7 SD-FV = 34.29

Analysis of Variance (Linear Model)

Source	DF	SS	MS	F	P	R^2
Regression	5	88069	17614	67.13	0.000	78.9
Residual Error	90	23615	262			
Total	95	111684				

Table 3.15 – ANOVA table, model 3 along the grain

MODEL 3 – ALONG GRAIN(NO ρ)

FV = - 22.1 + 2.08 τ + 65.4 δ - 0.397 MC + 0.0000422 Us + 0.0237 G
R-FV = 155.7 SD-FV = 34.29

Analysis of Variance (Linear Model)

Source	DF	SS	MS	F	P	R^2
Regression	5	88344	17669	68.13	0.000	79.1
Residual Error	90	23340	259			
Total	95	111684				

Table 3.16 – ANOVA table, model 4 along the grain

GLM ALONG 4 (NO G, NO ρ)

FV = - 17.5 + 2.44 τ + 65.4 δ - 0.573 MC + 0.0000389 Us

R-FV = 155.7 SD-FV = 34.29

Analysis of Variance (Linear Model)

Source	DF	SS	MS	F	P	R^2
Regression	4	87812	21953	83.69	0.000	78.6
Residual Error	91	23872	262			
Total	95	111684				

3.4 Discussion

3.4.1 Mechanical properties

Average response at failure has shown a negative correlation between the strength in bending (MOR) and strength in shear (τ) with respect to moisture content. The hardwoods are observed to yield higher strengths than the softwoods; approximately 70% higher in Bending and 45% higher in Shear. The results in the elastic region reflect the results at the point of fracture. The modulus of rigidity (G) for longitudinal shear was observed to be within the 15 – 230 MPa range for all wood species tested. The elastic modulus (MOE) in bending was observed to be within the range of 40000 – 80000 MPa. The toughness for longitudinal shear (Us) was measured to be in the range of 18000 – 50000 J/m^2 compared to the slightly larger range of 29000 – 50000 J/m^2 for bending (Ub). Although the toughness values were obtained from the same force vs. extension plots (once converted to stress vs. strain plots) as the elastic properties and material strength, they are in no way proportional. Remembering that the elastic modulus was obtained from the linear section of the force vs. extension plot and the ultimate strength was obtained at the point of fracture; the toughness is described in a different way. Fracture toughness is defined as the energy absorbed by the material up until the point of fracture, i.e. the area under the stress strain curve. The ultimate strength is not dependent upon strain however the toughness is. The elastic modulus is dependent upon the

extension, but only within the linear region of the curve. Beyond this region the material may deform plastically without fracture allowing more extension to occur. All of these results for mechanical properties are typical compared to previously recorded properties in literature [55, 59].

When comparing the cutting and thrust forces to this data, certain relationships become noticeable. Elastic moduli and stress at point of fracture have a negative gradient with respect to moisture content, the cutting and thrust forces have the same trend for both grain directions. The difference between the softwood and hardwood values at point of fracture is more prominent than that of the elastic region. The material strength (MOR and $\boldsymbol{\tau}$) follow exactly the same pattern with respect to moisture content and individual wood species as the major cutting force. Although the elastic properties (MOE and G) also follow these trends the magnitudes are much smaller suggesting that material strength has a more significant influence on the major cutting force than the elastic properties. This is discussed in greater detail using the findings from ANOVA in section 3.2.2.

3.4.2 Tool Forces

The average tool forces recorded in the experimental work was used to quantify the cutting mechanics for specific work-piece conditions. The average cutting, thrust and side force responses all exhibit a negative linear trend with respect to moisture content. The average cutting and thrust forces both increased linearly with respect to depth of cut; however the side force has a non-linear trend. As only three depths of cut were performed in the experiment the function of the curve was not obtained. The most probable cause for this type of trend is an increased contact between the lateral edge of the rip tooth and the work-piece for increased depths of cut.

Grain direction yielded the most interesting results. The average cutting forces machining across the grain yielded significantly higher values than machining along the grain. This is not the same for the thrust force or the side force. The average thrust forces observed are not significantly affected by the grain direction. The average side forces have an entirely different trend. The magnitude of the side force is much greater along the grain than across, up to 200% for the larger depths of cut.

When looking at the behaviour of the individual woods, certain trends are noticed. In general, the three hardwoods included in the experiment produced higher cutting and thrust forces than the softwoods with no discernable trend for side forces for the differing wood species. One exception to this rule is Siberian Larch which exhibits higher forces along the grain than its other softwood counterparts. Since wood is an anisotropic material, a wood species such as Siberian Larch can yield cutting force responses in one machining direction akin to softwoods. However, in the opposite direction it can yield forces similar to hardwoods. One explanation for this is the environmental factors associated with the growing conditions of the wood. Siberian Larch grows in extremely cold climates. The extended cold growing season results in the annual growth rings consisting of a larger proportion of the much denser latewood cells. In softwoods growing in the more temperate climates the ratio of earlywood to latewood cells would be approximately 1:1. Any factors attributed to growing conditions can influence the intrinsic properties of the wood.

Overall, the force in the direction of cutting is the most significant making the largest contribution to tool resistance during cutting. Average tool force values show that the cutting force is approximately 4.5 times larger than the thrust force and 25 times larger than the side force across the grain. Along the grain the cutting force is approximately 3.5 times larger than the thrust force and 10 times larger than the side force. It is for this reason that the ANOVA

and regression analysis focuses primarily on the recorded cutting force values as the response data.

3.4.3 Chip Formation

Similarities and differences in the chip formed during the rip tooth machining experiment have been compared with results from planing operations [66, 69, 71]. Despite the fact that the rip tooth has zero rake angle all types of chip formation along the grain, as postulated by Franz [66], were observed.

It has been established that increasing the contact of the tool face by operating with small/negative rake angles and by increasing the depth of cut can cause type III formation (this is exacerbated for rough tool faces). This only occurs for higher moisture contents.

In the case of dry woods, the chips start to resemble type I formation. A group of fibres are initially compacted causing a longitudinal crack to propagate in front of the tool. Eventually these fibres shear along the formed crack.

Type II formation usually requires a positive rake angle for continuous chip formation. In this instance the reason why this formation is observed is because optimum parameters have been achieved. A combination of optimum moisture content and low depth of cut must be achieved (10-20% at 0.4-0.8 mm and saturated at 0.4 mm) assuming that the tool used has been sharpened.

The work done to previously explain chip formation across the grain does not provide any useful information regarding the rip tooth machining experiment. The main reason for this is because no material removal occurred. Instead the rip tooth ploughed through the wood fibres. Woodson and Koch [71] investigated the mechanics of cutting across the grain for planing tools with large rake angles and concluded that the chip observed is caused by an initial tear in

compression followed by ongoing shear. For the rip tooth (which has zero rake angle) the failure mode was observed to be that of bending with no shearing taking place.

To elaborate further, bending was observed to be the primary failure mode for all depths of cut. However, the depths of cut that provided better visibility are 0.8 – 1.2 mm. Work-piece surface deformations seems to have been greatly affected by moisture content. For dry wood the work-piece appeared greatly deformed with a visible channel down the centre of the tool path. At 10-20% moisture content it is visible that the fibres have been ploughed through. However, there is less of a visible channel down the centre of the affected area. For saturated it appeared that even less of the ploughed area was deformed. In some instances it is even hard to see visible evidence that a tool has passed through it. This suggests that higher moisture content causes an increase in the elasticity of the wood fibres. For higher moisture content the fibres break and then attempt to spring back towards the initial position. For dry wood the fibres simply split and remain in that position.

3.4.4 Regression and ANOVA

Evidence from recently published literature shows regression analyses have been used to develop predictive cutting force models [6, 7, 72]. These models are mainly focused on the effects of varied tool geometry for band-saw teeth. A linear decrease in the cutting force for an increased positive rake angle (10° to 30°) has been observed [72], whilst at the same time a linear increase in cutting forces is observed for increased edge radii (5 to 20 μm).

The reader should be reminded that the experimental work detailed in this paper used only a simple orthogonal cutting tool with zero rake angle to limit the tool geometry parameters. The rationale behind this is to thoroughly evaluate the effects of work-piece properties for several wood species on the cutting force whilst limiting the tool geometry parameters and cutting conditions. It is furthermore assumed that the effects of edge recession (wear) had no

influence on the forces as the tool was sharpened during regular intervals. Furthermore, the test runs were randomized to remove systematic test run error.

Work-piece parameters have also previously been used as predictors in statistical modelling to describe force trends. The more commonly used parameters are moisture content, grain direction and density, although coefficients have previously been determined to discretely quantify wood species[6]. It is generally accepted that tool forces decrease with increased work-piece moisture content. An exception to this rule is for frozen wood specimens[7]. Furthermore, cutting the wood end grain yields the largest cutting forces with the lowest cutting forces observed machining along the fibre direction. In general, higher tool forces are observed when cutting wood species of greater density [6, 7]. Eyma et al [63] concluded that density alone acted as a poor work-piece parameter and that mechanical properties need to be utilised in order to develop more accurate cutting force relationships.

The analysis from this study shows that density is weighted as a much better categorical predictor across the grain compared to along the grain. This is by means of higher F and R^2 values across the grain (Fig. 7). The obtained strength properties (MOR, τ) and toughness (Ub, Us) are more consistent as categorical predictors. Coefficients were not calculated to represent the individual wood species tested. The logic behind this decision was to keep the regression models universal, i.e. independent of species. The cutting force can be predicted based upon the work-piece mechanical properties, density, and moisture content instead. This model proves that the intrinsic properties of the differing wood species have little influence on the cutting force when each species has been evaluated using a series of carefully obtained mechanical properties.

After using the R^2 and F (figure 3.17) values to determine the effects of each of the mechanical properties on cutting force, MOE was removed to re-predict the cutting force

across the grain. This did not improve the regression model, and it only reduced the R^2 value by 4%. Likewise, G and ρ were separately removed to re-predict two separate models. Also, G and ρ were removed simultaneously to re-predict an additional model. This once again did not improve the original R^2 value, but a decrease up to 1.4% was observed. These results confirm that the accuracy of cutting force prediction is not significantly influenced by MOE across the grain and G combined with ρ along the grain.

The predictive model across the grain has an R^2 value of 90% compared to 80% along the grain. The strength and toughness of the wood have consistently proven to be good predictors and the elastic properties have consistently proven to be poor predictors. Density is not consistent as it proves to be a good predictor along the grain and a poor predictor across the grain. The purpose of machining the radial wood plane was to engage the tool with approximately the same proportion of earlywood and latewood fibres. This was easily achieved across the grain as the tool path is perpendicular to the fibre direction. This was not so easily controlled along the grain. In most cases the radial grain pitch was larger than the 1 mm cutting edge making it extremely difficult to plan a tool path that engages the tool with both the less dense earlywood and denser latewood fibres. This leaves the author with three assumptions:

1. The tool passed through the earlywood fibres only
2. The tool passed through the latewood fibres only
3. The tool passed through a combination of both that cannot be confidently quantified

Regardless which of the assumptions is true, it explains why the density acts as a poor predictor along the grain resulting in a lower R^2 value for the respective model.

3.4.5 Regression Model Application

Dry Spruce was evaluated using the same three point bending and longitudinal shear methodologies. The obtained properties (table 3.17) were not used to develop either of the two regression models. Furthermore, controlled cutting tests were performed both along and across the wood grain at 0.8 mm depth of cut. The recorded cutting force values across and along the grain were 86.4 and 58.3N respectively.

The numerical regression models detailed for across (table 3.11) and along (table 3.14) the grain were used to return predictive cutting force values. These were calculated to be 64.1 and 45 N across and along the grain respectively. After superimposing these new observed and predicted cutting forces onto the regression plots (figure3.18), it became evident that the observed and predicted cutting values intersect within the 95% prediction intervals. This further proves that the regression models are species independent, i.e. only obtained properties are required to predict the cutting forces.

Table 3.17 – Recorded Mechanical Properties of Spruce

MOE (GPa)	MOR (MPa)	Ub (J/m^2)	G (MPa)	τ (MPa)	Us (J/m^2)	ρ (kg/m^3)	MC (%)	δ (mm)
6.83	62	25032	175	8.32	20122	627	7	0.8

3.5 Summary of Findings

1. The average thrust and side forces are measured to be only a fraction of the magnitude of the average cutting force. For this reason it was decided that no further analysis would be carried out on thrust and side force data collected. The major cutting force was the only quantified response evaluated during ANOVA and regression modelling.

2. The chip formation observed when machining along the grain can generally be described as an ongoing shearing process. The chips collected resembled the three main chip types as postulated by Franz. This indicates a similarity between the cutting mechanics for large orthogonal plaining tools and for the rip tooth used in these experiments. Moisture content and depth of cut were the major factors that influenced the observed chip types.
3. Optical microscope images of the work-piece surface formation machined across the grain shows that the wood fibres are subject to bending prior to failure with no evidence of shear taking place. Moisture content was the main factor that influenced the surface formation.
4. The wood shear properties (obtained through the longitudinal shear tests) exhibit the same trends as the major cutting force along the grain for the eight wood species evaluated. Likewise, the wood bending properties (obtained through the three point bending test) exhibit the same trends as the major cutting force across the grain for the eight wood species evaluated. This supports the findings from the microscope images of chip and surface formation that explicitly show evidence of shearing taking place along the grain and bending taking place across the grain.
5. The regression models prove that: i) the major cutting force for an orthogonal rip tooth can be predicted based upon obtained mechanical properties. ii) The intrinsic properties of wood species (of which there are many and difficult to evaluate) do not significantly influence the major cutting force as long as the wood work-piece has been thoroughly evaluated through mechanical testing. This also removes the need for calculated wood species coefficients. The recorded and predicted cutting force values for spruce (a species of wood not used to develop the model) fall within the 95%

prediction intervals of the models (figure 3.18). This further validates the significance of the models.

6. Results from ANOVA show that MOE carries little weight as a categorical predictor across the grain compared to the properties. By removing it from the model the R^2 is only reduced by 4% but the F statistic is increased by nearly 20. G and ρ carry little weight as categorical predictors along the grain and once removed from the model the R2 value only decreases by 1.4% but the F statistic increases by 23. This shows that although the fit of the model (R^2) is not improved the ratio of regression to residual variance (F) is improved.
7. The material strength (MOR and $\boldsymbol{\tau}$) and toughness (Ub and Us) carry the most weight as categorical predictors. Density (ρ) is weighted quiet highly for the predictive cutting force model across the grain however it carries little weight along the grain. It has been previously suggested in the discussion that this is due to the saw tooth failing to cut through the same proportion of both the earlywood and latewood fibres when machining along the grain. Machining across the grain the tooth is forced to machine through approximately the proportion of both the earlywood and latewood cells.

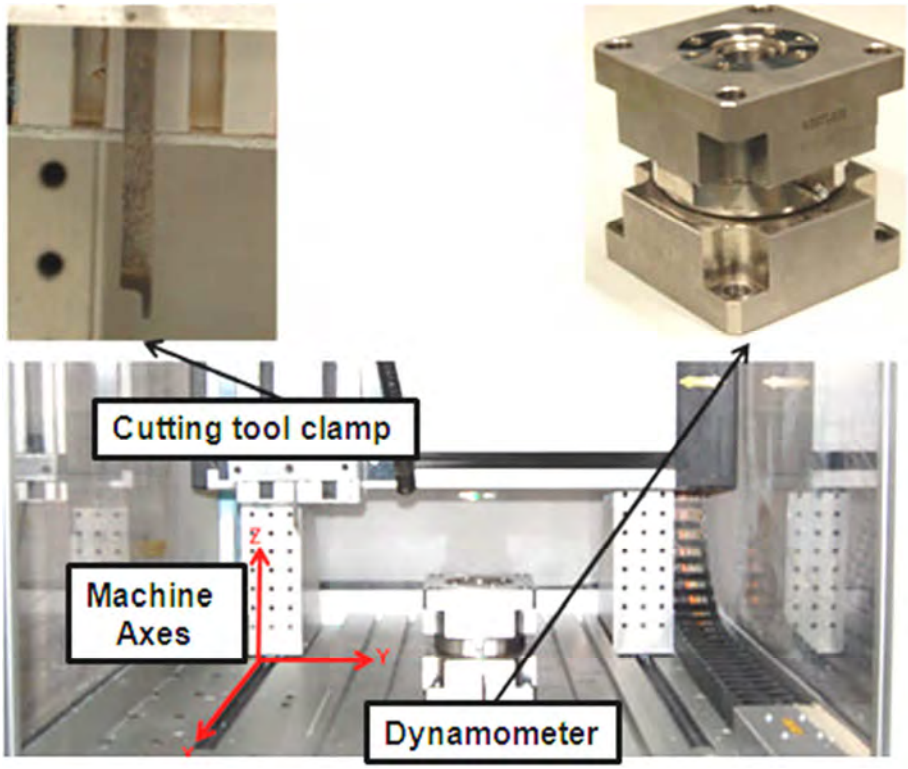

Figure 3.1 – Photograph of router machine test rig

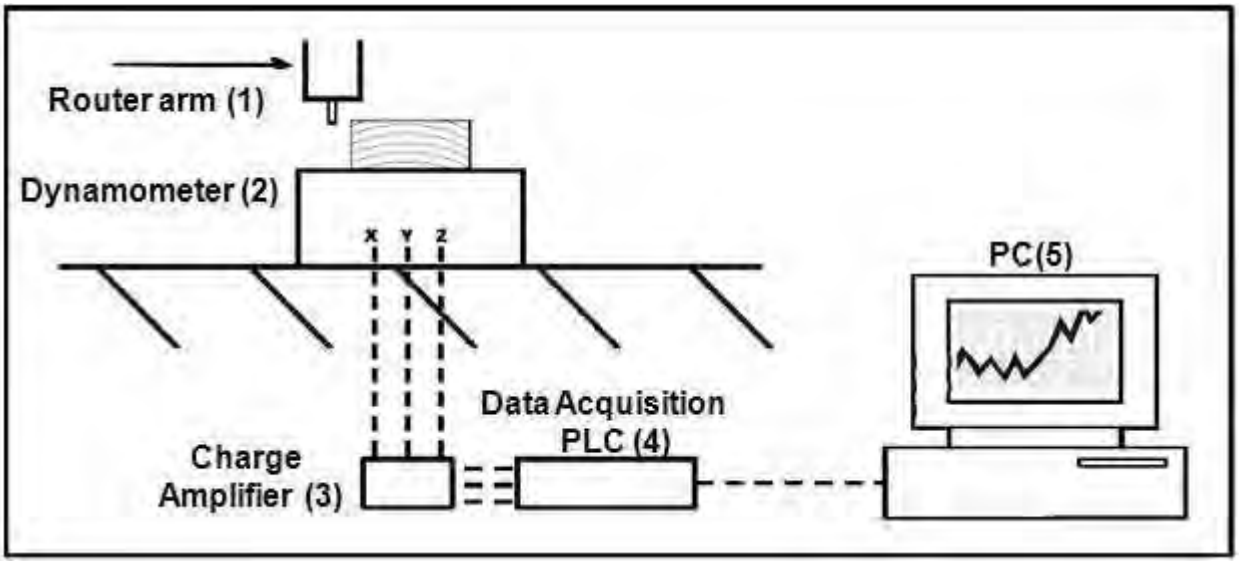

Figure 3.2 – Detailed test rig schematic diagram

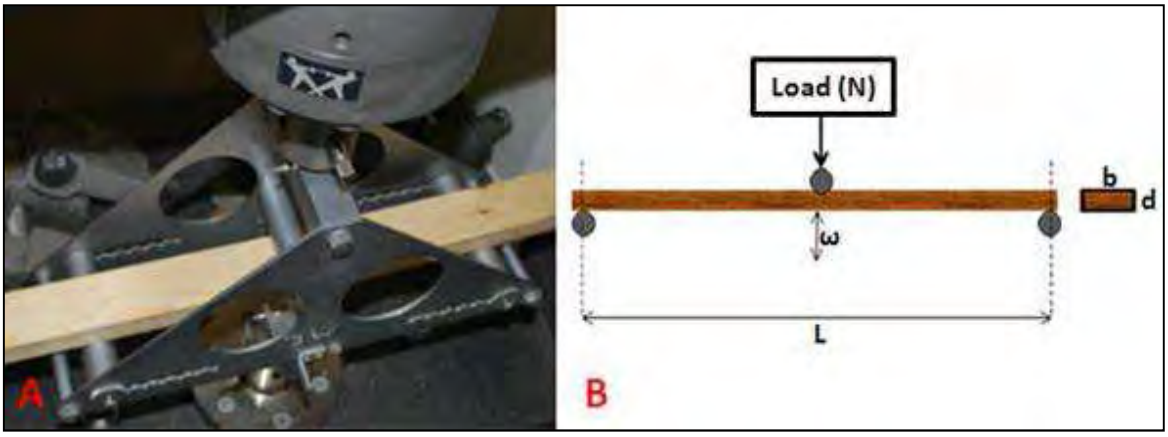

Figure 3.3 – A) Three point bending set up in universal testing machine. B) Schematic diagram

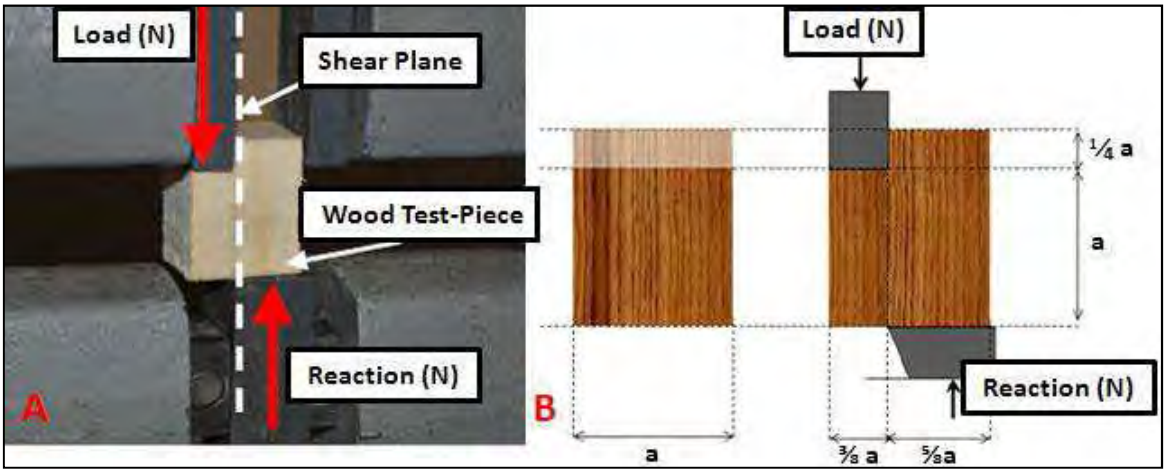

Figure 3.4 – A) Longitudinal shear set up in universal testing machine. B) Schematic diagram

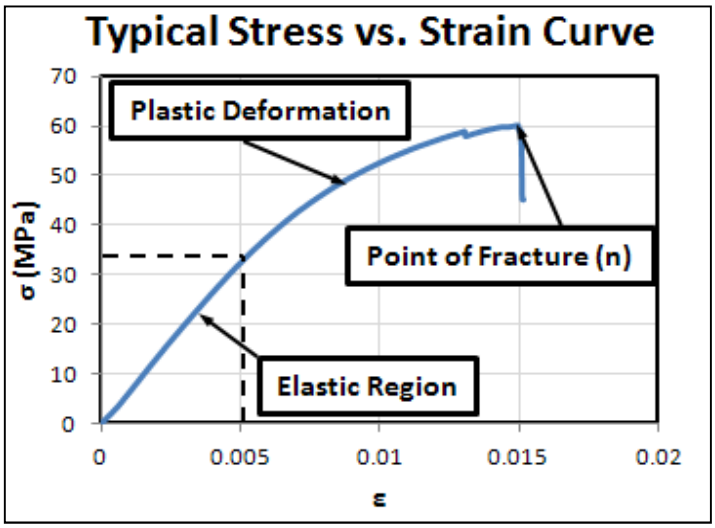

Figure 3.5 – Deformation zones on a typical stress vs. strain curve generated from the universal testing machine

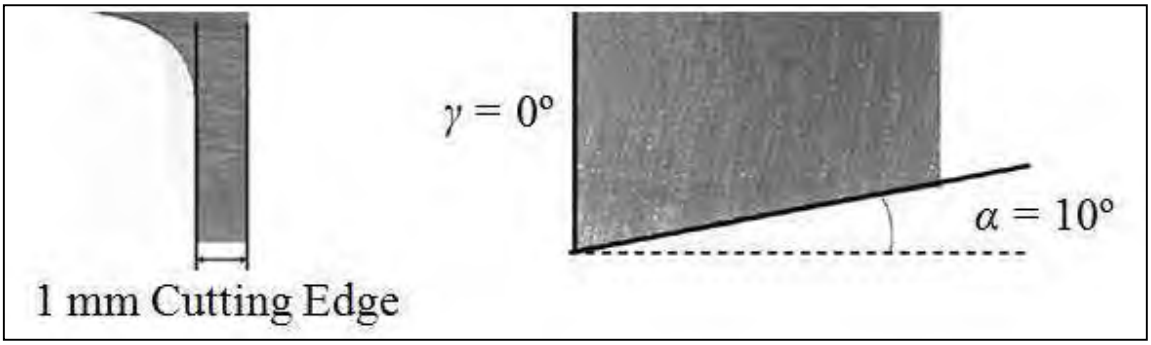

Figure 3.6 – Cutting tool geometry (Rip tooth)

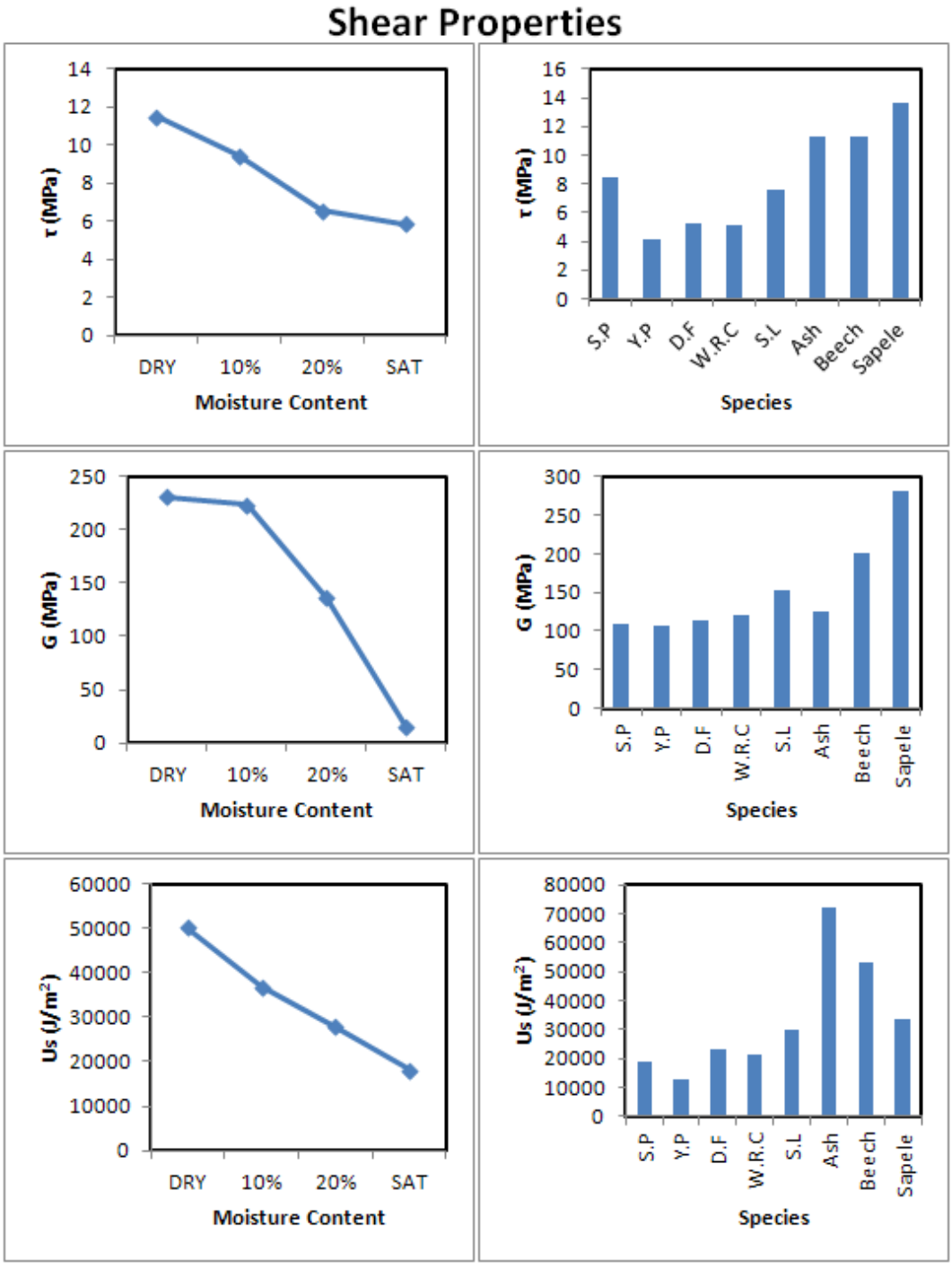

Figure 3.7 – Average shear plots

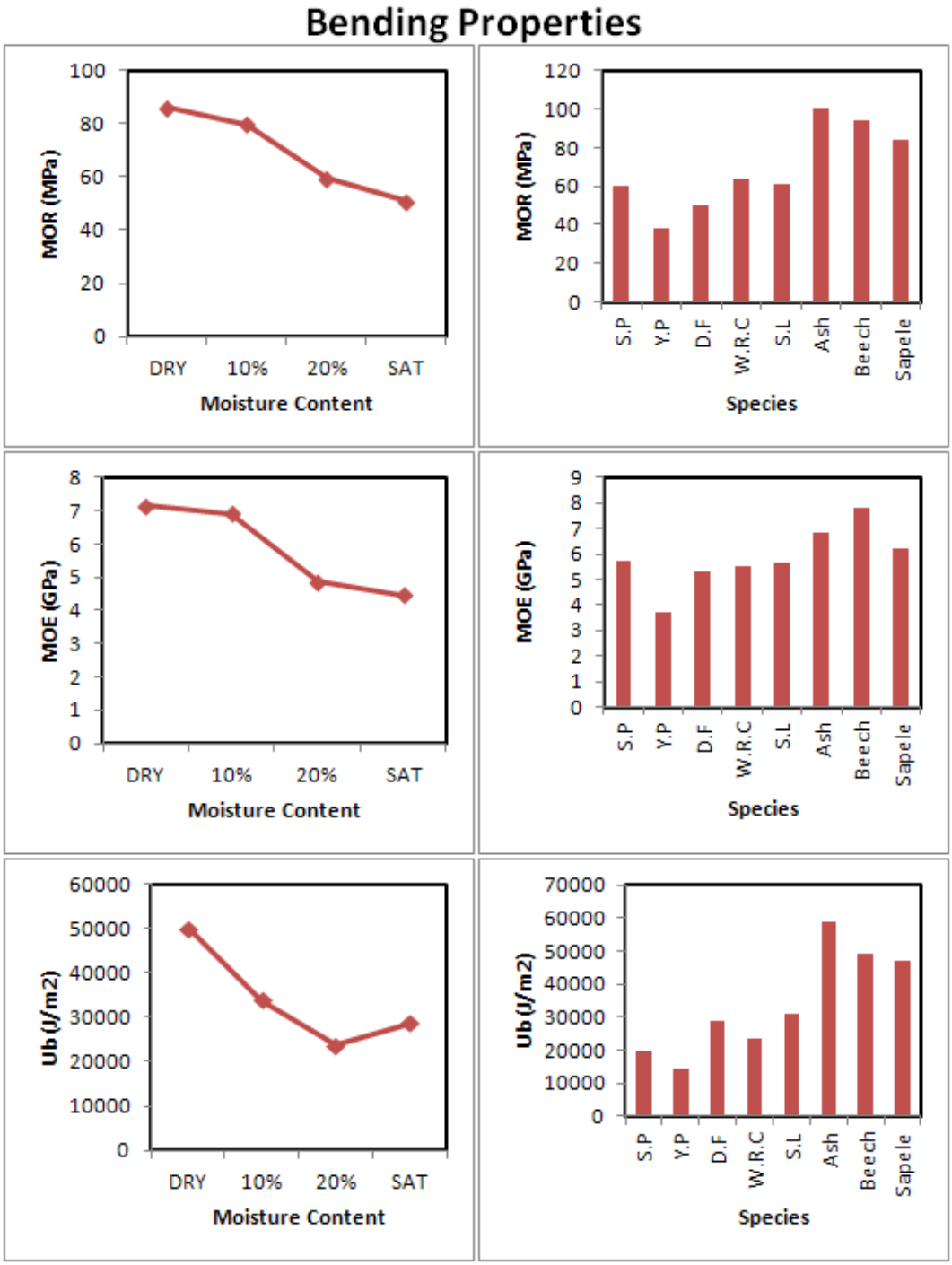

Figure 3.8 – Average bending plots

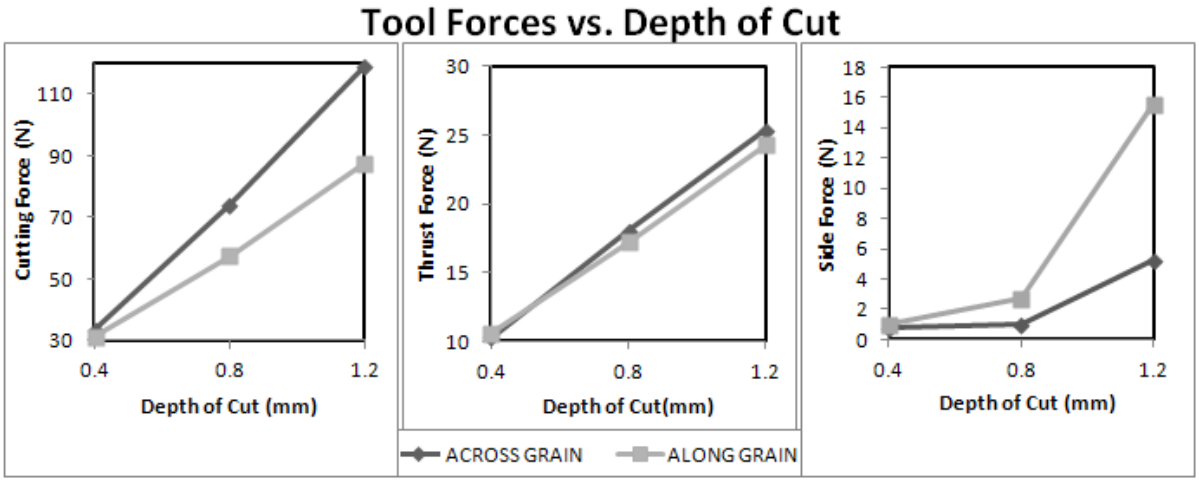

Figure 3.9 – Average tool forces with respect to depth of cut

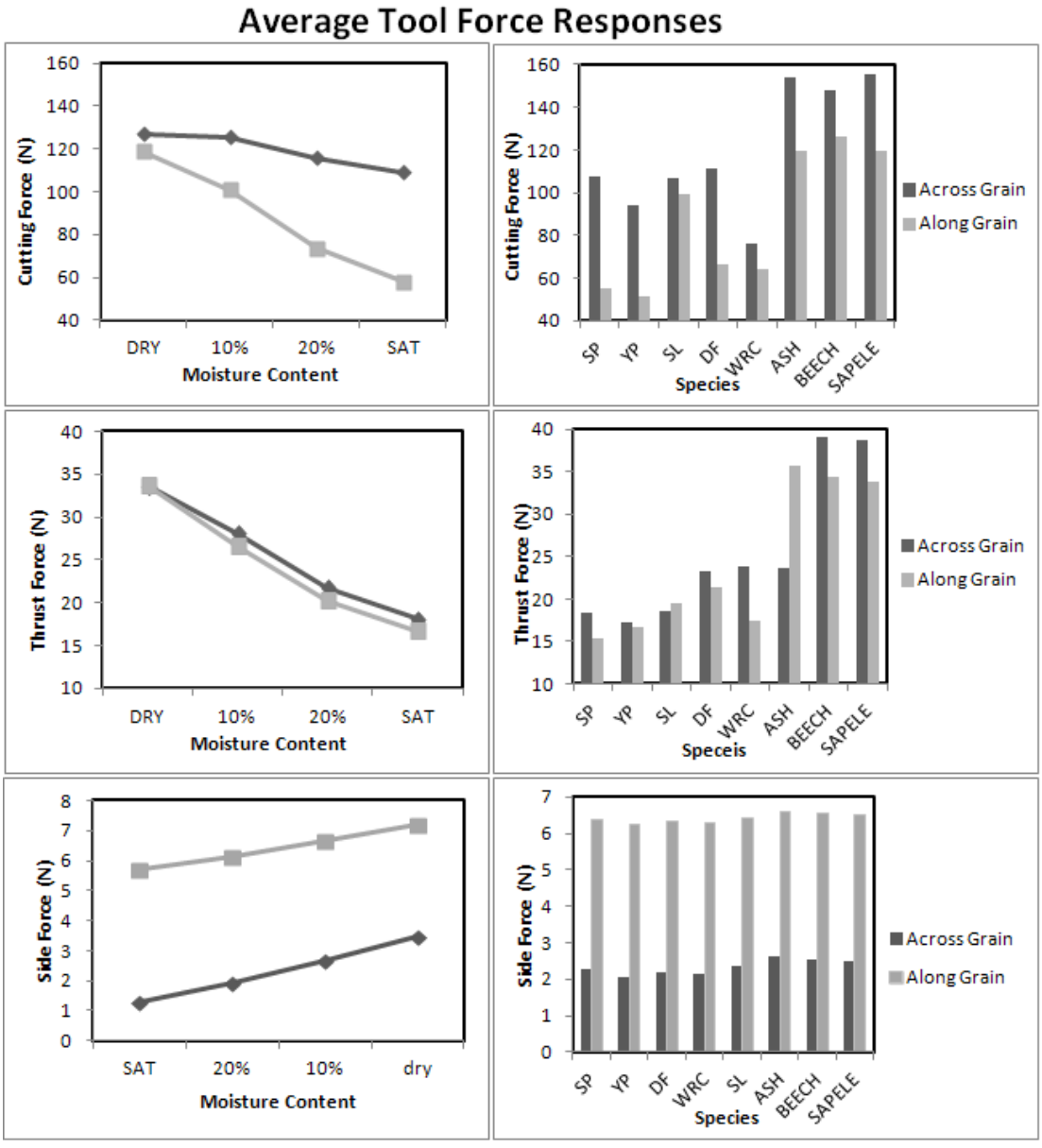

Figure 3.10 – Average tool force response plots

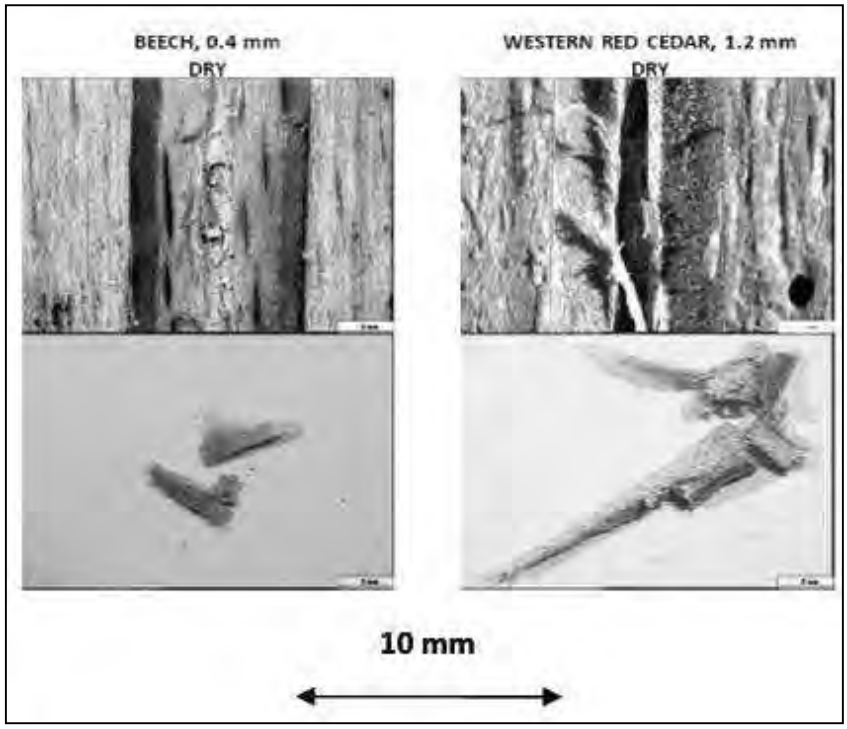

Figure 3.11 – Discontinuous (broken) chips

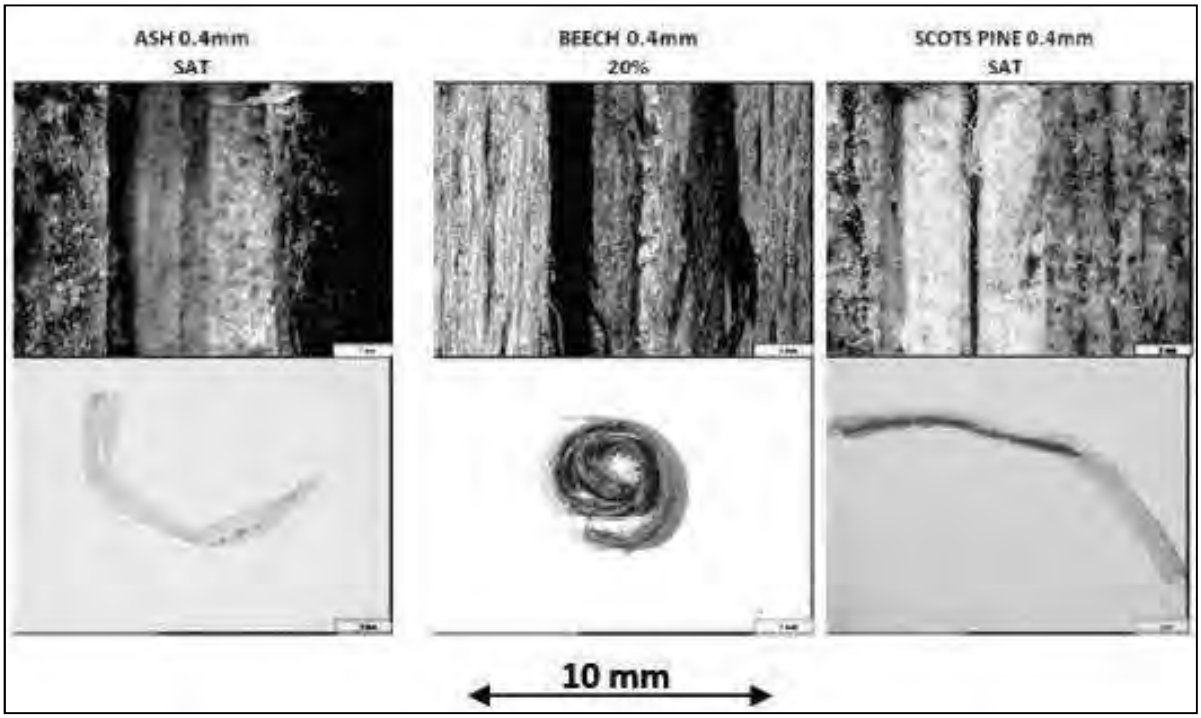

Figure 3.12 – Continuous chips

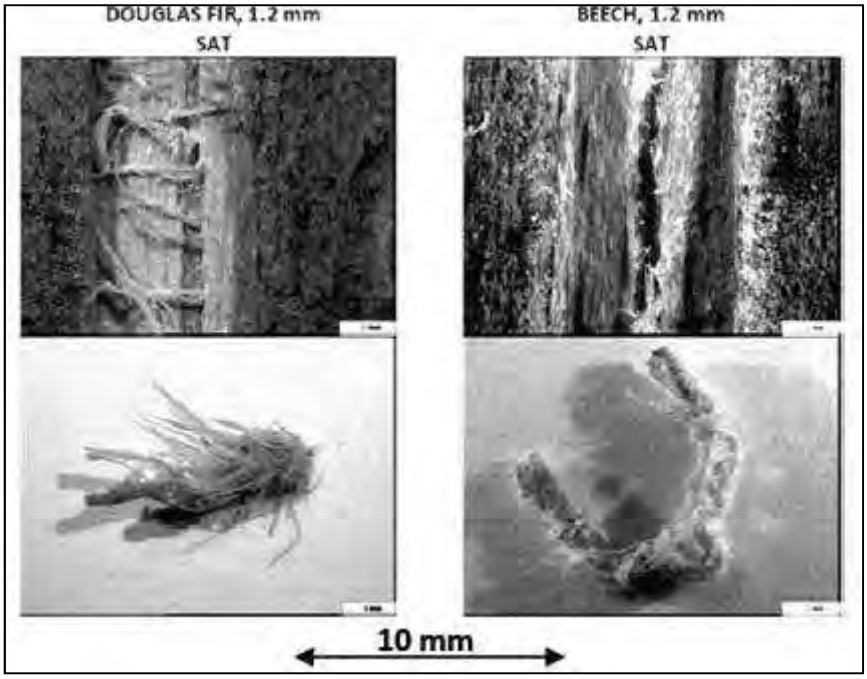

Figure 3.13 – Fuzzy chips

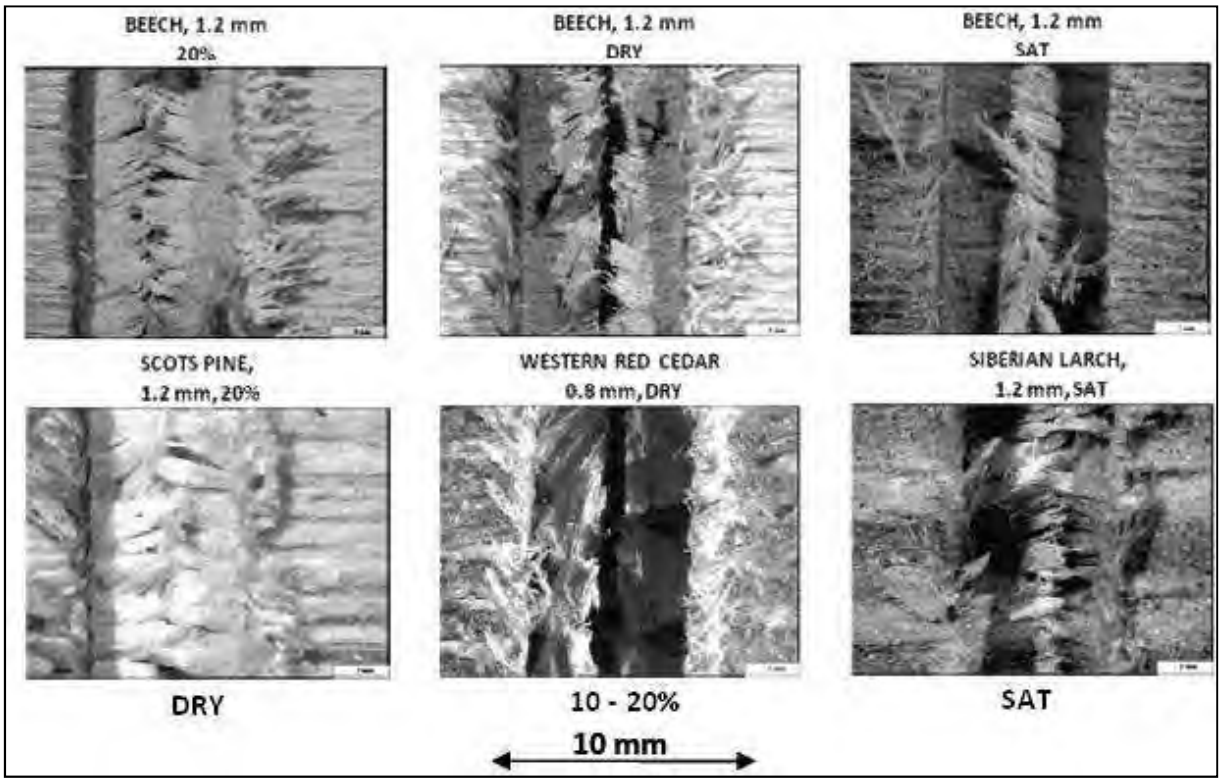

Figure 3.14 – Surface formation across grain

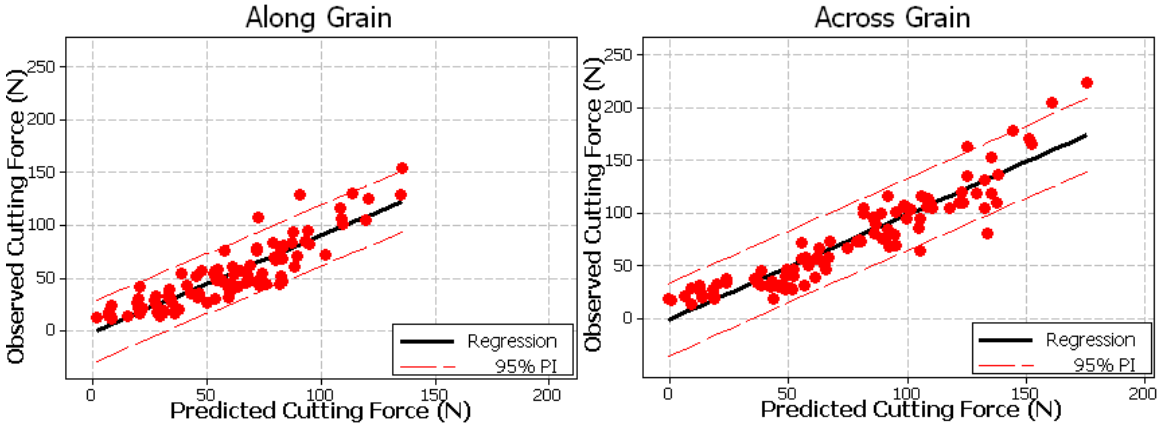

Figure 3.15 – Regression plots for cutting along and across the wood grain

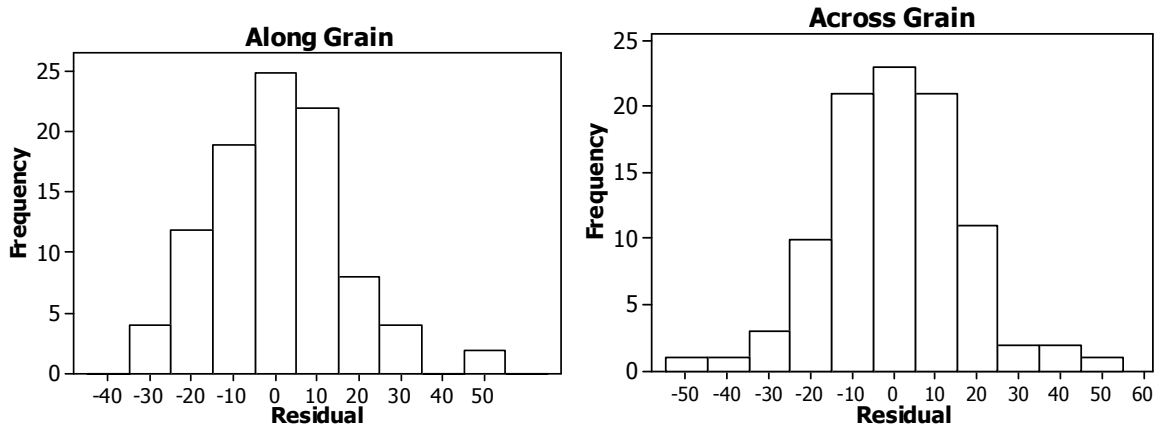

Figure 3.16 – Residual histogram plots of predictive models for cutting along and across the wood grain

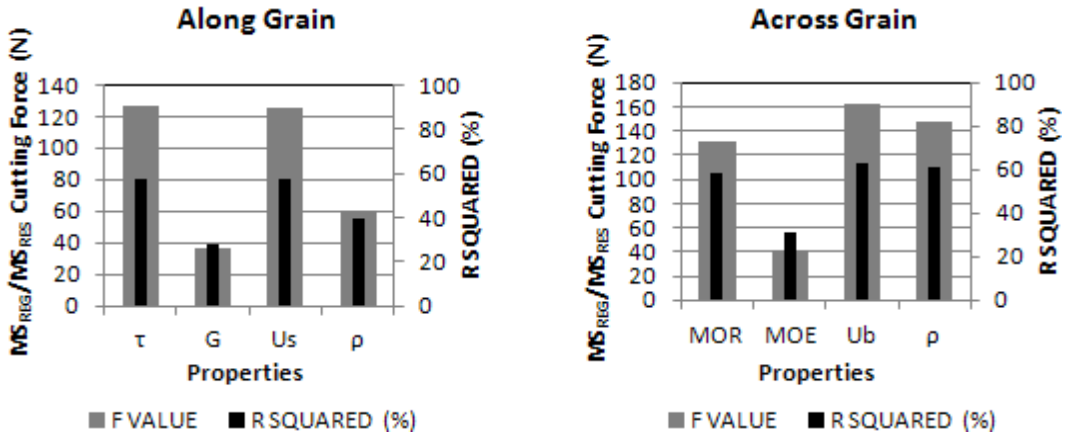

Figure 3.17 – Significance of the work-piece properties by means of simple least squares

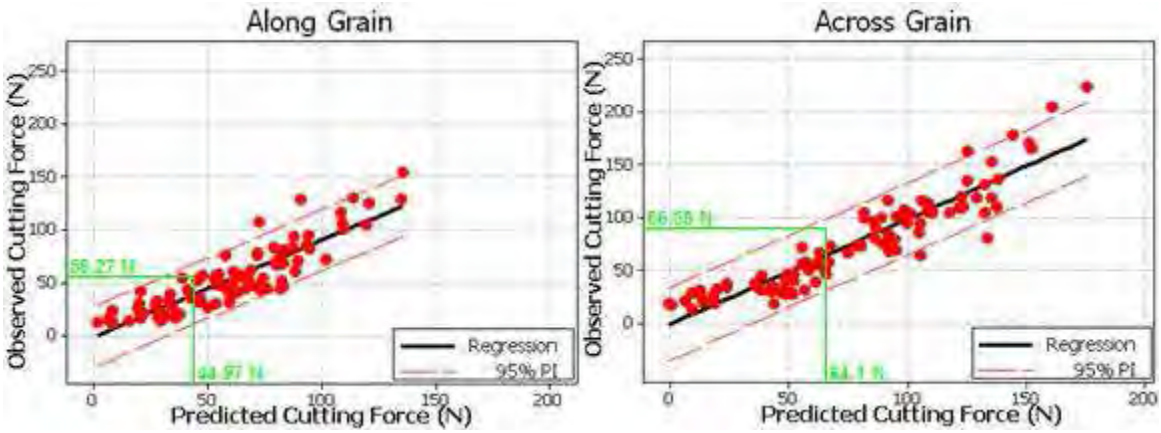

Figure 3.18 – Observed and predicted cutting force values for a random work-piece superimposed onto the existing regression models

CHAPTER 4
INFLUENCE OF TOOTH GEOMETRY FACTORS ON THE CUTTING MECHANICS

4.1 Introduction

The previous chapter details the findings of experimental work where a simple, orthogonal, rip tooth geometry was used. The purpose of this was to thoroughly investigate the effect of the varied work-piece properties on the cutting mechanics (recorded tool forces and chip formation) whilst limiting the tool geometry parameters. This chapter does the opposite; the work-piece parameters were limited whilst investigating the effects of varied tool geometry parameters. In general there are typically three types of handsaw tooth geometry:

1. Rip teeth – Have orthogonal cutting edges and un-bevelled rake and flank faces.
2. Bevelled teeth – Have bevelled rake and flank faces.
3. Compound teeth – Have bevelled rake and flank faces plus additional bevelled faces.

These different types of teeth are used to machine wood in different directions with respect to the grain (according to manufacturing product specifications, appendix 2).

- The un-bevelled (rip) teeth are used to remove material along the grain.
- The bevelled teeth are used to sever fibres across to the grain.
- The compound teeth are used to machine wood both along and across the grain.

The aim of this experimental research was to investigate the influence of specific geometric features of the three different saw teeth on the cutting mechanics. This aim was facilitated by

measuring the forces acting on the tooth and recording the chip formation using a high speed camera. These methods are elaborated upon further in this chapter.

4.2 Methodology

4.2.1 Selected teeth

Three tooth geometries were selected from Bahco™ handsaws (figure 4.1). The nominal blade thickness for all three geometries was 0.85 mm:

1. U0º – An un-bevelled (rip) tooth with an orthogonal cutting edge. This tooth has a negative rake angle (γ) of 13º and a flank angle (α) of 51º (figure 4.2).
2. U28º– A tooth with a bevelled rake and flank faces of 28º. This tooth has a negative rake angle of 15º and a flank angle of 48º (figure 4.3).
3. GT– A compound tooth with an additional bevelled face along with the 28º rake and flank faces. This tooth has a negative rake angle of 10º and a flank angle of 23º (figures 4.4).

The orientation of the cutting edge to the vertical differs between the three geometries. This is caused by the different grinding processes that provide the different bevel orientations. The U0° tooth has an orthogonal edge that subtends the vertical at 90º. The U28º has a 28º oblique rake face with a major edge that subtends the vertical at 60º. The GT tooth also has a 28 oblique rake face; the major edge subtends the vertical at 70º.

4.2.2 Average Depth per Tooth through Entire Saw Evaluation (appendix 8)

A series of manual tests were performed by ten experienced handsaw users. The average depth of cut per tooth and cutting velocity for saws containing the three selected tooth geometries were both determined. Only one species of wood (spruce) with cross sectional dimension of 50mm x 50mm was selected. This wood was acquired pre-seasoned from the supplier with a measured moisture content of 12%. Sawing was performed only across the wood grain. Each experienced user was instructed to saw to a marked depth of 45 mm using each of the three saws. Each blade was marked with ink. The length of the blade (***l***) where the ink was removed during cutting was used to indicate the average stroke length.

In addition to this a reciprocating test rig applying a vertical load of 58N to each saw was used to provide comparable values for depth of cut per tooth. An effective controlled stroke length (***l***) of 105 mm was used for each cutting test. This test was performed on only the U28° and GT saws.

The total number of strokes performed (***N***) and total time taken (***t***) to complete the 45 mm cut were recorded for both the manual and controlled tests. As the tooth pitch was known (7 teeth per 25.4 mm) the total number of teeth (***T***) used to perform the 45 mm cut was determined (equation 4.1):

$$\mathrm{T} = \frac{7(l \times \mathrm{N})}{25.4} \tag{4.1}$$

This was then used to calculate the average depth per tooth (equation 4.2):

$$\delta = \frac{45}{\mathrm{T}} \tag{4.2}$$

The average cutting speed was also determined using the data (equation 4.3):

$$Vc = \frac{l \times N}{t} \quad (4.3)$$

Table 4.1 – Average depth per tooth and cutting speed for entire saw

	Average Depth Per Tooth (mm)		Average Cutting Velocity (mm/s)	
Saw Used	**Manual Test Results**	**Controlled Test Results**	**Manual Test Results**	**Controlled Test Results**
U0°	0.08	-	473.5	-
U28°	0.11	0.11	524.1	924.5
GT	0.14	0.1	675.3	943.1

4.2.3 Apparatus and Error Evaluation (appendix 9)

4.2.3.1 Single Tooth Test-rig

A conventional shaper machine (figure 4.5) was procured to perform a linear cutting action using selected handsaw teeth. This consisted of a reciprocating arm driven by a 0.75 horsepower (660 Watt) motor. The main benefit of using the shaper over the router machine was greater machine stiffness which allowed for continuous, accurate, but most importantly, lower depths of cut to be achieved. The shaper performed the cutting action on the forward stroke of the cycle. The wooden work-piece was fed into the direction of cut at small even increments to ensure each stroke provided the same depth of cut per tooth.

4.2.3.1.1 Kinematics

Displacement plots were taken at regular intervals from a high speed video of the shaper arm. Referring to the displacement vs. time plot, for an entire stroke cycle, the velocity of the shaper arm was determined. During the first 20 mm of the forward stroke the shaper arm was accelerating. Likewise during the last 30 mm of the forward stroke the shaper arm was decelerating. The velocity in the remaining 120 mm was linear and was calculated to be 300 mm/s. This value is approximately 45% lower than the speeds observed during manual cutting, however previous research [67, 69] and controlled testing (appendix 4) finds that

cutting speed has no significant influence on the cutting forces (Fv). No machining was performed on the return stroke, however the velocity calculated in this linear region was 475 mm/s.

4.2.3.1.2 Vertical Stiffness

The stiffness set up determined the vertical stiffness of the shaper arm and hence its ability to maintain an accurate low depth of cut. The feed mechanism of the shaper gradually forced the rigid fixture into the tool holder; the resultant force was measured through the z axis channel of the dynamometer. A displacement dial gauge was positioned at the location where the single tooth performed the cutting action. Force readings were taken at every 0.05 mm increment of displacement. To prevent damage to the shaper arm the last reading was taken below 1 kN. As the force vs. displacement plot is linear the final readings were used to calculate the stiffness. The maximum Force and Displacement were 952 N and 0.00035 m respectively. These values were used to calculate the vertical stiffness of 2.72 MNm^{-1}.

4.2.3.2 Tool holder

The tool holder accommodated a group of set teeth inclined to assure that each tooth machined the same depth of cut. The group of teeth machined a groove parallel to the shaper arm allowing a subsequent single tooth to machine at a constant depth of cut. The depth of the single tooth was set using a feeler (thickness) gauge at the same thickness of the desired depth of cut. This measurement was taken as an offset from the last tooth from the group of teeth. The teeth were set using the raker pattern (L R N N L R N N). The final two teeth of the group were neutral, unset teeth. The following single tooth was also unset and of the same bevel orientation as the final tooth of the group.

A minimum of eight teeth were used to machine the grove. The left and right set teeth were offset from the blade at a nominal width of 0.3 mm to provide sufficient side clearance for the single tooth.

4.2.3.2.1 Control of Depth

Analysis of data from a series of manual handsaw tests (section 4.2.2) showed that the average depth of cut per tooth was in the range of 0.08 – 1.4 mm. The un-bevelled (U0°) teeth cut at the lowest depth in the range, the bevelled (U28°) cut at middle of the range and the compound teeth (GT) cut at the higher end of the range. Two depths were selected to determine the accuracy of the feeler gauge method; 0.05 mm and 0.1 mm.

In order to gauge the accuracy of the feeler gauge technique for controlling a depth of cut the tool set-up was used to machine through a homogenous work-piece (Obomodulan^{TM}) so that the bite profiles could be examined under an optical microscope. Two cuts in total were taken; the first provided the datum position for the measurement. The following cut was performed with the applied depth using the feeler gauge. The measurements using the optical microscope approximately matched the depths of cut applied using the feeler gauges.

4.2.3.2.2 Work-piece width

In order to assess the effect of work-piece width on tool forces a simple test was devised. This consisted of cutting two common timber widths, 25 mm and 50 mm both along and across the grain. A depth of 0.2 mm was used for dry Douglas fir only.

The mean tool forces measured do not vary significantly between the 25 mm and 50 mm widths. At this stage the decision was made to carry out all further controlled tests using the narrower 25 mm work-piece widths. This conforms to the space between the group and single tooth on the tool holder, allowing the tool force recordings to be distinguishable on the same shaper arm stroke.

4.2.3.3Force Measurement Instrumentation

The simplified test rig schematic (figure 4.6) shows the basics of how the tool forces were measured. The cutting tool (1) passed through the work-piece clamped to the dynamometer. The dynamometer platform fed into the cutting tool in even increments for each stroke (2). The forces applied to the work-piece stimulated a charge output from the transducers which then channelled through to the charge amplifiers (3). These amplified values were converted from analogue to digital (4) and finally were recorded on the PC (5). To elaborate, the dynamometer consisted of three piezoelectric transducers measuring forces in the x, y and z directions. The x and y axes transducers had a sensitivity of 7.5 pC/N and could measure up to 5 kN of force. The z axis had a sensitivity of 3.7 pC/N and could measure up to 10 kN of force. The signal output from each transducer was channelled into an analogue charge amplifier (one amplifier per transducer). The input sensitivity was calibrated to match the transducer sensitivity (in pC) and the output range was set to 100 N = 1 V up to a maximum output of 10 V (1 kN). The output from the charge amplifier was then sent to a data acquisition PLC, converting the analogue signal to digital allowing the forces to be recorded on a PC using LabView signal express.

4.2.3.3.1 Calibration

To verify that the data acquisition set up was accurately measuring the forces; loads were applied to each axis using a universal testing machine. This was performed within the loaded range of 1 – 5 kN measuring not only the force in the direction of the load but also the cross interference in the other two directions. The measurement of the forces started to lose accuracy beyond the 2 kN region, at the same point cross interference in the other two measured directions became more prominent. This was not seen as significant cause for concern, as all of the recorded forces for single tooth tests fell below 1 kN.

4.2.3.4 High Speed Camera Set-up

A high speed video camera was acquired to record footage at the tool work-piece interface. The camera was set up to record 1000 frames per second using a macro lens to capture chip formation at the macroscopic level. All test runs in the experimental design were recorded using this method. When recording the chip formation of a group of teeth the camera lens had to be tilted at a downward angle allowing it to view the longitudinal work-piece plane. Unlike the tool forces experiment, the interaction between the tooth and the work-piece had to be visible at all times. This meant that a group of teeth could not be passed through the work-piece before the single tooth. This difficulty was resolved by using a small inclined group of four unset teeth. The first tooth would perform little to no cutting action before each of the following three subsequent teeth passed through the work-piece. This allowed for a constant depth per tooth visible to the high speed camera. A 0.15 mm depth of cut was achieved by inclining the teeth by 3° (based on a uniform tooth pitch of 7 teeth per 25 mm). Typically the first tooth would perform little to no cutting with the second tooth performing the first cut. Subsequently the third and fourth teeth would each machine at a depth of 0.15 mm visible to the camera.

4.2.4 Experimental Design

4.2.4.1 For tool forces

A total of eight depths of cut were performed by the each single saw tooth; 0, 0.05, 0.1, 0.15, 0.2, 0.25, 0.3, 0.35, mm. The lowest four depths of cut were taken to represent the depth per tooth observed during manual sawing. The higher five depths of cut were taken to build an accurate trend of cutting force vs. depth of cut. The set, inclined group of teeth was first used to machine a groove parallel to the path of the shaper arm with adequate side clearance. Each tooth in the group machined at a depth of approximately 0.15 mm. For U0°, the final group tooth was unset to match the single tooth (figure 4.7). For the two bevelled geometries (U28°,

GT) the final group tooth was also unset and of the same bevel orientation as the single tooth (figure 4.8). All depths of cut for the single tooth were set using the feeler (thickness) gauges, providing the required vertical distance between the last tooth from the group and the adjustable single tooth.

Only one wood species (douglas fir) was used in this experiment. This was selected for its uniform grain pitch and low knot content. Four work-piece variations were used in the experimental design comprising of the two machining directions; along (90°-0°) and across (0°-90°) the grain, and two moisture contents; DRY (≈6%) and SATURATED (>30%). Each test run was performed 50 times to obtain statistically valid average tool forces (appendix 10).

4.2.4.2 For Chip Formation

High speed video footage was obtained for 12 cutting scenarios: using the U0°, U28° and GT teeth machining DRY and SATURATED douglas fir both along and across the grain. The unset, inclined group of teeth could only perform a single depth per tooth (approximately 0.15 mm) compared to the multiple depths performed for the tool force experiment. The chip and work-piece surface were both observed under the optical microscope to provide complimentary analysis to the high speed video.

4.3 Results

4.3.1 Tool Force Trends

4.3.1.1 Cutting Force (Fc)

The cutting force values wear measured to be significantly larger than both the thrust and side forces (figure 4.9). The values obtained for the U0° tooth geometry wear the largest ranging from 10 – 70 N for the increasing depths of cut. The trend for the recorded cutting force vs. depth of cut is linear for the U0° tooth geometry. The U28° tooth geometry exhibits a non-

linear trend for cutting force vs. depth of cut with values ranging from 5 – 25 N for increasing depths of cut. The GT tooth geometry also exhibits a non-linear trend for cutting force vs. depth of cut with values ranging from 5 – 50 N for increasing depths of cut. When evaluating the cutting force trends for specific work-piece conditions it is noticed that the trend is the same for each tooth geometry regardless of grain direction or moisture content. Only the magnitude of the forces was affected by grain direction. Generally the highest forces wear observed for dry work-pieces across the grain, however for U0° and U28° at 0 – 0.1 mm depth of cut saturated work-pieces across the grain yielded the highest forces. Dry work-pieces along the grain yielded lower forces with the lowest cutting forces yielded for saturated work-pieces along the grain.

As the trends for all three tooth geometries are the same, it was possible to determine work-piece coefficients for each work-piece variation. This was achieved in four steps (figure 4.10):

1. A column average was taken at each depth of cut from the empirical cutting force tables for each tooth geometry.
2. An augmented results table for each tooth was generated. This was done by dividing each empirical cutting force value by the column average.
3. A row average was taken from each row of the augmented table. This gave work-piece coefficients specific to each tooth geometry.
4. The row averages from the augmented tables for U0°, U28° and GT were aggregated providing general work-piece coefficients.

The work-piece coefficients were able to bring the magnitudes of each work-piece variation into the same approximate range (figure 4.11).

4.3.1.2 Thrust Force (Fp)

The recorded mean thrust force values exhibited the same trends as the cutting forces for all tooth geometries. For the U0° tooth the values wear approximately 12% the magnitude of the cutting forces, 10% for U28° tooth and 11% for GT tooth. There was very little difference between the thrust forces obtained along and across the grain. The values along the grain wear marginally (approximately 10%) smaller than across the grain for all three tooth geometries.

4.3.1.3 Side Force (Fr)

Once again, the side force values exhibited the same trends as the cutting forces for all tooth geometries. For the U0° tooth the values wear approximately 2% the magnitude of the cutting forces, 1.3% for U28° tooth and 1.6% for GT tooth. The side force values along the grain wear noticeably larger (approximately double) than across the grain. The difference between the values became more prominent with increasing depth of cut, particularly for the U0° tooth geometry.

4.3.2 Chip formation

4.3.2.1 Dry along the grain

From the high speed video it was evident that all three geometries yielded continuous chip formations for each tooth that made contact with the work-piece. Optical microscope images of the surface formation exhibited uniform, cleanly machined kerfs. This was complimented by the collected chip formation which was also uniform.

An important difference to make note of is the orientation of the chip formation with respect to the cutting edge. As the U0° formation is un-bevelled, the chip was formed parallel to the rest of the blade and is hence was forced into the gullet in tightly coiled spirals (figure 4.12). This did not occur for U28° (figure 4.13) and GT (figure 4.14) primarily due to the bevelled

rake face. The chip was formed instead parallel to the 28 bevel angle, with no interaction with the gullet observed.

4.3.2.2 Saturated Along the Grain

In general fuzzy chip formation was observed for all three tooth geometries evaluated. The wood fibres disintegrated when cut from the surface of the work-piece. It is evident from the high speed video that the chips did not form ahead of the tooth contrary to the observed footage for the dry work-pieces. The chips instead collapse in the opposite direction to the tool path. The collected chip formation observed under the microscope exhibits how the wood fibres disentangled. To further support this microscope images of the surface formation shows the corresponding disentangled fibres that were left behind in the kerf, indicators of the chip break-off points. There is little variation between the three tooth geometries in the chip types formed (figures 4.15 – 4.17).

4.3.2.3 Dry across the grain

In the frame by frame analysis of the U0° geometry (figure 4.18) the initial three frames show how the wood fibres deformed perpendicular to the grain, eventually failing in the fourth frame. The corresponding optical microscope image of the surface formation exhibits a very coarsely cut kerf. No material removal occurred during this process; the fibres were simply fractured and displaced.

For the U28° (figure 4.19) and GT (figure 4.20) formations the prolonged period of deformation observed perpendicular to the grain is not seen in the footage. The frame by frame analysis shows that cutting with these types of bevelled tooth is a much less aggressive procedure. This is supported by the surface formation microscope images which exhibit a much more cleanly cut kerf.

4.3.2.4 Saturated across the grain

Evidence of material removal was seen in the high speed footage for all geometries, contrary to the machined dry work-pieces across the grain. For instance, the optical microscope image of the surface formation showed sections of the kerf were the fibres have been completely uprooted (figure 4.21). It was apparent from the corresponding frame by frame analysis that these fibres were initially deformed in a similar way to the dry work-piece, however, as the fibres sprung back towards the tool path they were subsequently removed from the surface. It must be noted that the tooth that initially made contact with these fibres was only performing a ploughing action; the uprooting effect was caused by teeth that followed.

The high speed footage of the U28° (figure 4.22) geometry showed a tooth removing material in what appeared to be a similar fashion to the observed footage of chip along the grain. This only occurred for one tooth and the corresponding surface formation image did not provide conclusive evidence of continuous chip formation across the grain. It was evident from the high speed video that the GT (figure 4.23) geometry produced a very small amount of wood particles. The observed surface formation is comparable to that of the U28° geometry.

4.3.2.5 Chip Ratios

It was possible to the determine chip ratio and shear plane angle for the continuous chip types formed machining dry work-pieces along the grain. However, it was not possible to determine chip ratio and shear plane angle for the saturated work-pieces (figures 4.24 – 4.26). This is due to disintegration of the wood fibres after the tooth has liberated the chip from the work-piece surface.

The method of determining the chip ratio used was similar to that used in fundamental metal cutting research [3, 4] where:

$\mathbf{t_c}$ – Measured Chip Thickness (mm)

$\boldsymbol{\alpha}$ - Rake Angle

$\mathbf{t_u}$ - Un-deformed Chip Thickness = Depth of cut (mm)

$\mathbf{r_c}$ - Chip Ratio = $\mathbf{t_u/t_c}$

$\boldsymbol{\varphi}$ - Shear Plane Angle = arctan[($\mathbf{r_c}$ cos $\boldsymbol{\alpha}$) /(1 - $\mathbf{r_c}$ sin $\boldsymbol{\alpha}$)]

From the optical microscope images the chip thickness was measured at the inflection point of the helix. This was to ensure that the chip thickness was being measured and not the chip width. This proved difficult for the U28° geometry as the thickness and width were similar, so arbitrary points of chip thickness were measured. The U0° tooth geometry yielded $\mathbf{r_c}$ = 0.815 and $\boldsymbol{\varphi}$ = 34.7°, U28° yielded $\mathbf{r_c}$ = 0.882 and $\boldsymbol{\varphi}$ = 34.75° and GT yielded $\mathbf{r_c}$ = 0.857 and $\boldsymbol{\varphi}$ = 34.12°.

4.3.3 Parameters and Regression Models

4.3.3.1 Defined Parameters

The parameters were defined to develop the categorical predictors for the regression model. Five of the parameters used were geometric measurements taken from the three teeth:

- Rake angle, γ (°)
- Flank angle, α (°)
- Wedge angle, β (°) – Also called the sharpness angle. This is calculated as 90° minus both the rake and flank angles.
- Bevel angle, λ (°)
- Edge inclination angle, *k* (°)

Another five of the parameters used were based upon the interaction between the tooth and the work-piece. The CAD drawings (figures 4.27 – 4.28) show this interaction between the single tooth and the work-piece after a groove has been machined by the prior group of teeth.

- Depth of cut, δ (mm)
- Cutting area, A (mm^2) – Defined as the area enclosed between the tooth and the un-deformed work-piece (diametric view)
- Major edge contact length, L (mm) – The length of contact between the major cutting edge and the work-piece during cutting.
- Lateral contact length, L' (mm) – The length of contact between the lateral cutting edge and the work-piece during cutting.
- Cut perimeter, P (mm) – Defined as the sum of the major and lateral contact lengths.

Other parameters not directly related to the tool geometry or interaction with the work-piece:

- Work-piece coefficient, *WPC*

4.3.3.2 Average response plots and Analysis of Variance

The parameters used as categorical predictors in the regression models were evaluated by means of average response plots and analysis of variance. The tool geometry parameters (figure 4.29) work-piece coefficient (figure 4.30) and tool/work-piece interaction parameters (figure 31) were all evaluated in this way.

Only two tool geometry parameters were deemed appropriate as predictors for regression modelling:

1. The Bevel Angle (°) – The un-bevelled tooth (U0°) yielded double the average cutting force response than the two geometries that have a 28° rake face (U28° and GT). The

relationship has an R^2 value of 100% although this was inevitable as it was a straight line between two data points.

2. The Edge Inclination Angle (°) – The average cutting force response has an increasing linear trend with respect to the edge inclination angle. The relationship has an R^2 value of 99%.

The other geometric parameters do not have any distinctive trend with respect to the average cutting force response. There is only a small range in rake angles for the three geometries evaluate (5°). This is too small to influence the overall cutting forces and the lack of any distinctive trend deems this parameter to be insignificant. Cutting forces were only measured during the forward stroke; hence no interaction occurred with the rear of tooth. The null hypothesis that the Flank and Wedge angles do not have any significant effect on the cutting forces is confirmed by the lack of any distinctive trend with respect to the average cutting force response.

The work-piece coefficient has a linear trend with respect to the average cutting force response. This relationship is quantified by an R^2 of 99%. It must be remembered that the work-piece coefficient was originally determined through aggregation of the empirical cutting force data; hence it stands to reason that it has a near perfect fit with the average cutting force response.

Table 4.2 – Bevel Angle vs. Average Cutting Force Response

Bevel Angle - Analysis of Variance

Source	DF	SS	MS	F	P	R^2
Regression	1	161.82005	161.82005	∞	0.00	100
Residual	0	0	0			
Total	1	161.82005				

Table 4.3 – Edge Inclination Angle vs. Average Cutting Force Response

Edge Angle - Analysis of Variance

Source	DF	SS	MS	F	P	R^2
Regression	1	233.45	233.45	383.32	0.00	99.7
Residual	1	0.61	0.609			
Total	2	234.06				

Table 4.4 – Work-piece Coefficient vs. Average Cutting Force Response

Work-piece Coefficient - Analysis of Variance

Source	DF	SS	MS	F	P	R^2
Regression	1.00	244.43	244.43	1281.02	0.00	99.8
Residual	2.00	0.38	0.19			
Total	3.00	244.81				

Five tool/work-piece interaction parameters were selected for evaluation:

1. Depth of cut (mm) – This has a linear trend with respect to the average cutting force response with an R^2 value of 97.8%.
2. Cutting Area (mm2) – Each individual tooth geometry can be identified in this plot. This is not beneficial to the regression model as the overall R^2 value is low (12%) as a result of the distinguishable tooth geometries.
3. Major Edge Contact (mm) – Once again, each individual tooth geometry has a distinctive trend with respect to the average cutting force response. The relationship has an R^2 value of 40%.
4. Lateral Edge Contact (mm) – There is no distinctive trend for the three different tooth geometries. This results in a respectable R^2 value of 93.9%.
5. The Cutting Perimeter (mm) – This parameter is the combined sum of the major and lateral edge contact. The trends are similar to those of major edge contact (each geometry has a distinctive trend). This value has an R^2 of 64%.

Table 4.5 – Depth of Cut vs. Average Cutting Force Response

Depth of cut vs. Cutting Force - Analysis of Variance

Source	DF	SS	MS	F	P	R^2
Regression	1.00	311	311.2	272	0.00	98
Residual	6.00	6.88	1.15			
Total	7.00	318				

Table 4.6 – Cutting Area vs. Average Cutting Force Response

Cutting Area vs. Cutting Force - Analysis of Variance

Source	DF	SS	MS	F	P	R^2
Regression	1.00	347	347.3	2.72	0.11	12
Residual	20.00	2554	127.7			
Total	21.00	2901				

Table 4.7 – Major Edge Contact vs. Average Cutting Force Response

Major Edge Contact vs. Cutting Force – Analysis of Variance

Source	DF	SS	MS	F	P	R^2
Regression	1.00	327	327	10.12	0.01	40
Residual	15.00	484.5	32.30			
Total	16.00	811.4				

Table 4.8 – Lateral Edge Contact vs. Average Cutting Force Response

Lateral Edge Contact vs. Cutting Force – Analysis of Variance

Source	DF	SS	MS	F	P	R^2
Regression	1.00	1853	1853	153.3	0.00	94
Residual	10.00	121	12.08			
Total	11.00	1973				

Table 4.9 – Cutting Perimeter vs. Average Cutting Force Response

Cutting Perimeter vs. Cutting Force – Analysis of Variance

Source	DF	SS	MS	F	P	R^2
Regression	1.00	1979	1979	39.33	0.00	64
Residual	22.00	1107	50.31			
Total	23.00	3085				

Parameters 2-5 are partially influenced by the depth of cut. Average response plots were subsequently carried out to determine the influence of the depth of cut on each of the parameters (figure 4.32):

2. Cutting area (mm^2) has a linear relationship with respect to depth of cut. Trends for the individual tooth geometries cannot be identified. The overall R^2 value is 93.7%.

3. Major edge contact (mm) also has a linear relationship with respect to depth of cut. Trends for the individual tooth geometries cannot be identified. The overall R^2 value is 94.3%
4. Lateral edge contact (mm) once again has a linear relationship with respect to depth of cut. Trends for the individual tooth geometries cannot be identified. The overall R^2 value is 74%.
5. Cutting perimeter (mm) can still be divided into three separate trends for the respective tooth geometries. Each trend has a linear relationship with respect to depth of cut. The overall R^2 value for cutting perimeter vs. depth of cut is 82%.

Table 4.10 – Cutting Area vs. Depth of Cut

Cutting Area vs. Depth of Cut - Analysis of Variance

Source	DF	SS	MS	F	P	R^2
Regression	1.00	0.23	0.23	298	0.00	94
Residual	20.00	0.02	0.00			
Total	21.00	0.25				

Table 4.11 – Major Edge Contact vs. Depth of Cut

Major Edge Contact vs. Depth of Cut - Analysis of Variance

Source	DF	SS	MS	F	P	R^2
Regression	1.00	0.20	0.20	247	0.00	94
Residual	15.00	0.01	0.00			
Total	16.00	0.21				

Table 4.12 – Lateral Edge Contact vs. Depth of Cut

Lateral Edge Contact vs. Depth of Cut - Analysis of Variance

Source	DF	SS	MS	F	P	R^2
Regression	1.00	0.11	0.11	28.9	0.00	74
Residual	10.00	0.04	0.00			
Total	11.00	0.14				

Table 4.13 – Cutting Perimeter vs. Depth of Cut

Cutting Perimeter vs. Depth of Cut - Analysis of Variance

Source	DF	SS	MS	F	P	R^2
Regression	1.00	0.26	0.26	98.00	0.00	82
Residual	22.00	0.06	0.00			
Total	23.00	0.32				

4.3.3.3 Regression Models

The predicted cutting force equations were obtained using the linear multiple least squares method. Two models were generated using the selected categorical predictors (figure 4.33):

1. A model including depth of cut, major edge contact, lateral edge contact, un-deformed cut area, edge angle, bevel angle and work-piece coefficient (excluding cut perimeter).
2. A model including depth of cut, cutting perimeter, edge angle, bevel angle and work-piece coefficient (excluding major and lateral edge contact).

Model 1 has an overall R^2 value of 90% and model 2 has an R^2 value of 88%. There is little discrepancy between the two regression plots with regard to the dispersion of the residual data points.

Table 4.14 – Model 1 (Excluding Cutting Perimeter)

Model 1

FV = - 86.4 - 231 Depth of cut (mm) + 42.5 Major edge contact (mm) + 126 Lateral edge contact (mm) + 79.9 Undeformed Area (mm²) + 0.497 Bevel angle° + 0.512 Edge angle° + 22.9 WPC

R-FV = 67.53 SD-FV = 14.62

Analysis of Variance

Source	DF	SS	MS	F	P	R^2
Regression	7	18191.6	2598.8	108.40	0.000	89.6
Residual Error	88	2109.7	24.0			
Total	95	20301.4				

Table 4.15 – Model 2 (Excluding Both Major and Lateral Edge Contact Width)

Model 2

FV = - 240 - 237 Depth of cut (mm) + 170 Cut Perimeter (mm) - 26.5 Undeformed Area (mm²) + 1.59 Bevel angle° + 1.03 Edge angle°+ 22.9 WPC

R-FV = 67.53 SD-FV = 14.62

Analysis of Variance

Source	DF	SS	MS	F	P	R^2
Regression	6	17871.7	2978.6	109.11	0.000	88
Residual Error	89	2429.6	27.3			
Total	95	20301.4				

4.4 Discussion

4.4.1 Comparison to previous results

Both the U0° tooth and rip tooth described in chapter 3 both had orthogonal cutting edges making chip formation and tool forces comparable. To further aid the explanation of cutting mechanics using teeth with orthogonal edges, the high speed camera was available to provide explanations for the chip types observed in chapter 3.

4.4.1.1 Chip and Surface Formation

The first thing that must be mentioned is that the discontinuous, broken chips detailed in chapter 3 for the dry work-pieces at larger depths of cut (0.8 – 1.2 mm) were not formed by the U0° tooth. This is principally due to the fact that only comparably low depths of cut were performed in this experimentation (0 – 0.35 mm).

Continuous chips were produced using the U0° tooth geometry when machining dry work-pieces along the grain. The same types of chips were also observed machining using the rip tooth at low depths of cut for work-pieces ranging from dry to moderate moisture content (6-20%). The fuzzy chips were produced by both types of tooth only for saturated work-pieces along the grain. The high speed video and substantial collection of continuous chip formation provide conclusive evidence that cutting wood along the grain is a shearing process. It should further be noted that there is very little difference in the chip ratio and shear plane angle values for the dry work-piece along the grain. This suggests that the shear cutting mechanics along the grain is similar for all three tooth geometries. The only perceivable difference is the angle that the chip is formed in relation to the blade. For the bevelled teeth the chip is formed parallel to the bevelled rake face and hence is ejected at 28° to the normal of the blade. For the un-bevelled tooth the chip is formed normal to the blade and hence is forced to curl into the gullet.

High speed footage of the U0° tooth geometry shows how the initial fibres deform due to bending prior to fracture. The footage of the saturated work-piece does not illustrate this deformation process as well. The deformed, displaced fibres can be identified in the optical microscope images. The optical microscope images of the surfaces machined using the rip tooth are similar to U0°, although more fibres have been uprooted for U0° as more than one tooth performed the cut. The high speed video of the deformation prior to fracture along with the complimentary surface formation microscope images provide conclusive evidence that cutting wood across the grain is a bending process.

4.4.1.2 Tool forces

The recorded cutting force values from previous experimentation increased in a linear fashion for increasing depths of cut. This is mirrored by the linear trends observed machining using the U0° tooth geometry, albeit at much lower depths of cut (0-0.35 mm compared to 0.4 – 1.2 mm).

The thrust force values for U0°, U28° and GT are all have the same trend as their respective cutting force values and are hence proportional. There is very little difference in the magnitude of the thrust forces along and across the grain for increasing depths of cut. This mirrors the thrust force values recoded in the previous block of experimentation.

The side force values obtained cutting using the U0° tooth along the grain are noticeably larger than across the grain. This is similar to the side forces obtained machining using the rip tooth, although it is noticed that there is a dramatic non linear increase between 0.8 and 1.2 mm. This huge increase could be a possible effect of the interaction between the work-piece and lateral edges and would explain why it is not observed for the much lower depths of cut performed by the U0° tooth (0 – 0.35 mm). Contrary to the U0° tooth, both the U28° and GT teeth have noticeably higher side forces across the grain than along. Furthermore the gulf

between cutting force values for the two grain directions stays fairly constant for increasing depth of cut. The gap between the side force values along and across the grain for the U0° tooth increases with depth of cut. The cause of this observed phenomenon is the difference in lateral edge contact. For any given depth of cut the U0° tooth has double the lateral contact (constrained on both sides of the tooth) than the U28° or GT formations.

4.4.2 Parameters and Regression Modelling

Strong and weak correlations with the mean cutting force were identified in the main effects plot. In general, the parameters with distinct trends and high R^2 values proved to be the most suitable categorical predictors:

4.4.2.1 Geometric Parameters

Only the bevel angle and edge inclination angle were deemed suitable as predictors for the regression models. This was supported by the distinctive trends quantified by R^2 values ≈ 100%. There was only a small amount of variation (5°) between the three rake angles evaluated; furthermore no distinctive trend was identified between rake angle and the average cutting force response. There was no distinctive relationship with respect to the average cutting force response for both the flank and wedge angles. These two geometric parameters were dismissed as predictors due the lack of any trend, also because the cutting forces were only measured in the forward cutting direction (interaction with the rake side of the tooth only).

4.4.2.2 Interaction Parameters

When considering the tool/work-piece interaction parameters a general trend with respect to the average cutting force response was desired. This general trend was only observed for

depth of cut and lateral edge contact width. Discrete trends for each geometry evaluated were easily identified for the cutting area, major edge contact and cutting perimeter.

The cutting area, major edge contact width, lateral edge contact width and cutting perimeter all vary with respect to depth of cut. This provided the rationale for performing analysis of variance and average response plots for these parameters against the depth of cut. The cutting area, major edge contact with and lateral contact width all have a general relationship with respect to the depth of cut. The only parameter that has specific trends for each tooth geometry is the cutting perimeter. These three relationships are all linear and the bevelled teeth trends (U28° and GT) are much closer aligned than the un-bevelled tooth trend (U0°). This exercise demonstrates that the depth of cut parameter must be used to normalise the four other interaction parameters. This is comparable to the way that the work-piece coefficient normalises the empirical values for the four different work-pieces evaluated.

4.4.2.3 The Regression Models

Regression model 1 uses major and lateral edge contact width in place of cutting perimeter and has an R^2 value of 90%. Regression model 2 uses the cutting perimeter in place of major and lateral edge contact width and has an R^2 value of 88%. This is only a small discrepancy (2%) however it can be explained using the cutting perimeter, major and lateral edge contact width trends with respect to depth of cut. In essence the major and lateral edge contact parameters have general trends and the cutting perimeter has specific trends for each tooth. This results in the slightly higher R^2 value for model 1.

4.4.3 Hidden Variables

The effects of potentially hidden variables on the experimental results were considered. It was assumed that un-controlled environmental conditions such as room temperature and relative humidity were not significant and hence were not measured during the cutting tests.

The quality of the cutting edges at a microscopic level was evaluated. SEM images for the U0° (figure 4.35), U28° (figure 4.36) and GT (figure 4.37) are used to illustrate the scale of abrasion for 100 consecutive cuts. For these particular teeth the depth of cut used was 0.35 mm. First 50 cuts were performed on dry work-pieces along the grain then a further 50 cuts were performed on dry work-pieces across the grain. The following was observed:

- The teeth were initially covered with debris which was removed during the cutting process.
- The apex at which the major and lateral edges converge has a small radius before any cutting commences. This corner radius did not increase significantly after the 100 cuts were taken.
- Both the major and lateral cutting edges appear sharp at the microscopic level (i.e. the edge radius is too small to measure). Neither major nor lateral edges were worn post 100 cuts.

It can hence be assumed that the effects of abrasive wear did not have a negative impact on the quality of the cutting edges for the range of 100 cuts taken. The only visible difference post 100 cuts is the lack of debris on the rake and flank faces. The edge radii are too small to measure in this microscopic range and the corner radii range from only 4-8 μm. As a result the cutting edges and corners can be modelled as infinitely sharp when interacting with the lowest depth of cut from the controlled experiment (50μm). Because these SEM images show

the after effects of the most severe cutting scenario (cutting dry wood at the highest depth of cut) it can hence be assumed that all other cutting scenarios were unaffected by abrasive wear.

4.5 Summary of Findings

1. Frame by frame analysis of the high speed footage and optical microscope images were able to characterise the chip and surface formations for the U0°, U28° and GT tooth geometries. Cutting along the grain can confidently be described as a shearing process with quantified chip ratios and shear plane angles for the dry work-pieces. The key difference between the un-bevelled (U0°) and bevelled (U28° and GT) geometries was the formation of the chip with respect to the gullet. As U0° has an orthogonal edge the chip formed normal to the saw-blade and hence was transported into the gullet. As U28° and GT have 28° bevelled angles the chip was not transported into the gullet, it was instead ejected at a 28° tangent to saw blade.

2. The cutting mechanics across the grain for U0° can be confidently described as bending process. This bending process was evident from deformation observed from the high speed video. Furthermore the complimentary microscope images identified the same deformation points. These surface formation results mirror the results from chapter 3 using the rip tooth. It is not so clear weather cutting across the grain with U28° and GT is purely a bending process. This is due to the lack of visible deformation prior to deformation from the high speed video supported by the cleanly cut surfaces from the microscope images. Material removal was visible for all tooth geometries across the grain, although this is not by means of a single tooth alone. The

subsequent three teeth on each group were visibly responsible for removal of wood particles.

3. The average thrust and side forces wear measured to be only a fraction of the magnitude of the average cutting force. This mirrors the results from chapter 3 using the rip tooth. No further in depth analysis was carried out on thrust and side force data collected. Only the cutting force was used in the main effects plot (to evaluate the effect of defined parameters) and regression modelling.

4. The two geometric parameters that have the most influence on the cutting forces are the bevel angle and the edge inclination angle. All of the interaction parameters were used to develop the predictive cutting force models. Using major and lateral edge contact width yielded a model with slightly higher R^2 (2%) than the model using cutting perimeter.

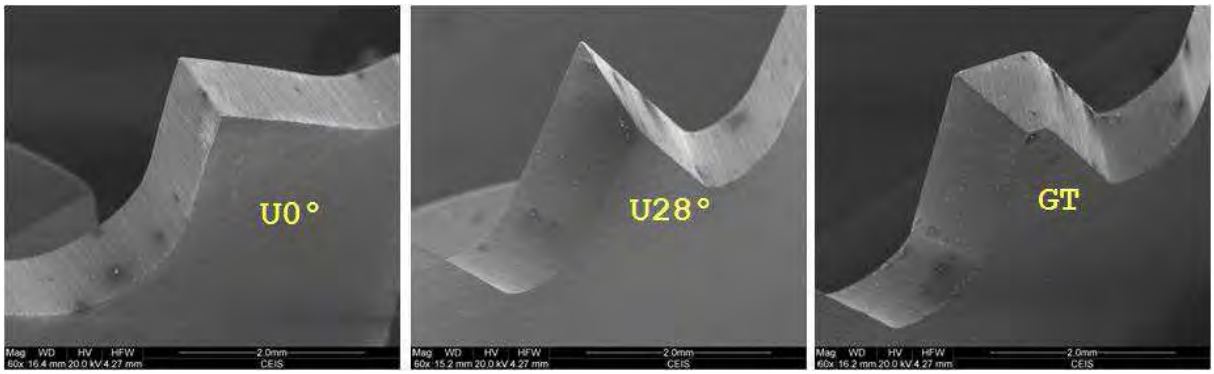

Figure 4.1 – Selected tooth geometries

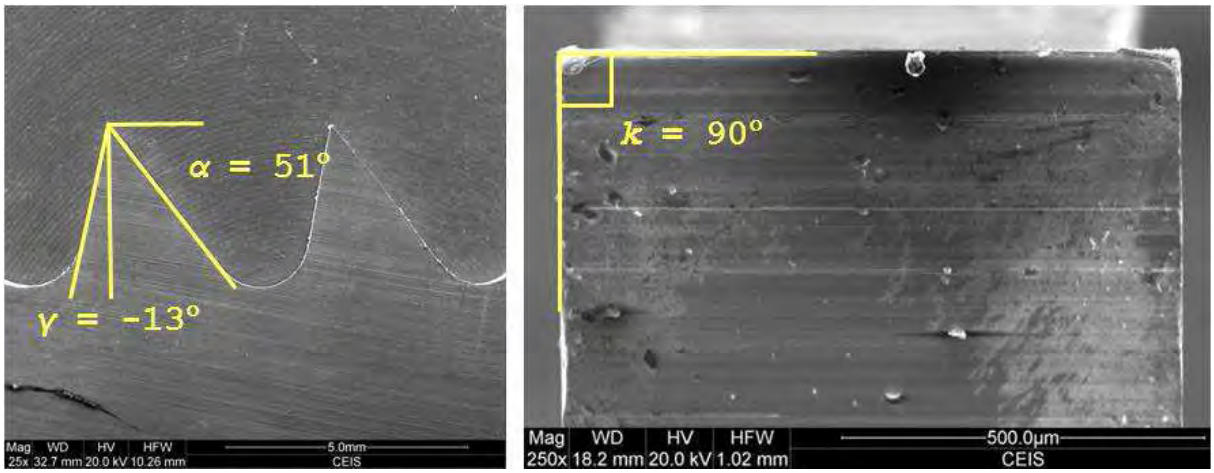

Figure 4.2 – U0° SEM measurements

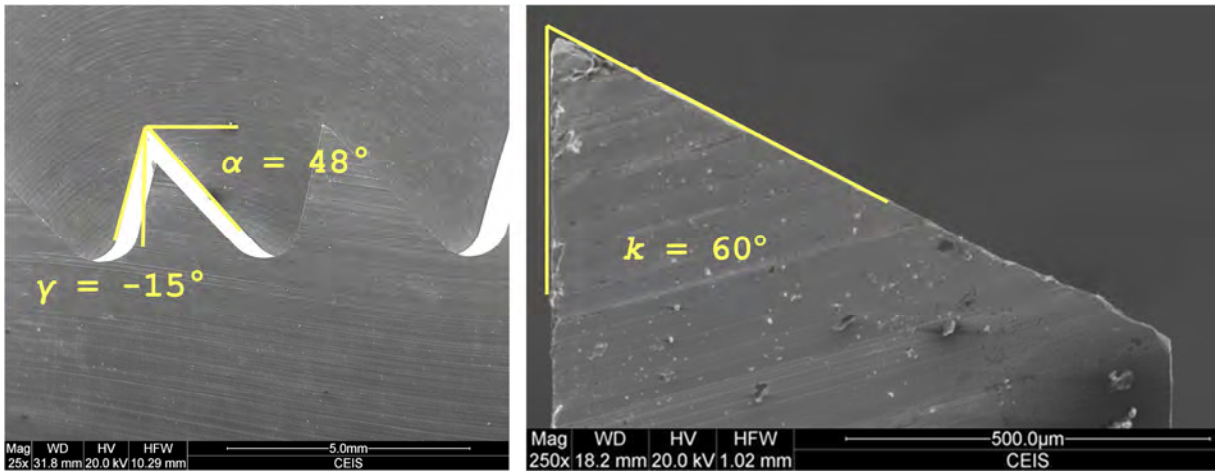

Figure 4.3 – U28° SEM measurements

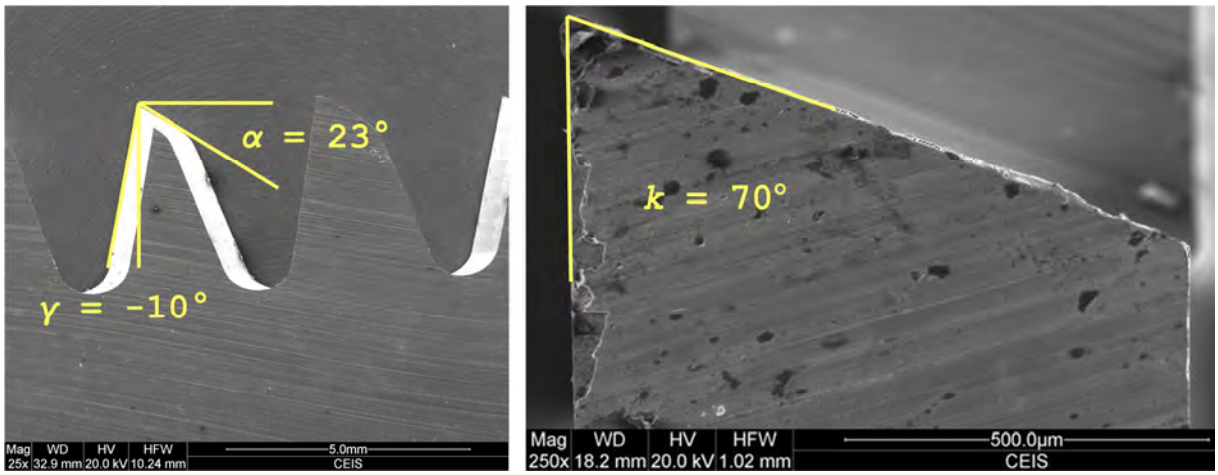

Figure 4.4 – GT SEM measurements

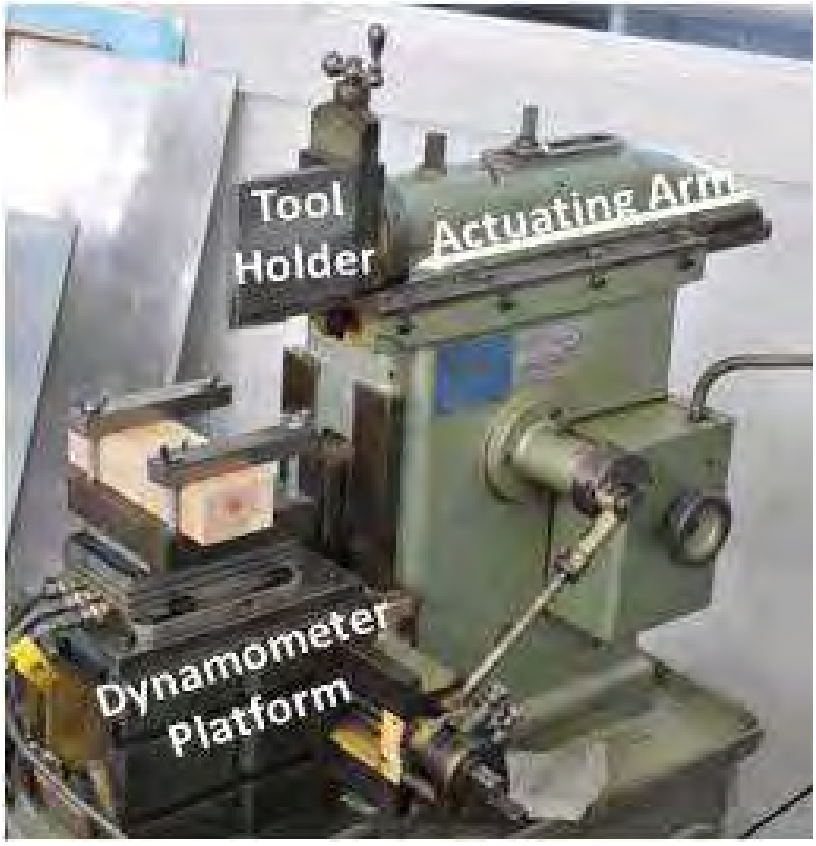

Figure 4.5 – Photograph of shaper machine test rig

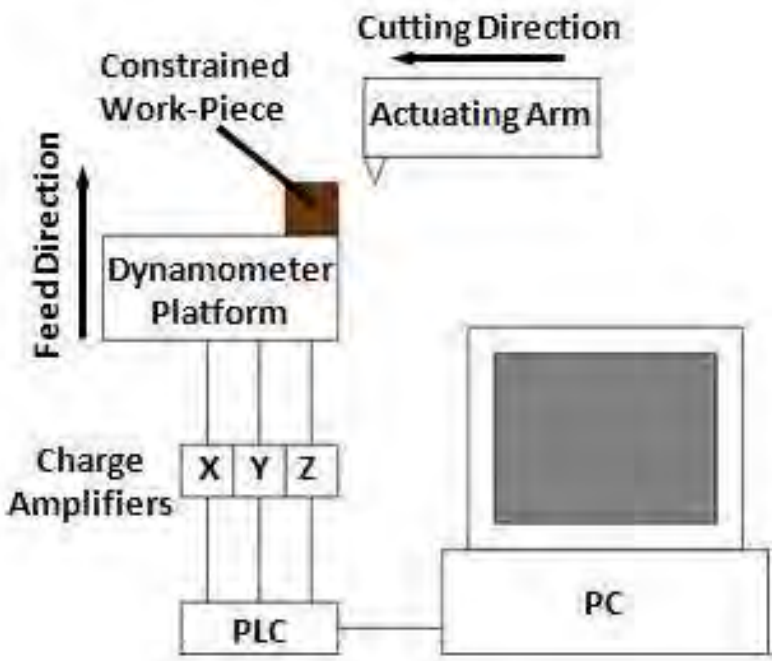

Figure 4.6 – Detailed test rig schematic diagram

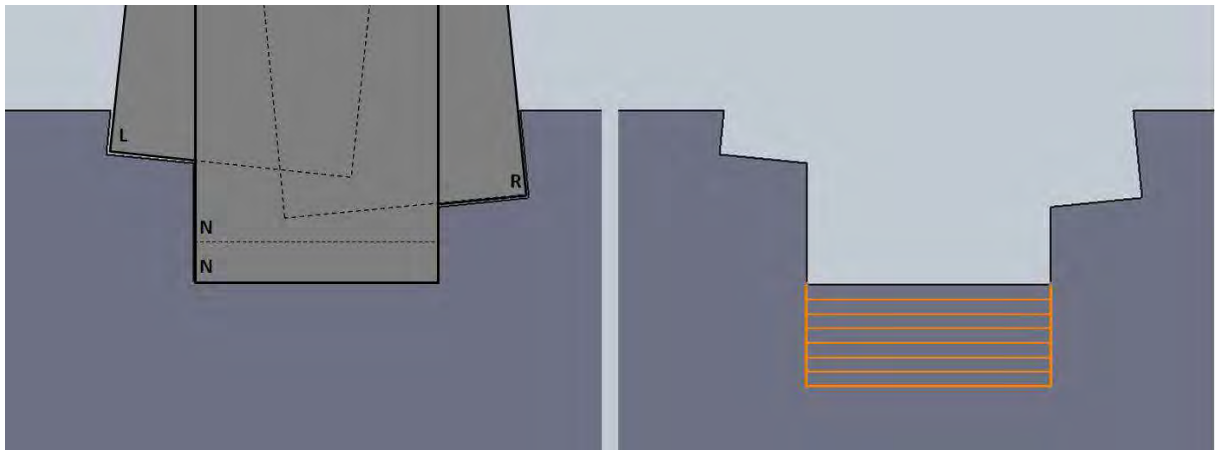

Figure 4.7 – CAD drawing of tool paths for un-bevelled (U0°) tooth

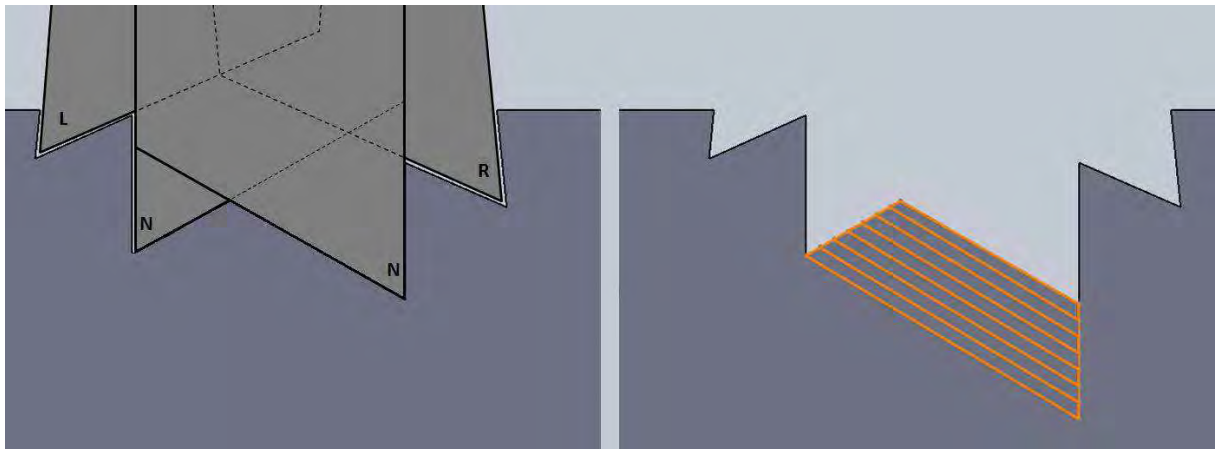

Figure 4.8 – CAD drawing of tooth paths for bevelled (U28° and GT) teeth

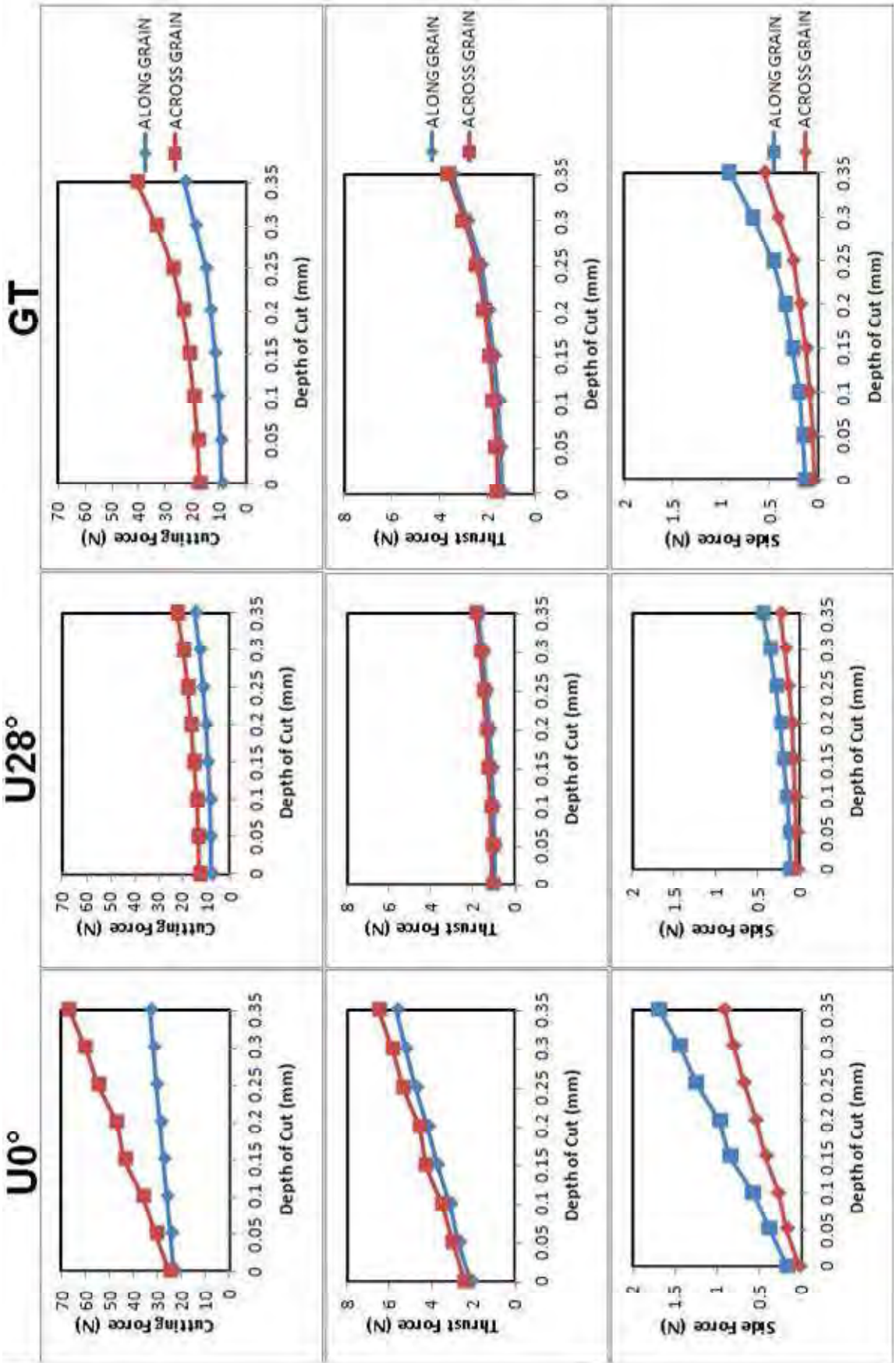

Figure 4.9 – Tool force average response plots

Figure 4.10 – Calculation of work-piece coefficient

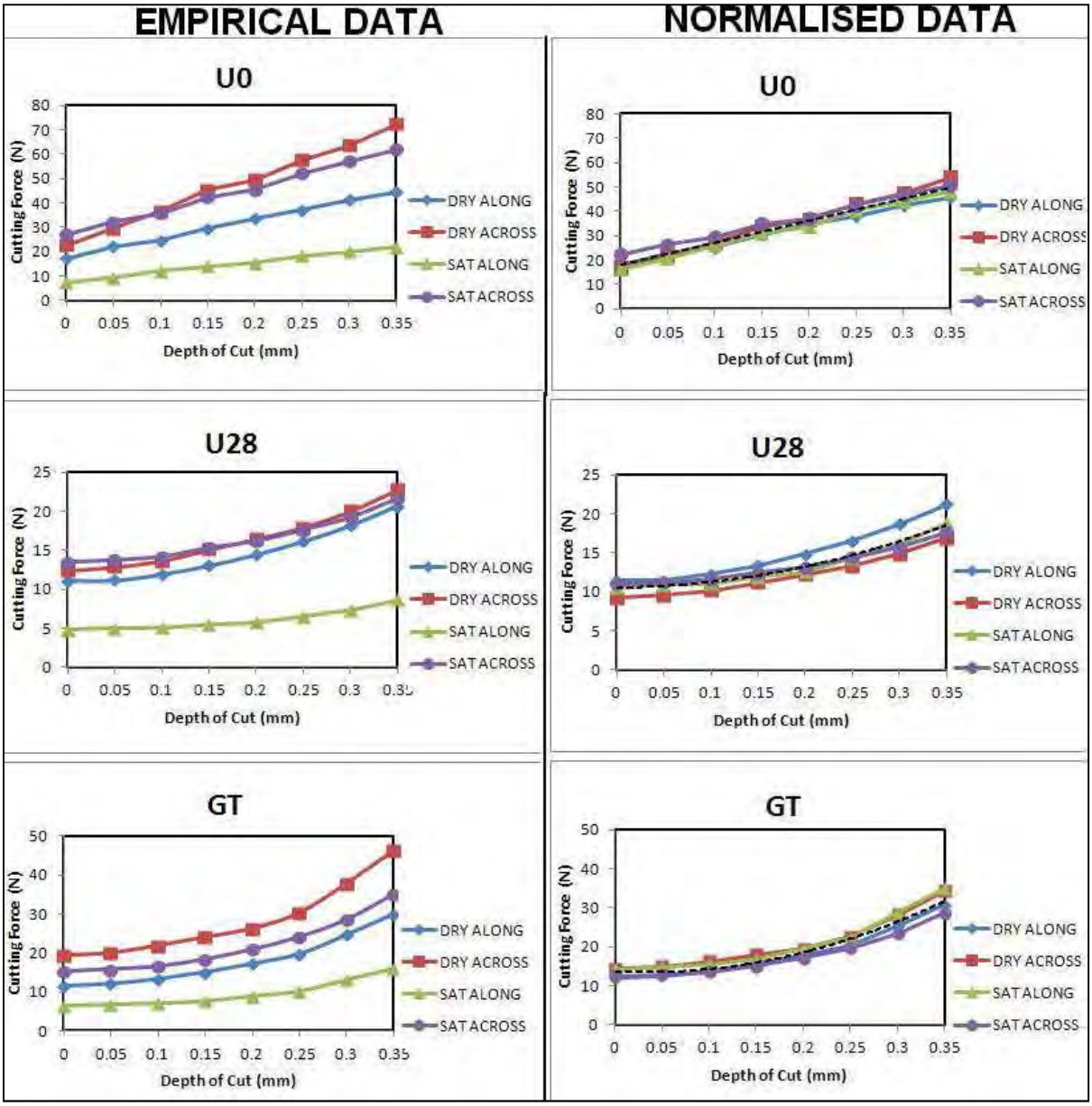

Figure 4.11 – Empirical and normalised cutting force values

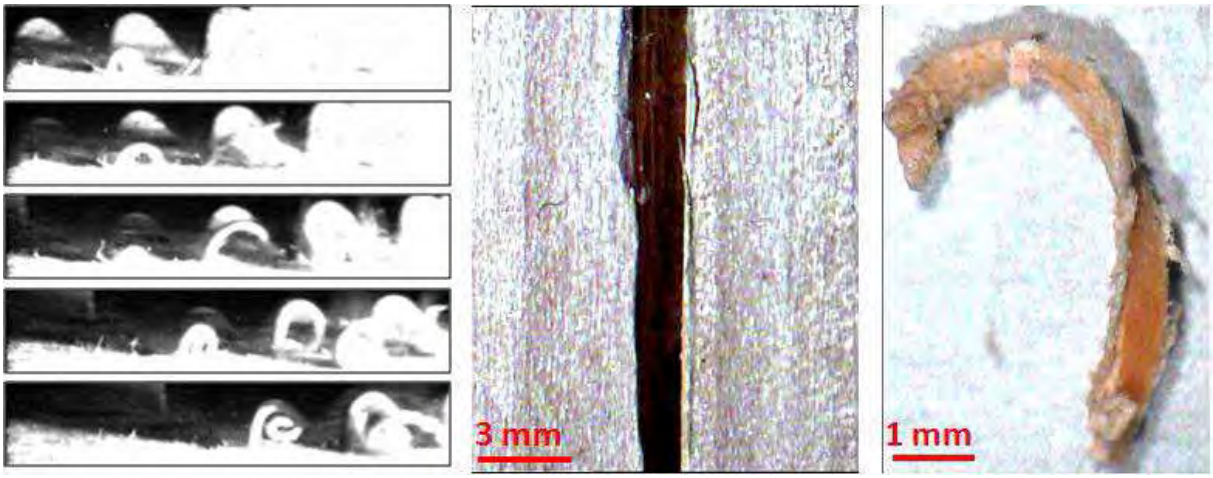

Figure 4.12 – U0° chip formation, dry, along the grain

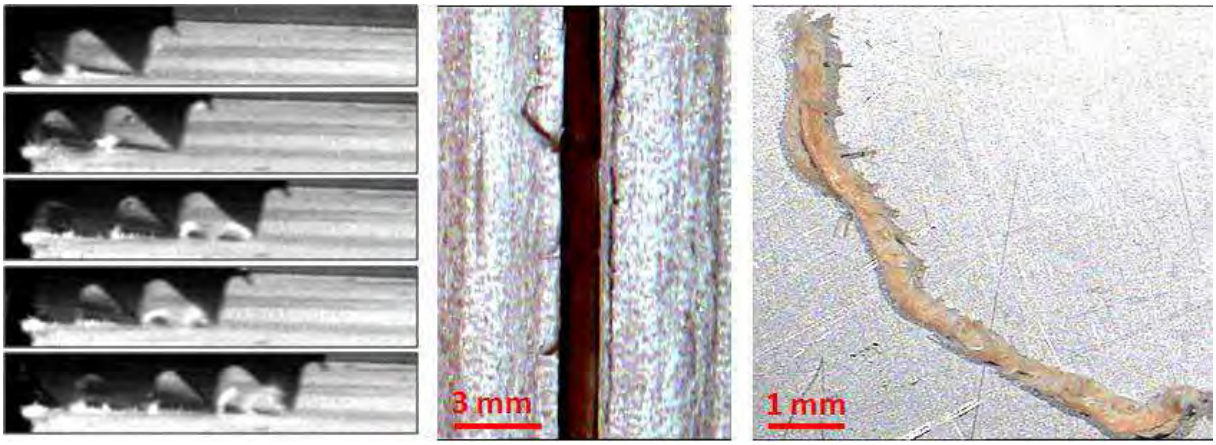

Figure 4.13 – U28° chip formation, dry, along the grain

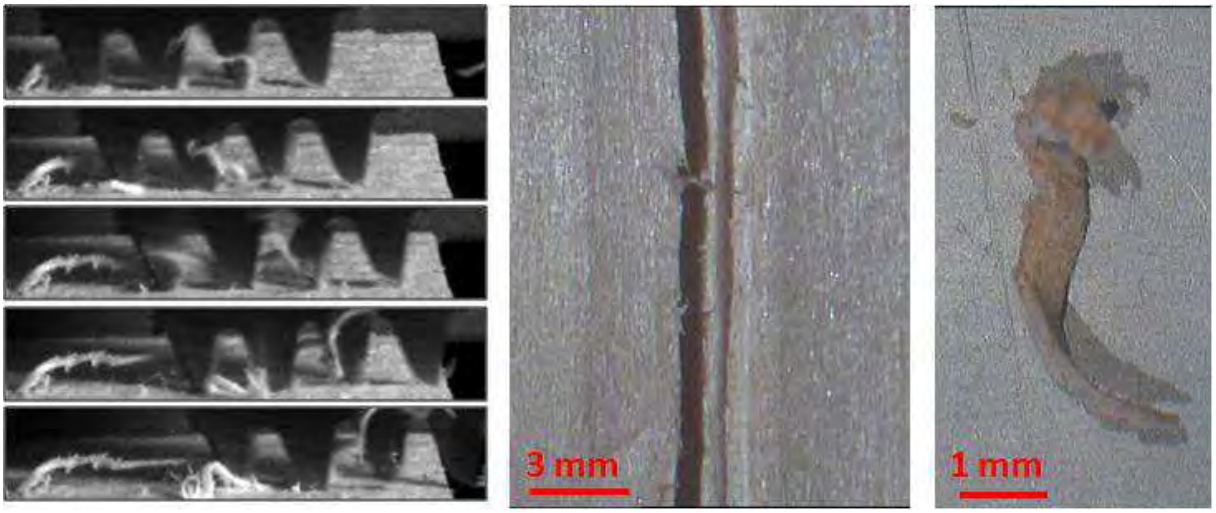

Figure 4.14 – GT chip formation, dry, along the grain

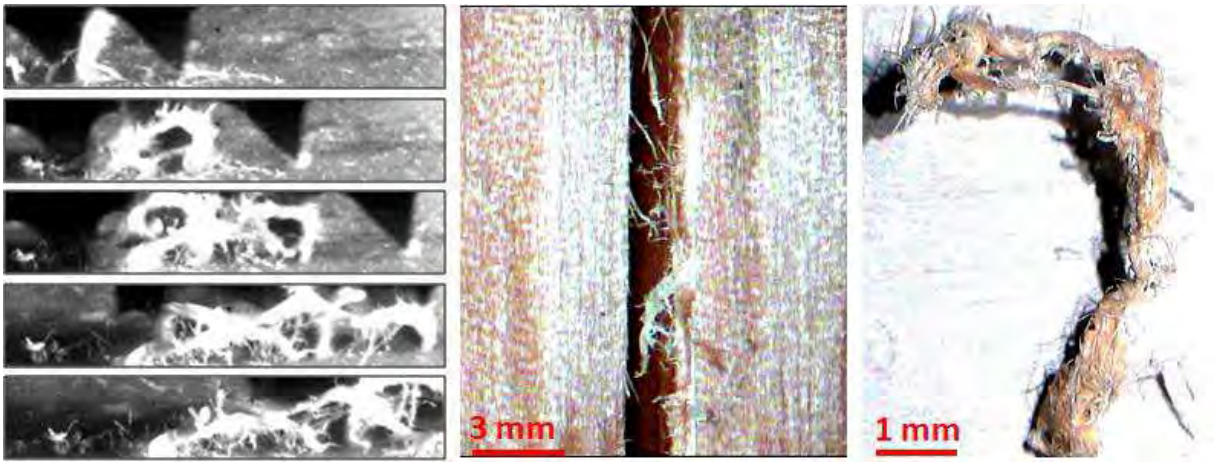

Figure 4.15 – U0° chip formation, saturated, along the grain

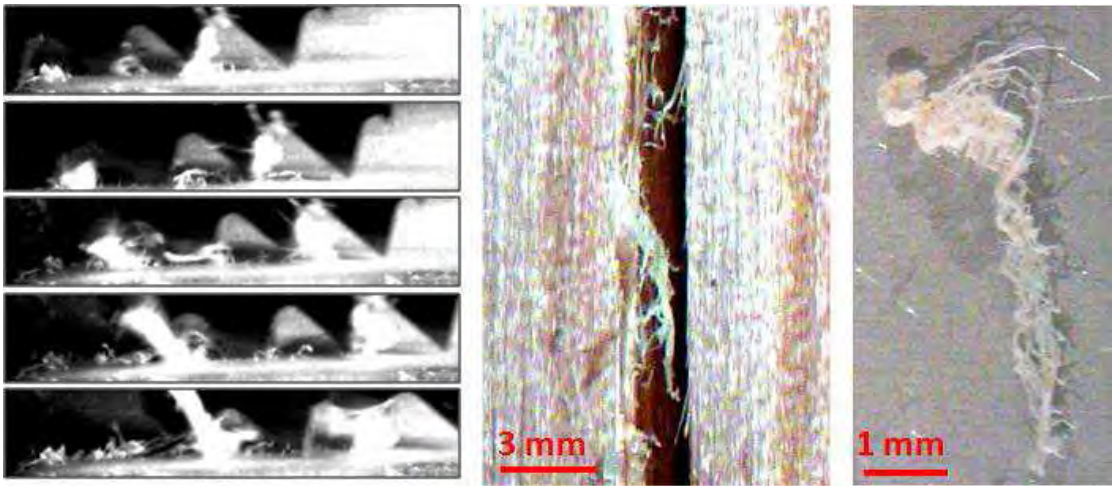

Figure 4.16 – U28° chip formation, saturated, along the grain

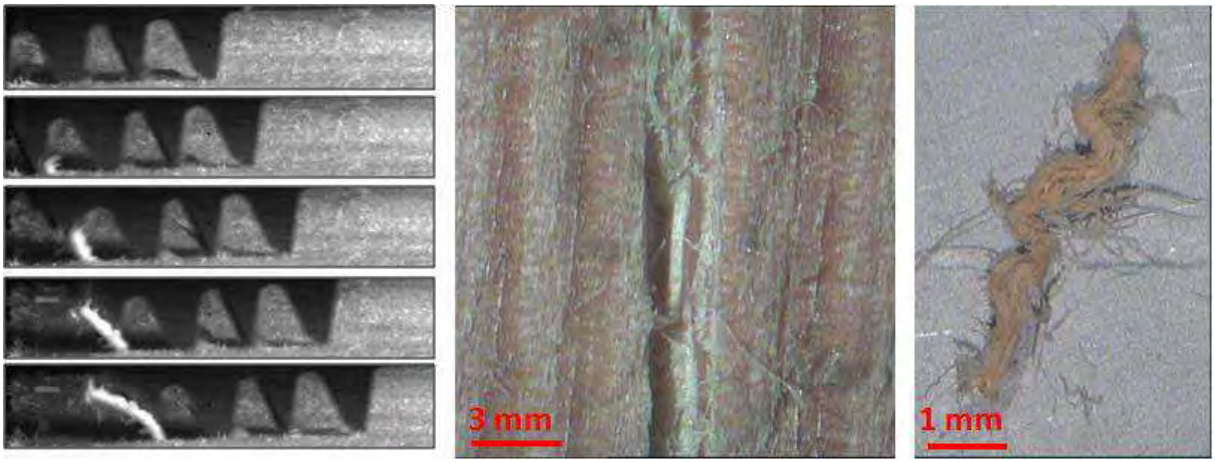

Figure 4.17 – GT chip formation, saturated, along the grain

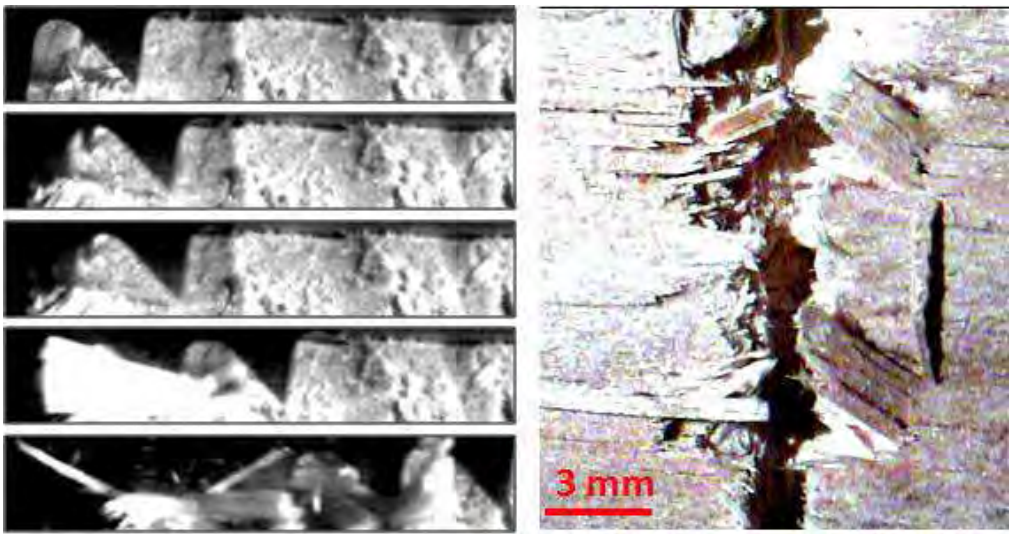

Figure 4.18 – U0° surface formation, dry, across the grain

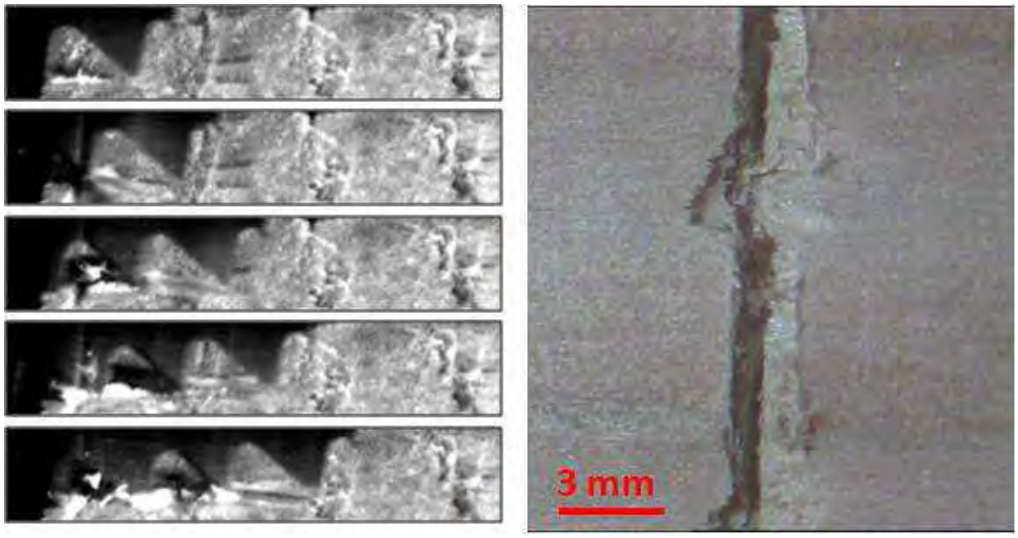

Figure 4.19– U28° surface formation, dry, across the grain

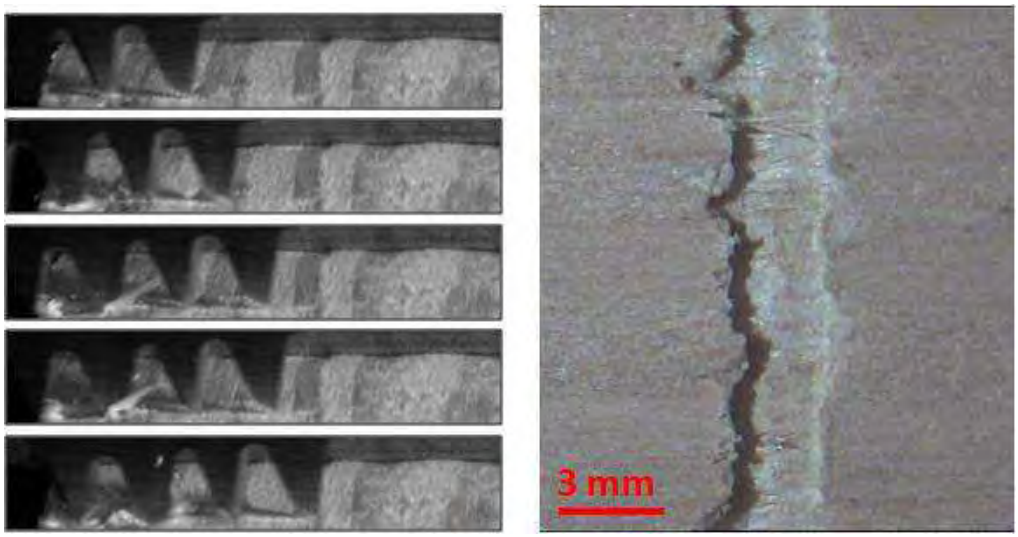

Figure 4.20– GT surface formation, dry, across the grain

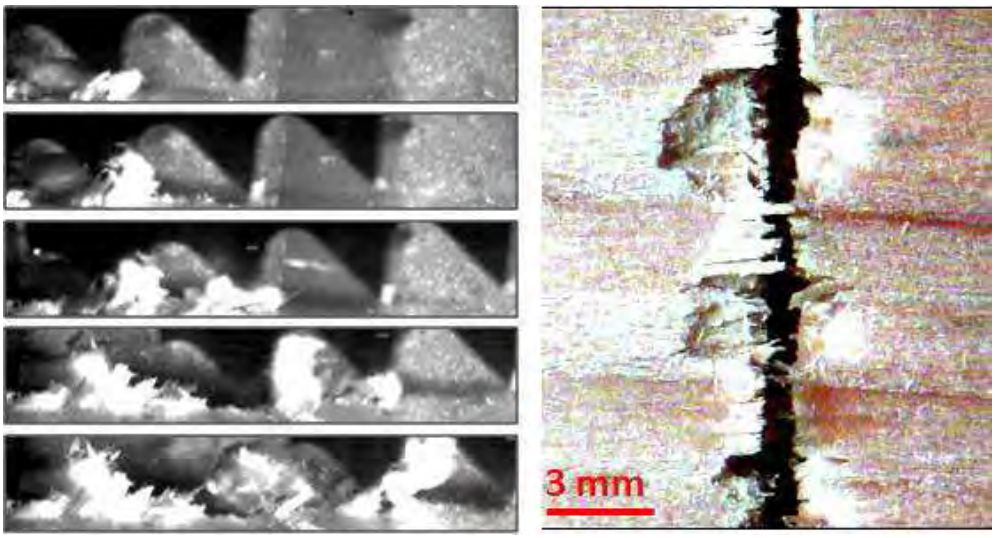

Figure 4.21 – U0° surface formation, saturated, across the grain

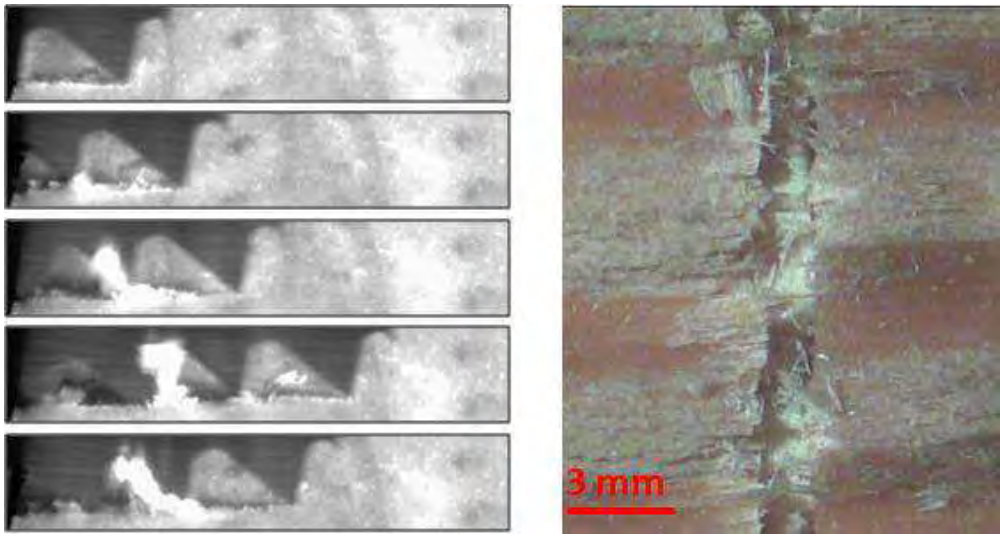

Figure 4.22 – U28° surface formation, saturated, across the grain

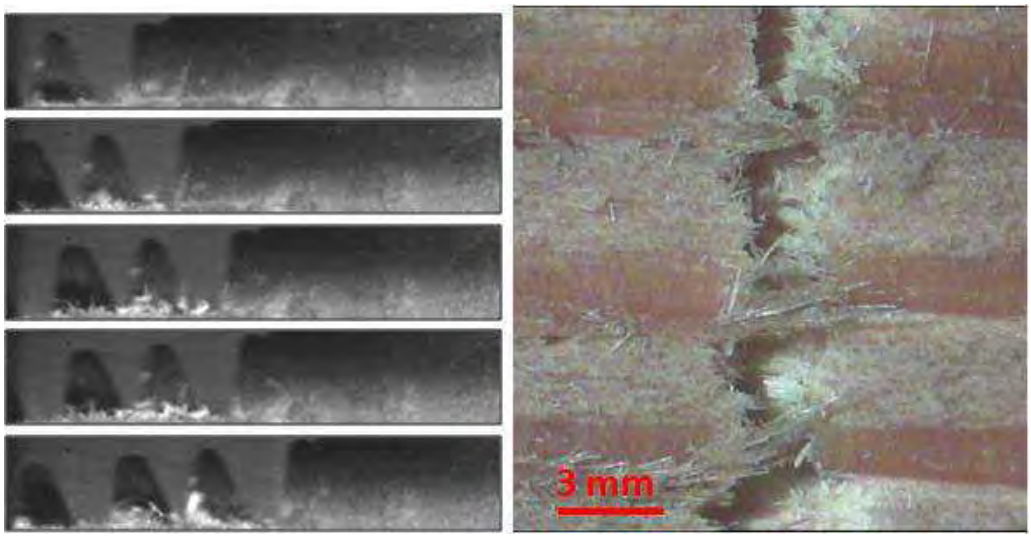

Figure 4.23 – GT surface formation, saturated, across the grain

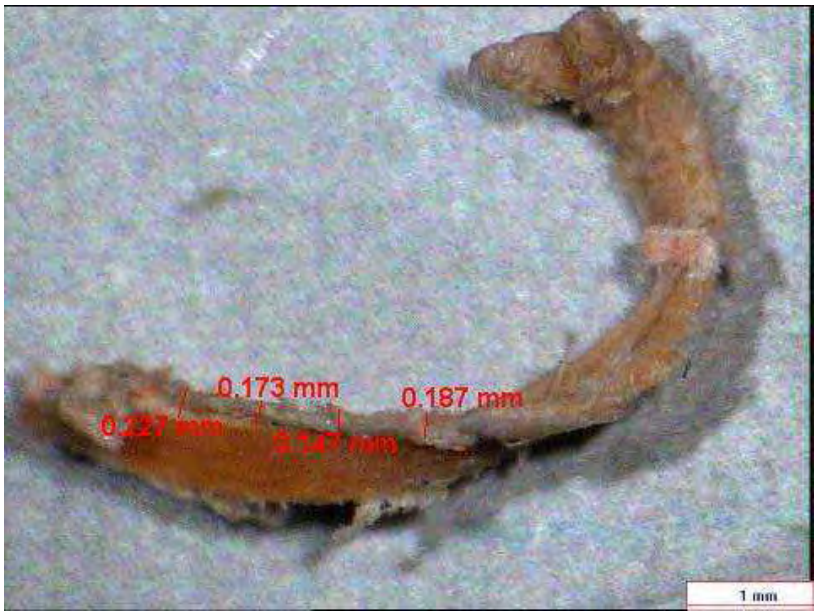

Figure 4.24 – Chip measurements, U0°, dry, along the grain

Figure 4.25 – Chip measurements, U0°, dry, along the grain

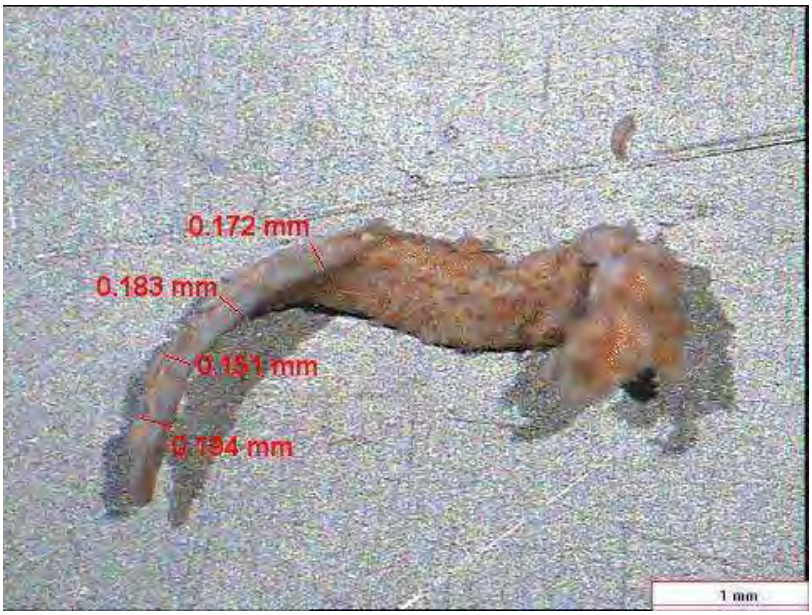

Figure 4.26 – Chip measurements, U0°, dry, along the grain

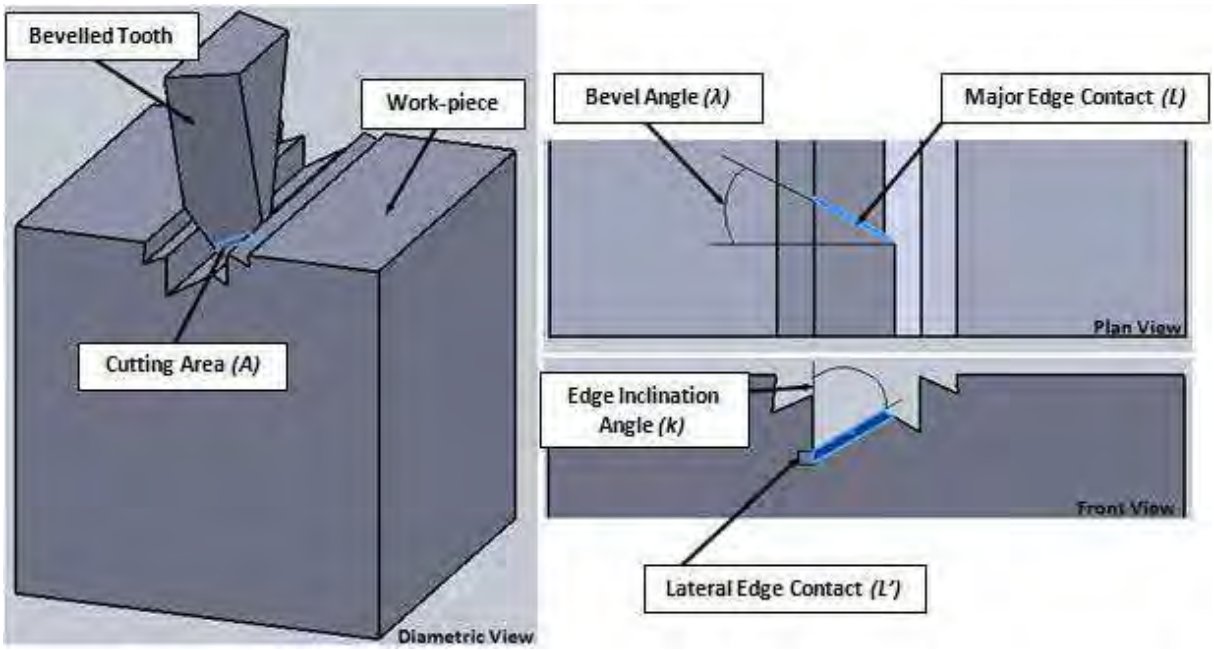

Figure 4.27 – CAD drawing of tool-work-piece interaction (un-bevelled tooth)

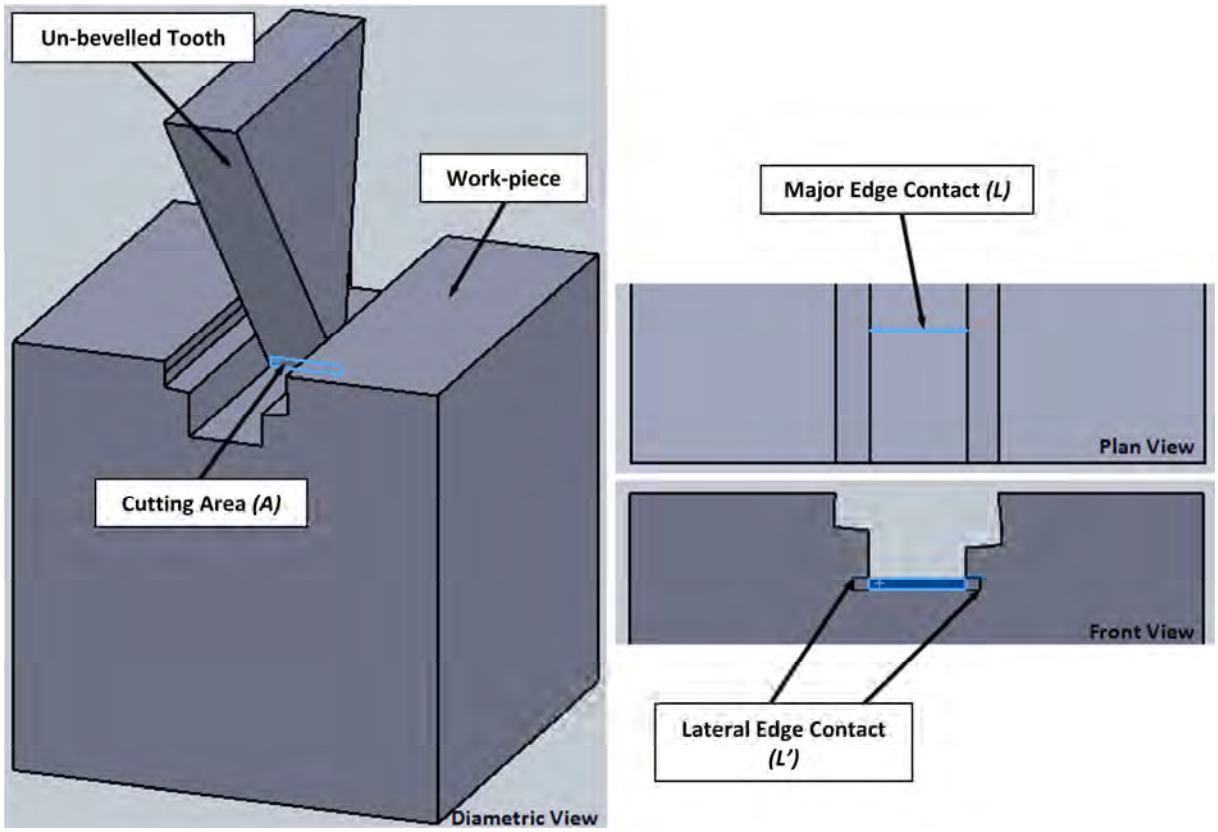

Figure 4.28 – CAD drawing of tool-work-piece interaction (bevelled tooth)

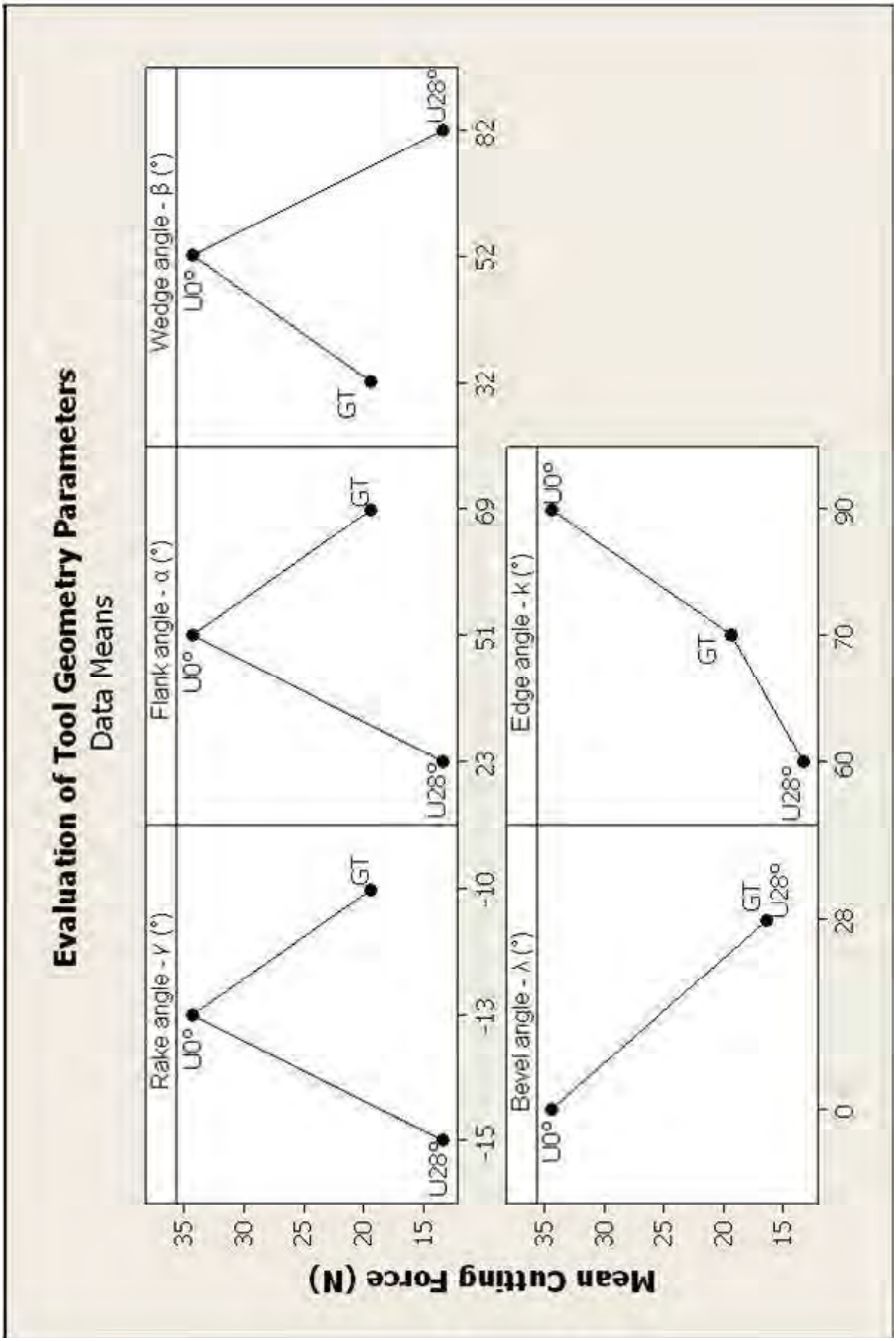

Figure 4.29 – Average cutting force responses for tool geometry parameters (effective flank and wedge angles)

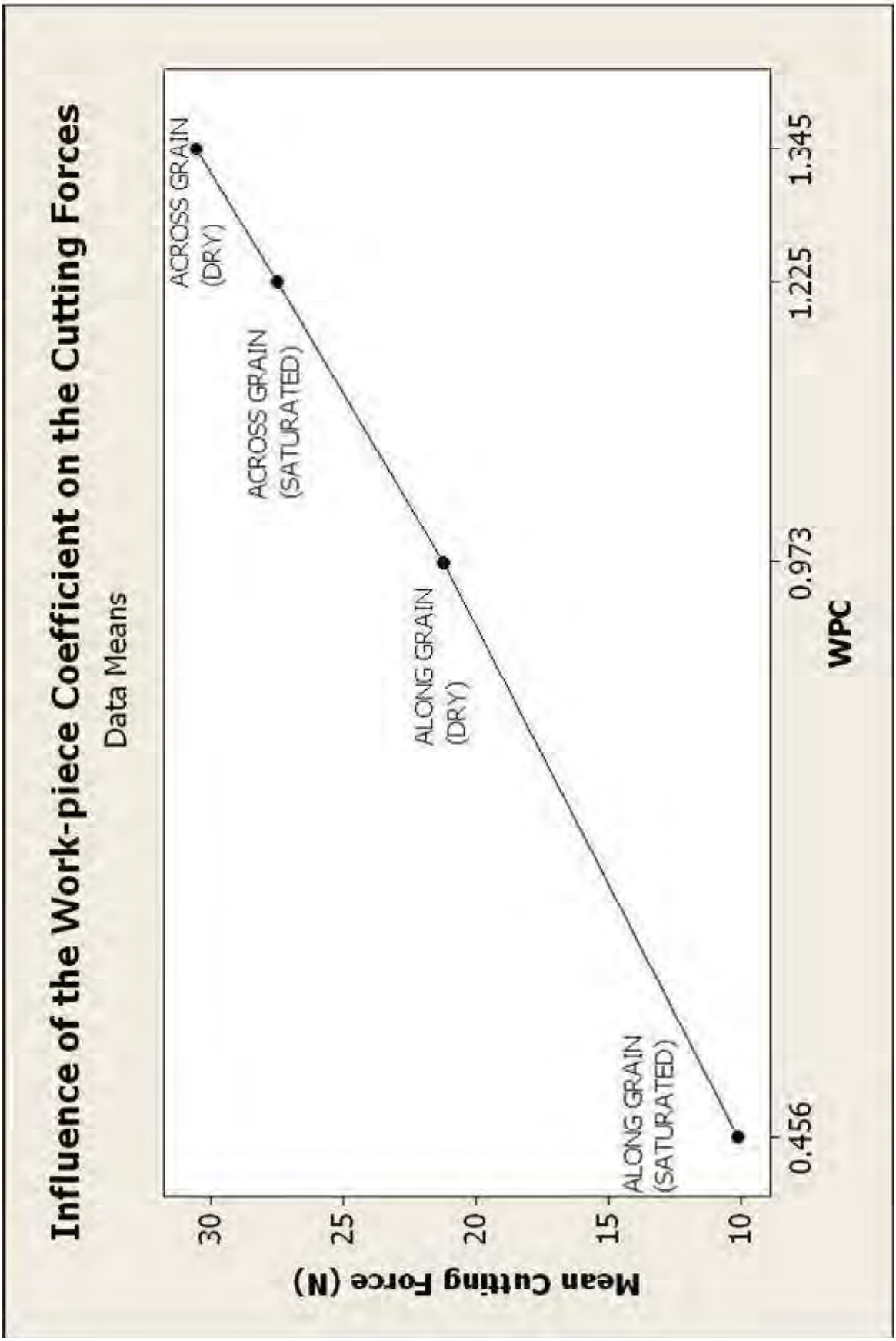

Figure 4.30 – Average cutting force response for work-piece coefficient

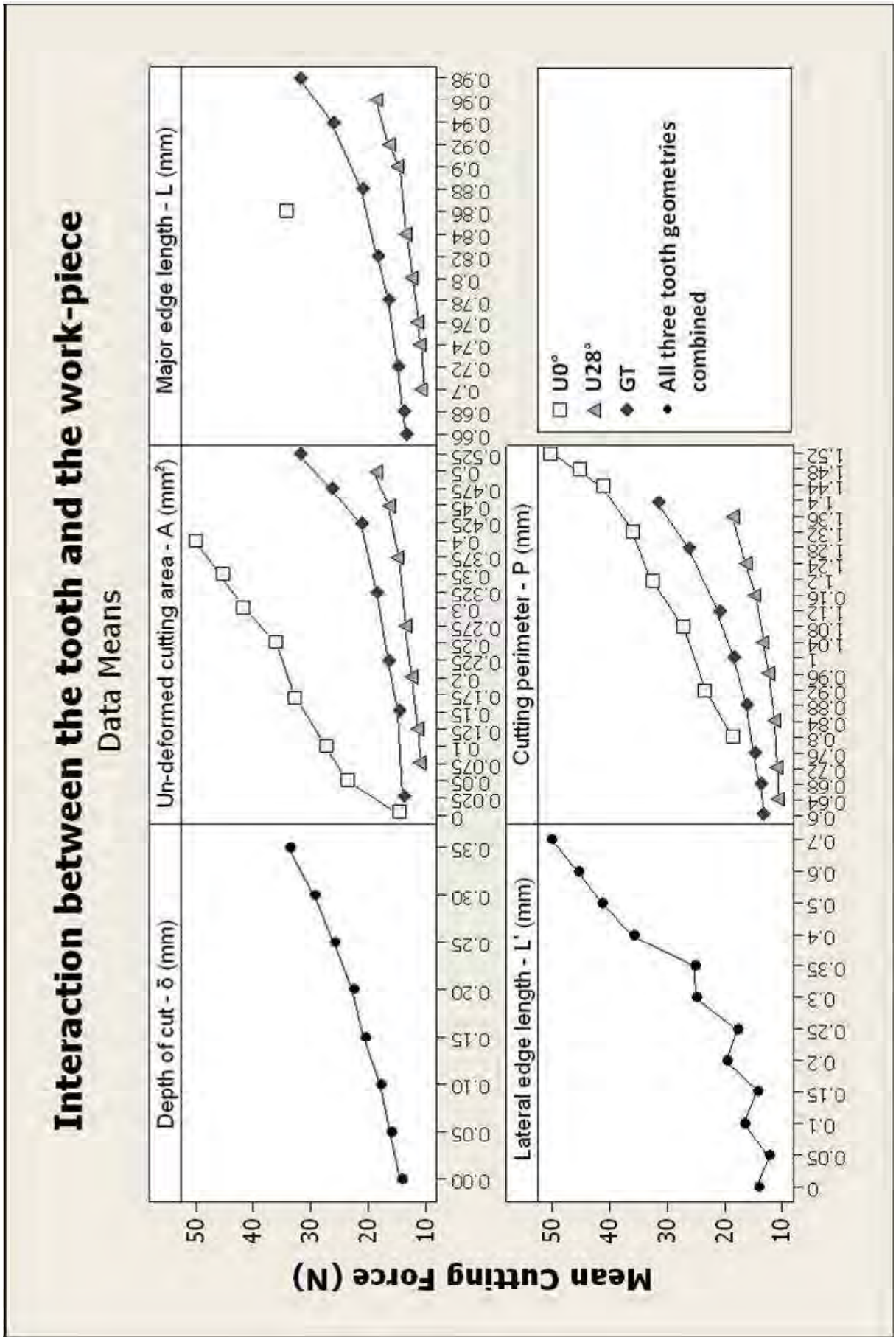

Figure 4.31 – Average cutting force responses for tool/work-piece interaction parameters

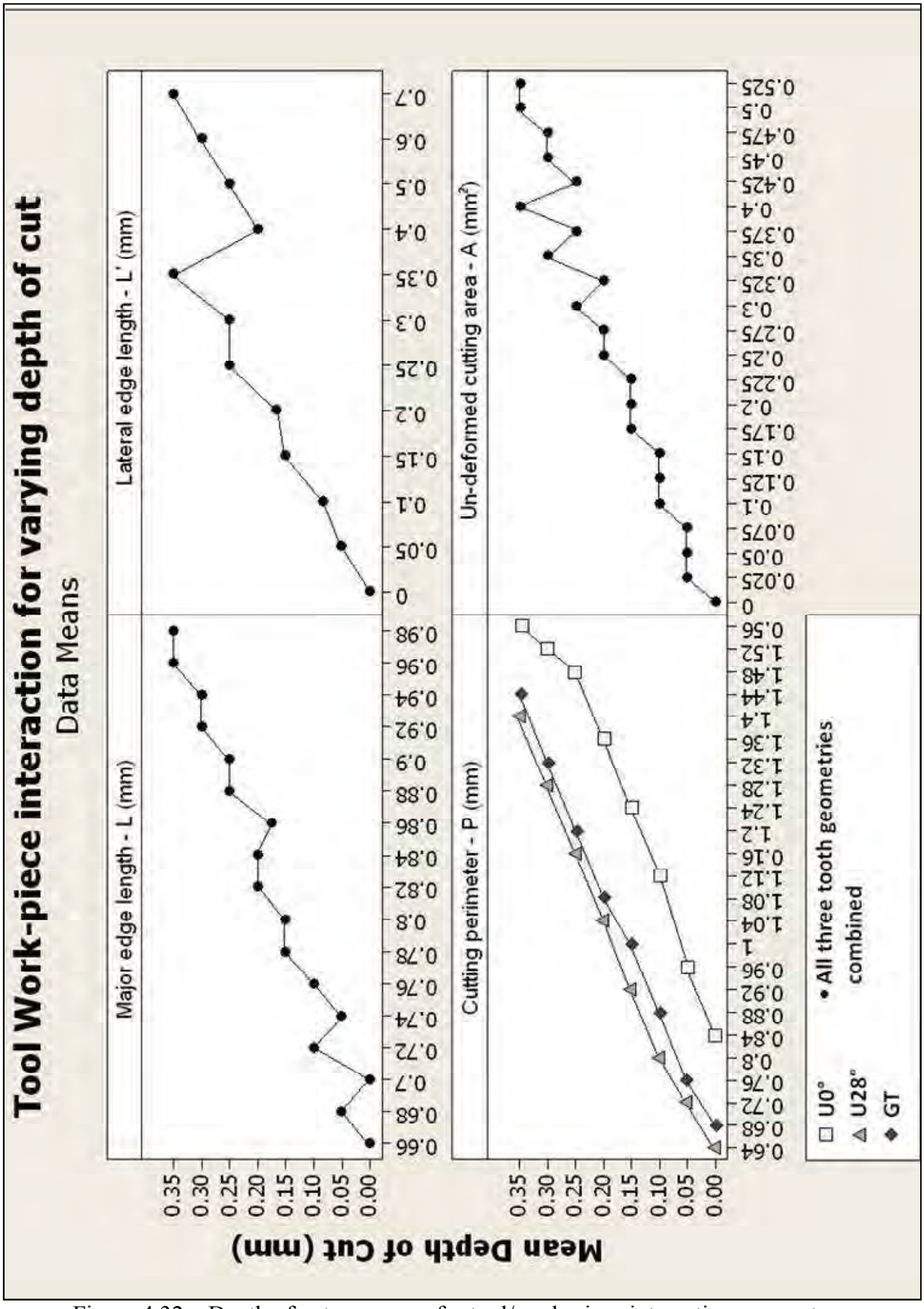

Figure 4.32 – Depth of cut responses for tool/work-piece interaction parameters

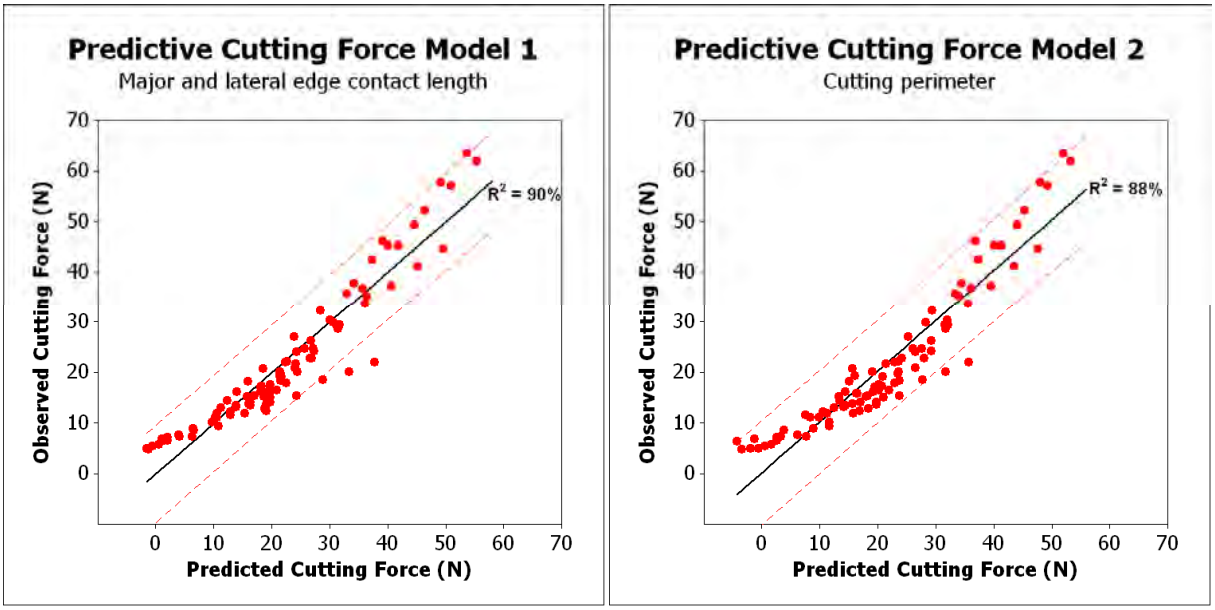

Figure 4.33 – Regression plots

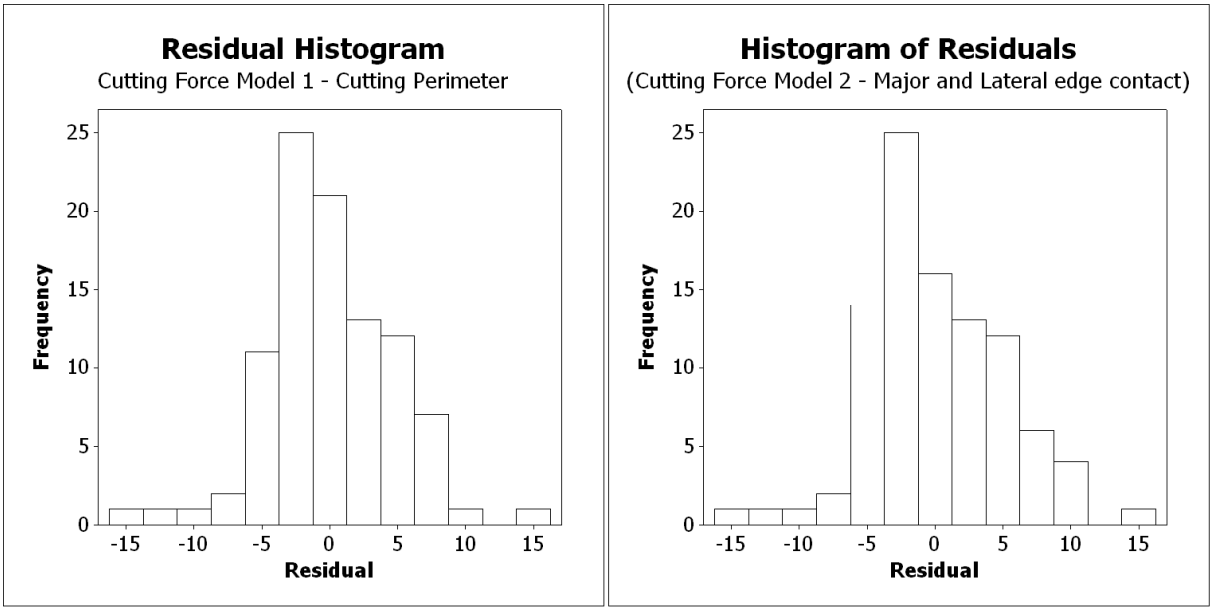

Figure 4.34 – Residual histograms

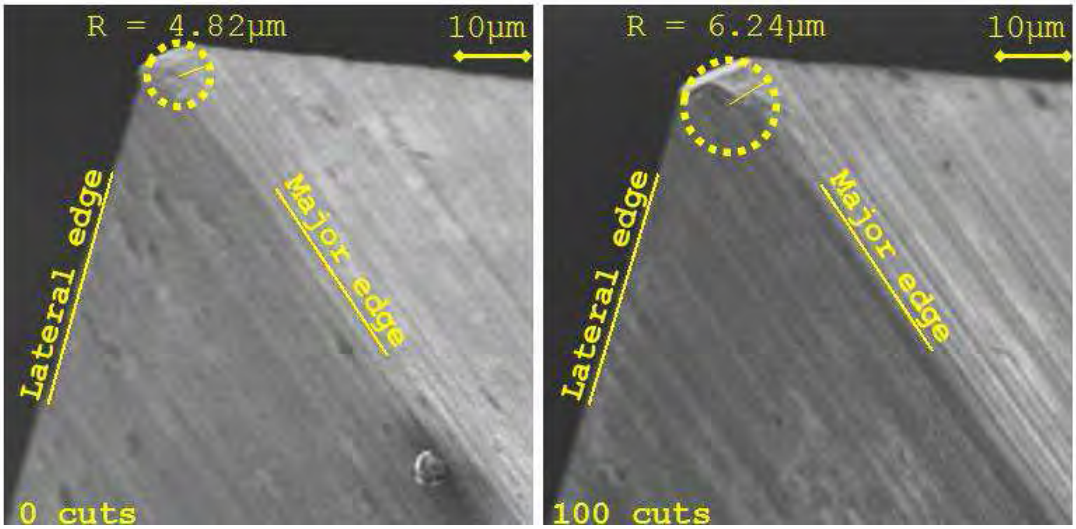

Figure 4.35 – U0º extreme tooth tip pre and post 100 cuts

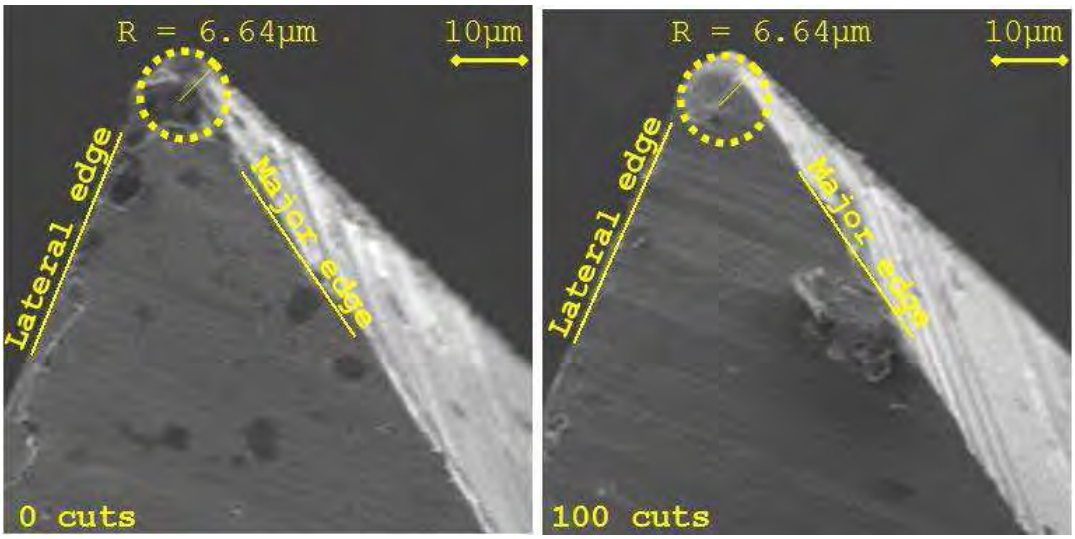

Figure 4.36 – U28º extreme tooth tip pre and post 100 cuts

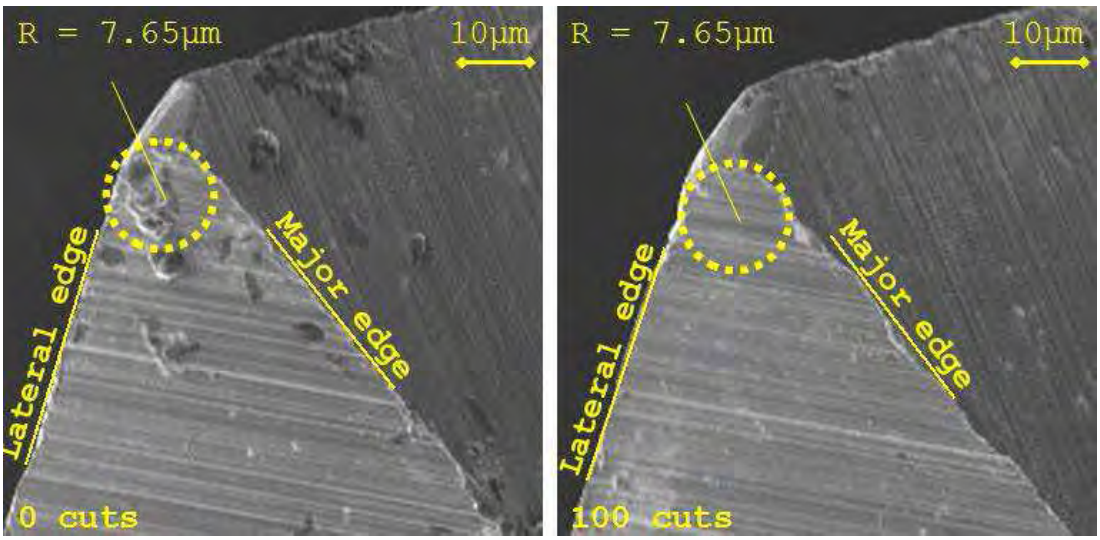

Figure 4.37 – GTº extreme tooth tip pre and post 100 cuts

CHAPTER 5
OVERALL DISCUSSION

5.1 Outcomes of Literature Review

A comprehensive review of literature related to both wood characteristics and machining operations was conducted. The outcome of this literature review revealed two significant gaps in the body of knowledge for this research area:

1. The majority of literature documents fundamental machining operations, i.e. orthogonal cutting using plaining tools. The small amount of literature that documents sawing processes focuses on high speed applications such as band-sawing and circular-sawing.
2. For all machining operations the effects of a wide variety of work-piece properties on the cutting mechanics were not considered. Often only physical properties such as density and moisture content were used to evaluate the work-piece prior to controlled cutting tests leaving mechanical properties neglected.

These two gaps in the body of knowledge warranted this authors original work detailed in chapters 3 and 4 of this thesis.

5.2 Cutting with Orthogonal Tooth Geometries

In chapter 3 a simple rip tooth with an orthogonal cutting edge was used for controlled experimentation. Only the recorded cutting force values (Fv) were used to develop the regression models. This is because the thrust force (Fp) and side force (Fr) values were measured to be significantly lower than the cutting force values. The regression models

provided a statistically valid grounding to make the following statements: i) cutting forces across the grain are influenced by properties obtained through bending tests, ii) cutting forces along the grain are influenced by properties obtained through shear tests.

The chip and surface formation was carefully evaluated under the microscope. The findings of which supported the two statements made after developing the regression models. No material removal occurred across the grain, however surface formation across the grain exhibited fibres bent out of position either side of the visible tool path (figure 5.1). Material removal did however occur along the grain, the collected chips were mainly uniform implying a failure shear mode (figure 5.2).

The un-bevelled (U0°) tooth formation described in chapter 4 has similar features to the rip tooth described in chapter 3 (both have an orthogonal cutting edge). High speed footage and microscope images of cutting using the U0° are very similar to the chip and surface formation described in chapter 3. Frame by frame analysis of the high speed video footage across the grain provided a dynamic representation of the wood fibres deformation in bending initiated by the un-bevelled tooth geometry (figure 5.3). Frame by frame analysis of the un-bevelled tooth along the grain shows continuous chip formation (figure 5.4). Each chip is formed normal to the orthogonal cutting edge and hence is transported into the gulled and removed from the kerf. This explained why the U0° tooth geometry is so often used along the grain. The chiselling action of the orthogonal edge and the role of the gullet ensure an efficient removal of material along the wood grain.

5.3 Cutting with Bevelled tooth Geometries

Analysis of the high speed footage for the bevelled tooth geometries (U28° and GT) also exhibits continuous chip formation implying a shear failure mode (figure 5.5). The only

difference between the bevelled and un-bevelled teeth is the direction of the chip formation. Frame by frame footage shows the chips formed normal to the bevelled rake face, which itself is at a tangent of 28° to the cutting direction (figure 5.6). The fact that the gullet plays no significant role for U28° and GT suggests that these two tooth geometries do not efficiently transport and remove the chip from the kerf. This explains why the two geometries are not often employed to machine along the wood grain.

Frame by frame analysis and microscope images of the bevelled teeth exhibits less deformation due to bending across the grain when compared to the same analysis for the un-bevelled teeth (figure 5.7). The wood fibres appear significantly less deformed and the kerf width is visibly narrower (figure 5.8). It is known from the numerical analysis detailed in chapter 4 that there is much less of an interaction between the tooth cutting area and the work-piece for the two bevelled tooth geometries. This lower contact area maintained during cutting results in the narrower kerf width.

It is also known from chapter 4 that the lateral edge contact plays a significant role in the regression modelling. The two bevelled teeth only have one lateral edge that interacts with the work-piece resulting in relatively low cutting forces. This is compared to the two lateral edges that simultaneously interact with the work-piece for the un-bevelled tooth which result in much higher cutting forces. As a result, the fibres are not excessively deformed prior to fracture. The single, bevelled lateral edge effectively behaves like the blade of a “knife”.

Prior to experimentation it was assumed that the GT tooth formation was able to machine equally well both along and across the wood grain. This was based upon the way that the compound tooth saws were marketed by the major manufacturers (appendix 2). It was established that the GT tooth geometry has only a slightly lower edge inclination angle than U28°. Furthermore, the cutting force trends and observed chip/surface formation are very

similar to that of U28°. The results from the single tooth experiment prove that the GT tooth formation cuts wood similar to the U28º geometry (knife like) than the U0º geometry (chisel like). This suggests that the GT tooth geometry is better suited to machining wood along the grain.

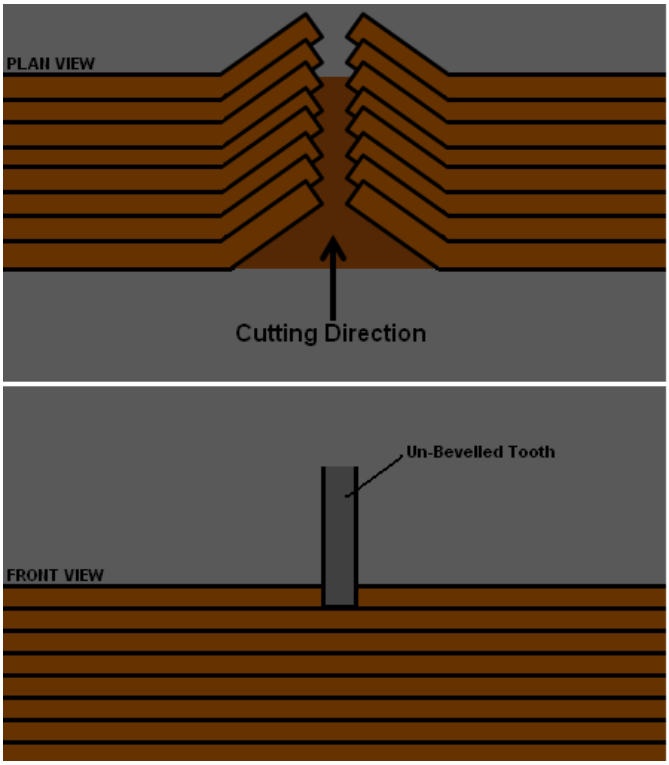

Figure 5.1 – Un-bevelled tooth machining across the grain

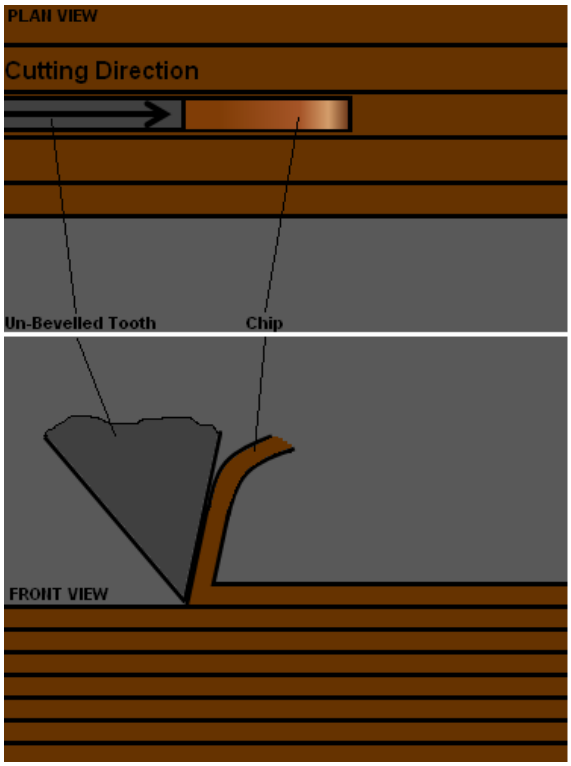

Figure 5.2 – Un-bevelled tooth machining along the grain

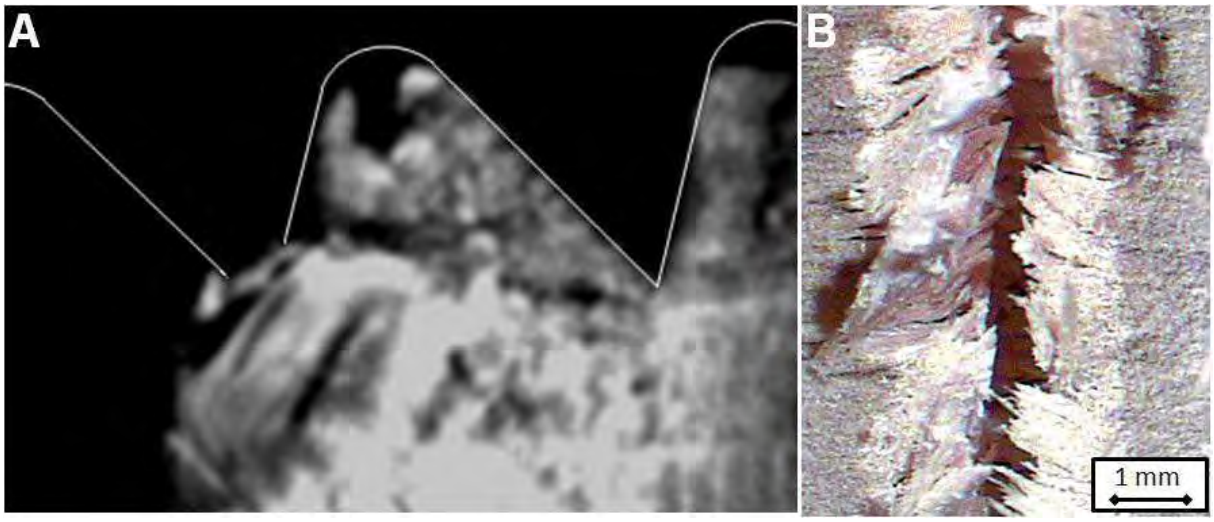

Figure 5.3 – A) High speed frame of an un-bevelled tooth cutting across the grain, B) Microscope image of surface formation post cut

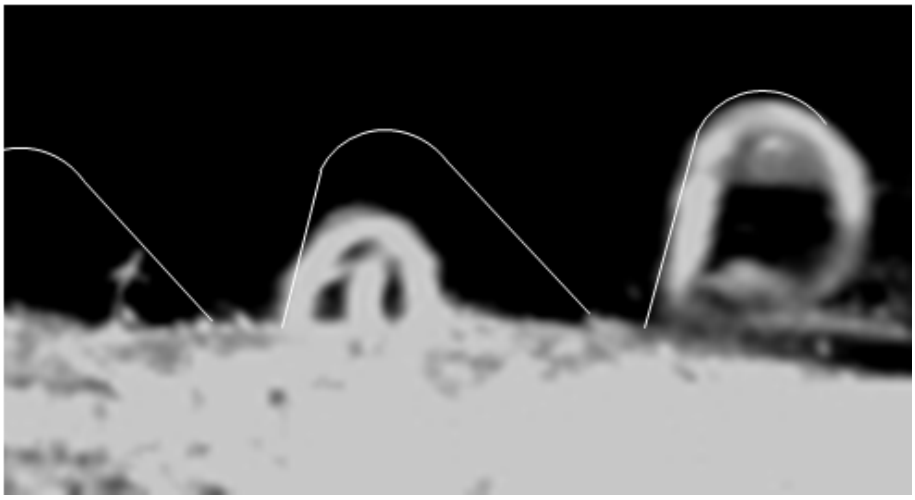
Figure 5.4 – High speed frame showing continuous chip formation for an un-bevelled tooth

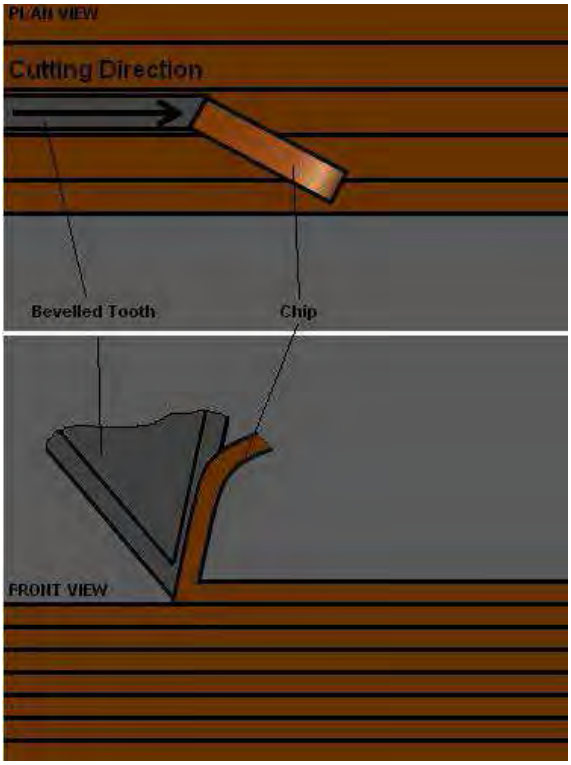

Figure 5.5 – Bevelled tooth machining along the grain

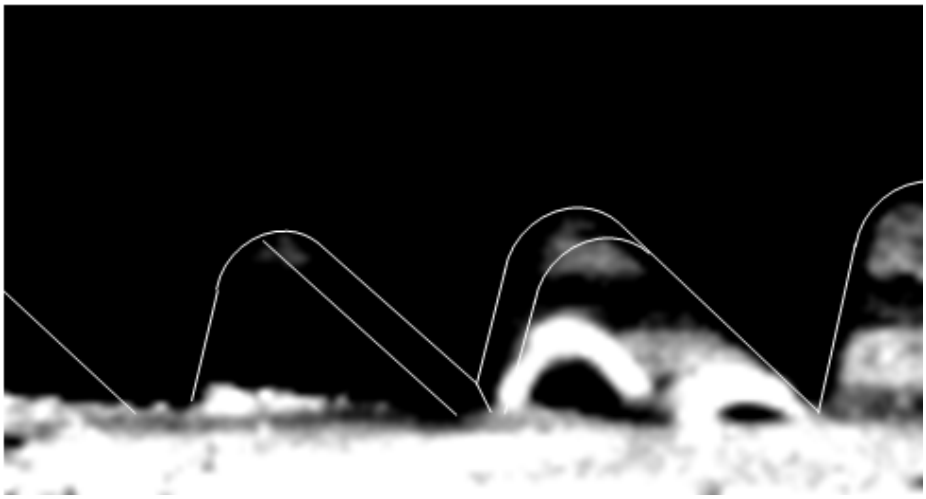
Figure 5.6 – High speed frame showing continuous chip formation for a bevelled tooth

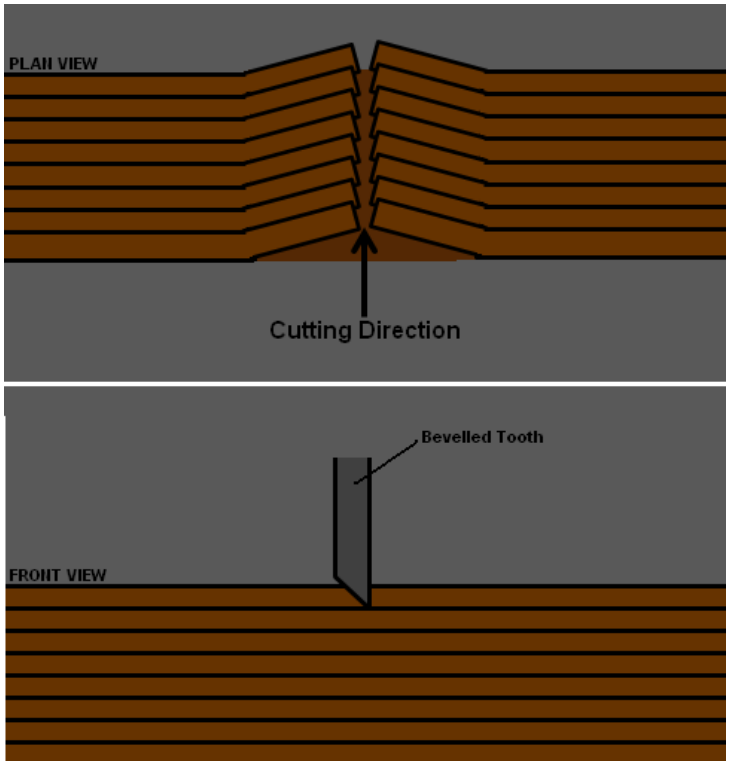

Figure 5.7 – Bevelled tooth machining across the grain

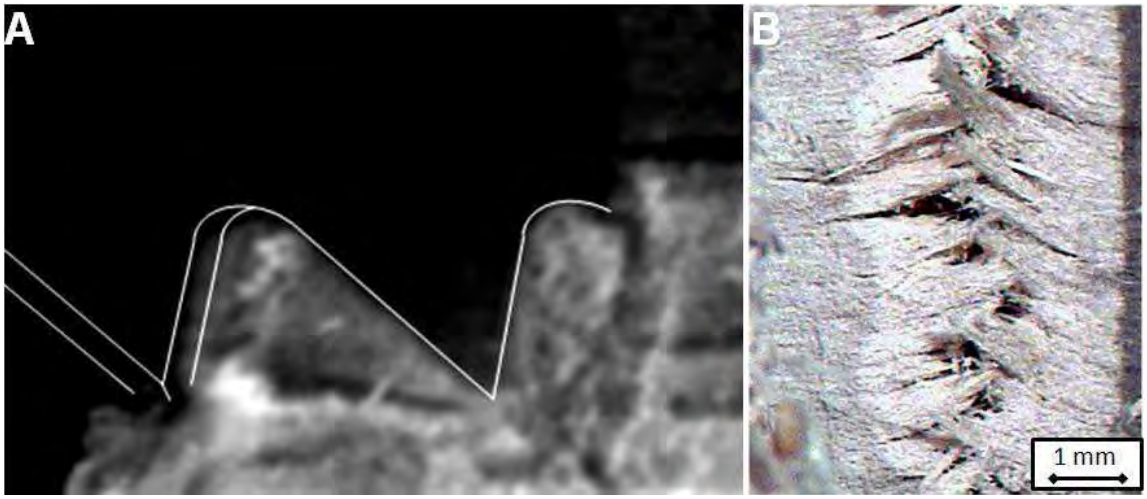

Figure 5.8 – A) High speed frame of a bevelled tooth cutting across the grain, B) Microscope image of surface formation post cut

CHAPTER 6
CONCLUSIONS AND FURTHER WORK

6.1 Conclusions

- Predictive cutting force models were developed using mechanical properties as predictors. The model for along the grain used shear properties and yielded R^2 of 80%. The model for across the grain used bending properties and yielded R^2 of 90%.
- Regression modelling was also used to predict cutting forces using tooth geometry parameters as predictors. Only one species of wood was used. Several permutations of parameters were used to develop models. The highest R^2 value yielded was 90%.
- Cutting along the grain with un-bevelled (orthogonal) teeth can be described as a shearing process. This has been proven both visually through high speed footage / microscope images and numerically through the statistically valid regression models.
- Cutting along the grain with bevelled tooth geometries can also be described as a shearing process. The chip formation is continuous (similar to un-bevelled teeth) the only difference is that the chip is formed at a tangent of 28º to the tool path.
- The un-bevelled geometry produces chip formation in the direction of the tool path. This forces the chip into the gullet hence efficiently removes material from the kerf. The bevelled tooth geometries do not effectively remove material from the kerf.
- Cutting across the grain with un-bevelled (orthogonal) teeth can be described as a bending process. Once again this has been proven both visually through high speed footage / microscope images and numerically through the regression models.
- The surface formation across the grain for the bevelled tooth reveals a visibly narrower kerf when compared to the un-bevelled tooth. This is because throughout the cutting process a smaller tooth contact area is maintained with the work-piece.

- The surface formation across the grain for the bevelled tooth exhibits less deformation prior to fracture than the un-bevelled tooth. This is because only one lateral cutting edge interacts with the work-piece (compared to two lateral edges for un-bevelled).
- The numerical analysis exhibit positive linear trends between both the tool contact area and the lateral edge contact length with respect to the cutting force. This explains why less deformation occurs when cutting across the grain with bevelled teeth.
- The cutting mechanics of the un-bevelled, U0º tooth geometry along the grain can be compared to "chiselling". The cutting mechanics of the bevelled, U28º tooth geometry across the grain can be compared to "knife cutting".
- The cutting mechanics of the thrice bevelled, GT tooth geometry is very similar to the mechanics for the U28°tooth geometry and hence be compared to "knife cutting". The cutting mechanics of the GT tooth much less comparable to that of the U0° tooth.
- This suggests that this type of compound tooth geometry is more suited to cutting across the grain. This contradicts the claims made by manufacturers which states that compound teeth perform equally well both along and across the grain (appendix 2).

6.2 Further Work

5.1.1 Design Optimization

In chapter 4 the following measured geometries of three different saw teeth were used to develop predictive cutting force models:

- γ - Rake angle (º)
- λ - Bevel angle (º)
- k - Cutting Edge inclination angle (º)

In the future, prototype saw teeth with multiple variations of each of these geometries could be developed. Either a full or fractional factorial experimental design for single tooth cutting could be performed. This would determine the optimum geometries for a desired low cutting force scenario.

5.2.2 Application of Regression Models

The regression model developed in chapter four could in future be used to predict the cutting forces for new proposed tooth geometries. The proposed tooth geometries here do not have bevelled rake and flank faces. Instead the tooth geometries incorporate chamfered features on both sides of the tooth. In total three new tooth geometries are proposed: C15° (figure 6.1), C22° (figure 6.2) and C30° (figure 6.3). The prefix "C" denotes that the teeth are chamfered and the following number denotes the angle at which the teeth are chamfered.

The geometric parameters for these new geometries have been used as categorical predictors in model 2 from chapter 4. The interaction between the tooth and prior machined groove (figures 6.4 - 6.6) were in addition used to determine the interaction parameters. These parameters were substituted into model 2[#] for depths of cut ranging from 0 - 0.35 mm. The predictive cutting force plots for the proposed tooth geometries (figure 6.7) are compared to the plots for the three geometries evaluated in chapter 4 (figure 6.8).

This brief exercise has identified that one of the proposed tooth geometries (C30°) yields lower predictive cutting forces than any of the teeth evaluated in chapter 4. It is hence viable to produce prototype versions of this tooth geometry for further controlled cutting tests.

[#] Model 2 (from chapter 4)

```
FV = - 240 - 237 Depth of cut (mm) + 170 Cut Perimeter (mm) - 26.5 Undeformed Area
(mm²) + 1.59 Bevel angle° + 1.03 Edge angle°+ 22.9 WPC
```

5.2.3 Additional Further Work

Related further work that goes beyond the scope of the research documented in this thesis includes:

- Wear testing and analysis of handsaw teeth.
- Studies based around the “micro” mechanical properties of wood (individual fibers).
- Process simulation and FEA.

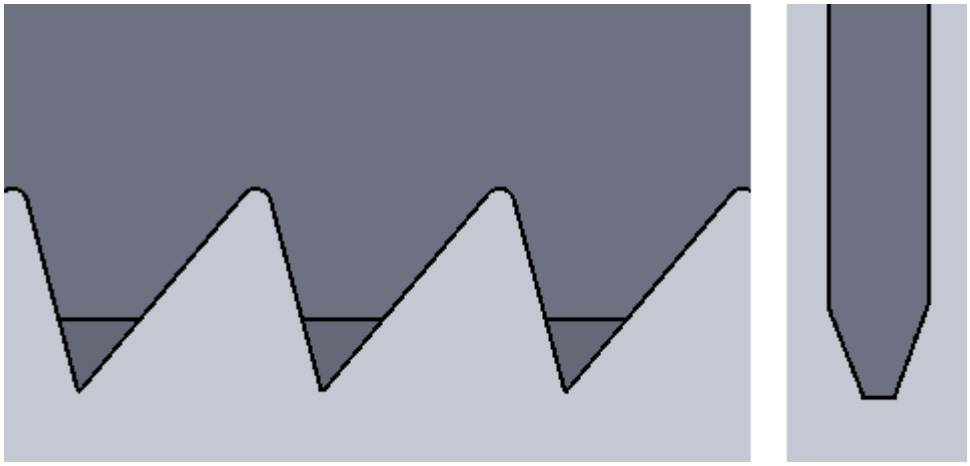

Figure 6.1 – C15° tooth geometry

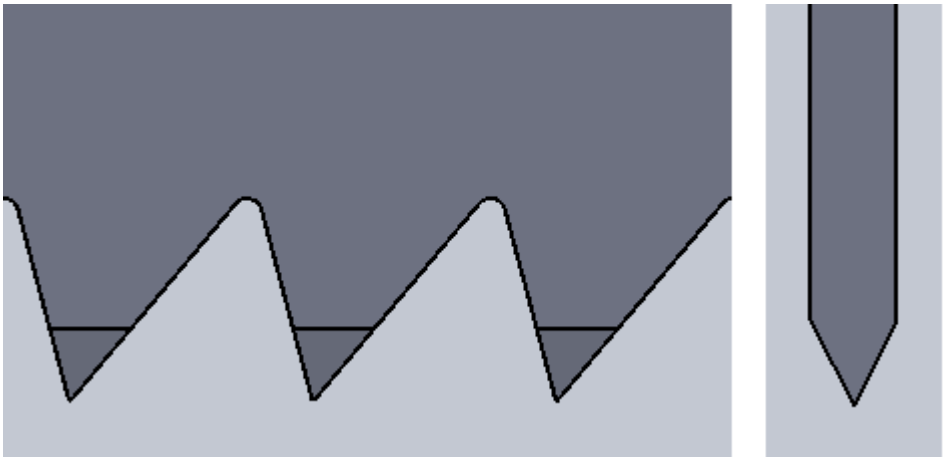

Figure 6.2 – C22° tooth geometry

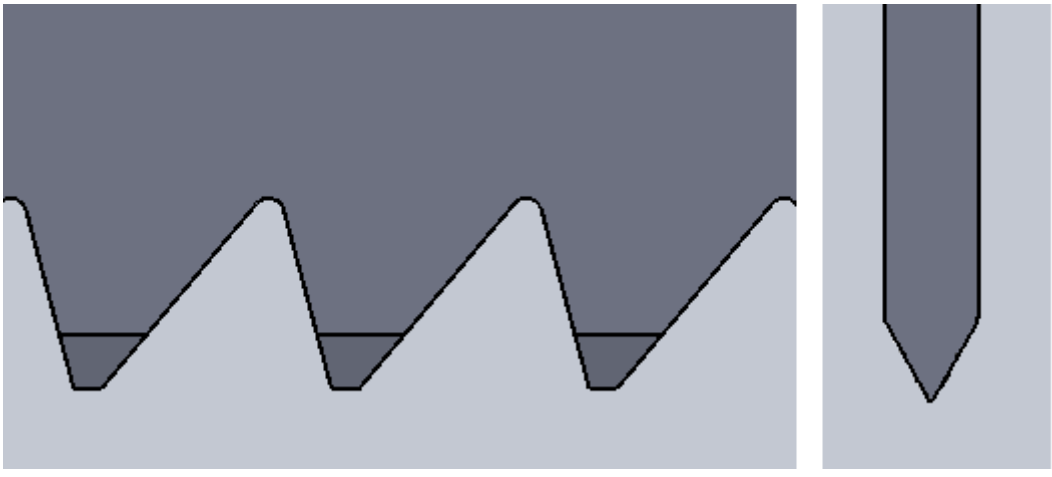

Figure 6.3 – C30° tooth geometry

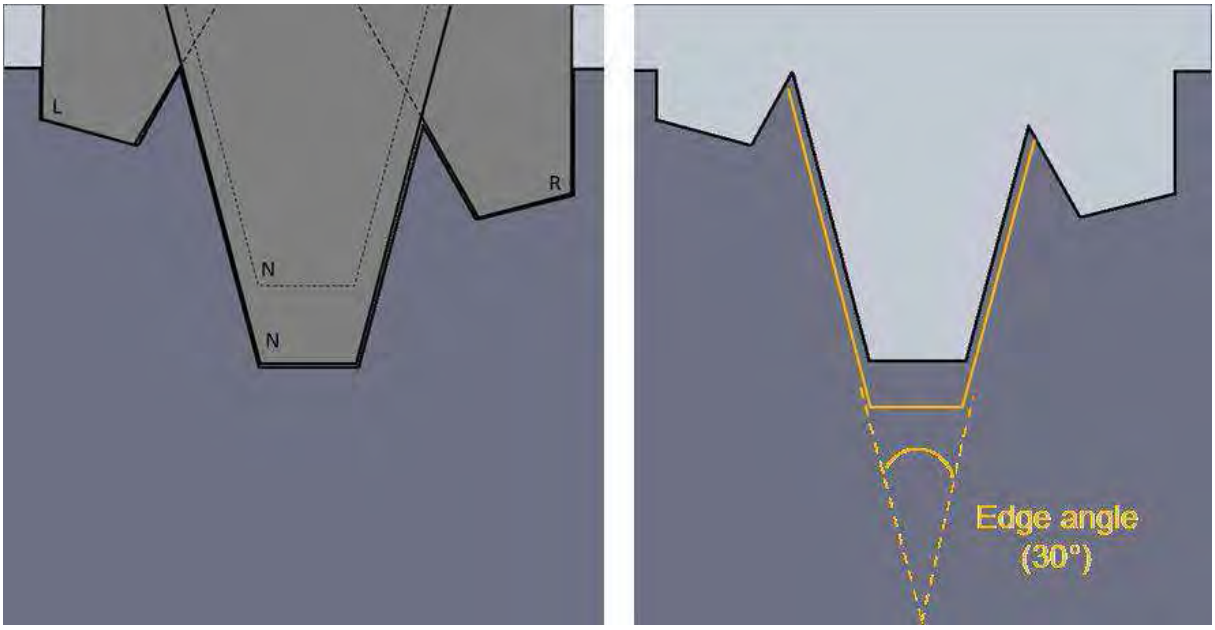

Figure 6.4 – Tool/Work-piece interaction C15°

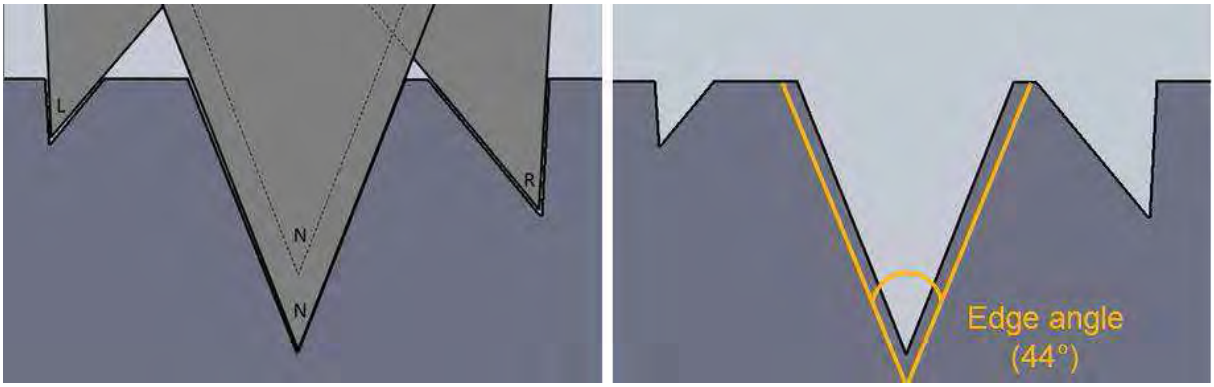

Figure 6.5 – Tool/Work-piece interaction C22°

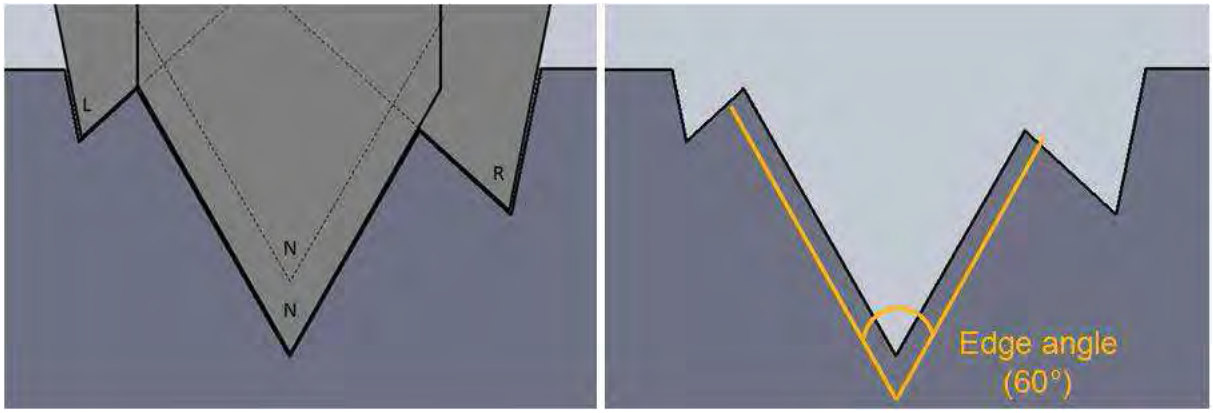

Figure 6.6 – Tool/Work-piece interaction C30°

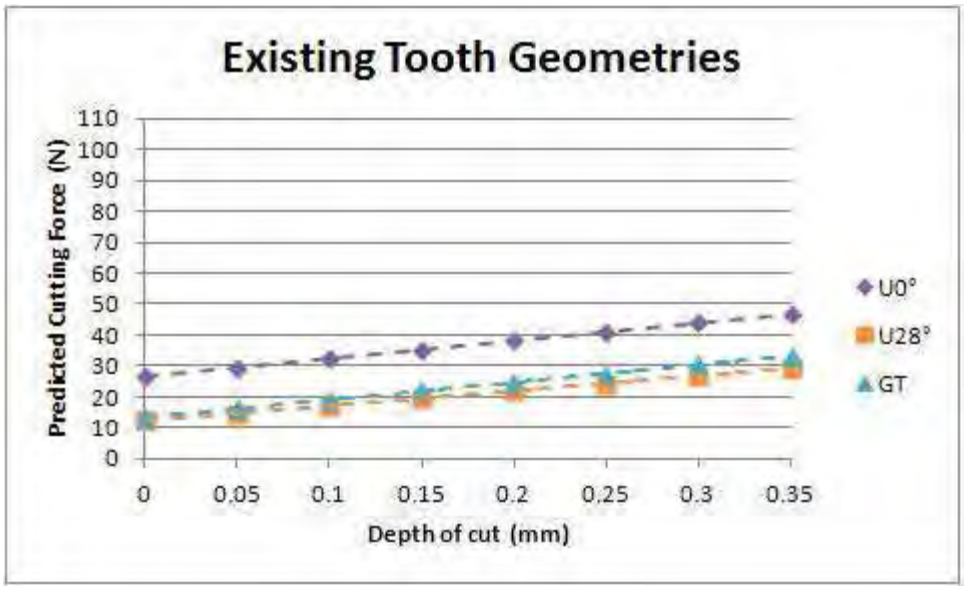

Figure 6.7 – Predictive cutting force vs. Depth of cut for geometries evaluated in chapter 4

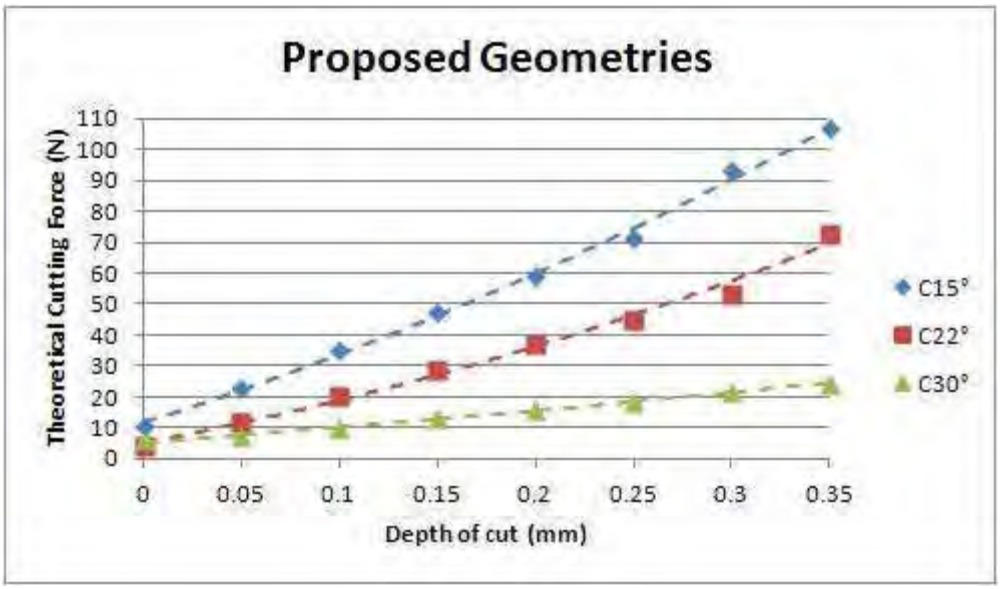

Figure 6.8 – Predictive cutting force vs. Depth of cut for new proposed tooth geometries

REFERENCES

[1] P. D. A. Jones and E. N. Simons, *Story of the Saw*. Sheffield: Spear and Jackson, Ltd, 1961.

[2] C. Suetonius-Tranquillus, "Caligula, Chapter 27," AD 119.

[3] H. Ernst, "Physics of Metal Cutting," in *National Metal Congress - American Society for Metals* Detroit, 1938.

[4] E. Merchant, "Basic Mechanics of the Metal-Cutting Process," *Journal of Applied Mechanics, ASME,* vol. 66, pp. 168-175, 1944.

[5] L. Cristóvão, O. Broman, A. Grönlund, M. Ekevad, and R. Sitoe, "Main cutting force for two species of tropical wood," in *20th International wood machining seminar* Skellefteå, Sweden, 2011.

[6] I. Lhate, L. Cristóvão, M. Ekevad, and R. Sitoe, "Cutting forces for wood of lesser used speceis from Mozambique," in *20th International wood machining seminar* Skellefteå, Sweden, 2011.

[7] B. Porankiewicz, B. Axelsson, A. Grönlund, and B. Marklund, "Main and normal cutting forces by machining wood of Pinus sylvestris," *BioResources,* vol. 6, pp. 3687-3713, 2011.

[8] I. Cooz and R. W. Meyer, "Cutting forces for tension and normal wood of maple," *Forest Products Journal,* vol. 56, pp. 26-34, 2006.

[9] M. Ekevad and B. Marklund, "Lateral cutting forces for different tooth geometreis and cutting directions," in *20th International wood machining seminar* Skellefteå Sweden, 2011.

[10] M. Ekevad, B. Marklund, and P. Gren, "Wood chip formation in circular saw blades studied by high speed photography," in *20th International wood machining seminar* Skellefteå, Sweden, 2011.

[11] M. F. Ashby and L. J. Gibson, *Cellular Solids: Structure and Properties*: Cambridge University Press, 1988.

[12] M. McBroom, "Wood Science - Chapter 3: The Woody Cell Wall," *Stephen F. Austin State University,* 2008.

[13] C. W. McMillin, "SEM technique for displaying the three-dimensional structure of wood," *Wood Science,* vol. 9, pp. 201-204, 1977.

[14] G. Modzel, F. Kamke, and F. De Carlo, "Comparative analysis of a wood: adhesive bondline," in *Wood Science and Technology*, 2010.

[15] K. Ando and H. Onda, "Mechanism for deformation of wood as a honeycomb structure I: Effect of anatomy on the initial deformation process during radial compression," *Journal of Wood Science,* vol. 45, pp. 120-126, 1999.

[16] C. Lehringer, G. Daniel, and U. Schmitt, "TEM/FE-SEM studies on tension wood fibres of Acer spp., Fagus sylvatica L. and Quercus robur L," *Wood Science and Technology,* vol. 43, pp. 691-702, 2009.

[17] The-University-of-Cambridge-(2006), "*The structure and mechanical behaviour of wood* - Available at: http://www.doitpoms.ac.uk/tlplib/wood/index.php " Accessed: 05 March 2010.

[18] M. P. Frankis, "Generic Inter-Relationships in Pinaceae," *Notes Royal Botanical Garden Edinburgh,* vol. 45, pp. 527-548, 1988.

[19] E. Wheeler, K. H. J. Buschow, W. C. Robert, C. F. Merton, I. Bernard, J. K. Edward, M. Subhash, and V. Patrick, "Wood: Macroscopic Anatomy," in *Encyclopedia of Materials: Science and Technology* Oxford: Elsevier, 2001, pp. 9653-9657.

[20] L. Finér, H. Mannerkoski, S. Piirainen, and M. Starr, "Carbon and nitrogen pools in an old-growth, Norway spruce mixed forest in eastern Finland and changes associated with clear-cutting," *Forest Ecology and Management,* vol. 174, pp. 51-63, 2003.
[21] K. Karlsson, "Height growth patterns of Scots pine and Norway spruce in the coastal areas of western Finland," *Forest Ecology and Management,* vol. 135, pp. 205-216, 2000.
[22] K. Nyström and M. Kexi, "Individual tree basal area growth models for young stands of Norway spruce in Sweden," *Forest Ecology and Management,* vol. 97, pp. 173-185, 1997.
[23] J. Puhe, "Growth and development of the root system of Norway spruce (Picea abies) in forest stands--a review," *Forest Ecology and Management,* vol. 175, pp. 253-273, 2003.
[24] R. A. Monserud and H. Sterba, "A basal area increment model for individual trees growing in even- and uneven-aged forest stands in Austria," *Forest Ecology and Management,* vol. 80, pp. 57-80, 1996.
[25] P. R. Ratcliffe and G. F. Peterken, "The potential for biodiversity in British upland spruce forests," *Forest Ecology and Management,* vol. 79, pp. 153-160, 1995.
[26] E. J. White, "Relationship between height growth of Scots pine (Pinus sylvestris L.) and site factors in Great Britain," *Forest Ecology and Management,* vol. 4, pp. 225-245, 1982.
[27] British-Standards-Institute, "BS EN 338: Structural timber - Strength classes," London, 2003.
[28] British-Standards-Institute, "BS EN 1912: Structural timber - Strength classes - Assignment of visual grades and species," London, 1998.
[29] British-Standards-Institute, "BS EN 14081-1: Timber structures - Strength graded structural timber with rectangular cross section - Part 1: General requirements," London, 2005.
[30] P. Ahlgren, J. Wood, and D. Goring, "The fiber saturation point of various morphological subdivisions of Douglas-fir and aspen wood," *Wood Science and Technology,* vol. 6, pp. 81-84, 1972.
[31] British-Standards-Institute, "BS 5268-2: Structural use of timber - Part 2: Code of practice for permissible stress design, materials and workmanship," London, 2002.
[32] British-Standards-Institute, "BS EN 13183-1: Moisture content of a piece of sawn timber - Part 1: Determination by oven dry method," London, 2002.
[33] British-Standards-Institute, "BS EN 13183-2: Moisture content of a piece of sawn timber - Part 2: Estimation by electrical resistance method," London, 2002.
[34] G. L. Amos, "Silica in timbers," *Division of Forest Products, Commonwealth Scientific and Industrial Research Organization, Australia,* 1951.
[35] G. Scarascia-Mugnozza, R. Valentiny, E. Kuzminski, and E. Giordano, "Freezing mechanisms, acclimation processes and cold injury in Eucalyptus species planted in the Mediterranean region," *Forest Ecology and Management,* vol. 29, pp. 81-94, 1989.
[36] J. Oja, L. Wallbäcks, S. Grundberg, E. Hägerdal, and A. Grönlund, "Automatic grading of Scots pine (Pinus sylvestris L.) sawlogs using an industrial X-ray log scanner," *Computers and Electronics in Agriculture,* vol. 41, pp. 63-75, 2003.
[37] J. Flodin, J. Oja, and A. Grönlund, "Fingerprint traceability of sawn products using x-ray log scanning and sawn timber surface scanning," in *Proceedings of the 53rd conference on Quality Control for Wood and Wood Products* Warsaw, Poland, 2007.
[38] M. Magnusson Seger and P.-E. Danielsson, "Scanning of logs with linear cone-beam tomography," *Computers and Electronics in Agriculture,* vol. 41, pp. 45-62, 2003.

[39] F. Longuetaud, J.-M. Leban, F. Mothe, E. Kerrien, and M.-O. Berger, "Automatic detection of pith on CT images of spruce logs," *Computers and Electronics in Agriculture,* vol. 44, pp. 107-119, 2004.
[40] F. Longuetaud, F. Mothe, and J.-M. Leban, "Automatic detection of the heartwood/sapwood boundary within Norway spruce (Picea abies (L.) Karst.) logs by means of CT images," *Computers and Electronics in Agriculture,* vol. 58, pp. 100-111, 2007.
[41] L. Yu and D. Qi, "Analysis and processing of decayed log CT image based on multifractal theory," *Computers and Electronics in Agriculture,* vol. 63, pp. 147-154, 2008.
[42] S. M. Bhandarkar, T. D. Faust, and M. Tang, "Design and prototype development of a computer vision-based lumber production planning system," *Image and Vision Computing,* vol. 20, pp. 167-189, 2002.
[43] S. Thawornwong, L. G. Occeña, and D. L. Schmoldt, "Lumber value differences from reduced CT spatial resolution and simulated log sawing," *Computers and Electronics in Agriculture,* vol. 41, pp. 23-43, 2003.
[44] E. Sarigul, A. L. Abbott, and D. L. Schmoldt, "Rule-driven defect detection in CT images of hardwood logs," *Computers and Electronics in Agriculture,* vol. 41, pp. 101-119, 2003.
[45] L. Moberg, "Models of internal knot properties for Picea abies," *Forest Ecology and Management,* vol. 147, pp. 123-138, 2001.
[46] C. L. Todoroki, E. C. Lowell, and D. Dykstra, "Automated knot detection with visual post-processing of Douglas-fir veneer images," *Computers and Electronics in Agriculture,* vol. 70, pp. 163-171, 2010.
[47] M. Öhman and M. Chernykh, "Predicting the propagation of diving grain in the vicinity of sound knots," in *20th International wood machining seminar* Skellefteå, Sweden, 2011.
[48] H. T. Lyhykäinen, H. Mäkinen, A. Mäkelä, S. Pastila, A. Heikkilä, and A. Usenius, "Predicting lumber grade and by-product yields for Scots pine trees," *Forest Ecology and Management,* vol. 258, pp. 146-158, 2009.
[49] A. Kantola, S. Härkönen, H. Mäkinen, and A. Mäkelä, "Predicting timber properties from tree measurements at felling: Evaluation of the RetroSTEM model and TreeViz software for Norway spruce," *Forest Ecology and Management,* vol. 255, pp. 3524-3533, 2008.
[50] A. Reiterer and S. E. Stanzl-Tschegg, "Compressive behaviour of softwood under uniaxial loading at different orientations to the grain," *Mechanics of Materials,* vol. 33, pp. 705-715, 2001.
[51] S. Korkut, M. Akgül, and T. Dündar, "The effects of heat treatment on some technological properties of Scots pine (Pinus sylvestris L.) wood," *Bioresource Technology,* vol. 99, pp. 1861-1868, 2008.
[52] M. J. Manríquez and P. D. Moraes, "Influence of the temperature on the compression strength parallel to grain of paricá," *Construction and Building Materials,* vol. 24, pp. 99-104.
[53] S.-C. Oh, "Applying failure criteria to the strength evaluation of 3-ply laminated veneer lumber according to grain direction by uniaxial tension test," *Construction and Building Materials,* vol. 25, pp. 1480-1484.
[54] J. Galicki and M. Czech, "Tensile strength of softwood in LR orthotropy plane," *Mechanics of Materials,* vol. 37, pp. 677-686, 2005.

[55] Forest-Products-Laboratory, *Method for evaluating Shear Properties of Wood*. Madison, WI: U.S. Department of Agriculture, Forest Service, Forest Products Laboratory, 1968.
[56] British-Standards-Institute, "BS EN 408:Timber structures - Structural timber and glued laminated timber - Determination of some physical and mechanical properties " London, 2003.
[57] ASTM, "D143-09: Standard Test Methods for Small Clear Specimens of Timber," Pennsylvania, 2009.
[58] S. I. Gustafsson, "Mechanical Properties of some Swedish hard wood species," *Proceedings of the Institution of Mechanical Engineers,* vol. 215, pp. 125-131, 2001.
[59] Forest-Products-Laboratory, *Wood handbook—Wood as an engineering material, Gen. Tech. Rep. FPL–GTR–113*. Madison, WI: U.S. Department of Agriculture, Forest Service, Forest Products Laboratory, 1999.
[60] C. Coutand, G. Jeronimidis, B. Chanson, and C. Loup, "Comparison of mechanical properties of tension and opposite wood in Populus," *Wood Science and Technology,* vol. 38, pp. 11-24, 2004.
[61] A. Wechsler and S. Hiziroglu, "Some of the properties of wood-plastic composites," *Building and Environment,* vol. 42, pp. 2637-2644, 2007.
[62] AFNOR, "NF B51-012: Wood Shear Test," Paris, 1942.
[63] F. Eyma, P.-J. Méausoone, and P. Martin, "Strains and cutting forces involved in the solid wood rotating cutting process," *Journal of Materials Processing Technology,* vol. 148, pp. 220-225, 2004.
[64] D. M. Moses and H. G. L. Prion, "Anisotropic Plasticity and Failure Prediction in Wood Composites," *Paper presentation for ANSYS Inc. Ninth International Conference and Exhibition,* 2000.
[65] P. J. Méausoone, "Choice of optimal cutting conditions in wood machining using the coupled tool–material method," in *Proceedings of the 15th International Wood Machining Seminar*, 2001, pp. 37–47.
[66] N. C. Franz, *An Analysis of the Wood-Cutting Process*. Ann Arbor: University of Michigan Press, 1958.
[67] E. Kivimaa, "Cutting force in woodworking." vol. 18 Helsinki: VTT Julkaisu, 1950, p. 101.
[68] P. Koch, *Wood Machining Process*. New York: Ronald Press Co, 1964.
[69] W. M. McKenzie, "Fundamental analysis of the wood cutting process," in *Department of Wood Technology*: University of Michigan, 1961.
[70] B. Axelsson, "Lateral cutting force during machining of wood due to momentary disturbances in the wood structure and degree of wear of the cutting tool," *European Journal of Wood and Wood Products,* vol. 52, pp. 198-204, 1994.
[71] G. E. Woodson and P. Koch, "Tool Forces and Chip Formation In Orthogonal Cutting Of Loblolly Pine," U.S. Department of Agriculture, Forest Service, Southern Forest Experiment Station, New Orleans, LA 1970.
[72] B. Axelsson, Å. Lundberg, and J. Grönlund, "Studies of the main cutting force at and near a cutting edge," *European Journal of Wood and Wood Products,* vol. 51, pp. 43-48, 1993.
[73] Y. Huang, "Cutting Force Components in Orthogonal Cutting Parallel to the Grain (90-0) 1 - Effects of the Rake angles," *Mokuzai Gakkaishi,* vol. 40, pp. 1134-1140, 1994.
[74] N. C. Franz, "An Analysis of Chip Formation in Wood Machining," *Forest Products Journal,* vol. 10, pp. 332-336, 1955.

[75] G. Goli, M. Fioravanti, N. Sodini, L. Uzielli, and A. Del Taglia, "Wood Processing: a contribute to the interpretation of surface origin according to grain orientation," in *COST Action E35* Rosenheim, 2005.

[76] G. Goli, M. Fioravanti, R. Marchal, L. Uzielli, and S. Busoni, "Up-milling and down-milling wood with different grain orientations – the cutting forces behaviour," *European Journal of Wood and Wood Products,* 2009.

[77] J.-P. Costes, P. L. Ko, T. Ji, C. Decès-Petit, and Y. Altintas, "Orthogonal cutting mechanics of maple: modeling a solid wood-cutting process," *Journal of Wood Science,* vol. 50, pp. 28-34, 2004.

[78] G. Goli, L. Bleron, R. Marchal, L. Uzielli, and M. Negri, "Measurment of Cutting Forces in Routing Wood at varous Grain Angles: Initial Results with Douglas-Fir," in *Wood Science and Engineering in the Third Millennium* Transilvania University, 2002.

[79] G. Goli, R. Marchal, L. Uzielli, and M. Negri, "Measuring cutting forces in routing wood at various grain angles - Study and comparison between up- and down- milling techniques, processing Douglas Fir and Oak," in *16th International Wood Machining Seminar*, Matsue, 2003.

[80] E. H. Lee and B. W. Shaffer, "The theory of plasticity applied to a problem of machining," *Journal of Applied Mechanics, ASME,* vol. 18, pp. 405-413, 1951.

[81] G. Goli, R. Marchal, and M. Negri, "Industrial Machining of Douglas Fir with Varous Tools and Materials," in *Proceedings of the 15th International Wood Machining Seminar* Los Angeles, California, 2001.

[82] G. Goli, L. Bleron, R. Marchal, L. Uzielli, and M. Negri, "Formation and Quality of Wood Surfaces Processed at Various Grain Angles: Douglas-Fir and Oak," *Wood Structure and Properties,* pp. 91-98, 2002.

[83] G. Goli and L. Uzielli, "Mechanisms of Wood Surface Formation and Resulting Final Condition after Planing," in *Proceedings of the 2nd International Symposium on Wood Machining - Properties of Wood and Wood Composites related to Machining* Vienna, 2004.

[84] G. Goli, R. Marchal, M. Negri, and J.-P. Costes, "Surface quality: comparison among visual grading and 3D roughness measurements," in *Proceedings of the 15th International Wood Machining Seminar* Los Angleles, California, 2001.

[85] W. Jin and L. Cai, "Study and analysis on cutting forces of oblique cutting of wood," *Holz Roh Werkst,* vol. 54, pp. 283-286, 1996.

[86] W. Jin and L. Cai, "Study on the normal component force in oblique cutting of wood," *Holz Roh Werkst,* vol. 55, pp. 118-120, 1997.

[87] H. A. Stewart, "Chip formation when orthogonally cutting wood against the grain," *Wood Science and Technology,* vol. 3, pp. 193-203, 1971.

[88] H. A. Stewart, "Fixed knife-pressure bar system for surfacing dry wood," *Forest Products Journal,* vol. 36, pp. 52-56, 1986.

[89] L. Fernando, "Characheristics of sugar maple wood surfaces machined with fixed-obliqe knife pressure-bar cutting system," *Wood Science and Technology,* vol. 41, pp. 17-29, 2007.

[90] L. de Moura and R. Herandez, "Charachteristics of sugar maple wood surfaces produced by helical planing," *Wood and Fiber Science,* vol. 38, pp. 166-178, 2006.

[91] R. Fischer, C. Gottlöber, M. Oertel, A. Wagenführ, and W. Darmawan, "Effects of wood cutting with extreme inclined cutting edges," in *20th International wood machining seminar* Skellefteå, Sweden, 2011.

[92] B. E. Klamecki, "A review of wood cutting tool literature," *Holz als Roh - und Werkstoff,* vol. 37, pp. 265-276, 1979.

[93] J. A. Bailey, A. E. Bayoumi, and J. S. Stewart, "Wear of some cemented tungsten carbide tools in machining oak " *Wear,* vol. 85, pp. 69-79, 1983.
[94] A. E. Bayoumi, J. A. Bailey, and J. S. Stewart, "Comparison of the wear resistance of various grades of cemented carbides that may find application in wood machining," *Wear,* vol. 89, pp. 185-200, 1983.
[95] A. E. Bayoumi, J. A. Bailey, and J. S. Stewart, "Comparison of the wear resistance of selected steels and cemented carbide cutting tool materials in machining wood," *Wear,* vol. 105, pp. 133-144, 1985.
[96] G. D. Mohan and B. E. Klamecki, "The susceptibility of wood-cutting tools to corrosive wear," *Wear,* vol. 74, pp. 85-92, 1982.
[97] M. Scholl and P. Clayton, "Wear behaviour of wood cutting edges," *Wear,* vol. 120, pp. 221-232, 1987.
[98] W. M. McKenzie and W. E. Hillis, "Evidence of chemical acceleration of wear in cutting plant materials," *Wear,* vol. 8, pp. 238-243, 1965.
[99] C. Müller, R. Deetz, U. Schwarz, and V. Thole, "Agricultural residues in panel production - Impact of ash and silica content," in *20th Internationa wood machining seminar* Skellefteå, Sweden, 2011.
[100] M. Gauvent, P. J. Méausoone, and P. Brenot, "Corrosion of materials used as cutting tools of wood," *WEAR,* vol. 261, pp. 1051 - 1055, 2006.
[101] W. M. McKenzie and R. L. Crowling, "The early stages of edge wear in cutting wood," in *IUFRO - Section 41 Meeting*, 1969.
[102] G. Pahlitzsch and H. Jostmeier, "Beobachtugen uber das - Abstumphfungsverhalten beim Fasen von Schichtstoff-Verbundplatten," *Holz Roh Werkst,* vol. 23, pp. 121-125, 1965.
[103] E. Bartz and H. Breier, "Kurzverfahren zur prufung der Vershliebwirkung und der Zerspanberkeit von holz und holzwersktoffen," *Holz Roh Werkst,* vol. 27, pp. 148-152, 1969.
[104] H. Bier and P. Hanicke, "Die speizifiche schnittkraftals funktion der shneidenabstumphfung beim frasen " *Holztechnologie,* vol. 4, pp. 158-162, 1963.
[105] W. M. McKenzie and R. L. Cowling, "A factorial experiment in transverse-plane (90-90) cutting of wood: part 1 - cutting force and edge wear," *Wood and Fiber Science,* vol. 3, pp. 204-213, 1971.
[106] British-Standards-Institute, "BS 3159-1: Woodworking saws for hand use - Part 1: Specification for hand saws," London, 1999.
[107] S. J. Lundstrum, "Balanced Saw Performance," United States Department of Agriculture - Forest Service, Madison, WI 1985.
[108] C. Andersson, M. T. Andersson, and J. E. Ståhl, "Bandsawing. Part I: cutting force model including effects of positional errors, tool dynamics and wear," *International Journal of Machine Tools and Manufacture,* vol. 41, pp. 227-236, 2001.
[109] W. M. McKenzie, "Effects of bevelling the teeth of rip saws," *Wood Science and Technology,* vol. 34, pp. 125-133, 2000.
[110] J. Ratnasingam and F. Scholz, "Optimising the cutting of tension wood in rubberwood: An economic and quality perspective," in *20th International wood machining seminar* Skellefteå, Sweden, 2011.
[111] S. Loehnertz and I. Cooz, "Sawtooth forces in cutting tropical hardwoods native to South America," *FPL – RP – 567,* p. 16 p, 1998.
[112] T. J. Ko and H. S. Kim, "Mechanistic cutting force model in band sawing," *International Journal of Machine Tools and Manufacture,* vol. 39, pp. 1185-1197, 1999.

[113] K. Orlowski, T. Ochrymiuk, and A. Atkins, "Applications of fracture mechanics for energetic effects predictions while wood sawing," in *20th International wood machining seminar* Skellefteå, Sweden, 2011.
[114] K. Orlowski and B. Palubicki, "Recent progress in research on the cutting processes of wood," *Holzforschung,* vol. 63, pp. 181-185, 2009.
[115] I. Vazquez-Cooz and R. W. Meyer, "Cutting forces for tension and normal wood of maple," *Forest Products Journal,* vol. 56, pp. 26-34, 2006.
[116] R. Okai, S. J. Mitchual, and K. Frimpong-Mensah, "Optimisation techniques for minimising saw teeth deflection and lumber thickness variation," *Precision Engineering,* vol. 30, pp. 39-46, 2006.
[117] C. Andersson, J. E. Ståhl, and H. Hellbergh, "Bandsawing. Part II: detecting positional errors, tool dynamics and wear by cutting force measurement," *International Journal of Machine Tools and Manufacture,* vol. 41, pp. 237-253, 2001.

APPENDIX 1 – PUBLICATIONS

Journal Articles

1. Naylor, A. Hackney, P. Perera, N. and Clahr E. 2012. A Predictive Model for the Cutting Force in Wood Machining Developed using Mechanical Properties. *BioRes. 7:2883-2894*

A PREDICTIVE MODEL FOR THE CUTTING FORCE IN WOOD MACHINING DEVELOPED USING MECHANICAL PROPERTIES

Andrew Naylor,[a,*] Phil Hackney,[a] Noel Perera,[a] and Emil Clahr [b]

In this study a number of work-piece variations were evaluated whilst limiting the cutting conditions. Eight wood species controlled at four moisture levels were machined along and across the wood grain. The tool used during cutting was designed to resemble a rip saw tooth with zero rake angle and narrow edge width. Each work-piece variation machined in the cutting tests was subjected to mechanical tests that evaluated bending properties across the grain and shear properties along the grain. The regression model establishes a relationship between the bending properties for cutting forces across the grain, as well as shear properties for cutting forces along the grain. F and R^2 values show that the elastic properties of the wood in bending and shear have less influence on the cutting forces when compared to the strength and toughness. Additionally, density is seen to have less influence on the cutting force along the grain. This is explained by the tool passing through an unquantifiable proportion of early and latewood fibers from the annual growth rings. Cutting across the grain, the tool is forced to machine through approximately the same proportion of earlywood and latewood fibres.

Keywords: Wood machining; Manual wood sawing; Mechanical testing; Regression modeling

Contact information: a: School of Computing, Engineering and Information Sciences, Ellison Building, Northumbria University, Newcastle Upon Tyne, NE1 8ST, United Kingdom; b: Research and Development Centre for Wood Working, SNA Europe, Box 1103 82113 Bollnäs, Sweden
**Corresponding author: andrew2.naylor@northumbria.ac.uk*

INTRODUCTION

Fundamental wood machining research typically uses characterized chip formation, coupled with tool forces in order to explain the cutting mechanics. Franz (1955; 1958) characterized chip formation along the grain (90° to 0°) with varied rake angles and edge radii, concluding that although all chip types observed have very different characteristics, the primary cutting mechanics machining in this direction is shearing. Woodson and Koch (1970) evaluated the chip formation across the grain (0° to 90°) by means of a veneer peeling case study. They concluded that the chip is formed by an initial tear caused by compression, followed by an ongoing shearing process with some tensile failure. McKenzie (1961) studied the cutting mechanics machining the wood end grain (90° to 90°) with the observation that the chip is formed by a tensile failure mode, causing parallel gaps to propagate between the wood fibers. All of these studies implemented the use of planning tools, removing wood across the entire width of the work-piece. Furthermore, none of these studies have thoroughly investigated the influence of mechanical properties on tool forces.

A2

More recent research (Axelsson *et al.* 1991; Cristovao *et al.* 2011) looks at the effects of moisture content and density on tool forces. In these studies the density is measured by taking grayscale images of the internal wood structure using CT scanning. Additionally, wood fracture mechanics during sawing has been investigated (Orlowski *et al.* 2009, 2011). Loehnertz and Cooz (1998) recorded saw tooth cutting, thrust, and side forces for many hardwood species. This study focused on the machining the wood end grain (sawmill applications) for dry and saturated work-pieces. Eyma *et al.* (2004, 2005) used density and hardness combined with mechanical properties obtained parallel to the grain such as: shear stress, compressive stress, elastic modulus, and toughness to develop cutting force relationships.

Published work (Naylor *et al.* 2011) details the findings of cutting tests performed in the test rig described in the methodology. Optical microscope images of the chip formed cutting along the grain are comparable to the chip formation types characterized by Franz (1955, 1958). Dry work-pieces are noted to be the cause of the discontinuous and broken chips whilst work-pieces with higher moisture content are seen to yield the fuzzy chip types. The continuous chips are produced by machining wood at moisture content ranging from 10 to 20%. Observed surface formation cutting across the grain does not bear any resemblance to the chip observed by Woodson and Koch (1970); instead, a bending of the wood fibers perpendicular to the grain is seen. Furthermore, it is observed that increased moisture content leads to an increase in elasticity, causing the fibers to spring back and cover the machined tool path.

The existing body of work often has a limited consideration for the effects of multiple mechanical properties on the tool forces. Furthermore, often only one wood grain direction and/or species is selected as the work-piece. In this study, properties obtained using a longitudinal shear methodology was used as parameters for predicting cutting force along the grain. Properties obtained via a three-point bending test methodology were used as parameters for predicting cutting force across the grain. Multiple wood species and moisture levels were used.

EXPERIMENTAL METHODOLOGY

The experimental test rig comprised of a cutting tool driven by a 3-axis CNC router machine. The tool was rigidly attached to the actuating arm of the router machine and was driven at a single speed of 100 mm/s for each cut performed. The work-piece was mounted on a force dynamometer equipped with piezoelectric load cells that measured the cutting, thrust, and side force components acting on the tool. Only the cutting and thrust force components were taken into consideration for this analysis. The test rig schematic diagram (Fig. 1) details the set-up of the data acquisition system. To obtain tool force data, the cutting tool **(1)** was used to machine through the work-piece attached to the force dynamometer **(2)**. The three piezoelectric transducers in the dynamometer each generated a charge in response to the cutting forces (3.9 pC/1 N in X and Y directions, 1.95 pC/1 N in the Z direction). These signals fed into the charge amplifier **(3)**, where the signals were calibrated for a 10V input to the data acquisition PLC **(4)** (3900 pC/10 V in X and Y directions, 1950 pC/10 V in Z direction: Hence 1 N =

0.01 V). The PLC converted the signals from analogue to digital, and the data was then analysed using LabView signal express software **(5)**.

The high speed steel tool used in the experiment has geometry similar to the hand-saw rip tooth formation (Fig. 2). The tool has an orthogonal cutting edge with a width of 1 mm and a rake angle (α) of zero. To ensure that the cutting edge was sharp, the tool was sharpened using precision grinding equipment prior to performing the test runs. The two machining directions selected for the experiment were 90° to 0° (along the grain) and 0° to 90° (across the grain) as these are deemed to be the most common directions for manual wood sawing. This is specifically relevant to the scope of this author's research into the performance of individual handsaw teeth. Machining was performed along and across the radial wood plane rather than the tangential. This is because the ratio of earlywood to latewood bands on the radial plane is approximately 1:1; it was expected that the tool would pass through both earlywood and latewood fibres. Eight species of wood were evaluated in the experiment: five softwoods (Scots pine, yellow pine, Siberian larch, Douglas fir, and western red cedar) and three hardwoods (ash, beech, and sapele). Each of these wood species had four separate moisture levels: DRY (≈6%), 10%, 20%, and SATURATED (>30%). Including the two machining directions, this amounts to 64 work-piece variables. Each of the 64 work-piece variations were machined at three cut depths: 0.4, 0.8, and 1.2 mm, providing a total of 192 cutting force values for analysis.

Moisture content was determined electronically using a hand held protimeter. An average was taken of a minimum of six measurements from the radial plane of each wood work-piece at a minimum depth of 5 mm. Density was determined through manual measurements of the work-piece using a digital vernier calliper combined with measurement of the mass using calibrated electronic scales. A minimum of six depth and breadth measurements were taken from various positions for a specified work-piece length. The average depth, breadth, and length were used to estimate the volume of the work-piece. The general equation: $\rho = m/v$ (kg/m^3), was used to determine the final density value.

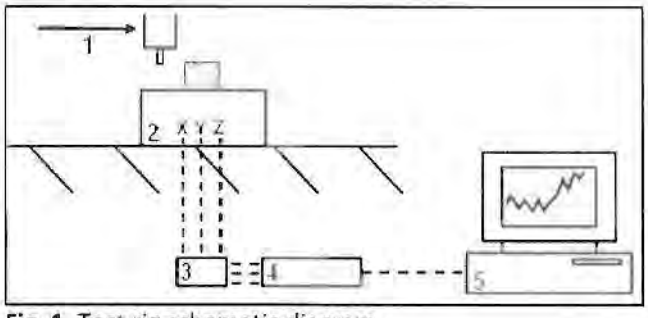

Fig. 1. Test rig schematic diagram

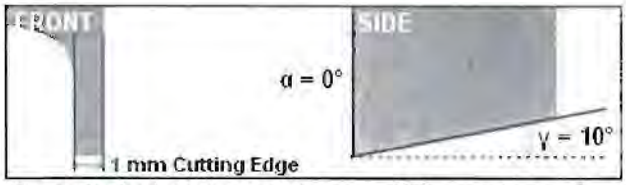

Fig. 2. Optical microscope images of the cutting tool

A4

Only clear specimens of each selected wood species were used as test samples for mechanical testing. This was to eliminate the detrimental effects of knots or distorted grain on the obtained results. A total of 32 work-piece variations were evaluated for each mechanical test. This was based upon the eight wood species and four moisture variations. No repeats were performed for any given variation however the test sequence was randomised to eliminate any systematic error.

ASTM D143-09 (2009) standard test procedures for longitudinal shear (Fig. 3) and three-point bending (Fig. 4) were carried out in a universal testing machine to characterize wood strength across and along the grain, respectively. The longitudinal shear specimen is placed between the crosshead of the testing machine and an anvil allowing the wood to shear parallel to the grain direction. A 0.6 mm/min crosshead speed was maintained throughout testing until failure. Derived shear stress and strain, Eq.1 and Eq.2 respectively, are noted. The span (L) of the three-point bending specimens was limited to 300 mm with a 20 mm depth (d); this is in keeping with the specified 14:1 minimum span to depth ratio. An additional criterion that was also specified by the standard was a 1.3 mm/min crosshead maintained throughout testing until failure. Derived bending stress and strain, Eq.3 and Eq.4 respectively, are also noted.

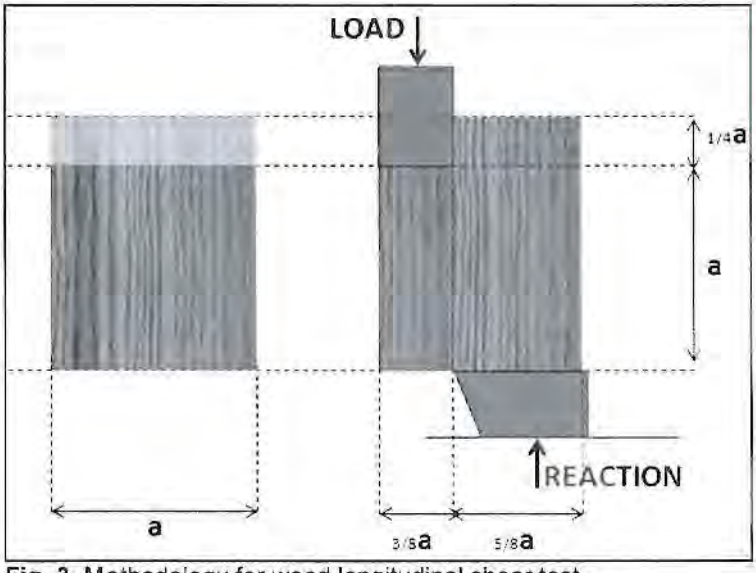

Fig. 3. Methodology for wood longitudinal shear test

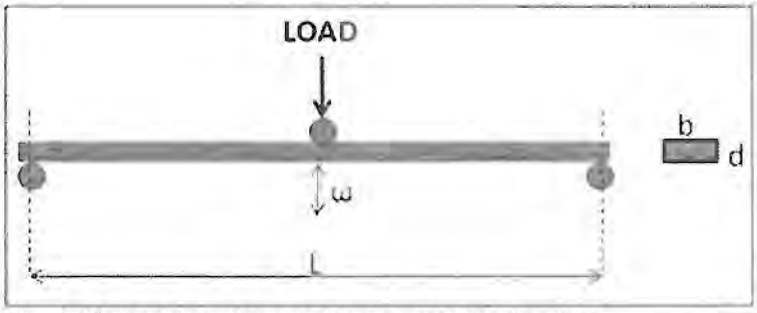

Fig. 4. Methodology for wood three-point bending test

Measurements of recorded Force (**F**) vs. Displacement (ω) were taken by the universal testing machine. Each **F** vs. ω plot was easily converted to a Stress vs. Strain plot, with the curve taking the form of a quadratic polynomial. The gradient of the plot in the linear elastic region provided the modulus of elasticity (**MOE**) for bending and the shear modulus (**G**). Likewise the modulus of rupture (**MOR**) for bending and the shear strength (τ) were taken as the stress at point of fracture. Toughness (**U**) was obtained by taking a definite integral of the function between zero and point of fracture (**n**) (Eq. 5).

The prepared wood specimens for the three point bending tests, longitudinal shear tests, and controlled cutting tests were carefully cut from the same one meter length of timber. This was to ensure that the mechanical properties and cutting forces obtained were for near identical work-pieces. In summary, the observed response taken from the cutting tests was the tool force in the direction of cutting. The controlled variables were machining direction, moisture content (**MC**), and depth of cut (**δ**) with the measured variables of mechanical properties and density (**ρ**). Each work-piece was machined along and across the grain, disregarding the wood end-grain direction. The model parameters acted as predictors for two separate models cutting along and across the grain.

$$\gamma = \frac{\omega}{3/8\,a} \tag{1}$$

$$\tau = \frac{F}{a^2} \tag{2}$$

$$\sigma = \frac{3FL}{2bd^2} \tag{3}$$

$$\varepsilon = \frac{6\omega d}{L^2} \tag{4}$$

$$U = \int_n^0 f(\varepsilon) = \int_n^0 a\varepsilon^2 + b\varepsilon + c \tag{5}$$

STATISTICAL METHODS

Multiple least squares method was used to develop the regression models based upon several categorical predictors. In both cases, force in the direction of cutting, **Fc** (N), was the measured response with **MOE**, **MOR**, **ρ**, **Ub**, **MC**, and **δ** as predictors for the model across the grain and **G**, **τ**, **ρ**, **Us**, **MC**, and **δ** as predictors for the model along the grain (Table 1).

Simple least squares method was subsequently used to weight the effects of the obtained mechanical properties on the cutting force. Specific cutting force (**Fsp**) defined as force over depth of cut was used as the response value for the selected categorical predictors. Across the grain these predictors are: **MOE**, **MOR**, **ρ**, and **Kb**. Along the

grain the predictors are; **G**, **τ**, **ρ**, and **Ks**. Moisture content was not selected for these trials in order to keep an emphasis on the properties obtained through mechanical testing. The **F** and $\mathbf{R^2}$ values were used to quantify the influence of the obtained mechanical properties on the predicted cutting force (Eq. 6 and Eq. 7).

Table 1. Categorical Predictors Used for Regression Models

Symbol	*Description*	*Units*
MOR	Bending strength across the grain	MPa
τ	Shear strength along the grain	MPa
MOE	Bending elastic modulus across the grain	MPa
G	Shear elastic modulus along the grain	MPa
Ub	Bending toughness across the grain	J/m^2
Us	Shear toughness along the grain	J/m^2
MC	Moisture content	%
δ	Depth of cut	mm

$$\text{F Value} = \frac{\text{explained variance}}{\text{unexplained variance}} = \frac{MS_{REG}}{MS_{RES}} \quad (6)$$

$$R^2 = \frac{SS_{REG}}{(SS_{REG} + SS_{RES})} \quad (7)$$

RESULTS

Mechanical Properties

For all moisture levels evaluated, the mean values for **MOR** range from 50 to 90 MPa. A linear decrease was observed for increased moisture content, with the highest values yielded by the three hardwood species tested, on average 70% greater than the softwood values. The mean values **MOE** ranged from 40000 to 80000 MPa, with a linear decrease observed for increased moisture content. There was no discernable pattern to suggest that the hardwoods yield higher **MOE** values than the softwoods. **Ub** on average ranged from 29000 to 50000 J/m^2. Once again a linear decrease in magnitude was observed for increased moisture content. The hardwoods yielded significantly higher values, on average 120% greater than the softwood values.

The mean **τ** values ranged from 5 to 12 MPa. The highest values represented the three hardwoods tested, which were approximately 45% greater than the softwoods. Furthermore a linear decrease in strength was observed with an increase in moisture content. The mean **G** values ranged from 15 to 230 MPa with the larger values once again representing the hardwoods. These values were approximately 50% greater than the softwoods. **G** was significantly influenced by moisture content with the average values obtained for the saturated work-pieces measuring only 6% the magnitude of the values obtained for the dry work-pieces. **Us** on average ranges from 18000 to 50000 J/m^2. Again a linear decrease in magnitude was observed for increased moisture content. In a similar

way to Ub, Us yielded significantly higher values for the three hardwood species tested, on average 150% greater than the softwood values.

Average values for ρ also showed a negative linear trend for increased moisture content. The hardwoods yield values approximately 45% greater in magnitude than the softwoods. For the nominal values of DRY (≈6%), 10%, and 20%; the measured moisture content values had a low standard deviation in proportion to the range. Furthermore the measured values did not deviate too far from the nominal values. The measured values for nominally SATURATED work-pieces have an average of 35% moisture content. The range and standard deviation are larger; this is due to the variation in wood fibre saturation for the different species.

Table.2. Obtained Mechanical Properties

	Species	MOE (MPa)	MOR (MPa)	Ub (J/m^2)	G (MPa)	τ (MPa)	Us (J/m^2)	ρ (kg/m^3)	MC (%)
DRY (NOMINAL)	Scots Pine	62800	79.21	33250	151.47	9.53	26650	576.64	6.00
	Yellow Pine	50800	47.72	24910	286.27	6.28	17100	484.80	6.00
	Douglas Fir	69200	72.01	49000	236.51	7.58	34080	496.62	6.00
	Western Red Cedar	91500	99.28	40600	52.78	8.62	31730	671.57	6.00
	Siberian Larch	73300	65.24	49020	260.16	9.31	54000	638.46	6.00
	Ash	57500	105.57	84000	277.03	17.06	94300	912.87	6.00
	Beech	88900	127.44	61750	363.83	15.55	86400	669.00	6.00
	Sapele	78000	92.73	58050	219.11	18.17	57200	819.08	6.00
	AVERAGE	**71500**	**86.15**	**50070**	**230.90**	**11.51**	**50180**	**658.63**	**6.50**
	RANGE	**40700**	**79.72**	**59090**	**311.05**	**11.89**	**77200**	**428.07**	**2.00**
	STANDARD DEVIATION	**14400**	**25.24**	**18350**	**94.06**	**4.65**	**28200**	**148.44**	**0.93**
10% (NOMINAL)	Scots Pine	58300	61.99	21000	152.64	7.97	25200	559.04	14.00
	Yellow Pine	40300	47.62	19200	91.30	5.69	16120	436.15	11.00
	Douglas Fir	61400	58.57	24750	43.32	3.97	26850	478.93	14.00
	Western Red Cedar	39500	54.60	22100	268.98	4.76	26250	460.96	11.00
	Siberian Larch	67000	88.62	28840	208.32	10.34	27280	615.38	11.00
	Ash	82300	119.09	61740	123.21	14.20	84000	850.73	10.00
	Beech	113600	95.04	47250	211.37	14.15	60750	696.65	11.00
	Sapele	91100	113.05	45500	691.02	14.31	28600	759.75	8.00
	AVERAGE	**69200**	**79.82**	**33790**	**223.77**	**9.42**	**36880**	**607.20**	**11.25**
	RANGE	**74100**	**71.47**	**42540**	**647.70**	**10.34**	**67880**	**414.58**	**6.00**
	STANDARD DEVIATION	**25400**	**27.77**	**15670**	**202.15**	**4.43**	**23080**	**151.22**	**1.98**
20% (NOMINAL)	Scots Pine	64900	53.85	8750	128.55	10.85	15260	546.36	20.00
	Yellow Pine	32400	30.57	3840	46.22	2.22	11700	416.88	25.00
	Douglas Fir	44700	40.92	20470	152.23	4.85	21000	462.60	25.00
	Western Red Cedar	46900	56.63	10330	138.98	3.74	16640	434.53	25.00
	Siberian Larch	40800	48.80	22500	136.96	5.76	24080	604.35	20.00
	Ash	77600	103.94	42750	84.88	7.32	70950	714.17	24.00
	Beech	51100	78.47	42000	209.07	7.17	35500	737.15	27.00
	Sapele	31500	62.47	38740	195.14	10.64	28250	632.64	23.00
	AVERAGE	**48700**	**59.46**	**23670**	**136.50**	**6.57**	**27920**	**568.59**	**23.63**
	RANGE	**46100**	**73.37**	**38910**	**162.85**	**8.63**	**59250**	**320.27**	**7.00**
	STANDARD DEVIATION	**15800**	**22.93**	**15730**	**53.23**	**3.08**	**18980**	**124.04**	**2.50**
SAT (NOMINAL)	Scots Pine	44100	47.00	15400	6.21	5.70	9100	530.23	32.00
	Yellow Pine	24900	26.65	10200	7.75	2.31	7100	407.70	35.00
	Douglas Fir	36600	29.59	22000	25.20	4.42	11600	448.67	35.00
	Western Red Cedar	43300	43.84	21930	19.91	3.49	11000	354.88	30.00
	Siberian Larch	44500	40.83	22800	7.71	4.71	14200	575.65	32.00
	Ash	56200	73.15	45990	18.45	6.34	40000	708.26	45.00
	Beech	58400	76.76	45600	16.20	8.35	31200	787.75	40.00
	Sapele	47800	69.15	45000	19.54	11.39	21000	595.21	31.00
	AVERAGE	**44500**	**50.88**	**28610**	**15.12**	**5.84**	**18150**	**551.04**	**35.00**
	RANGE	**33500**	**50.11**	**35790**	**18.99**	**9.08**	**32900**	**432.87**	**15.00**
	STANDARD DEVIATION	**10600**	**19.64**	**14610**	**7.02**	**2.89**	**11760**	**147.96**	**5.13**

Cutting Force Models

Force in the direction of cutting was used as the only measured response for the regression models. Measured thrust and side forces were negligible compared to the

cutting force. Multiple least squares method was used to develop the regression equations (Eq. 8 and Eq. 9), the regression plots shown with 95% prediction intervals (Fig. 5), and the residual histograms (Fig. 6). The models exhibited R^2 values of 80% and 90% along and across the grain, respectively. Additionally, the ratio of range to standard deviation is considered (**R/SD**). These values evaluate the spread of the data and the variance. They were 4.54 and 4.66 along and across the grain, respectively.

The simple least squares method was used to quantify the influence of the obtained properties on the cutting force. The spread of the residual **Fsp** values had a data range of 159 N/mm across the grain and 168 N/mm along the grain. Standard deviation was also calculated with values of 34 across the grain and 33.5 along the grain. The ultimate material strength values yielded the highest R^2 and F values with values for toughness following the same pattern (Fig. 7). The elastic properties yielded the lowest F and R^2 values. Density, however, yielded very high F and R^2 values across the grain with comparably low values along the grain.

Models excluding selected categorical predictors were also developed. Predicting the cutting force (FC_P) along the grain by negating G returned an R^2 value of 78.9%. Negating ρ along the grain returned an R^2 value of 79.1%. Negating both G and ρ along the grain returned an R^2 value of 78.6%. These only differ by a very small amount from the R^2 value of 80% when all categorical predictors are used. Predicting the cutting force across the grain by negating **MOE** returns an R^2 value of 85.9%, compared to the slightly larger value of 90% when using all categorical predictors. It is also noticed that the F values vary when using different combinations of categorical predictors. Along the grain, these vary from 59.33 using all of the categorical predictors, 67 excluding G, 68 excluding ρ and 84 excluding both G and ρ. When using all of the categorical predictors in the cutting force model across the grain, an F value of 90.54 is returned. By excluding **MOE** from this group of categorical predictors, a larger F value of 110 is returned.

Eq. 8. Regression equation along the Grain

$$FC_P = -15.3 + 0.0243\,G + 2.54\,\tau - 0.0246\,\rho + 65.4\,\delta - 0.301\,MC + 0.00492\,Us$$

$R^2 = 0.8$ **Range** = 155.7 **SD** = 34.29

Eq. 9. Regression equation across the Grain

$$FC_P = -72.7 - 0.000093\,MOE + 0.235\,MOR + 0.0594\,\rho + 108\,\delta - 0.129\,MC + 0.00526\,Ub$$

$R^2 = 0.9$ **Range** = 210.4 **SD** = 45.12

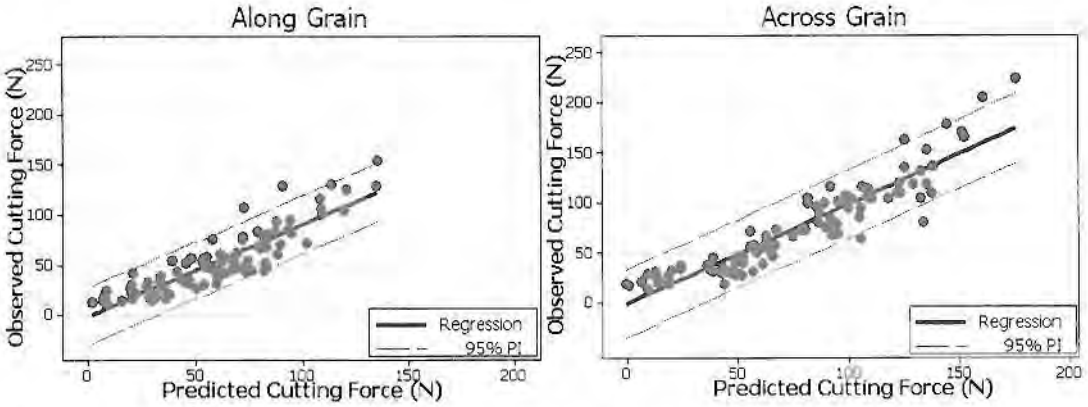

Fig. 5. Regression plots for cutting along and across the wood grain

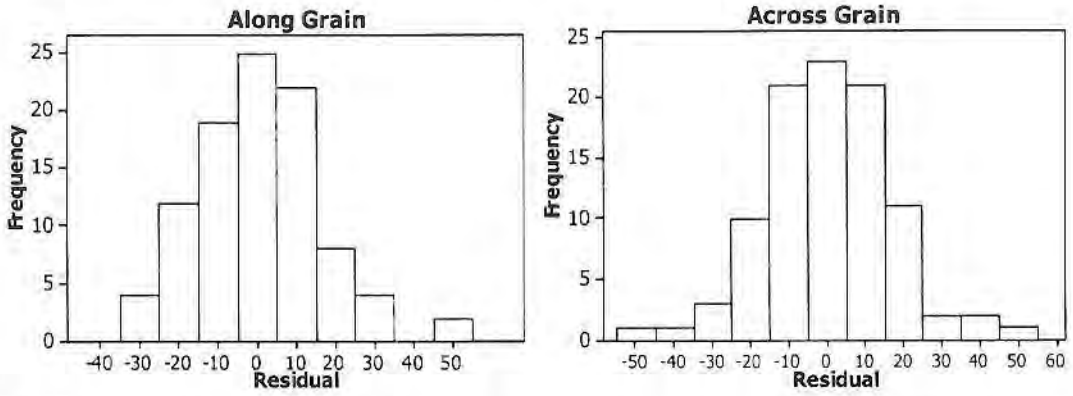

Fig. 6. Residual histogram plots of predictive models for cutting along and across the wood grain

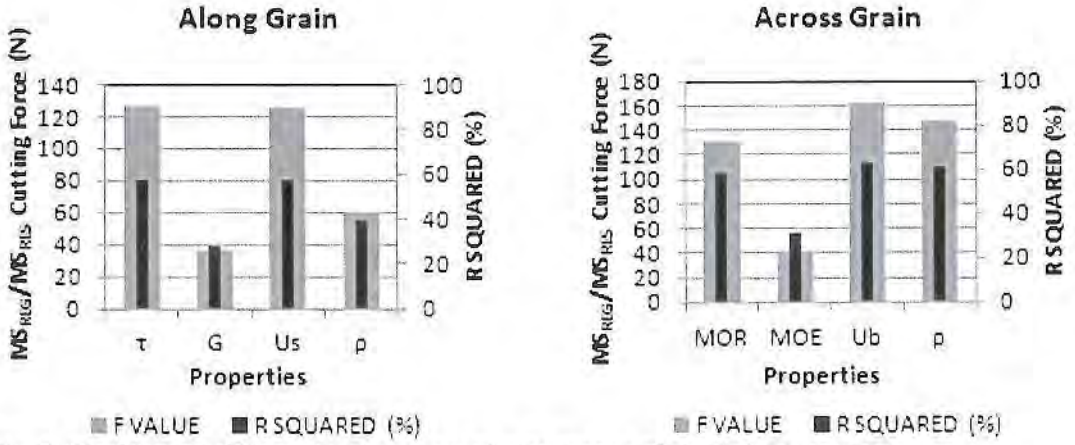

Fig. 7. Significance of the work-piece properties by means of simple least squares

DISCUSSION

Evidence from recently published literature shows regression analyses have been used to develop predictive cutting force models (Axelsson *et al.* 1993; Lhate *et al.* 2011; Porankiewicz *et al.* 2011). These models are mainly focused on the effects of varied tool geometry for band-saw teeth. A linear decrease in the cutting force for an increased positive rake angle (10° to 30°) has been observed (Axelsson *et al.* 1993), whilst at the same time a linear increase in cutting forces is observed for increased edge radii (5 to 20 μm).

The reader should be reminded that the experimental work detailed in this paper used only a simple orthogonal cutting tool with zero rake angle to limit the tool geometry parameters. The rationale behind this is to thoroughly evaluate the effects of work-piece properties for several wood species on the cutting force whilst limiting the tool geometry parameters and cutting conditions. It is furthermore assumed that the effects of edge recession (wear) had no influence on the forces, as the tool was sharpened during regular intervals. Furthermore, the test runs were randomized to remove systematic test run error.

Work-piece parameters have also previously been used as predictors in statistical modelling to describe force trends. The more commonly used parameters are moisture content, grain direction, and density, although coefficients have previously been determined to discretely quantify wood species (Lhate *et al.* 2011). It is generally accepted that tool forces decrease with increased work-piece moisture content. An exception to this rule is for frozen wood specimens (Porankiewicz *et al.* 2011). Furthermore, cutting the wood end grain yields the largest cutting forces, with the lowest cutting forces observed machining along the fibre direction. In general, higher tool forces are observed when cutting wood species of greater density (Lhate *et al.* 2011; Porankiewicz *et al.* 2011). Eyma *et al.* (2004) concluded that density alone acted as a poor work-piece parameter and that mechanical properties need to be utilised in order to develop more accurate cutting force relationships.

The analysis from this study shows that density is weighted as a much better categorical predictor across the grain compared to along the grain. This is by means of higher **F** and $\mathbf{R^2}$ values across the grain (Fig. 7). The obtained strength properties (**MOR, τ**) and toughness (**Ub, Us**) are more consistent as categorical predictors. Coefficients were not calculated to represent the individual wood species tested. The logic behind this decision was to keep the regression models universal, *i.e.* independent of species. The cutting force can be predicted based upon the work-piece mechanical properties, density, and moisture content instead. This model proves that the intrinsic properties of the differing wood species have little influence on the cutting force when each species has been evaluated using a series of carefully obtained mechanical properties.

After using the $\mathbf{R^2}$ and **F** values to determine the effects of each of the mechanical properties on cutting force, **MOE** was removed to re-predict the cutting force across the grain. This did not improve the regression model, and it only reduced the $\mathbf{R^2}$ value by 4%. Likewise, **G** and **ρ** were separately removed to re-predict two separate models. Also, **G** and **ρ** were removed simultaneously to re-predict an additional model. This once again did not improve the original $\mathbf{R^2}$ value, but a decrease up to 1.4% was observed. These results confirm that the accuracy of cutting force prediction is not significantly influenced by **MOE** across the grain and **G** combined with **ρ** along the grain.

The predictive model across the grain has an $\mathbf{R^2}$ value of 90% compared to 80% along the grain. The strength and toughness of the wood have consistently proven to be good predictors and the elastic properties have consistently proven to be poor predictors. Density is not consistent as it proves to be a good predictor along the grain and a poor predictor across the grain. The purpose of machining the radial wood plane was to engage the tool with approximately the same proportion of earlywood and latewood fibres. This was easily achieved across the grain as the tool path is perpendicular to the fibre direction. This was not so easily controlled along the grain. In most cases the radial grain pitch was larger than the 1 mm cutting edge making it extremely difficult to plan a tool path that engages the tool with both the less dense earlywood and denser latewood fibres. This leaves the author with three assumptions:

1. The tool passed through the earlywood fibres only
2. The tool passed through the latewood fibres only
3. The tool passed through a combination of both that cannot be confidently quantified

Regardless which of the assumptions is true, this situation explains why the density acts as a poor predictor along the grain resulting in a lower R^2 value for the respective model.

CONCLUSION

1. The regression models establish novel relationships between the bending properties and cutting forces across the grain and between the shear properties and cutting forces along the grain.
2. The models are completely species independent, *i.e.* no coefficients for species were factored into the models. Only the obtained mechanical properties of the individual wood species were used.
3. Strength (**MOR, τ**) and toughness (**Ub, Us**) have a strong influence on the cutting force both along and across the grain. This has been proven by weighting the categorical predictors used in the regression models.
4. The elastic properties (**MOE, G**) have a weak influence on the cutting force both along and across the grain.
5. **ρ** has a stronger influence on the cutting force across the grain than along. This is evident from the simple least squares analysis and can explain the lower $\mathbf{R^2}$ value and hence more disperse residual plots for the model cutting along the grain.

REFERENCES

ASTM, (2009). "D143-09: Standard test methods for small clear specimens of timber," Pennsylvania.

Axelsson, B., Grundberg, S., and Grönlund, J. (1991). "The use of gray scale images when evaluating disturbances in cutting force due to changes in wood structure and tool shape," *European Journal of Wood and Wood Products* 49, 491-494.

Axelsson, B., Lundberg, Å., and Grönlund, J. (1993). "Studies of the main cutting force at and near a cutting edge," *European Journal of Wood and Wood Products* 51, 43-48.

Cristovao, L., Broman, O., Grönlund, A., Ekevad, M., and Sitoe, R. (2011). "Main cutting force models for two species of tropical wood," Proceedings of the 20th International Wood Machining Seminar, June 7-10, Skellefteå, Sweden.

Eyma, F., Méausoone, P., Martin, P. (2004) "Study of the properties of thirteen tropical wood species to improve the prediction of cutting forces in mode B," *Ann. For. Sci.* 61, 55-64.

Eyma, F., Méausoone., Larricq, P., and Marchal, R. (2005). "Utilization of a dynamometric pendulum to estimate cutting forces involved during routing. Comparison with actual calculated values," *Ann. For. Sci.* 62, 441-447.

Franz, N. C. (1955). "An analysis of chip formation in wood machining," *Forest Products Journal* 10, 332-336.

Franz, N. C. (1958). *An Analysis of the Wood-Cutting Process*, University of Michigan Press, Ann Arbor.

Lhate, I., Cristóvão, L., Ekevad, M., and Sitoe, R. (2011). "Cutting forces for wood of lesser used speceis from Mozambique," in 20th International Wood Machining Seminar, Skellefteå, Sweden.

Loehnertz, S. and Cooz, I. (1998). "Sawtooth forces in cutting tropical hardwoods native to South America," *FPL – RP* – 567, 16 pp.

McKenzie, W. M. (1961). "Fundamental analysis of the wood cutting process," Department of Wood Technology, University of Michigan.

Naylor, A., Hackney, P., and Clahr, E. (2011). "Machining of wood using a rip tooth: Effects of work-piece variations on cutting mechanics," Proceedings of the 20th International Wood Machining Seminar, June 7-10, Skellefteå, Sweden.

Orlowski, K., and Palubicki, B. (2009). "Recent progress in research on the cutting processes of wood. A review," *Holzforschung.* 63, 181-185.

Orlowski, K., Ochrymiuk, T., and Atkins, A. (2011). "Application of mechanics for energetic effects predictions while sawing," Proceedings of the 20th International Wood Machining Seminar June 7-10, Skellefteå, Sweden.

Porankiewicz, B., Axelsson, B., Grönlund, A., and Marklund, B. (2011). "Main and normal cutting forces by machining wood of *Pinus sylvestris*," *BioResources* 6, 3687-3713.

Woodson, G. E., and Koch, P. (1970). "Tool forces and chip formation in orthogonal cutting of loblolly pine," U.S. Department of Agriculture, Forest Service, Southern Forest Experiment Station, New Orleans, LA.

Article submitted: March 13, 2012; Peer review completed: May 8, 2012; Revised version received and accepted: May 18, 2012; Published: May 22, 2012.

Conference Papers

1. Naylor, A. Hackney, P. and Clahr, E. 2011. Machining of Wood using a Rip Tooth: Effects of Work-piece Variations on Cutting Mechanics. Proceedings of the 20th International Wood Machining Seminar. Skellefteå, Sweden. 305-314

1. Naylor, A. Hackney, P. and Perera, N. 2012. Determination of wood strength properties through standard test procedures. Proceedings of the 10th International Conference on Manufacturing Research. Aston, UK. 372-377

2. Naylor, A. Hackney, P. and Perera, N. 2012. Evaluation of handsaw tooth performance through the development of a controlled cutting test rig. Proceedings of the 10th International Conference on Manufacturing Research. Aston, UK. 594-599

Machining of Wood using a Rip Tooth: Effects of Work-piece Variations on Cutting Mechanics

Naylor, Andrew.[1*] Hackney, Philip.[1] Clahr, Emil.[2]

[1]School of Computing, Engineering and Information Sciences, Ellison Building, Northumbria University, Newcastle upon Tyne, NE1 8ST, United Kingdom
[2]Research and Development Centre for Wood Working, SNA Europe, Box 1103 82113 Bollnäs, Sweden

ABSTRACT

Genetics and environmental conditions during the growth of wood are known to affect the intrinsic characteristics influencing cutting mechanics. To evaluate this, a full factorial experiment has been performed investigating the effects of three significant factors involved in wood machining; wood species, moisture content and grain direction. A variety of woods were evaluated (five softwood and three hardwood species) at four moisture levels. As all woods are heterogeneous, anisotropic materials, machining was performed parallel and perpendicular to the grain direction. A three axis CNC router was used to drive a tool resembling a rip tooth, at low velocity, through each of the sixty-four wooden work-piece variations at three different depths of cut. To collect quantitative data, a piezoelectric dynamometer was used with a data acquisition system to measure and record the cutting and thrust force components acting on the tool. Chip formation and work-piece deformation were observed using images taken from an optical microscope. This paper compares the published results [1-7] for planing operations with findings from the rip tooth experiment.

INTRODUCTION

Research performed into optimum wood machining conditions [1, 2] suggests that there are three significant types of factor that affect the cutting mechanics:

1. Factors attributed to the machining process
2. The species of the wood
3. The moisture content of the wood

Wood has three orthogonal planes of symmetry; axial, radial and tangential. Corresponding to these planes of symmetry are several different cutting directions by which different machining processes can be described. When referring to a machining direction the nomenclature states a labelling system consisting of two numbers. The first number denotes the orientation of the cutting edge to the wood grain direction; the second number denotes the movement of the tool with respect to the grain direction. To illustrate this, the three main cutting directions as shown in *figure 1.*

Corresponding Author** ***Tel: +44 (0) 1912273624
Email: andrew2.naylor@northumbria.ac.uk

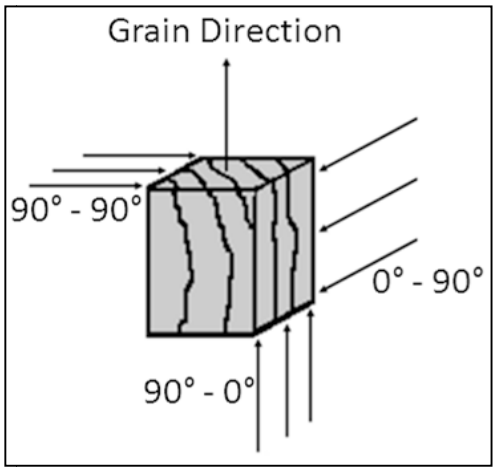

Figure 1 – Machining directions with respect to wood grain

- **90°-90°** - The axial plane or the wood end grain. Both the cutting edge and tool movement are perpendicular to the grain.
- **0°-90°** - The radial and tangential planes, cutting across the grain. The cutting edge is parallel to the grain but the tool movement is perpendicular.
- **90°-0°** - The longitudinal plane, cutting along the grain. The cutting edge is perpendicular to the grain but the tool movement is parallel.

Evidence from fundamental literature [3, 4] suggests that cutting velocity has negligible effect on the forces acting on the tool. This is for the ranges of 0.2 mm/s – 6.3 m/s along the grain and 2.5 m/s – 50 m/s across the grain.

A Review of Planing Operations

Kivmaa [3] used Finish birch in a study investigating the geometric factors of the tool on cutting performance and found that the main cutting force was inversely proportional to the sharpness of the tool. It is also stated at this point that the thrust force is caused by contact between the rake face and the chip. The larger the rake angle the thicker the chip and hence the lower the thrust force. This is because the chip is not being compressed. Although it is observed that there is no significant effect of cutting velocity on the major cutting force, the orientation of the tool with respect to the grain does have a significant effect on the cutting forces. For this planing scenario, the highest cutting forces are observed to be in the 90°-90° direction with the lowest cutting forces in the 90°-0° direction (cutting along the grain). In the same study, the tool sharpness and rake angle remain constant for the testing of 21 different species of wood. Analysis of data found a linear trend between the density of the wood and the major cutting force. From this empirical data a predictive model for cutting force was created.

Extensive work into the chip formation produced through varied cutting conditions has been carried out by Franz [4, 5], McKenzie [6], Woodson and Koch [7]. The cutting tools used in the experiments represent a wood plane that removes material across the entire width of the work-piece. Regarding machining in the 90°-0° direction (along the grain) it was found that large rake angles result in negative thrust forces (acting upwards relative to the work-piece). The wood fibres split ahead of the tool and finally fail due in tension. This type of chip is beneficial where quick removal of material is required. Continuous chip formation is achieved when using a very sharp tool edge and a diagonal plane of shear, providing an excellent surface finish to the work-piece. This process can be described as ongoing shear. Dull tool edges, and very small or negative rake

angles cause a *fuzzy chip*. It is also suggested that very large depths of cut may form this chip where there is too much contact with the blade surface. This type of chip causes a raised *fuzzy grain* where wood fibres become protruded, hence producing a poor surface finish.

An investigation into the mechanics of cutting across the grain (0°-90°) considers the veneer peeling process as a case study. This process uses high rake angles (approximately 70°) and small depths of cut (less than 1 mm). The material removal in veneer peeling is described as an ongoing shearing process initiated by a tear in compression perpendicular to the grain.

McKenzie [6] investigated the effects of cutting in the 90°-90° direction. In general the cutting mechanics specify a tensile failure mode causing parallel gaps to propagate along the grain. It is noted that these gaps become larger as the moisture content decreases. Cutting forces in this direction are strongly affected by cell type, moisture content, depth of cut, and rake angle

A Review of Single Tooth Operations

The limited research performed on the effects of single point cutting tools focuses on the optimisation of cutting conditions for industrial sawing processes. From the available literature [8-11] it is apparent that the responses desired from experimentation are the forces along the major cutting edge. Chip formation is not heavily investigated.

Machining in the 90°-90° direction, Axelsson [8-10] developed the prior knowledge of the machining process obtained using planing operations by investigating the effects on cutting mechanics using single point cutting tools. For sawing processes, the tool used has a side clearance of 1 mm either side to represent the set of a saw-blade. Using computerised tomography (CT) a linear relationship between the density of the wood for a specified tool path and the cutting forces was established. This linear relationship is clearly shown when cutting through a knot of much higher density to the un-defected wood-grain.

Interesting results were produced from research into the effects of changing the rake angle of band-saw teeth, machining wood in the 90°-90° direction [11]. Three teeth with 25°, 30° and 35° rake angles were examined, it was found that the largest rake angle produced the lowest cutting forces and the smallest rake angle produced the largest cutting forces. Initially, it appeared that the 25° and 35° rake angles produced a smooth work-piece finish after machining, whilst the 30° rake angle produced a rough finish with fuzzy grain. Microscope images showed that the 25° rake angle only appeared smooth when in fact the machining caused fuzzy grain which was then compressed due to the low rake angle of the tooth.

METHODOLOGY

Test Equipment

The experimental test rig comprised of a cutting tool driven by a 3 axis CNC router machine. The work-piece was mounted on a force dynamometer equipped with piezoelectric load cells measuring the cutting, thrust and side force components acting on the tool. Only the cutting and thrust force components were taken into consideration for this analysis. The test rig schematic diagram *(figure 2)* details the set-up of the data acquisition system. To obtain tool force data, the cutting tool **(1)**

was used to machine through the work-piece attached to the force dynamometer **(2)**. The three piezoelectric transducers in the dynamometer each generate a charge in response to the cutting forces (3.9 pC/1 N in X and Y directions, 1.95 pC/1 N in the Z direction). These signals feed into the charge amplifier **(3)** where the signals are calibrated for a 10V input to the data acquisition PLC **(4)** (3900 pC/10 V in X and Y directions, 1950 pC/10 V in Z direction: Hence 1 N = 0.01 V). The PLC converts the signals from analogue to digital and the data can be analysed using appropriate software.

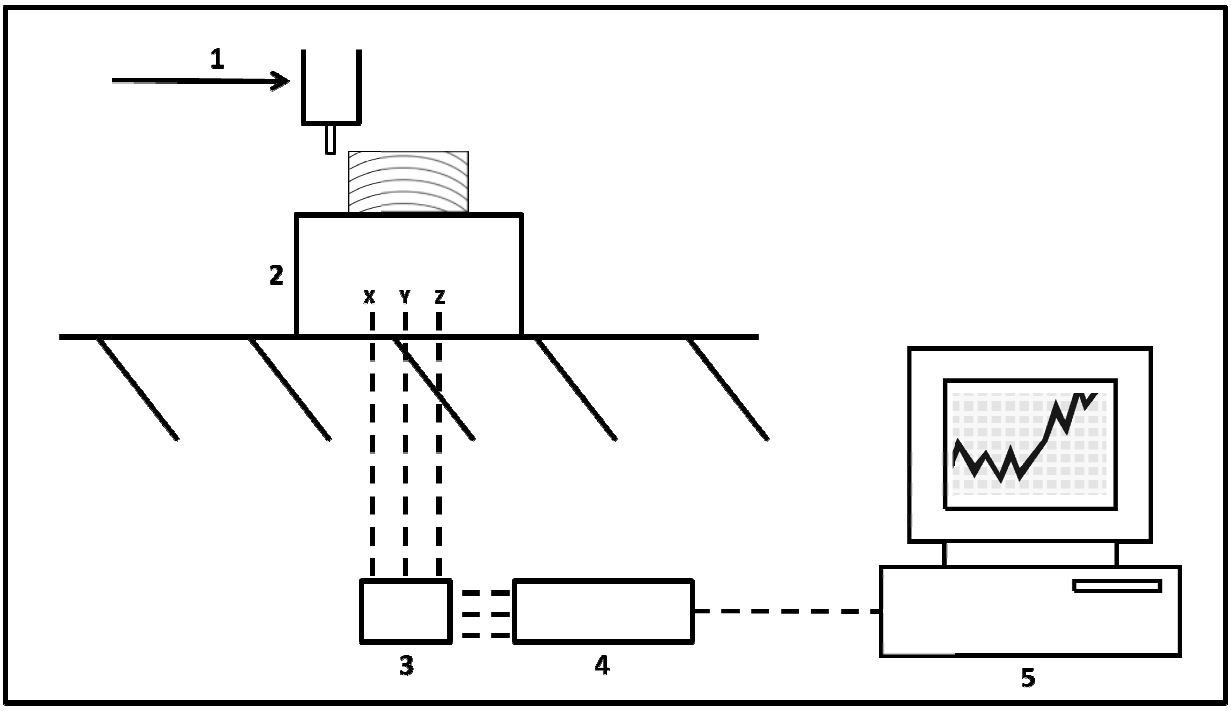

Figure 2 - Test rig schematic with data acquisition system

Experimental design

The tool used in the experiment has geometry similar to the rip tooth formation *(figure 3).* The tool has an orthogonal cutting edge with a width of 1 mm and a rake angle of zero. To ensure that the cutting edge was sharp the tool was sharpened using precision grinding equipment prior to performing the test runs. The two machining directions selected for the experiment were 90°-0° (along the grain) and 0°-90° (across the grain) as these are deemed to be the most common directions for manual wood-sawing.

Eight species of wood where evaluated in the experiment, five softwoods (Scots Pine, Yellow Pine, Siberian Larch, Douglas Fir and Western Red Cedar) and three hardwoods (Ash, Beech and Sapele). Each of these wood species had four separate moisture levels; Dry (<6%), 10%, 20% and Saturated (>30%). Including the two machining directions this amounts to sixty-four work-piece variables. Each of the sixty-four work-piece variations was machined at three depths of cut; 0.4, 0.8 and 1.2 mm, providing a total of one hundred and ninety-two cutting and thrust force values for analysis.

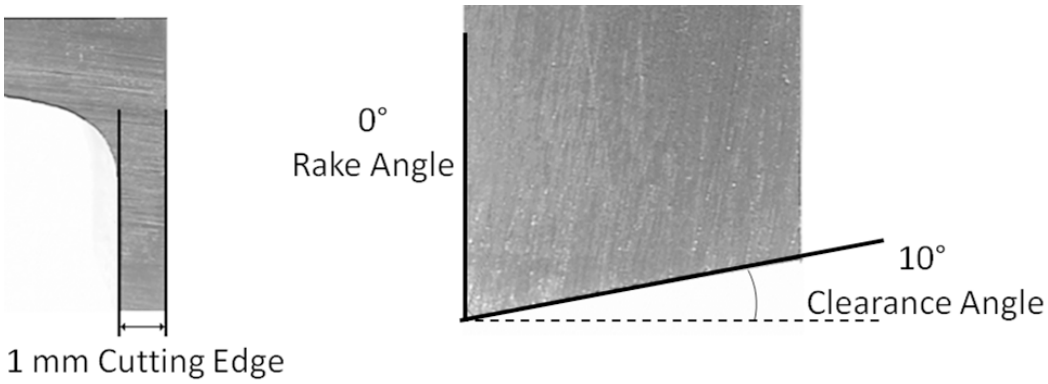

Figure 3 - Optical microscope images of tool

RESULTS AND DISCUSSION

Cutting Force data

The cutting force is observed to increase with depth of cut for all woods at all moisture levels tested *(figure 4)*. Furthermore, cutting across the grain yields higher cutting forces than along the grain. This trend becomes more prominent for increased depths of cut. Thrust force values are also seen to increase with depth of cut. However, wood grain direction is seen to have negligible effect on the magnitude of these forces.

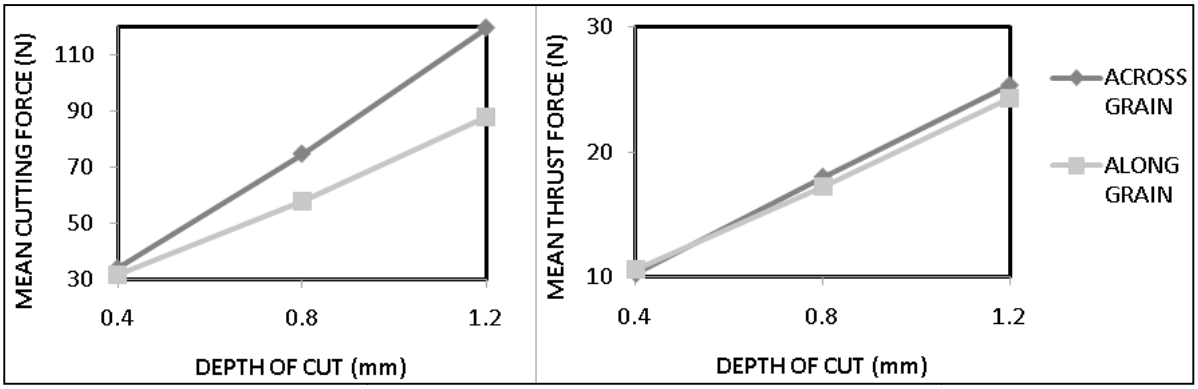

Figure 4 – Cutting/Thrust Force vs. Depth of Cut

When focusing on the average behaviour of all of the woods *(figure 5)*, a linear relationship is observed for the tool forces with regard to moisture content. The highest forces are observed for dry woods and the lowest forces are observed for the saturated woods. The machining direction does not have any significant effect on the thrust force. However, the cutting force is heavily influenced by the machining direction. This is more prominent for increasing depths of cut where machining across the grain yields higher forces than along the grain.

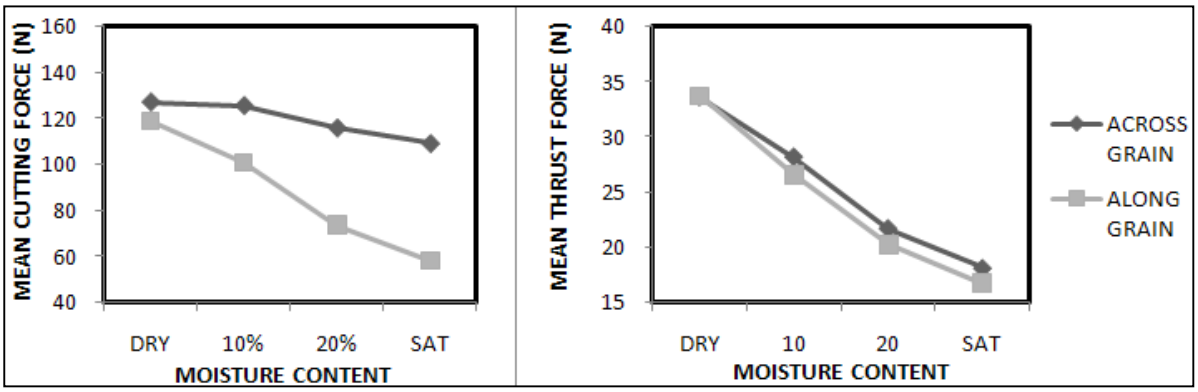

Figure 5 – 1.2 mm depth of cut: Cutting/Thrust Force vs. Moisture Content

When looking at the behaviour of the individual woods *(figure 6)*, certain trends are noticed. In general, the three hardwoods included in the experiment produced higher cutting and thrust forces than the softwoods. One exception to this rule is Siberian Larch which exhibits higher forces along the grain than its other softwood counterparts. Since wood is an anisotropic material, a wood species such as Siberian Larch can yield cutting force responses in one machining direction akin to softwoods. However, in the opposite direction it can yield forces similar to hardwoods. One explanation for this is the environmental factors associated with the growing conditions of the wood. Siberian Larch grows in extremely cold climates. The extended cold growing season results in the annual growth rings consisting of a larger proportion of the much denser latewood cells. In softwoods growing in the more temperate climates the ratio of earlywood to latewood cells would be approximately 1:1. Any factors attributed to growing conditions can influence the intrinsic properties of the wood.

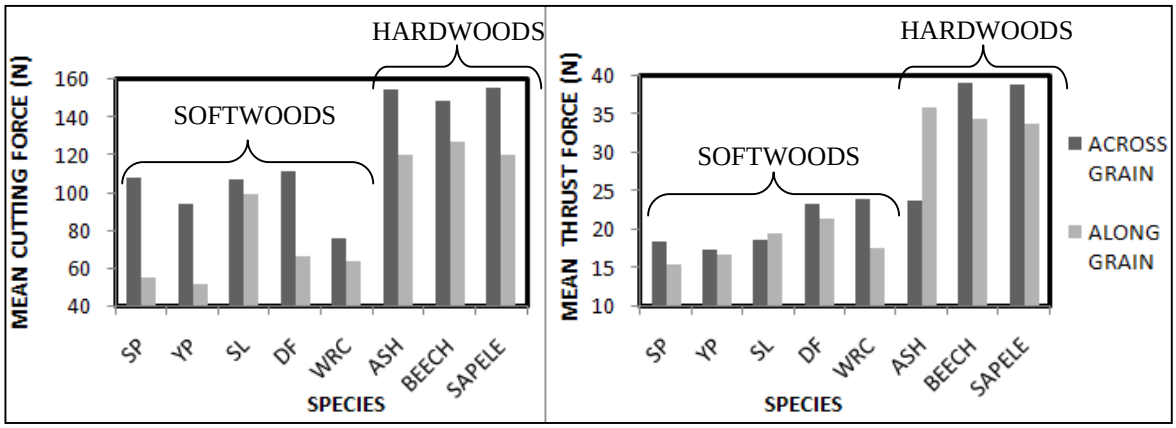

Figure 6 – 1.2 mm depth of cut: Cutting/Thrust Force vs. Species

Chip Formation

Similarities and differences in the chip formed during the rip tooth machining experiment have been compared with results from planing operations [4, 6, 7]. Despite the fact that the rip tooth has zero rake angle all types of chip formation along the grain, as postulated by Franz [4], were observed.

Type I chips were observed for dry wood of all species and depths of cut *(figure 7)*. The chips were discontinuous (broken) and the surface finish of the affected part of the area appeared poor due to several break-off points for the chip.

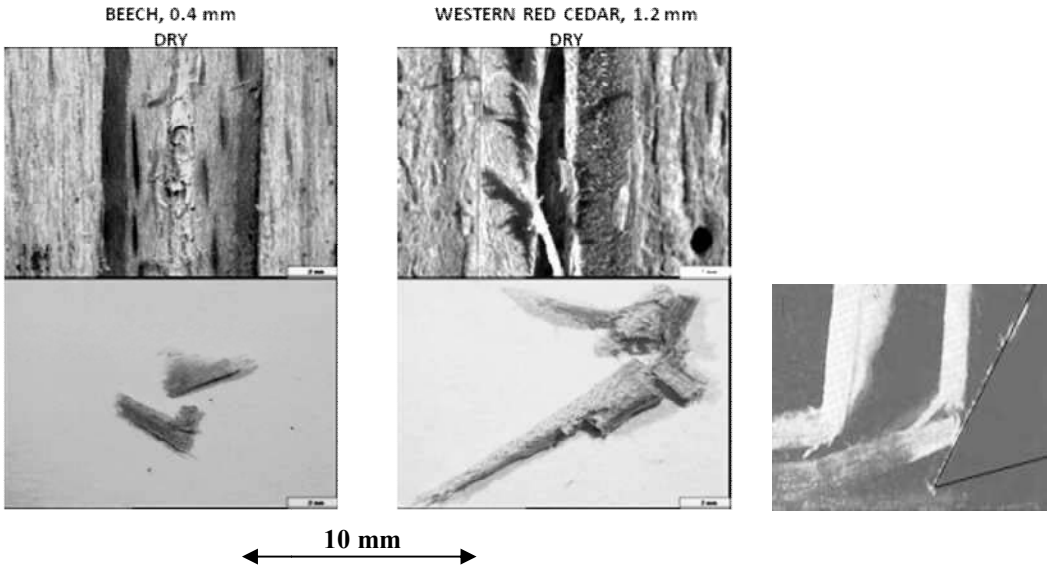

Figure 7 – Type I chip formation along the grain

Type II chip formation occurred at 10-20% moisture content for 0.4-0.8 mm depth of cut as well as for saturated at 0.4 mm depth of cut *(figure 8)*. The area left behind by this formation appeared to have high quality surface finish on account of the continuous (un-broken) chip.

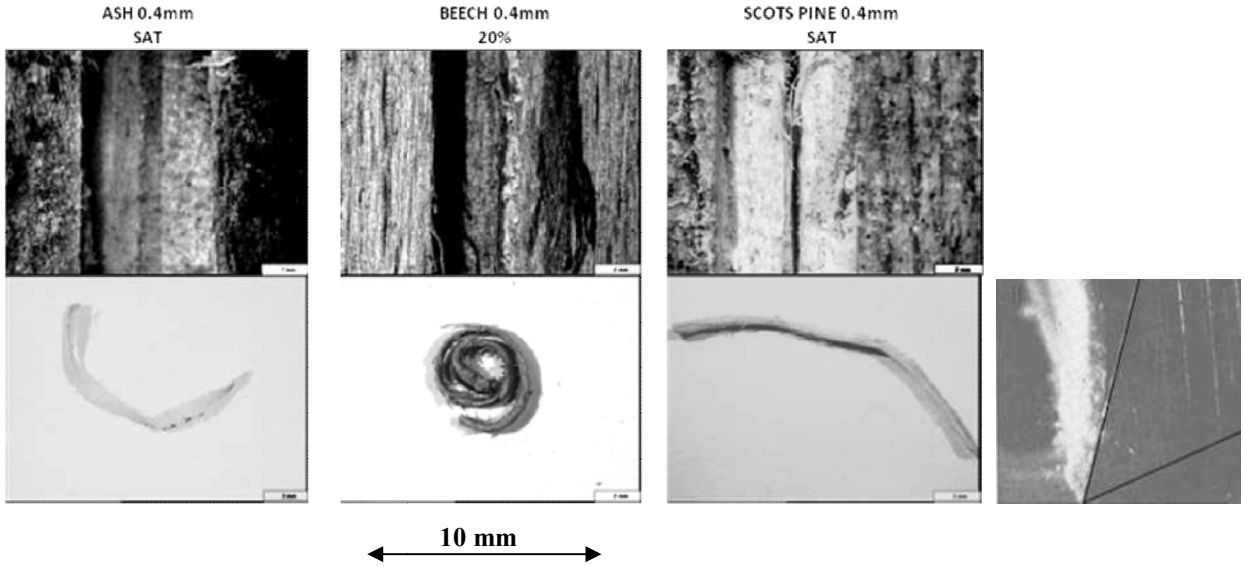

Figure 8 – Type II chip formation along the grain

Type III chip formation occurred mainly for saturated work-pieces (with some occurring at 20% moisture content) at the larger depths of cut of 0.8 and 1.2 mm *(figure 9)*. The surface finish of the

work-piece was seen as *fuzzy*, with up-rooted wood fibres left behind in the groove. It is apparent from the microscope images that this type of formation occurred more frequently for softwoods than hardwoods.

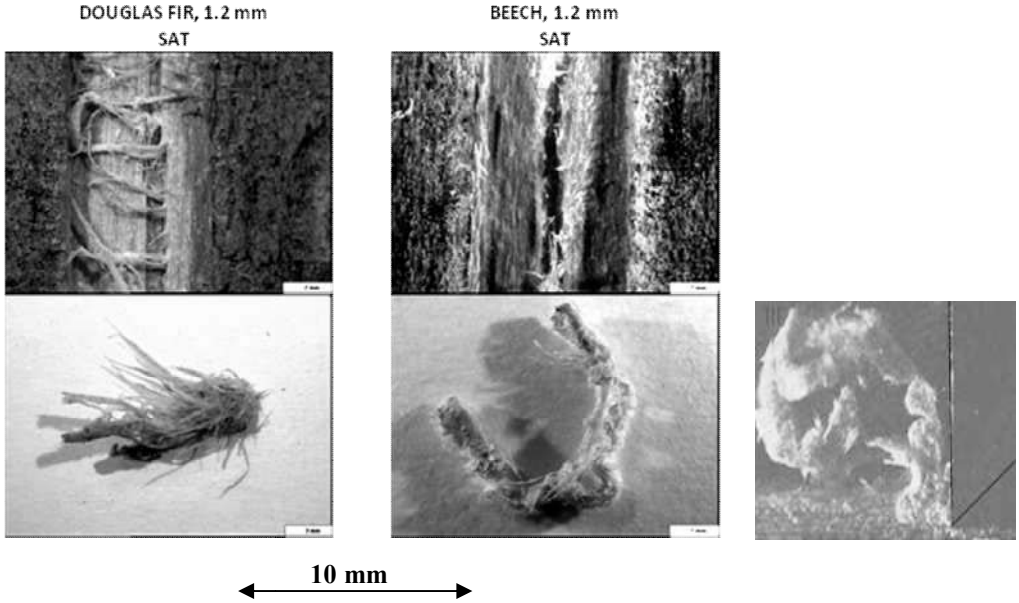

Figure 9 – Type III chip formation along the grain

It has been established that increasing the contact of the tool face by operating with small/negative rake angles and by increasing the depth of cut can cause type III formation (this is exacerbated for rough tool faces). This only occurs for higher moisture contents. In the case of dry woods, the chips start to resemble type I formation. A group of fibres are initially compacted causing a longitudinal crack to propagate in front of the tool. Eventually these fibres shear along the formed crack. Type II formation usually requires a positive rake angle for continuous chip formation. In this instance the reason why this formation is observed is because optimum parameters have been achieved. A combination of optimum moisture content and low depth of cut must be achieved (10-20% at 0.4-0.8 mm and saturated at 0.4 mm) assuming that the tool used has been sharpened.

The work done to previously explain chip formation across the grain does not provide any useful information regarding the rip tooth machining experiment. The main reason for this is because no material removal occurred. Instead the rip tooth ploughed through the wood fibres. Woodson and Koch [7] investigated the mechanics of cutting across the grain for planing tools with large rake angles and concluded that the chip observed is caused by an initial tear in compression followed by ongoing shear. For the rip tooth (which has zero rake angle) the failure mode was observed to be that of bending with no shearing taking place.

To elaborate further, bending was observed to be the primary failure mode for all depths of cut. However, the depths of cut that provide better visibility are 0.8 – 1.2 mm *(figure 10).* Work-piece deformation seems to have been greatly affected by moisture content. For dry wood the work-piece appeared greatly deformed with a visible channel down the centre of the tool path. At 10-20% moisture content it is visible that the fibres have been ploughed through. However, there is no channel down the centre of the affected area. For saturated it appeared that even less of the ploughed area was deformed. In some instances it is even hard to see visible evidence that a tool has passed through it. This suggests that higher moisture content causes an increase in the elasticity

of the wood fibres. For higher moisture content the fibres break and then attempt to spring back towards the initial position. For dry wood the fibres simply split and remain in that position.

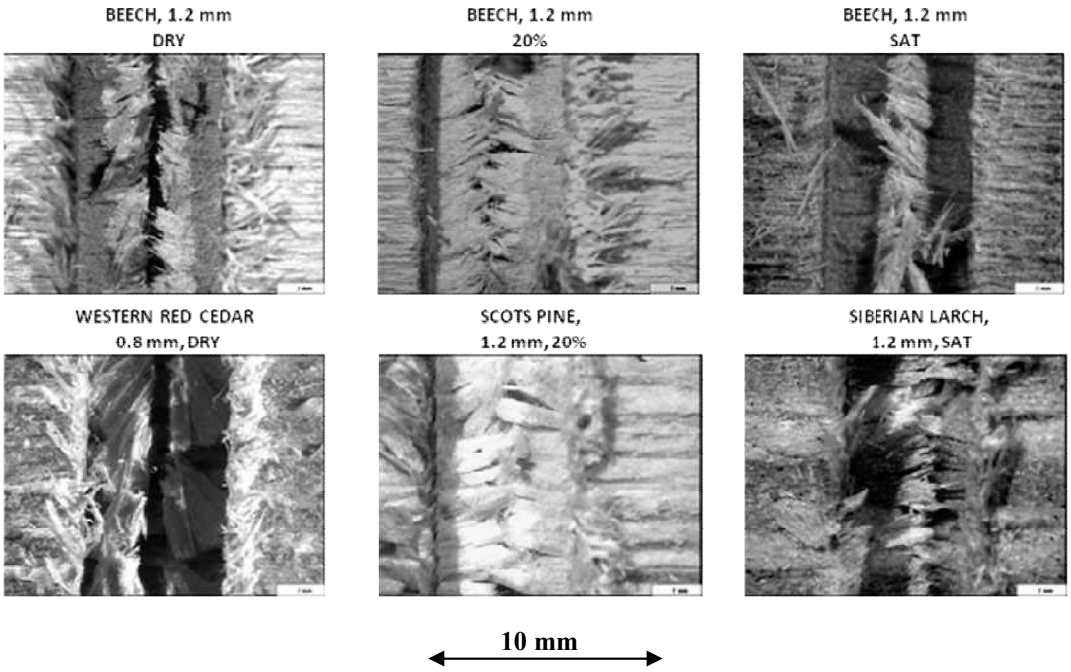

Figure 10 - Observed chip formation across the grain

CONCLUSION

When machining with a single rip tooth the cutting mechanics along the grain consisted of an ongoing shearing process which is heavily influenced by moisture content. Dry wood generally required larger cutting forces to remove material in a stubborn process. This produced chip formation type I, where as saturated wood exhibited liberal material removal at relatively low cutting forces generating chip type III. If chip type II is desirable, parameters for optimum surface finish were observed to be low depths of cut at 10-20% moisture content.

The cutting mechanics across the grain was caused by failure of the wood fibres in bending. The cutting forces across the grain were significantly higher than along the grain. However, there was less difference between dry and saturated average force values. This suggests that the bending effect across the grain was not as significantly affected by moisture content than the shearing effect along the grain. Higher moisture content sees an increase in the elasticity of the wood fibres allowing them to spring back to their original position after ploughing. This however could cause a detrimental effect during the sawing process. Average force responses show that the wood grain direction does not significantly affect the thrust forces.

A further programme of work is required to provide complimentary data. ASTM D143-09 standard test procedures for three point bending and longitudinal shear will be implemented to characterize wood strength across and along the grain respectively. Regression analysis will establish a relationship between the collected cutting force data and the obtained mechanical properties (Fracture Stress and Elastic Modulus).

REFERENCES

[1] P. J. Méausoone, "Choice of Optimal Cutting Conditions in Wood Machining with the "Tool-Material Pairing" Method," in *Proceedings of the 15th International Wood Machining Seminar*, 2001, pp. 37–47.

[2] F. Eyma, P.-J. Méausoone, and P. Martin, "Strains and cutting forces involved in the solid wood rotating cutting process," *Journal of Materials Processing Technology,* vol. 148, pp. 220-225, 2004.

[3] E. Kivimaa, "Cutting force in woodworking." vol. 18 Helsinki: VTT Julkaisu, 1950, p. 101.

[4] N. C. Franz, *An Analysis of the Wood-Cutting Process*. Ann Arbor: University of Michigan Press, 1958.

[5] N. C. Franz, "An Analysis of Chip Formation in Wood Machining," *Forest Products Journal,* vol. 10, pp. 332-336, 1955.

[6] W. M. McKenzie, "Fundamental analysis of the wood cutting process," in *Department of Wood Technology*: University of Michigan, 1961.

[7] G. E. Woodson and P. Koch, "Tool Forces and Chip Formation In Orthogonal Cutting Of Loblolly Pine," U.S. Department of Agriculture, Forest Service, Southern Forest Experiment Station, New Orleans, LA 1970.

[8] B. Axelsson, "Lateral cutting force during machining of wood due to momentary disturbances in the wood structure and degree of wear of the cutting tool," *European Journal of Wood and Wood Products,* vol. 52, pp. 198-204, 1994.

[9] B. Axelsson, S. Grundberg, and J. Grönlund, "The use of gray scale images when evaluating disturbances in cutting force due to changes in wood structure and tool shape," *European Journal of Wood and Wood Products,* vol. 49, pp. 491-494, 1991.

[10] B. Axelsson, Å. Lundberg, and J. Grönlund, "Studies of the main cutting force at and near a cutting edge," *European Journal of Wood and Wood Products,* vol. 51, pp. 43-48, 1993.

[11] I. Vazquez-Cooz and R. W. Meyer, "Cutting forces for tension and normal wood of maple," *Forest Products Journal,* vol. 56, pp. 26-34, 2006.

DETERMINATION OF WOOD STRENGTH PROPERTIES THROUGH STANDARD TEST PROCEDURES

Andrew Naylor
Philip Hackney
Noel Perera
School of Computing, Engineering and Information Sciences
Northumbria University, Ellison Building
Newcastle Upon Tyne, NE1 8ST, UK
andrew2.naylor@northumbria.ac.uk

ABSTRACT

In this study a review of existing recognised standards for wood mechanical testing was conducted. This review considers tensile, compressive, bending and shear test methodologies from a range of sources. In addition, values for wood mechanical properties were obtained through controlled experimentation using a universal material testing machine. Selected standard procedures were used to obtain wood strength properties both along and across the grain. These consist of a three point bending procedure used to evaluate the wood strength across the grain and a longitudinal shear procedure used to evaluate the wood strength along the grain. Strength properties obtained through controlled experimentation are compared to values available in existing literature with little discrepancy.

Keywords: Mechanical Test Procedures, Universal Testing Machine, Wood Strength Properties

1 INTRODUCTION

Wood is anisotropic and hence some mechanical test procedures are often performed both along and across the grain. Tension and compression tests have been successfully performed both along and across the grain. Compression tests show that wood has much larger strength and modulus of elasticity values along the grain rather than across (Reiterer and Stanzl-Tschegg 2001, Manríquezand Moraes 2009). The trend for tensile tests is the same as compressive (Oh 2011, Galicki and Czech 2005) (larger values along the grain). However, the magnitude of the compressive strengths is significantly larger than tensile, typically ten times larger. Due to the nature of the test procedure, static bending test procedures are mainly implemented to characterise wood strength across the wood grain. Shear test procedures have been implemented in all three wood machining directions (Munthe and Ethington 1968) revealing that only a true shear failure mode occurs along the wood grain.

1.1 Static Bending

Four point bending is recommended by British Standards for wood as failure occurs at the point of maximum displacement between the two loaded anvils (British Standards 2003). This eliminates the excessive compressive forces that would occur with the use of a single anvil and reduces likely-hood of shear along the grain. American Standards for three point bending specifies a span to depth ratio of 1:14 (ASTM 2009). Once again this ensures that the failure mode is bending with no shear along the grain or compressive deformation caused by the loaded anvil.

Previous research into the properties of Finnish birch (Gustafsson 2001) has evaluated both the British and American test procedures. The findings reveal an average modulus of elasticity (**MOE**) of 11.2 GPa for three point bending compared to 14.9 GPa for four point bending, an increase of approximately 25%. Comprehensive records (Bergman et al 1999) reveal an **MOE** value of 13 GPa in static bending which lies between these two values, showing that results from both test procedures are

within an appropriate range. The modulus of rupture (**MOR**), commonly referred to as bending strength, is calculated to be the same regardless of the testing procedure.

Despite the discrepancy between the two test procedures for determination of **MOE**, evidence from literature shows that **MOE** has been accurately determined using the three point method. This was used to evaluate Green wood (Coutand et al 2004) and wood plastic composites (Wechsler and Hiziroglu 2007)

$$MOR = \frac{3FL}{2bd^2}, \quad \textbf{At point of fracture} \tag{1}$$

$$MOE = \frac{FL^3}{4bd^3\omega}, \quad \textbf{At elastic limit} \tag{2}$$

1.2 Shear

Shear occurs most commonly along the grain direction hence values in this direction are referred to as longitudinal shear. French standards for longitudinal shear incorporate a test specimen with three separate shear zone where failure can occur (AFNOR 1942). This standard has been used previously to determine the modulus of rigidity for a predictive cutting force model where a tool machines wood along the grain (Eyma et al 2004). Alternatively, American standards have developed a method for accurately measuring the shear strength (**τ**) and modulus of rigidity (**G**) (ASTM 2009). The set-up consists of a test piece that can fail along only one zone of shear.

$$\tau = \frac{F}{A}, \quad \textbf{At point of fracture} \tag{3}$$

$$G = \frac{\tau}{\gamma} = \frac{FL}{Ax}, \quad \textbf{At elastic limit} \tag{4}$$

A previous study on wood shear (Munthe and Ethington 1968) using spruce, applied the American standard methodology and apparatus to all three orthogonal planes of symmetry with respect to the wood grain direction. The results indicate that the wood is much stronger along the grain. Tests both across the fibre direction and growth rings (end grain) yield **τ** values approximately 20% that of along the grain and **G** values of approximately 3%. Furthermore, only true shear was observed along the wood grain. This was illustrated by a uniform fault line propagating along the wood grain. Other failure modes were observed: Buckling of the annual growth rings at the wood end grain and bending of the fibres across the grain which are both referred to as “rolling shear”.

2 METHODOLOGY

A programme of work was completed using the American standard test procedures for three point bending and longitudinal shear. These determined wood properties across and along the grain respectively. Eight wood species including both hardwoods and softwoods were selected. The American test standards were favoured as they were easier to implement in the universal testing machine. Hence the question must be asked; does this more simple approach produce results comparable to results obtained via other well established methods?

2.1 Three point Bending

All tests were performed using the American standard methodology described in sub-sections 1.1 and 1.2. The span (**L**) of all of test specimens was kept at 300mm with a 20mm depth (**d**); this is in keeping with the specified 14:1 minimum span to depth ratio. An additional criterion that was also specified by the standard was a 1.3 mm/min crosshead maintained throughout testing until failure. The wood was placed into the experimental set-up in the universal testing machine (Figure 1) where the apparatus was placed between a moving crosshead and a 10 kN load cell. Force vs. Displacement plots were initially

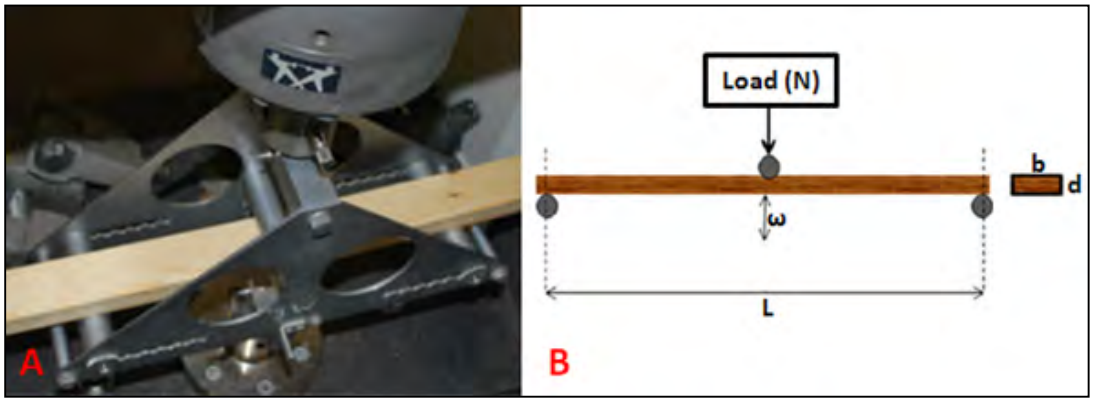

Figure 1: A) Three point bending set up in universal testing machine. B) Schematic diagram

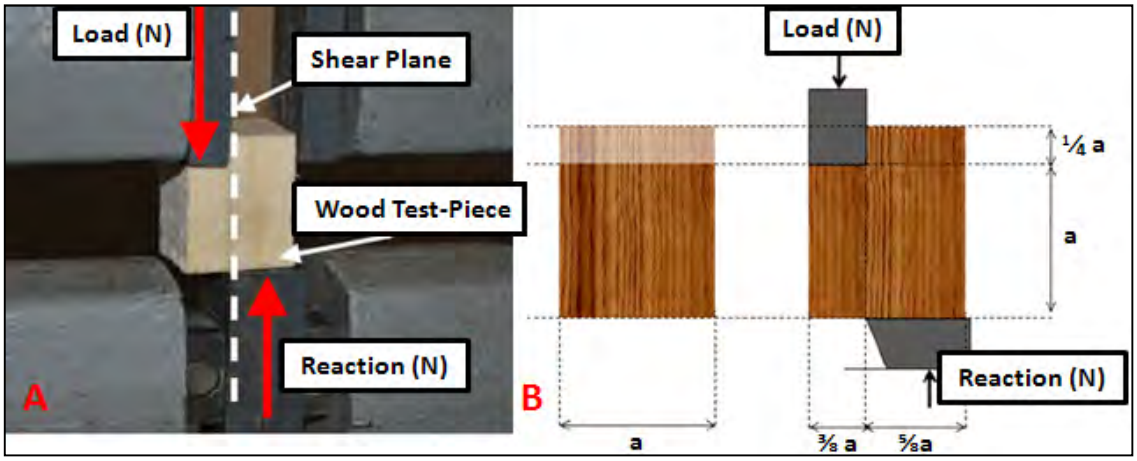

Figure 2: A) Longitudinal shear set up in universal testing machine. B) Schematic diagram

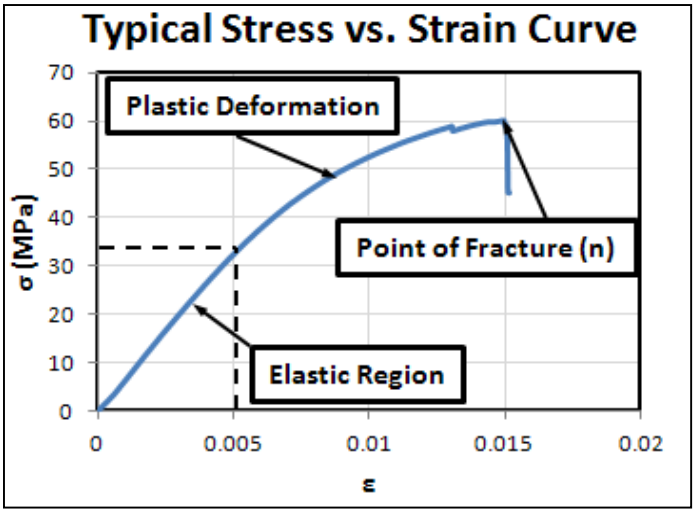

Figure 3: Deformation zones on a typical stress vs. strain curve

generated by the test machine data acquisition system. The linear region where Force was directly proportional to Displacement was taken to be the elastic region where no permanent deformation occurs. Force and Displacement measurements from this region are used to calculate **MOE**. The Force measurement at the point of fracture was subsequently used to calculate **MOR**.

2.2 Longitudinal Shear

As with three point bending, all tests were performed using the American standard methodology. The experimental set up also used the 10 kN load cell. All proportions for the test piece used in experimentation are detailed (Figure 2). A 0.6 mm/min crosshead was maintained throughout testing until failure. As the shear zone was approximately square, both the length and width were taken to be ***a***. Equations 3 and 4 could be modified to accommodate the standard test specimen. Once again Force vs. Displacement plots were acquired to determine the elastic region and the point of fracture **τ** and **G** were calculated using equations 5 and 6 respectively.

$$\tau = \frac{F}{a^2}, \qquad \textbf{At point of fracture} \tag{5}$$

$$G = \frac{Fa}{a^2 x} = \frac{F}{ax}, \quad \textbf{At elastic limit} \tag{6}$$

2.3 Toughness

Toughness was calculated as the area under the stress (**σ**) vs. strain (**ε**) curves (Figure 3) generated from the universal testing machine force extension plots. The stress strain curve was in the form of a quadratic polynomial. Toughness (**U**) was obtained by taking the definite integral of the quadratic function between zero and the point of facture (**n**) (equation 7).

$$U = \int_n^0 f(\varepsilon) = \int_n^0 (a\varepsilon^2 + b\varepsilon + c) \tag{7}$$

3 RESULTS

In general the average strength of the wood species tested across the grain (denoted by **MOR**) obtained through the three point bending tests (table 1) was measured to be over eight times greater than the strength along the grain (denoted by **τ**) obtained through the longitudinal shear tests. However, the average elasticity of the wood across the grain (denoted by **MOE**) was measured to be nearly 40 times greater than along the grain (denoted by **G**).

3.1 Bending

For all moisture levels evaluated, values for mean **MOR** for the wood species evaluated range from 50-90 MPa with a linear decrease in strength observed for increased moisture content. The values for mean **MOE** of the wood species evaluated ranges from 4-8 GPa with a linear decrease in elasticity also observed for increased moisture content. The results from the force extension plots show there is no discernible pattern to suggest that the hardwoods yield higher **MOE** values than the softwoods.

3.2 Shear

The average **τ** values range from 5-12 MPa. The highest values represent the three hardwoods tested which have values approximately 45% greater than the softwoods. Furthermore a linear decrease in strength is observed with an increase in moisture content. The average **G** values of the wood species evaluated range from 15-230 MPa with the larger values once again representing the hardwoods. These values are approximately 50% greater than the softwoods. **G** exhibits a negative linear trend with respect to moisture content.

Table 1: Properties obtained through mechanical testing

	Species	MOE (GPa)	MOR (MPa)	Ub (J/m^2)	G (MPa)	τ (MPa)	Us (J/m^2)	ρ (kg/m^3)	MC (%)
DRY (NOMINAL)	Scots Pine *(SW)*	6.28	79.21	33250	151.47	9.53	26650	576.64	6.00
	Yellow Pine *(SW)*	5.08	47.72	24910	286.27	6.28	17100	484.80	6.00
	Douglas Fir *(SW)*	6.92	72.01	49000	236.51	7.58	34080	496.62	8.00
	Western Red Cedar *(SW)*	9.15	99.28	40600	52.78	8.62	31730	671.57	6.00
	Siberian Larch *(SW)*	7.33	65.24	49020	260.16	9.31	54000	638.46	8.00
	Ash *(HW)*	5.75	105.57	84000	277.03	17.06	94300	912.87	6.00
	Beech *(HW)*	8.89	127.44	61750	363.83	15.55	86400	669.00	6.00
	Sapele *(HW)*	7.80	92.73	58050	219.11	18.17	57200	819.08	6.00
	AVERAGE	**7.15**	**86.15**	**50070**	**230.90**	**11.51**	**50180**	**658.63**	**6.50**
	RANGE	**4.07**	**79.72**	**59090**	**311.05**	**11.89**	**77200**	**428.07**	**2.00**
	STANDARD DEVIATION	**1.44**	**25.24**	**18350**	**94.06**	**4.65**	**28200**	**148.44**	**0.93**
10% (NOMINAL)	Scots Pine *(SW)*	5.83	61.99	21000	152.64	7.97	25200	559.04	14.00
	Yellow Pine *(SW)*	4.03	47.62	19200	91.30	5.69	16120	436.15	11.00
	Douglas Fir *(SW)*	6.14	58.57	24750	43.32	3.97	26850	478.93	14.00
	Western Red Cedar *(SW)*	3.95	54.60	22100	268.98	4.76	26250	460.96	11.00
	Siberian Larch *(SW)*	6.70	88.62	28840	208.32	10.34	27280	615.38	11.00
	Ash *(HW)*	8.23	119.09	61740	123.21	14.20	84000	850.73	10.00
	Beech *(HW)*	11.36	95.04	47250	211.37	14.15	60750	696.65	11.00
	Sapele *(HW)*	9.11	113.05	45500	691.02	14.31	28600	759.75	8.00
	AVERAGE	**6.92**	**79.82**	**33790**	**223.77**	**9.42**	**36880**	**607.20**	**11.25**
	RANGE	**7.41**	**71.47**	**42540**	**647.70**	**10.34**	**67880**	**414.58**	**6.00**
	STANDARD DEVIATION	**2.54**	**27.77**	**15670**	**202.15**	**4.43**	**23080**	**151.22**	**1.98**
20% (NOMINAL)	Scots Pine *(SW)*	6.49	53.85	8750	128.55	10.85	15260	546.36	20.00
	Yellow Pine *(SW)*	3.24	30.57	3840	46.22	2.22	11700	416.88	25.00
	Douglas Fir *(SW)*	4.47	40.92	20470	152.23	4.85	21000	462.60	25.00
	Western Red Cedar *(SW)*	4.69	56.63	10330	138.98	3.74	16640	434.53	25.00
	Siberian Larch *(SW)*	4.08	48.80	22500	136.96	5.76	24080	604.35	20.00
	Ash *(HW)*	7.76	103.94	42750	84.88	7.32	70950	714.17	24.00
	Beech *(HW)*	5.11	78.47	42000	209.07	7.17	35500	737.15	27.00
	Sapele *(HW)*	3.15	62.47	38740	195.14	10.64	28250	632.64	23.00
	AVERAGE	**4.87**	**59.46**	**23670**	**136.50**	**6.57**	**27920**	**568.59**	**23.63**
	RANGE	**4.61**	**73.37**	**38910**	**162.85**	**8.63**	**59250**	**320.27**	**7.00**
	STANDARD DEVIATION	**1.58**	**22.93**	**15730**	**53.23**	**3.08**	**18980**	**124.04**	**2.50**
SAT (NOMINAL)	Scots Pine *(SW)*	4.41	47.00	15400	6.21	5.70	9100	530.23	32.00
	Yellow Pine *(SW)*	2.49	26.65	10200	7.75	2.31	7100	407.70	35.00
	Douglas Fir *(SW)*	3.66	29.69	22000	25.20	4.42	11600	448.67	35.00
	Western Red Cedar *(SW)*	4.33	43.84	21930	19.91	3.49	11000	354.88	30.00
	Siberian Larch *(SW)*	4.45	40.83	22800	7.71	4.71	14200	575.65	32.00
	Ash *(HW)*	5.62	73.15	45990	18.45	6.34	40000	708.26	45.00
	Beech *(HW)*	5.84	76.76	45600	16.20	8.35	31200	787.75	40.00
	Sapele *(HW)*	4.78	69.15	45000	19.54	11.39	21000	595.21	31.00
	AVERAGE	**4.45**	**50.88**	**28610**	**15.12**	**5.84**	**18150**	**551.04**	**35.00**
	RANGE	**3.35**	**50.11**	**35790**	**18.99**	**9.08**	**32900**	**432.87**	**15.00**
	STANDARD DEVIATION	**1.06**	**19.64**	**14610**	**7.02**	**2.89**	**11760**	**147.96**	**5.13**

3.3 Toughness

The average toughness values (**Ub** and **Us**) range from 18000-50000 J/m^2. These values are not as significantly affected by the grain direction as the materials strength (**MOR** and **τ**) or elasticity (**MOE** and **G**). The mean values obtained by **σ** vs. **ε** plots in three point bending (**U**b) yielded approximate values only 10% greater than the mean values obtained by **σ** vs. **ε** plots in longitudinal shear (**U**s).

4 DISCUSSION

Established values in literature (Bergman et al 1999) are compared to the obtained mechanical properties in this study (for woods of low moisture content ≈ 6-12%):

- The **MOR** values in this study are 5% lower than the values in literature for the hardwood and 8% lower for the softwoods.
- The **MOE** values are 14% lower for the hardwoods and 41% lower for the softwoods.

- The **Ub** values are 28% lower for the hardwoods and 41% lower for the softwoods.
- The **τ** values in this study 20% higher for the hardwoods and 7% lower for the softwoods.

There were no readily available values of **Us** or **G** from literature to compare to the obtained values documented in this study. **MOE** and **Ub** recorded values collate less well to established values in literature than **MOR** and **τ** recorded values. Both **MOE** and **Ub** are dependent upon strain however **MOR** and **τ** are not. The source of this discrepancy must hence originate from different measurements of strain. A possible cause of this could be variations in the crosshead speed of the universal testing machine. American standards (ATSM 2009) specify speeds of 1.3 mm/min and 0.6 mm/min for the bending and shear tests respectively. Crosshead speeds in the comparable study (Bergman et al 1999) are not specified.

5 CONCLUSION

In general, the American standards for testing (ATSM 2009) were accurately able to determine strength properties, i.e. **τ** and **MOR** (although a small percentage of error in **τ** was observed for the hardwood species evaluated). A larger degree of error was however noticed for the elastic and toughness properties. The values for the bending toughness values (**Ub**) and elastic modulus (**MOE**) documented in this study are noticeably lower than values from literature (Bergman et al 1999). Documented values of shear toughness (**Us**) and modulus of rigidity (**G**) were not readily available from literature to compare to the values recorded in this study. Hence further work is warranted to investigate how values of **Us** and **G** (obtained using the American standard) compare to values using other test methodologies.

REFERENCES

1942. AFNOR NF B51-012: Wood Shear Test, *French National Organisation for Standardisation*, Paris

Munthe, B.P and Ethington, R.L. 1968. Method for evaluating Shear Properties of Wood. *U.S. Department of Agriculture Forest Service,* Madison, WI

Bergman, R. Cai, Z. Carll, C.G. Clausen, C.A.; Dietenberger, M.A. Falk, R.H. Frihart, C.R.; Glass, S.V.; Hunt, C.G. Ibach, R.E. Kretschmann, E. Rammer, D.R.; Ross, R.J. Star, N.M. Wacker, J.P. Wang. X. White, R.H, Weidenhoeft, A.C. Weimann, M.C. Zelinka, S.L. 1999. Wood Handbook, Wood as an Engineering Material*, U.S. Department of Agriculture Forest Service,* Madison, WI

Gustafsson, S. I. 2001. Mechanical Properties of some Swedish hard wood species, *Proceedings of the Institution of Mechanical Engineers,* 215:125-131

Reiterer, A. and Stanzl-Tschegg, S. E. 2001. Compressive behaviour of softwood under uniaxial loading at different orientations to the grain. *Mechanics of Materials,* 33:705-715

2003. BS EN 408: Timber structures - Structural timber and glued laminated timber - Determination of some physical and mechanical properties. *British Standards Institute*, London

Coutand, C. Jeronimidis, G. Chanson, B. and Loup, C. 2004. Comparison of mechanical properties of tension and opposite wood in Populus, *Wood Science and Technology,* 38:11-24

Eyma, F. Méausoone, P.J. and Martin, P. 2004. Strains and cutting forces involved in the solid wood rotating cutting process. *Journal of Materials Processing Technology, 148:*220-225

Galicki, J. and Czech, M. 2005. Tensile strength of softwood in LR orthotropy plane. *Mechanics of Materials,* 37:677-686

Wechsler, A. and Hiziroglu, S. 2007. Some of the properties of wood-plastic composites. *Building and Environment,* 42:2637-2644

2009. ASTM D143-09: Standard Test Methods for Small Clear Specimens of Timber. *American Society for Testing and Materials*. West Conshohocken, PA

Manríquez, M. J. and Moraes, P. D. 2009. Influence of the temperature on the compression strength parallel to grain of paricá. *Constr Build Mater,* 24: 99-104

Oh, S.C. 2011. Applying failure criteria to the strength evaluation of 3-ply laminated veneer lumber according to grain direction by uniaxial tension test *Constr Build Mater,* 25:1480-1484

International Conference on Manufacturing Research
(ICMR) 2012
11 – 13 September 2012, Aston Business School

Aston Business School

BEST 3rd YEAR ICMR DOCTORAL PAPER AWARD

presented to:

Andrew Naylor, Philip Hackney and Noel Perera

for their paper:

Determination of wood strength properties through standard test procedures

Signed: on behalf of COMEH and the ICMR 2012 organising committee

A33

EVALUATION OF HANDSAW TOOTH PERFORMANCE THROUGH THE DEVELOPMENT OF A CONTROLLED CUTTING TEST RIG

Andrew Naylor
Philip Hackney
Noel Perera
School of Computing, Engineering and Information Sciences
Northumbria University, Ellison Building
Newcastle Upon Tyne, NE1 8ST, UK
andrew2.naylor@northumbria.ac.uk

ABSTRACT

In this study a conventional shaper machine has been converted into a controlled cutting test rig. A specially designed tool holder was attached to the actuating arm of the shaper machine. This tool holder constrained a small group of handsaw teeth designed to machine a groove followed by an adjustable single tooth that machined a specified depth of cut. A work-piece dynamometer was attached to the platform of the shaper machine. The three force transducers that compose the dynamometer were used to measure resultant cutting, thrust and side forces in the relative X, Y and Z axes. These are measured as the single tooth passes through the work-piece. In addition to force measurement, a high speed video camera was utilised to capture footage of the chip/surface formation where the tooth interacts with the wood work-piece. The recorded forces and captured footage of chip formation validate published findings that machining along the wood grain is a shearing process and machining across wood the grain is a bending process.

Keywords: Wood Machining, Sawing Processes, High Speed Photography

1 INTRODUCTION

The two parameter groups that influence the cutting mechanics in wood machining are: 1) Parameters associated with the tool geometry, i.e. rake angle, edge width, edge radii etc. 2) Parameters associated with the work-piece, i.e. moisture content, grain direction, physical/mechanical properties etc. The cutting process itself is scrutinised by two separate methods, findings of which can then be combined to make well rounded conclusions. The first method is the measurement of forces acting on the cutting edge of the tool; this is usually done by using force transducers. The second method is the characterisation of chip and surface formation; this can be a simple process of viewing collected chip/surfaces under the microscope or a more sophisticated process of recoding high speed video of the cutting process. The fundamental literature detailing the chip and surface formation across the grain (Franz 1955, Woodson and Koch 1970) details only processes where a large orthogonal tool removes material across the entire work-piece width. This process and the sawing process differ far too greatly to attempt to draw comparisons between the chip/surface formations of the two. From other fundamental literature three distinctive types of chip formation have been observed to occur along the grain (McKenzie 1961). The first type (type I) is caused by a large rake angle producing a negative thrust forces (acting in a positive vertical direction relative to the work-piece). The wood fibres split ahead of the tool and finally fail due to bending. This type of chip is beneficial where quick removal of material is required. The second type (type II) is formed by a very sharp tool edge and a diagonal plane of shear. Excellent surface finish is achieved due to the continuous chip formation. The third type is caused by dull tool edges, and very small or negative rake angles. It is also suggested that very large depths of cut may form this chip where there is too much contact with the blade surface. This third type (type III) of chip causes a raised *fuzzy grain*

where wood fibres become protruded, hence a poor surface finish. It is important to note that evidence from the fundamental literature (McKenzie 1961, Woodson and Koch 1970, Franz 1955, Kivemaa 1950) infers that varying the cutting velocity has a negligible effect on the tool forces.

A high speed camera has been previously utilised to capture footage of the cutting process for single circular saw teeth (Ekevad et al. 2011). The camera was set up to record 40,000 frames per second for a circular saw rotating at a speed of 3250 RPM. Green, dry and frozen wood was machined in the 90°-0° direction (along the grain) using single rip teeth with rake angles of 0°, 10°, 20° and 30°. The only observed continuous chip formation (type II) was for green wood, with the dry and frozen work-pieces yielded smaller broken wood particles (type I). Furthermore the footage was able to evaluate the action of the gullet. Reduced rake angle leads to a reduction in gullet volume, still images from this footage show a build up of wood particles for the larger rake angles (lower gullet volume), as the wood chips/particles are prevented from curling past the much smaller root radii. This results in an impaction of wood particles in the gullet impeding the material removal from the kerf.

A study conducted to compare the fundamental chip formation types along the grain to chips formed cutting using a rip saw tooth (Naylor et al. 2011) found that fuzzy chips (type III) occurred machining work-pieces of high moisture content, discontinuous chips (type I) occurred machining dry work-pieces at high depths of cut and the continuous chips (type II) were formed machining dry to moderate moisture content work-pieces at lower depths of cut. Machining across provided no chip for analysis, only a deformed work-piece surface. This surface formation consisted of the fracturing of fibres perpendicular to the grain. Dry work-pieces exhibited a visible tool path with extremely deformed fibres bent out of position. Saturated work-pieces exhibited no visible tool path; this is due to the severed fibres, of increased moisture content, springing back to cover the tool path.

A related study (Naylor et al. 2012) uses properties of the wood obtained through mechanical testing to develop two predictive cutting force models. This study also uses a rip saw tooth of the same geometry as mentioned in the previous paragraph. The first regression model has an R^2 of 90%, it took properties obtained from a three point bending test procedure (used to evaluate the wood strength across the grain) and cutting forces obtained machining across the grain. The second regression model has an R^2 of 80% it took properties obtained from a longitudinal shear test (used to evaluate the wood strength along the grain) and cutting forces obtained machining along the grain.

The aim of the research discussed in this paper was to develop a controlled cutting test rig capable of determining the cutting mechanics for single saw teeth. This aim was facilitated by obtaining footage and still images of the chip formation process to further validate the novel statements regarding the mechanics of cutting; *"cutting along the grain is a shearing process"* and *"cutting across the grain is a bending process".* High speed footage and optical microscope images were obtained to characterise the chip and surface formation. Tool forces were recorded for varied depth of cut to provide a comparison to the tool forces obtained using the rip tooth in prior related research (Naylor et al. 2011 and 2012).

2 METHODOLOGY

2.1 Single Tooth Test-rig

The saw-tooth geometry selected for the experiment has an orthogonal cutting edge of 0.85 mm, a negative rake angle of 12° and a flank angle of 50° (Figure 1). In industry this tooth geometry is described as a rip tooth due to the low negative rake and lack of bevelled edges that would provide obliquity during cutting. Saws with this type of tooth geometry are typically used only along the grain with each tooth removing material in a chisel like action. In this study machining took place both along and across the wood grain for only one species (douglas fir).

A conventional shaper machine was procured to perform a linear cutting action using selected handsaw teeth (Figure 2.A). The simplified test rig schematic (Figure 2.B) shows the basics of how the tool forces were measured. The cutting tool (1) passed through the work-piece clamped to the dynamometer. The dynamometer platform fed into the cutting tool in even increments for each stroke (2).

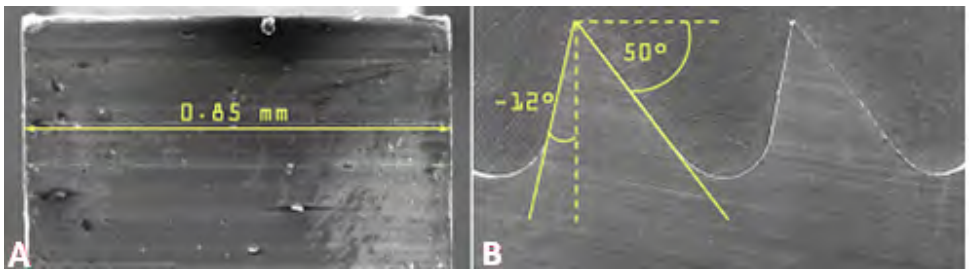

Figure 1: A) Edge Width: B) Rake and Flank of Tooth

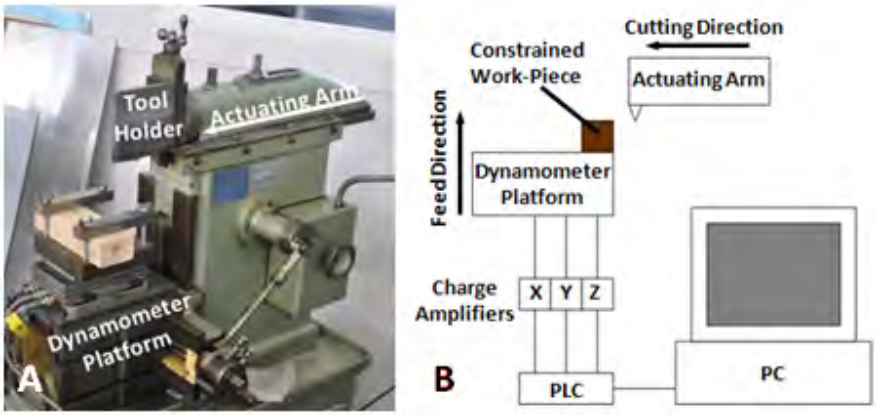

Figure 2: A) Shaper Machine Set-Up: B) Detailed Test-Rig Schematic

The forces applied to the work-piece stimulated a charge output from the transducers which then channelled through to the charge amplifiers (3). These amplified values were converted from analogue to digital (4) and finally were recorded on the PC (5). To elaborate, the dynamometer consisted of three piezoelectric transducers measuring forces in the x, y and z directions. The x and y axes transducers had a sensitivity of 7.5 pC/N and could measure up to 5 kN of force. The z axis had a sensitivity of 3.7 pC/N and could measure up to 10 kN of force. The signal output from each transducer was channelled into an analogue charge amplifier (one amplifier per transducer). The input sensitivity was calibrated to match the transducer sensitivity (in pC) and the output range was set to 100 N = 1 V up to a maximum output of 10 V (1 kN). The output from the charge amplifier was then sent to a data acquisition PLC, converting the analogue signal to digital allowing the forces to be recorded on a PC using LabView signal express.

2.2 Recording High Speed Video Footage

A high speed camera capable of recording 1000 frames per second was acquired for this experiment. A group of four teeth were used to perform the cut. This group of teeth was inclined in the tool holder at 3° ensuring that each tooth performed a depth of 0.15 mm (based on a pitch of 7 teeth per 25 mm). Cutting was performed along and across the wood grain for both dry and saturated work-pieces. Typically the first tooth would perform little to no cutting with the second tooth performing the first cut. Subsequently the third and fourth teeth would each machine at a depth of 0.15 mm visible to the camera.

2.3 Single Tooth Tests

Tests performed using only single teeth were not recorded using the high speed camera. This was because most of the tooth was obscured from view by a prior machined groove. The purpose of the groove was to

provide a level cutting surface parallel to the tool path ensuring that a constant depth of cut was maintain for the entire work-piece surface. Depths of cut of 0, 0.05, 0.15, 0.2, 0.25, 0.3, 0.35 mm were performed along and across the wood grain for both dry and saturated work-pieces. The offset between the single tooth and the prior machined groove was controlled using feeler gauges ensuring an accurate depth of cut.

3 RESULTS

3.1 Chip Formation

Machining the dry work-piece along the grain yielded continuously formed, unbroken wood chips and a cleanly cut surface. In contrast to this, machining the saturated work-piece along the grain yielded fuzzy chips. It is apparent from the high speed video frames that the wood fibres in these chips disintegrated when removed from the work-piece surface by the saw tooth. Furthermore, similar disintegrated wood fibres were left behind on the surface.

Initial deformation perpendicular to the grain is observed in the high speed video frames when machining the dry work-piece across the grain. This was followed by an instantaneous failure and more aggressive cutting process from the following teeth. Machining the saturated work-piece across the grain exhibits a less aggressive cutting process. It is apparent from the frame by frame analysis that these fibres are initially deformed in a similar way to the dry work-piece. The fibres spring back towards the tool path and are subsequently removed from the surface. It must be noted that the tooth that initially makes contact with these fibres is only performing a ploughing action; the uprooting effect is caused by teeth that follow.

3.2 Tool Forces

The mean tool forces (Figure 5B) combine all work-piece conditions to provide average response data for cutting, thrust and side forces. The magnitudes of the thrust forces are approximately 12% the magnitude of the cutting forces, for all depths of cut (i.e. the thrust forces are proportional to the cutting forces as they both increase with depths of cut). The side forces exhibit no noticeable trend for increasing depths of cut with magnitudes ranging from 2 to 5 % of that of the cutting forces.

When evaluating the measured cutting forces for all work-piece variations (Figure 5A) a few trends are noticed. On average machining along the grain yields approximately half the cutting force observed across the grain. Machining saturated work-pieces yields lower cutting forces; in the range of 70 – 80 % of the values observed for the dry work-pieces (this excludes 0 and 0.05 mm depth of cut for saturated, across the grain, which are slightly larger force values than observed for dry, across the grain). In summary, the cutting forces for the different work-piece conditions all have the same linear trend with respect to depth of cut. The only thing that differs between the different work-pieces is the magnitude of the forces.

4 DISCUSSION

4.1 Chip Formation

The chip and surface formation observed draw similarities to formations observed from fundamental literature (McKenzie 1961) and previous study where a single rip saw tooth was used (Naylor et al. 2011). Machining the dry work-piece along the grain forms continuous chips (type II) and machining the saturated work-piece along the grain forms fuzzy chips (type III). No discontinuous chips (type I) were formed as only the relatively low depth of 0.15 mm was performed. Surface formation machining across the grain also draws some similarities to the previous study. The surface formation of the dry work-piece displays permanently deformed fibres with a visible tool path. The surface formation of the saturated

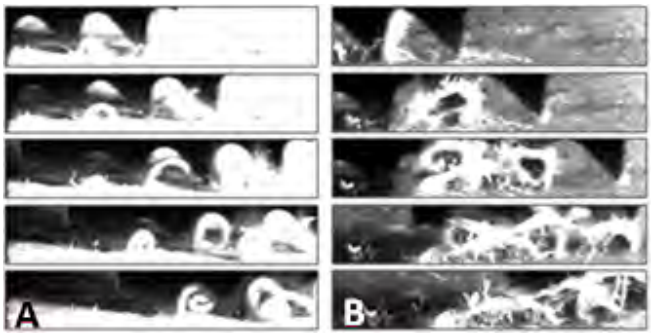

Figure 3: A) Chip Formation Along the Grain, Dry; B) Along the Grain, Saturated

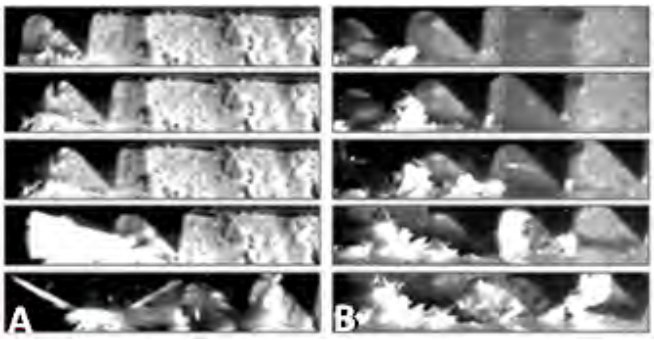

Figure 4: A) Surface Formation Across the Grain, Dry; B) Across the Grain, Saturated

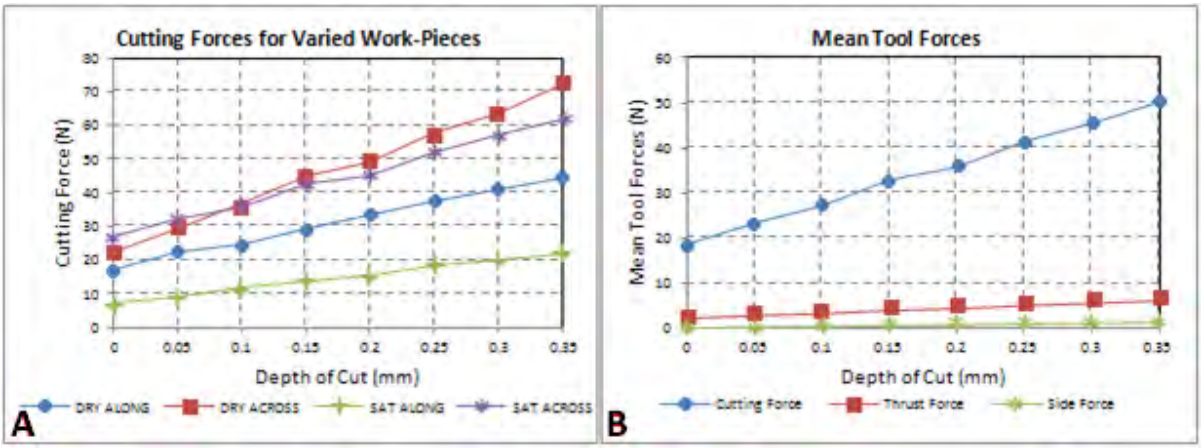

Figure 5: A) Cutting Force vs. Depth of Cut for all Work-piece's; B) Mean Tool Forces vs. Depth of Cut

work-piece shows some sections along the length of the kerf were fibres have sprung back over the tool path, but other sections where fibres have been uprooted by the subsequent teeth in the group. No major chip formation comparisons can be drawn to the circular saw study (Ekevad et al. 2011), which also used high speed video footage to analyse the chip. The reasons for this are the difference in work-piece (**1**) (the circular saw study uses green and frozen wood) and a focus on the gullet performance rather than the interaction with the wood and the major cutting edge (**2**). A key difference is noticed for machining dry work-pieces along the grain, which yielded discontinuous wood chips (type I). This is most probably due to the circular saw tooth geometries which have large positive rake angles.

4.2 Tool Forces

From prior research (Naylor et al. 2011 and 2012) average tool force values show that the cutting force is approximately 4.5 times larger than the thrust force and 25 times larger than the side force across the grain. Along the grain the cutting force is approximately 3.5 times larger than the thrust force and 10 times larger than the side force. Analysis of the mean tool forces in this study (combining both along and across the grain) show the cutting force to be approximately 8 times larger than the thrust force and in the range of 20 – 50 times larger than the side force. This discrepancy is due to the difference in tooth geometry and cutting conditions. The geometry of the tooth used in prior research had zero rake and a 1 mm cutting edge. The geometry of the tooth used in this research had a negative rake of 15° and a 0.85 mm cutting edge. Furthermore the depths of cut performed in the prior research where in the range of 0.4 – 1.2 mm. The depth of cut range used in this study was much lower, 0 – 0.35 mm.

4.3 A Statement on the Mechanics of Cutting

It is important to note that the high speed video footage provides frame by frame evidence to support findings from related research (Naylor et al. 2012). The statement that machining along the grain is a shearing process is supported by the visible shearing action providing ongoing continuous formation with no break off points. The statement that machining across the grain is a bending process is supported by the high speed video showing the fibres deforming in a bending process prior to fracture.

5 CONCLUSION

It has been proven that the test rig developed can effectively evaluate the cutting mechanics for single saw teeth. This has been demonstrated through the high speed recordings of chip formation and the tool force measurements. The most significant of the measured tool forces is that in the direction of cutting ranging from 20 – 50 N (based on an average of all work-piece variations). The thrust force is less significant, approximately 12% of the cutting force. The side force is the least significant force with recorded values under 5% the magnitude of the cutting forces. The cutting force values show that the different work-piece variations all have the same linear trend with respect to depth of cut; only the magnitude of the forces varies. Typically cutting dry work-pieces yielded higher forces than saturated work-pieces, cutting across the grain yielded higher forces than cutting along the grain.

The still frames from the high speed video of the chip and surface formations provided supporting evidence to two novel statements with regard to the mechanics of cutting using teeth with orthogonal edges: 1) *Cutting across the grain is a bending process;* 2) *Cutting along the grain is a shearing process.*

REFERENCES

Kivimaa, E. 1950. Cutting force in woodworking. *VTT Julkaisut*, 18:1-101

Franz, N. C. 1955. An Analysis of Chip Formation in Wood Machining. *Forest Prod J*, 10:332-336.

McKenzie, W. M. 1961. Fundamental analysis of the wood cutting process. *Department of Wood Technology*, University of Michigan, MI

Woodson, G. E. and Koch, P. 1970. Tool Forces and Chip Formation in Orthogonal Cutting of Loblolly Pine. *U.S. Department of Agriculture Forest Service*, New Orleans, LA

Ekevad, M. Marklund, B. and Gren, P. 2011. Wood chip formation in circular saw blades studied by high speed photography. *Proceedings of the 20th International wood machining seminar.* Skellefteå, Sweden. 55-61

Naylor, A. Hackney P. and Clahr, E. 2011. Machining of Wood using a Rip Tooth: Effects of Work-piece Variations on Cutting Mechanics. *Proceedings of the 20th International wood machining seminar.* Skellefteå, Sweden. 305-314

Naylor, A. Hackney, P. Perera, N. and Clahr E. 2012. A Predictive Model for the Cutting Force in Wood Machining Developed using Mechanical Properties. *BioRes.* 7:2883-2894

APPENDIX 2 – MARKETING OF SAWS BY MAJOR MANUFACTURES

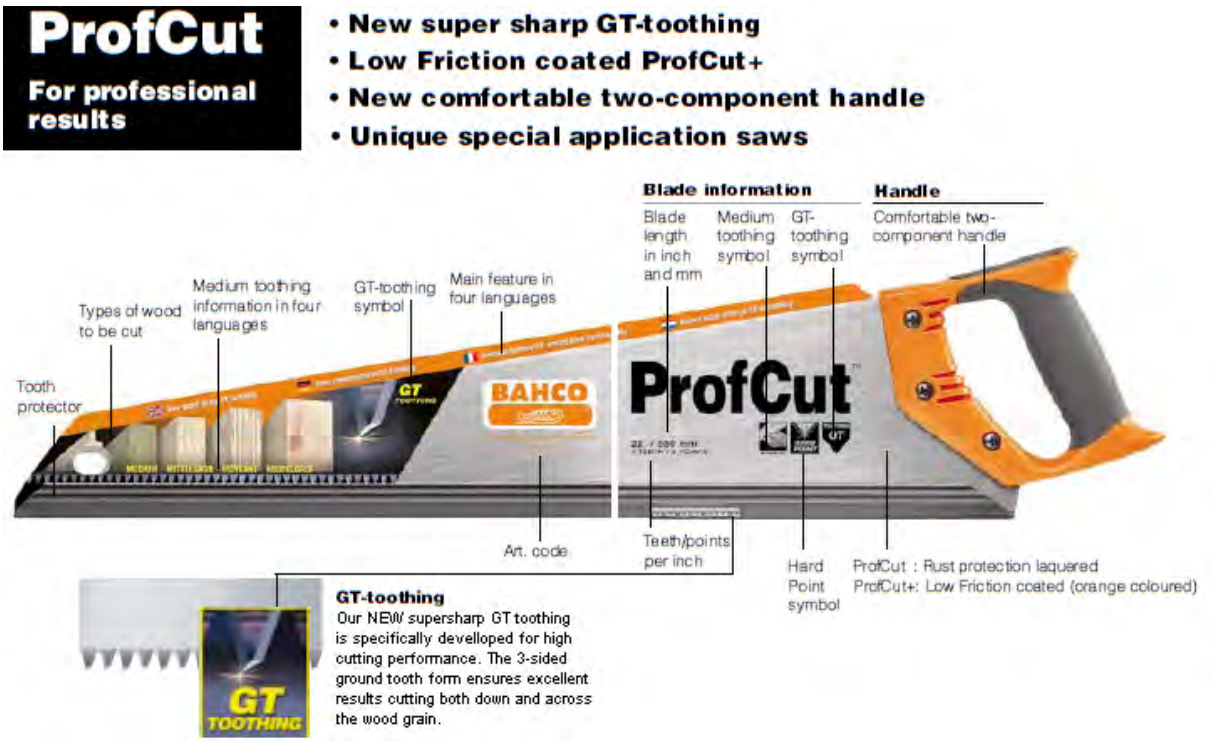

BAHCO promotional leaflet for ProfCut™ saw (GT tooth geometry)

STANLEY promotional leaflet for JETCUT™ saw (triple tooth geometry)

IRWIN promotional leaflet for JACK™ saw (universal triple ground tooth geometry)

APPENDIX 3–TOOTH GEOMETRY STANDARDS (BRITISH STANDARDS: BS 3159-1)

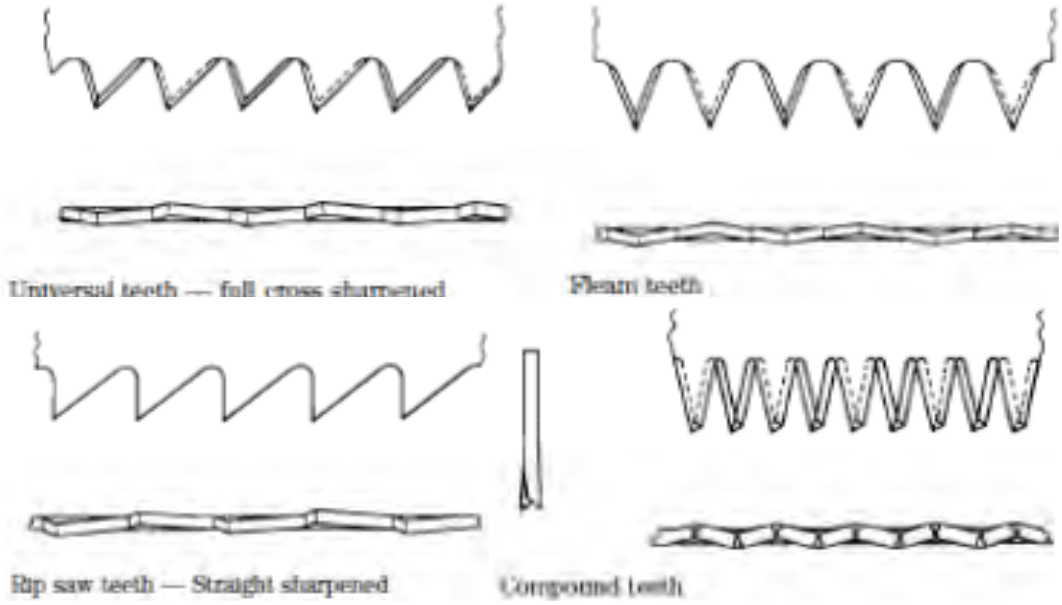

Different varieties of saw teeth

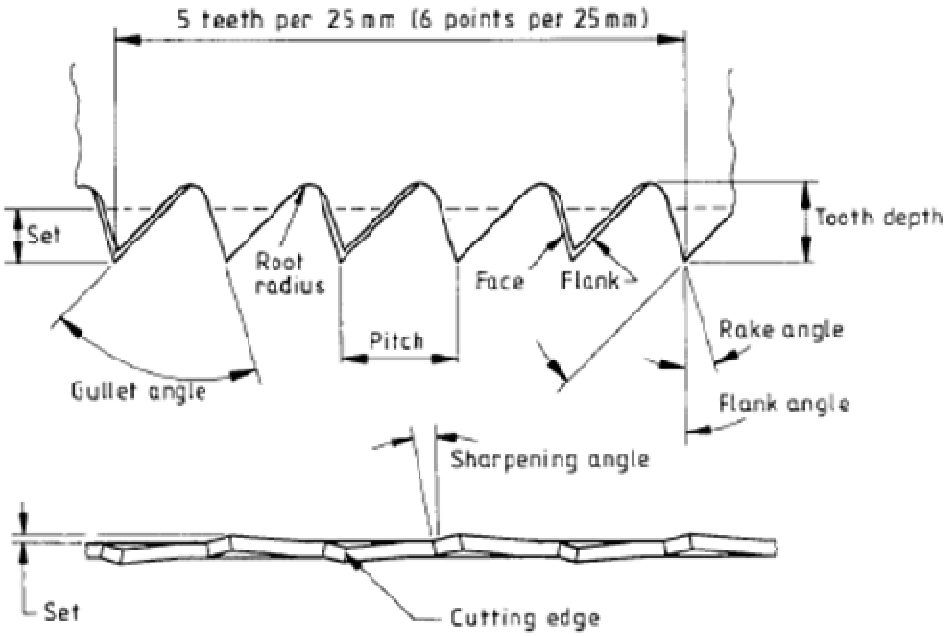

Defined geometric parameters

Specified geometries for the different varieties of saw teeth

	Rake Angle		Flank Angle		Bevel Angle		Gullet Angle
Saw Type	**Min**	**Max**	**Min**	**Max**	**Min**	**Max**	**Nominal**
General and Cross Cut Saws	-10°	-20°	40°	50°	10°	30°	60°
Rip Saws	0°	-10°	50°	60°	-	-	60°
Fleam Saws	-20°	-25°	20°	25°	10°	30°	-
Compound Saws	-10°	-20°	10°	25°	10°	30°	-

Number of teeth per 25 mm for specified length

	Number of Points per 25 mm			
Blade Length (mm)	**General and Cross Cut Saws**	**Rip Saws**	**Fleam Saws**	**Compound Saws**
450	8, 10	-	-	-
500	8, 10	-	8	8, 10, 12
550	7, 8, 10	-	8	8, 10
600	5, 6, 7, 8	-	7, 8	8, 10
650	5, 6, 7, 8	4, 4.5, 5	4.5, 5, 6	7, 8

Blade thicknesses for specified length

	Blade Thickness (mm)			
Blade Length (mm)	**Class 1**	**Class 2**	**Class 3**	**Class 4**
450	0.86	0.86	0.71	0.71
500	0.86	0.86	0.71	0.71
550	0.86	0.86	0.71	0.71
600	0.94	0.91	0.89	0.89
650	0.94	0.91	0.89	0.89

Class 1 – Best quality blades for highly skilled craftsmen
Class 2 – Good quality blades for experienced craftsmen
Class 3 – General use industrial saws
Class 4 – DIY purpose saws

• Raker Set –	N	L	N	R	N	L	L= Left Set
• Straight Set – Set	L	R	L	R	L	R	R=Right
• Wave Set – Set	L	L	L	R	R	R	N=Neutral

Setting Patterns

APPENDIX 4 – INFLUENCE OF THE CUTTING SPEED ON THE CUTTING MECHANICS

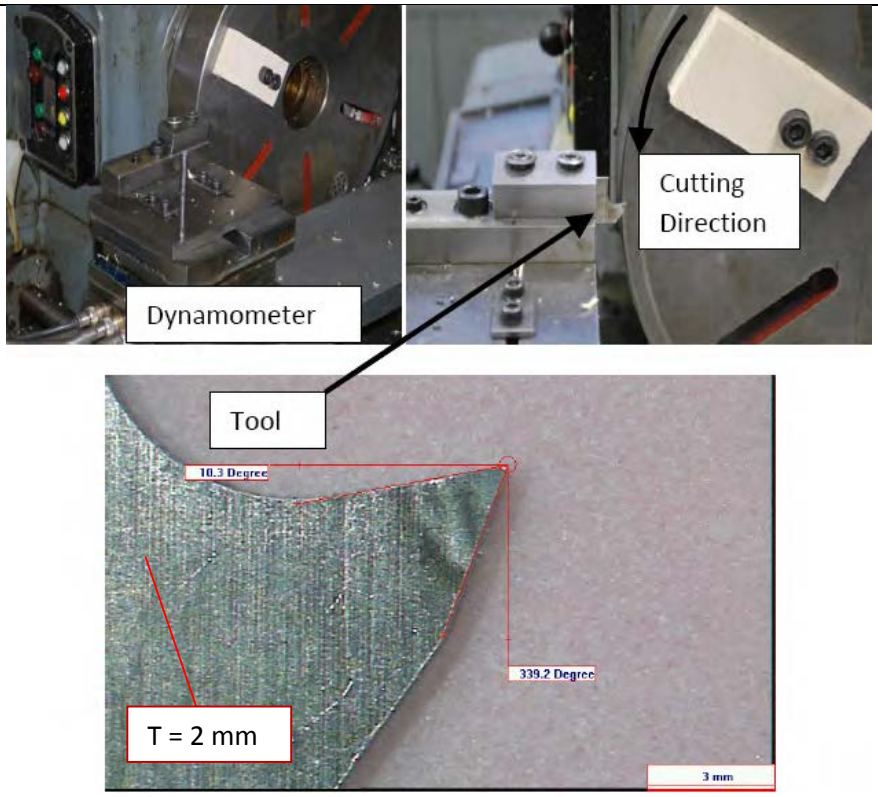

Rip tooth constrained to a dynamometer feed bed & Work-piece constrained to lathe

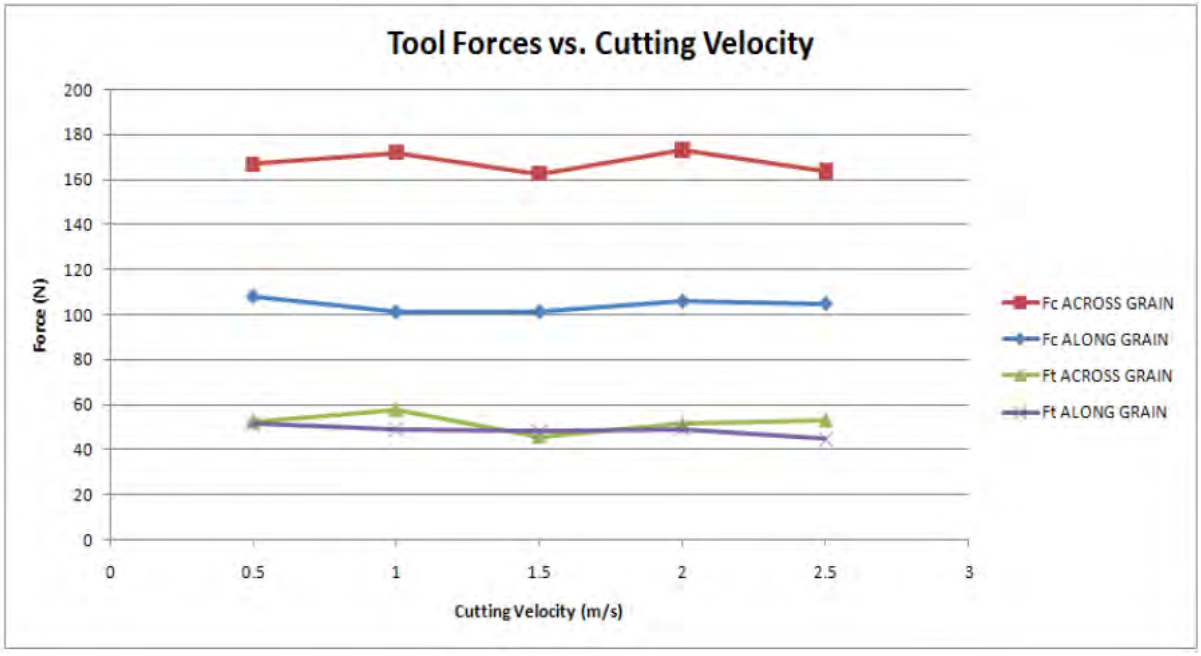

Mean Cutting and Thrust Forces

Chip formation and kerf for varied cutting speeds

APPENDIX 5 – CONTROL AND MEASURMENT OF MOISTURE CONTENT

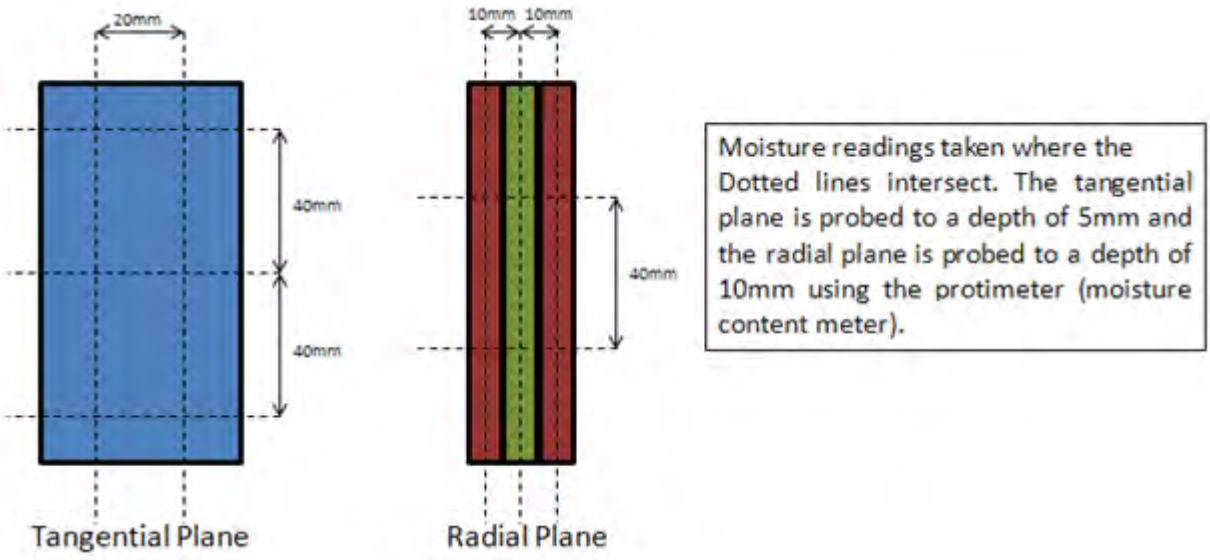

Probe locations on the wood work-piece

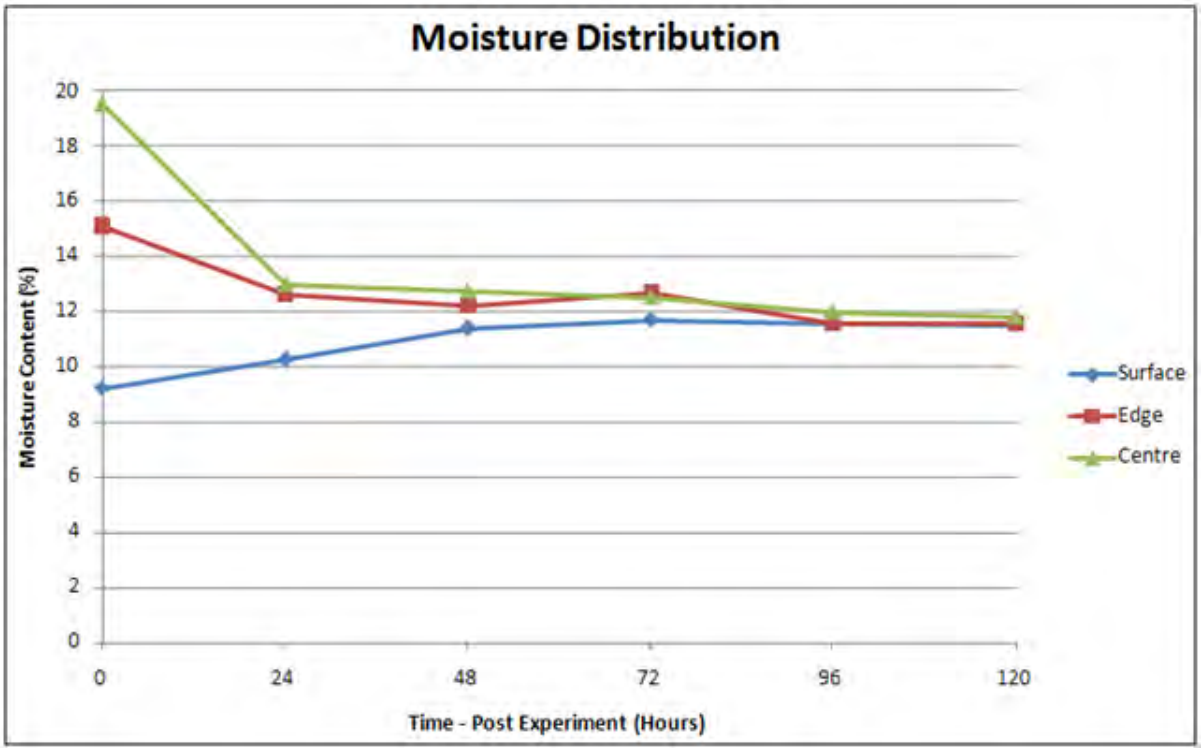

Redistribution of moisture for the 10% nominal work-piece (work-piece sealed in an air tight container)

A calibration check device (Calcheck) is supplied with the instrument for checking the Measure mode calibration. Hold the Calcheck across the electrode pins as shown. A correctly calibrated SurveyMaster will read 18.2 ±1.0. Contact your supplier if the instrument is reading incorrectly.

Check the Search mode operation by holding the instrument against a reference wall that is assumed to be in a stable condition and that does not have any pipes or wires running through it. Note and record the relative value that is displayed. Check the instrument at the same position on the reference wall at regular intervals. Contact your supplier if the reading varies by more than ±50 from the original reference value.

Calibration of the york protimeter

APPENDIX 6 – ROUTER TEST RIG: APPARATUS AND ERROR EVALUATION

KISTLER
Type 9377C

3-Component Force Link

120x120x125 mm, –150 … 150 kN

Quartz force link for measuring the three orthogonal components of a dynamic or quasistatic force acting in an arbitrary direction.

- Accurate measurement independent of the force application point
- Wide frequency range
- Easy installation
- Stainless, sealed sensor case
- Rugged multipole plug connection

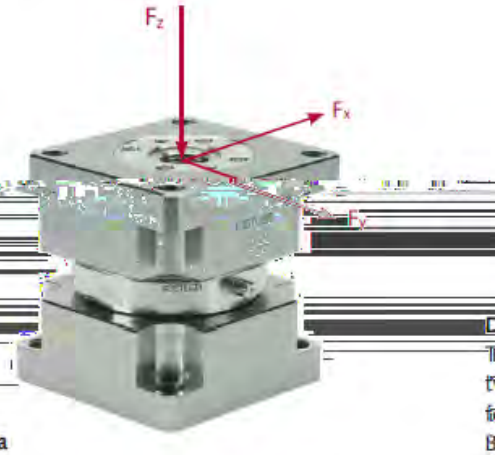

Description

The 3-component force sensor is mounted under preload between two plates and measures both tensile and compression forces in all directions.

Based on the piezoelectric principle, a force produces a proportional electric charge. This is conducted via an electrode-to-the appropriate connector.

The simple and vibration-resistant design of the force link is very rigid resulting in a high natural frequency, which is a requirement for highly dynamic force measurements.

The 3-pole connector V3 neg. (design protected) is provided with a positioning aid. This guarantees accurate assignment and centering of the connector pins and sockets before connection. The plug connection is protected against rotation.

After correct installation, the sensor is ready for use without recalibration.

Quartz 3-component force links allow simple, direct and very precise measurements.

Application

3-component force links measure:

- Cutting forces during machining
- Impact forces in crash tests
- Recoil forces of rocket engines
- Vibration forces of components for space travel
- Friction forces
- Forces in product testing
- Ground reaction forces in biomechanics
- Vehicle forces on a road and a test stand
- Forces on a wind tunnel balance

Technical Data

Range (Without moment loading, e.g. when four force links are mounted in a force plate)	F_x, F_y	kN	–75 … 75
Range (Example with force application point on the surface of the cover plate)	F_x, F_y	kN	–30 … 30
Range (Force application point centric)	F_z	kN	–150 … 150
Overload	F_x, F_y, F_z	%	10
Calibrated range (Force application point 10 mm below the surface of the cover plate)	F_x, F_y	kN	0 … 30 0 … 3
Calibrated range (Force application point centric)	F_z	kN	0 … 150 0 … 15
Permissible moment load ($M_z = 0$; $F_z = 0$)	M_x, M_y	N·m	–2 040/2 040
Permissible moment load ($M_{x,y} = 0$, $F_z = 0$)	M_z	N·m	–2 040/2 040
Threshold		N	≤0,01
Sensitivity	F_x, F_y	pC/N	≈–3,9
	F_z	pC/N	≈–1,95

Kistler dynamometer type K9377 technical specifications

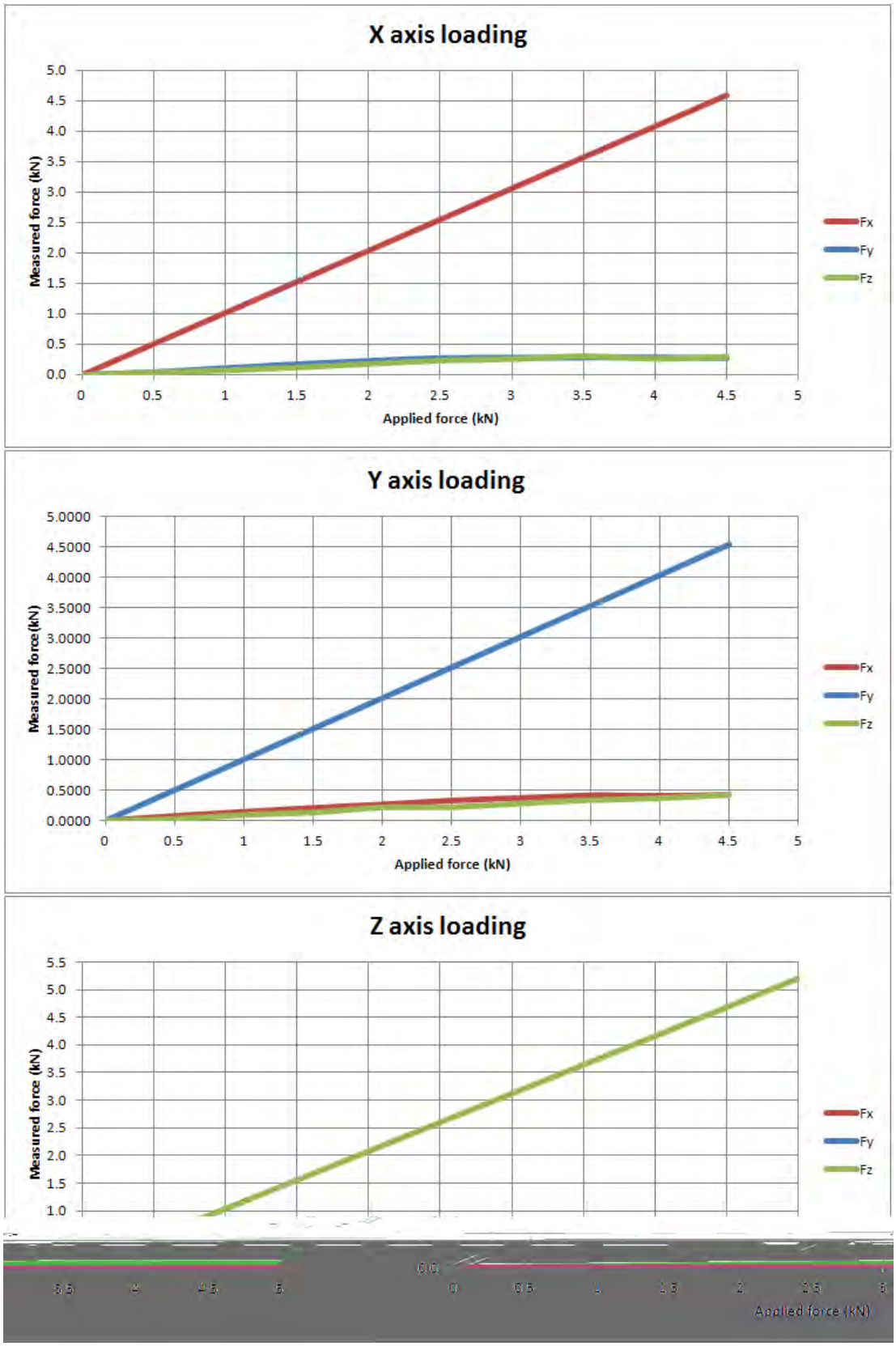

Loading of the K9377C dynamometer in the universal testing machine (with cross interference in un-tested directions)

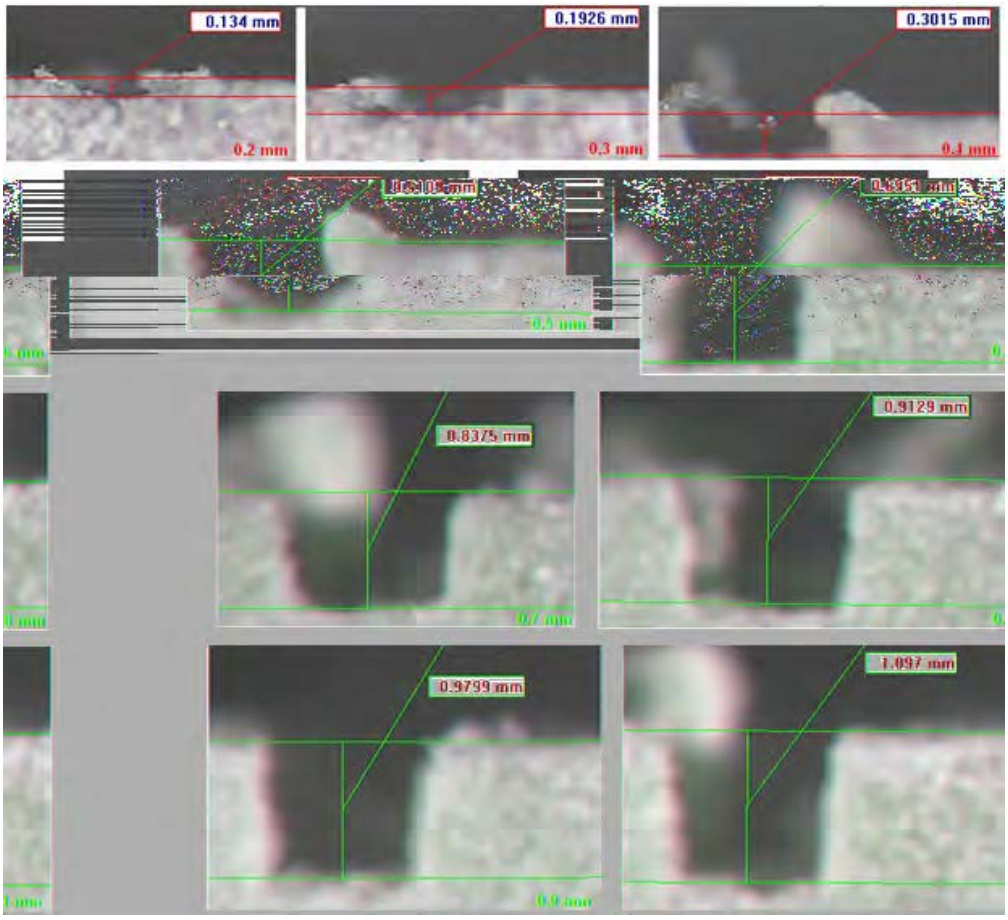

Programmed depths of cut (red) and measured depth of cut (blue) using the CNC router machine

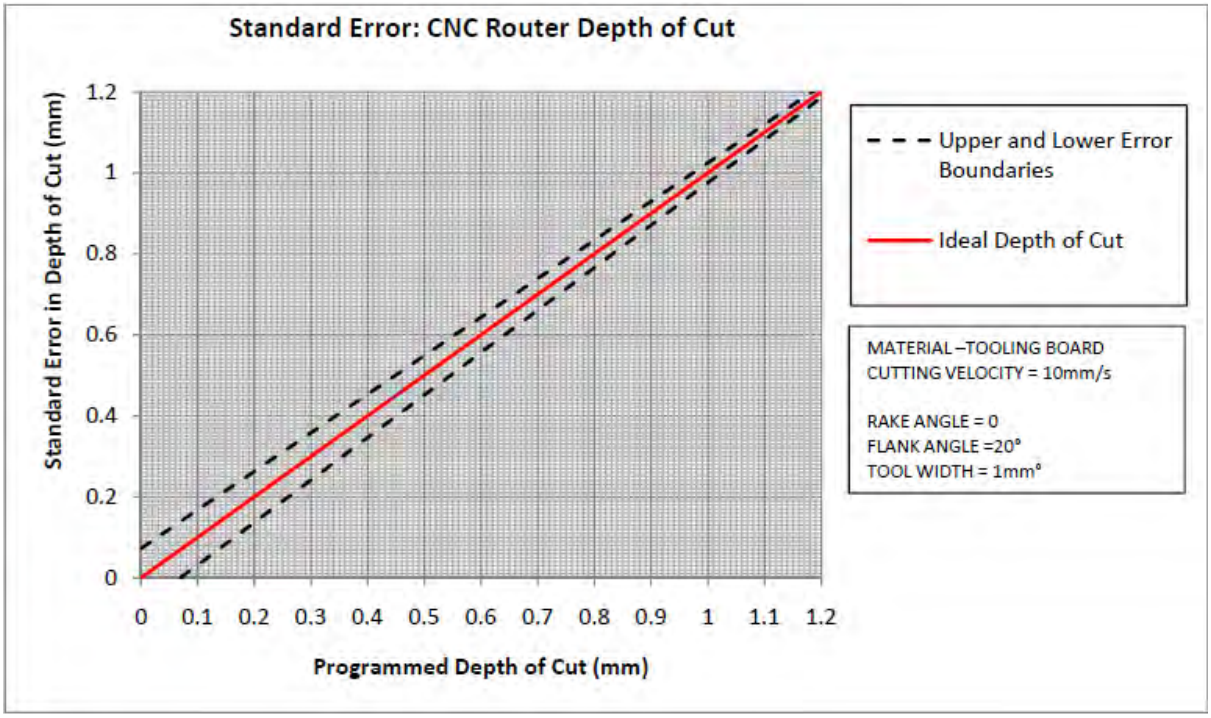

Observed error for selected depths of cut

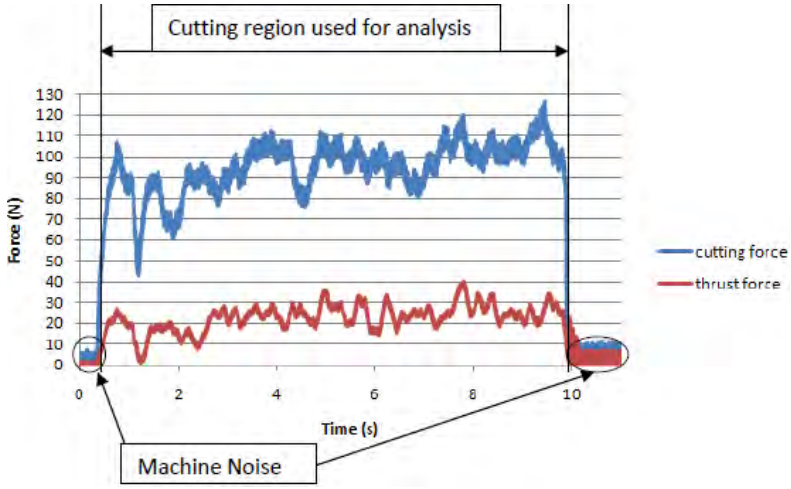

Force vs. time plot measuring the cutting force (Y axis) and thrust force (Z axis)

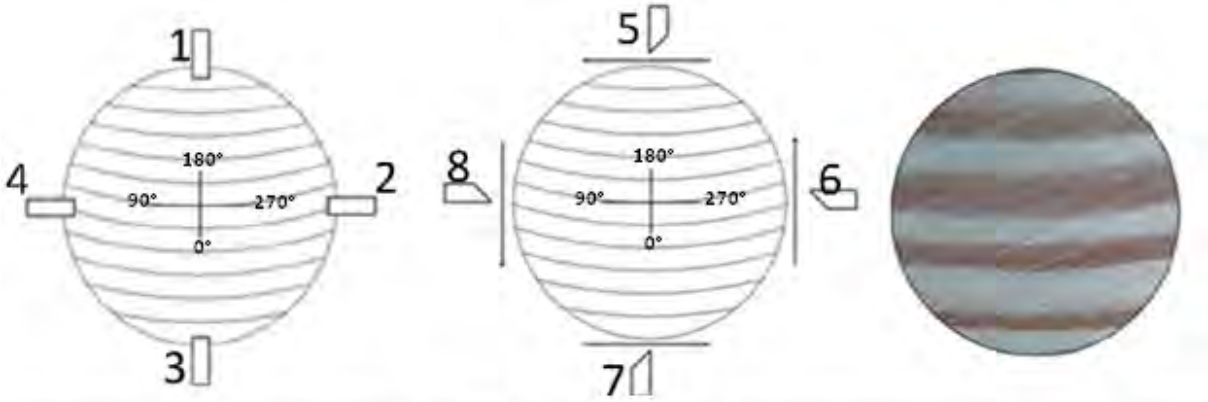

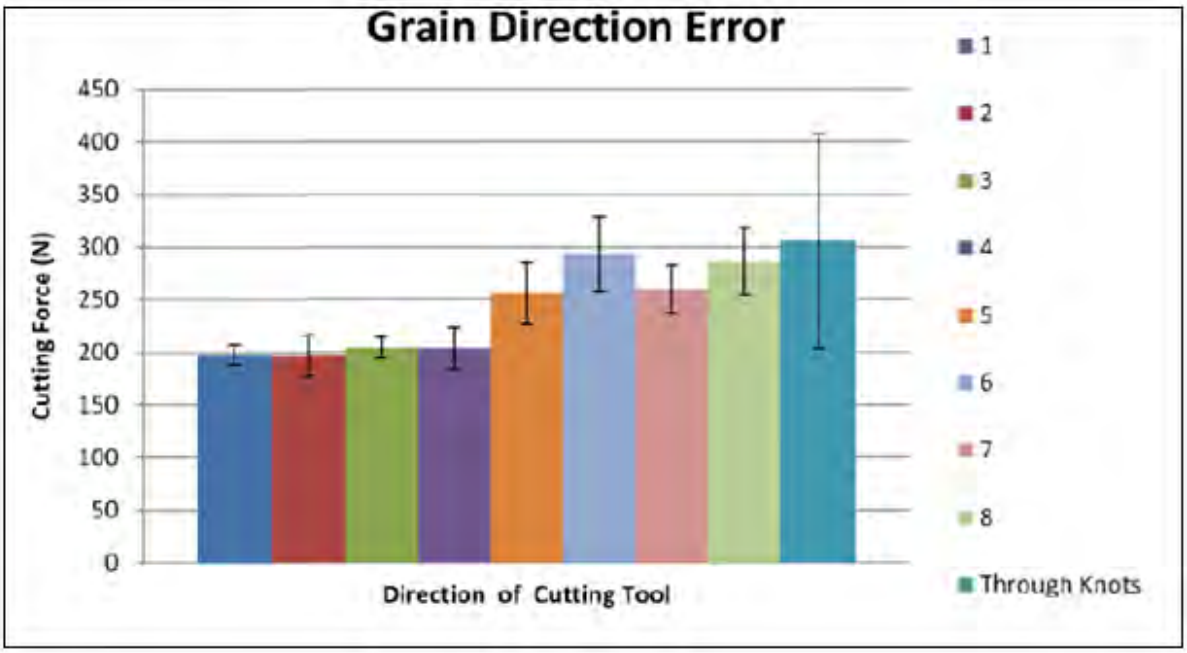

Average cutting forces (and error) observed for different machining directions with respect to the annual growth rings

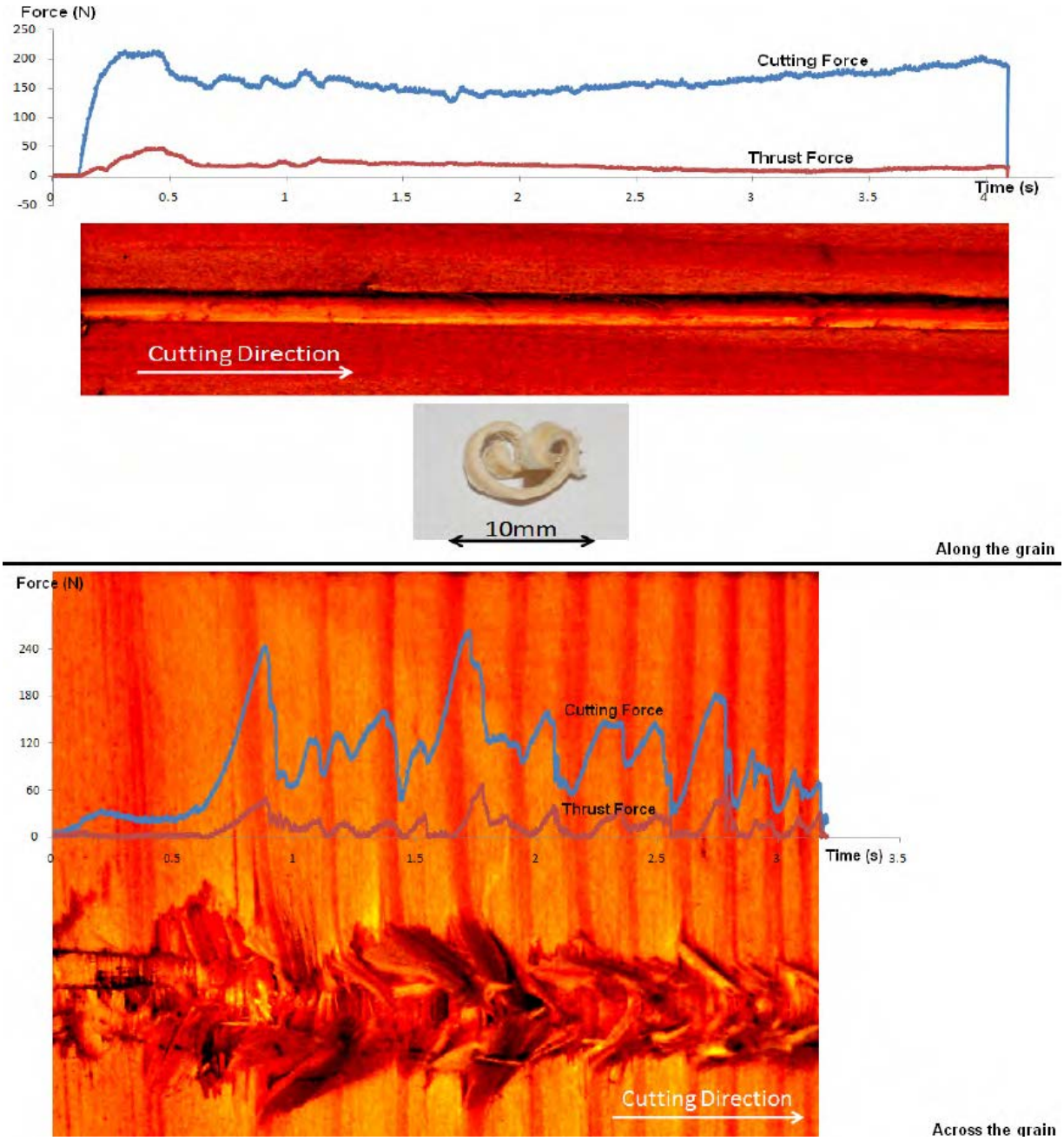

Typical cutting and thrust force plots and resultant chip/surface formation observed both along and across the grain

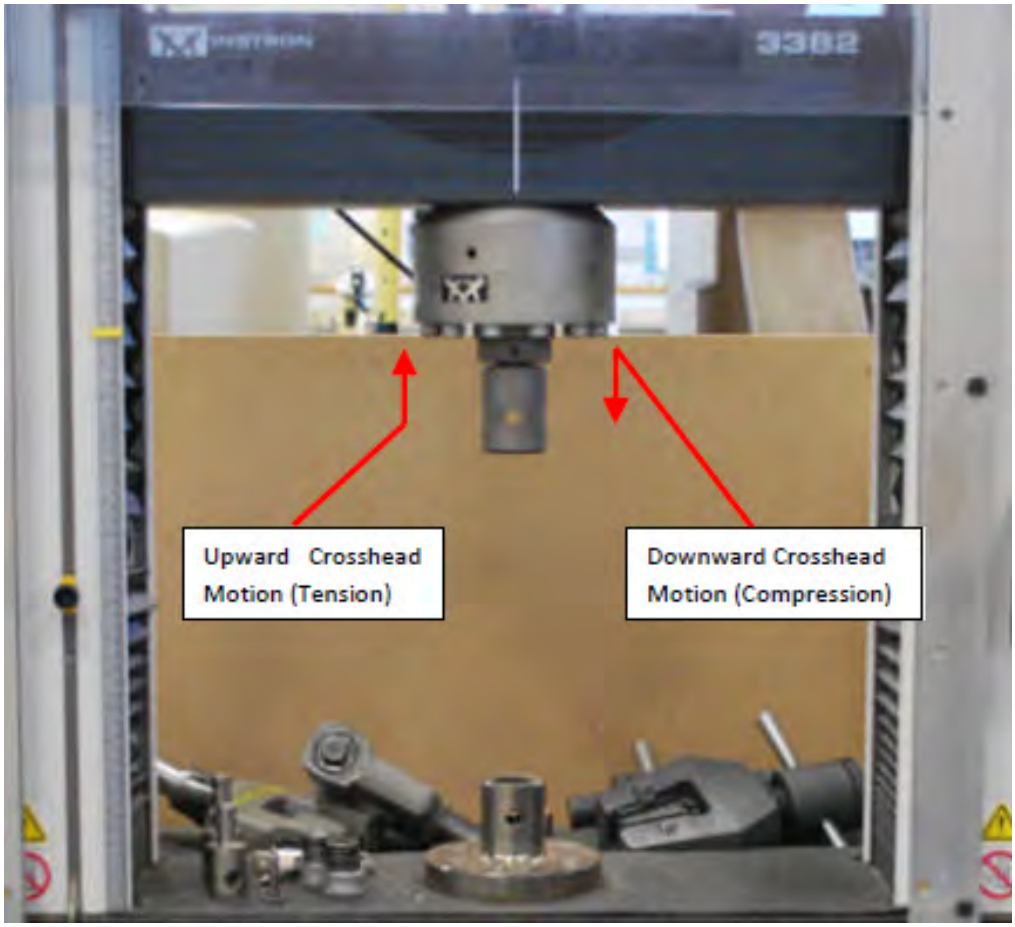

Universal materials testing machine (Instron)

APPENDIX 7– OPTICAL MICROSCOPE IMAGES OF CHIP AND SURACE FORMATION FROM ROUTER MACHINE EXPERIMENT

For each page of results the microscope images are arranged in the order denoted by the table below, with moisture content va rying along the columns. The scale width of each image is 13 mm.

	DRY	10%	20%	SATURATED
Across Grain (Work-piece)	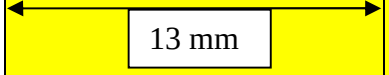			
Along Grain (Work-piece)				
Along Grain (Chip)				

SCOTS PINE

0.4 mm Depth of Cut

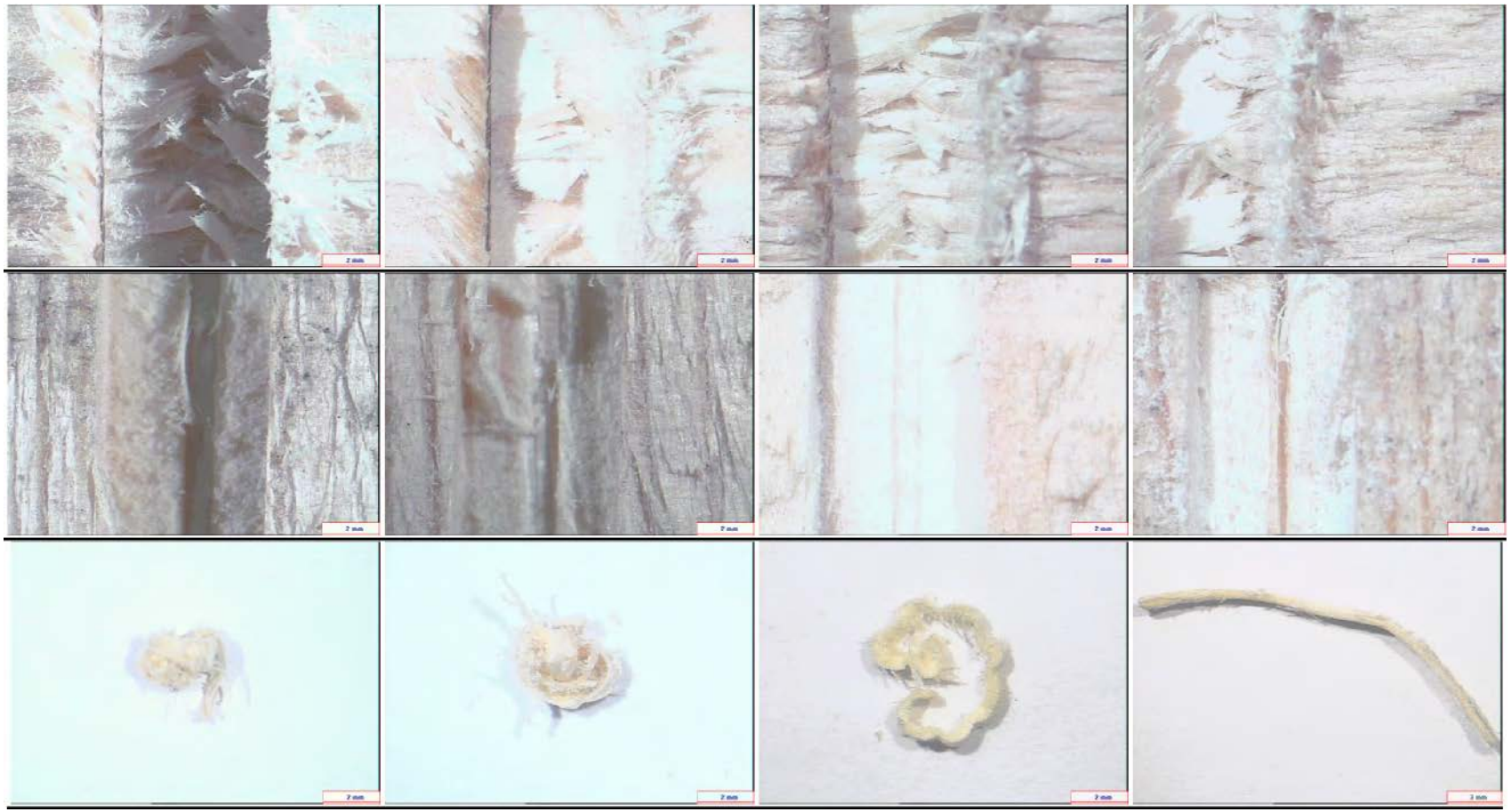

SCOTS PINE

0.8 mm Depth of Cut

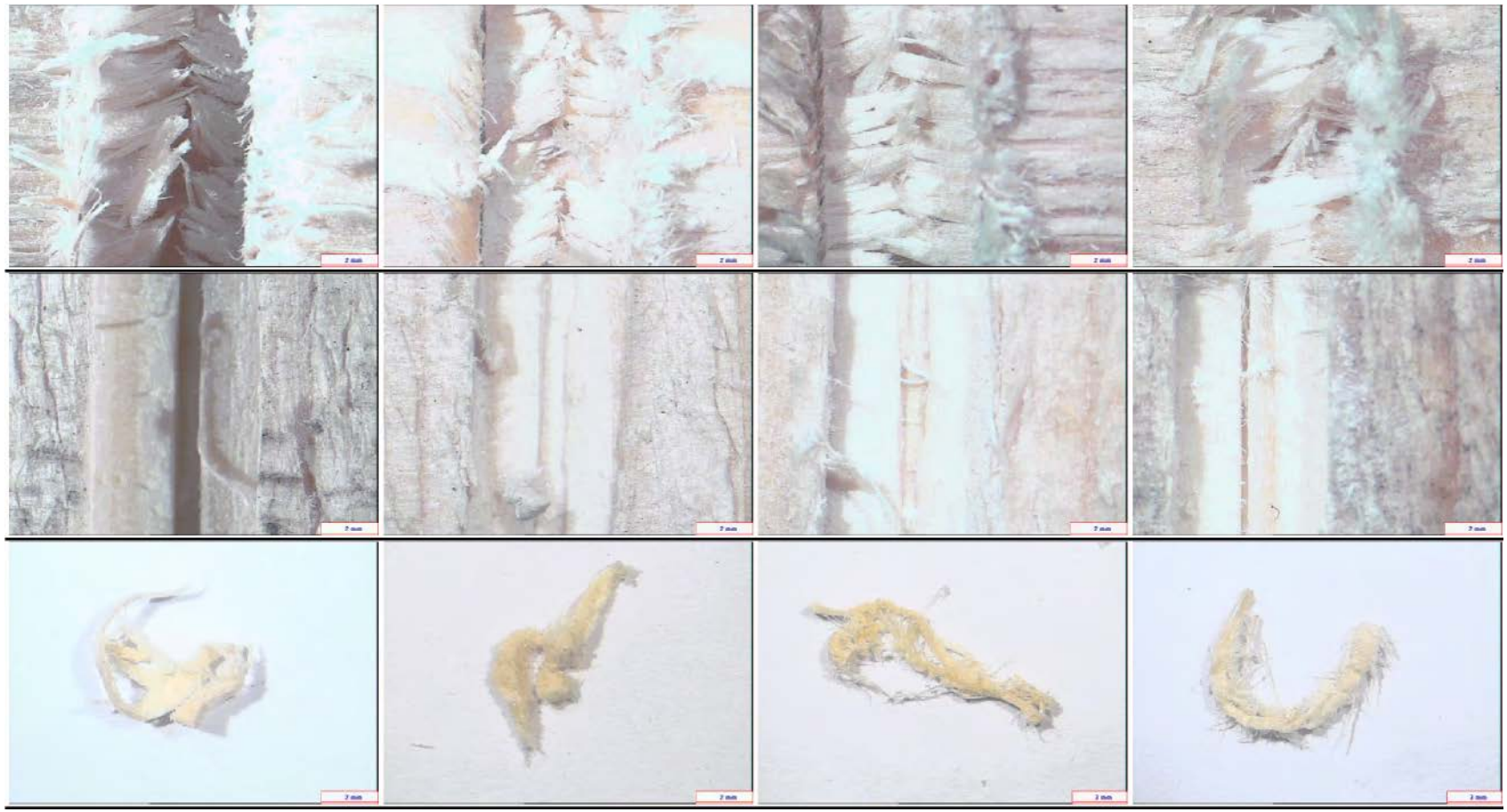

SCOTS PINE

1.2 mm Depth of Cut

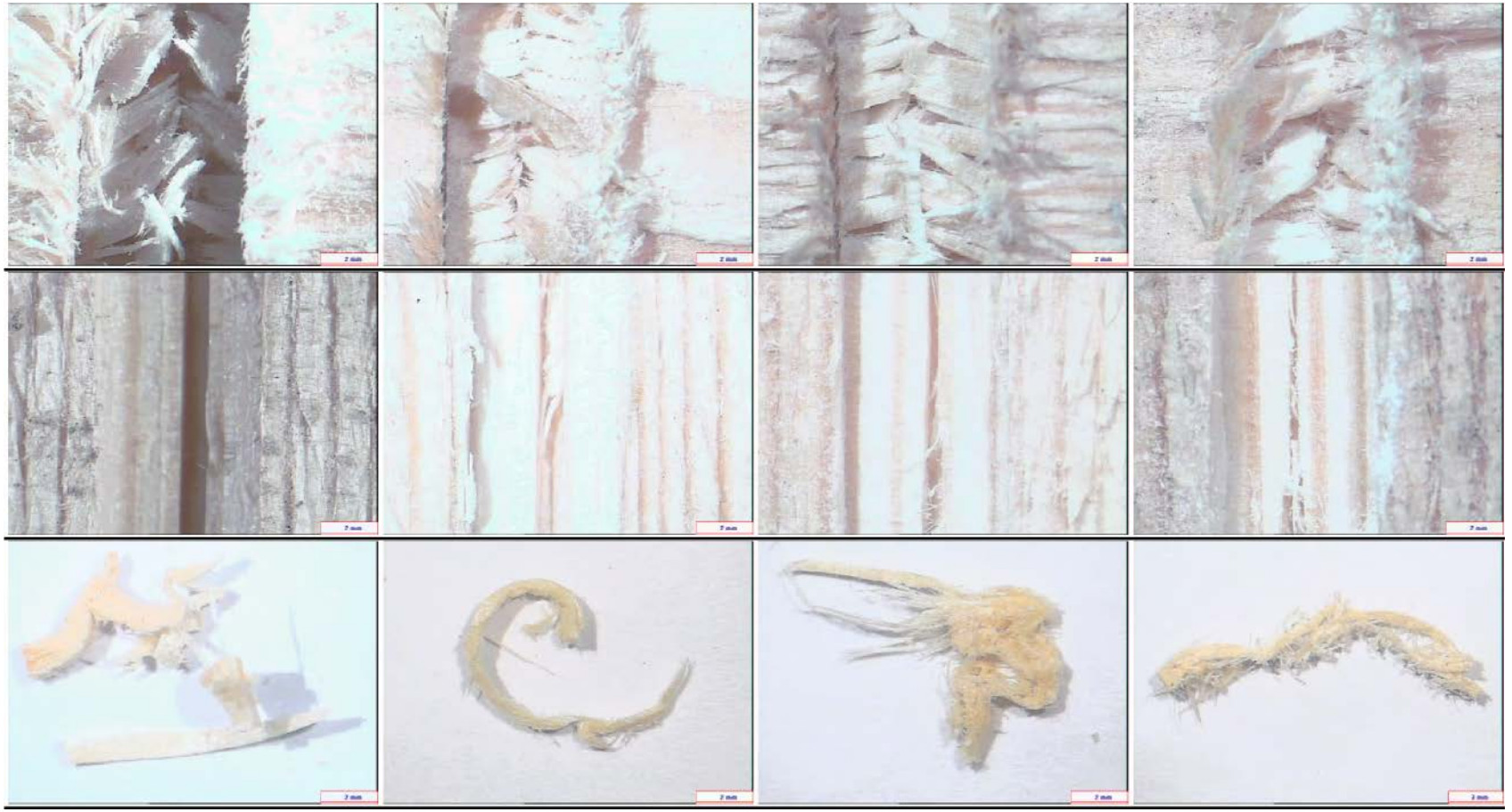

YELLOW PINE

0.4 mm Depth of Cut

YELLOW PINE

0.8 mm Depth of Cut

YELLOW PINE

1.2 mm Depth of Cut

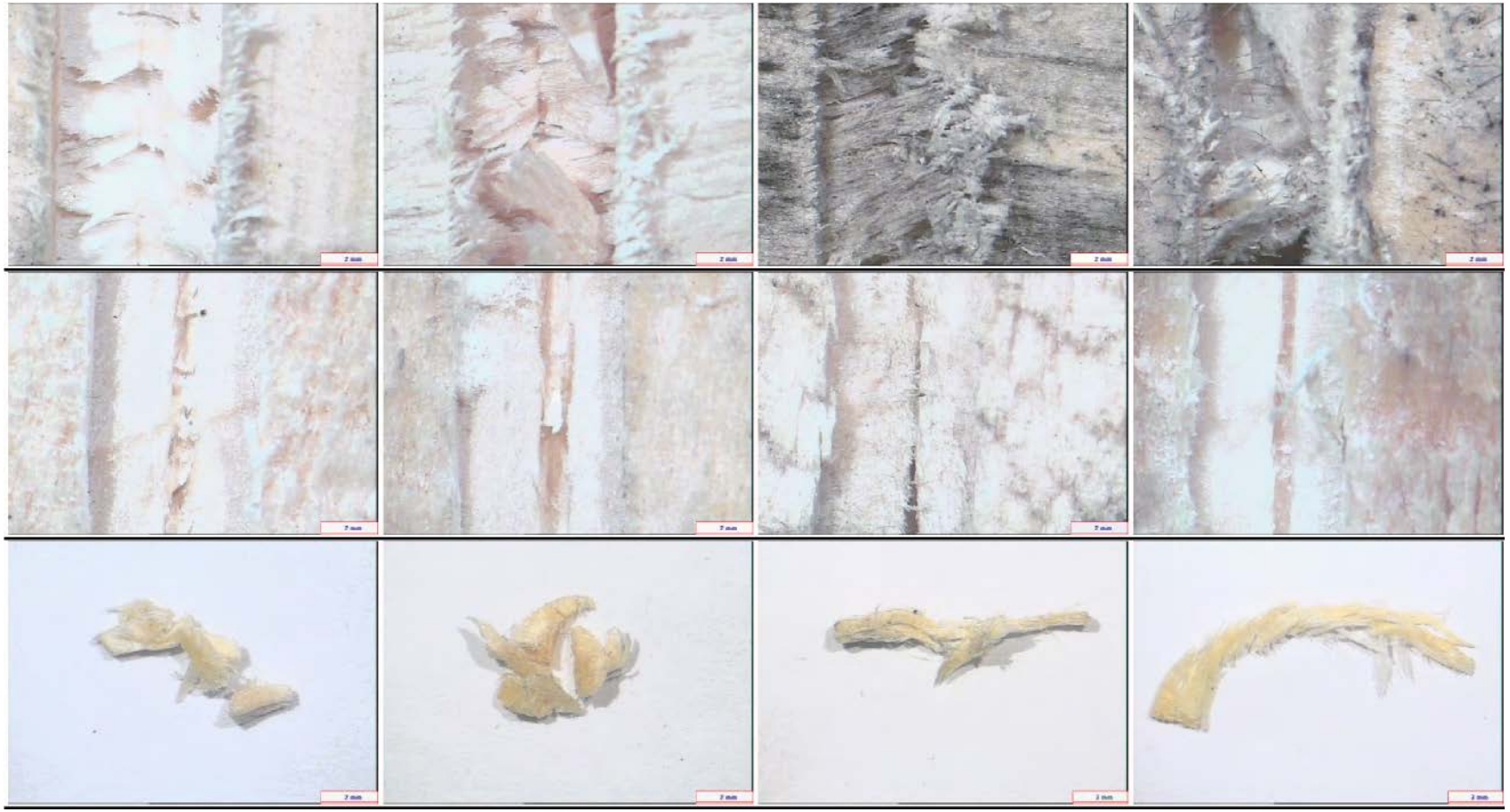

SIBEREAN LARCH

0.4 mm Depth of Cut

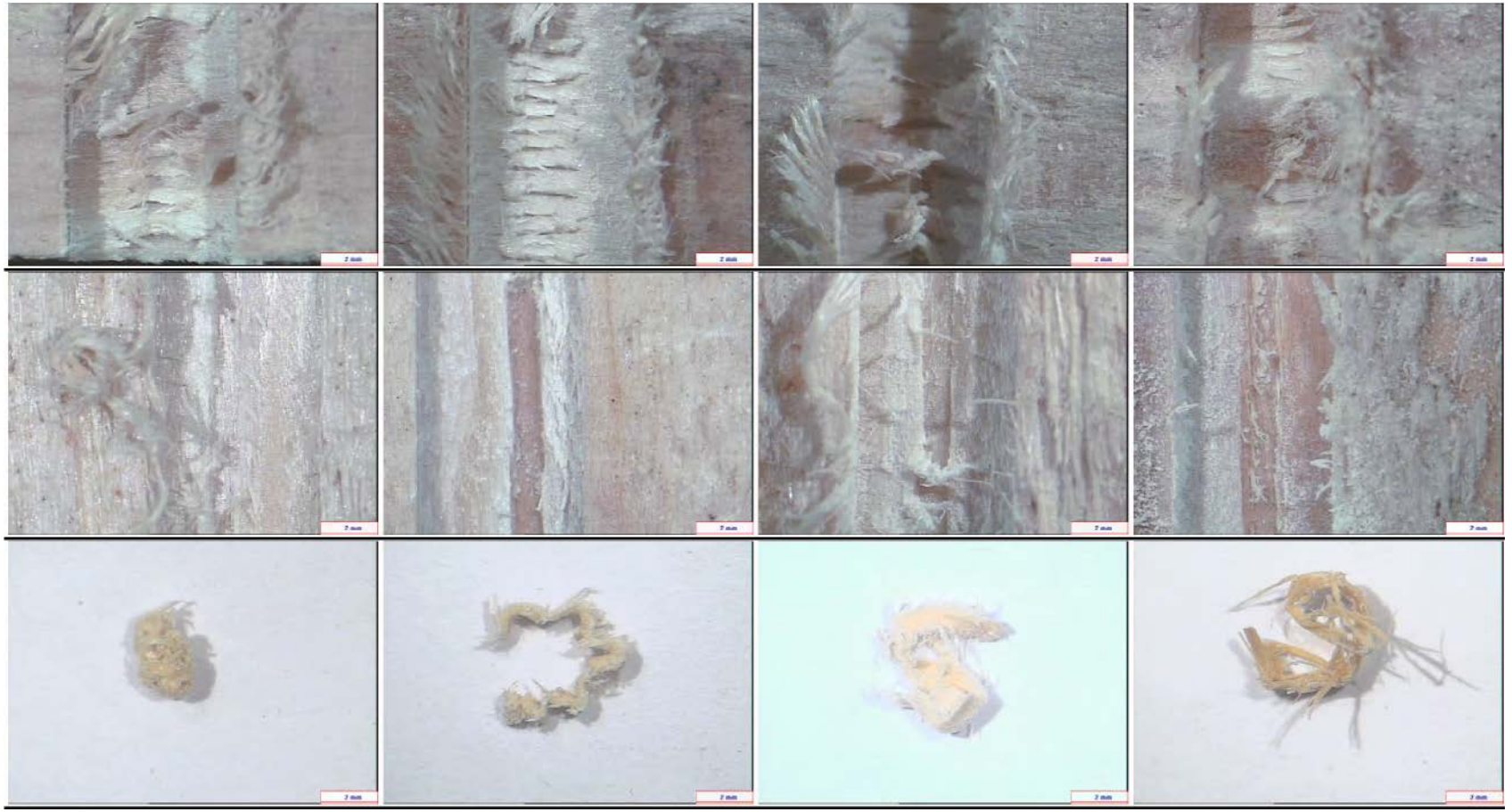

SIBEREAN LARCH

0.8 mm Depth of Cut

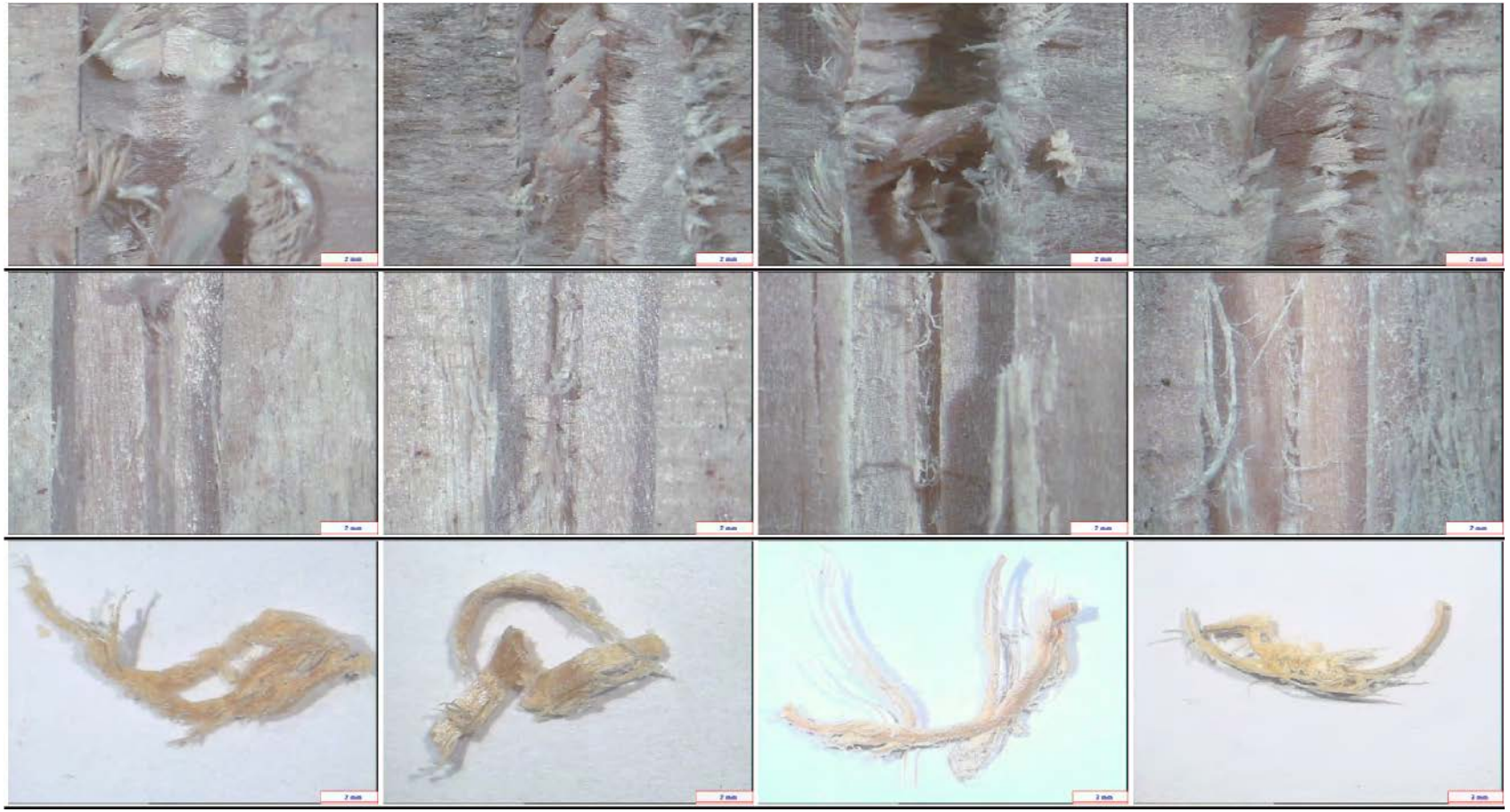

SIBEREAN LARCH

1.2 mm Depth of Cut

DOUGLASS FIR

0.4 mm Depth of Cut

DOUGLASS FIR

0.8 mm Depth of Cut

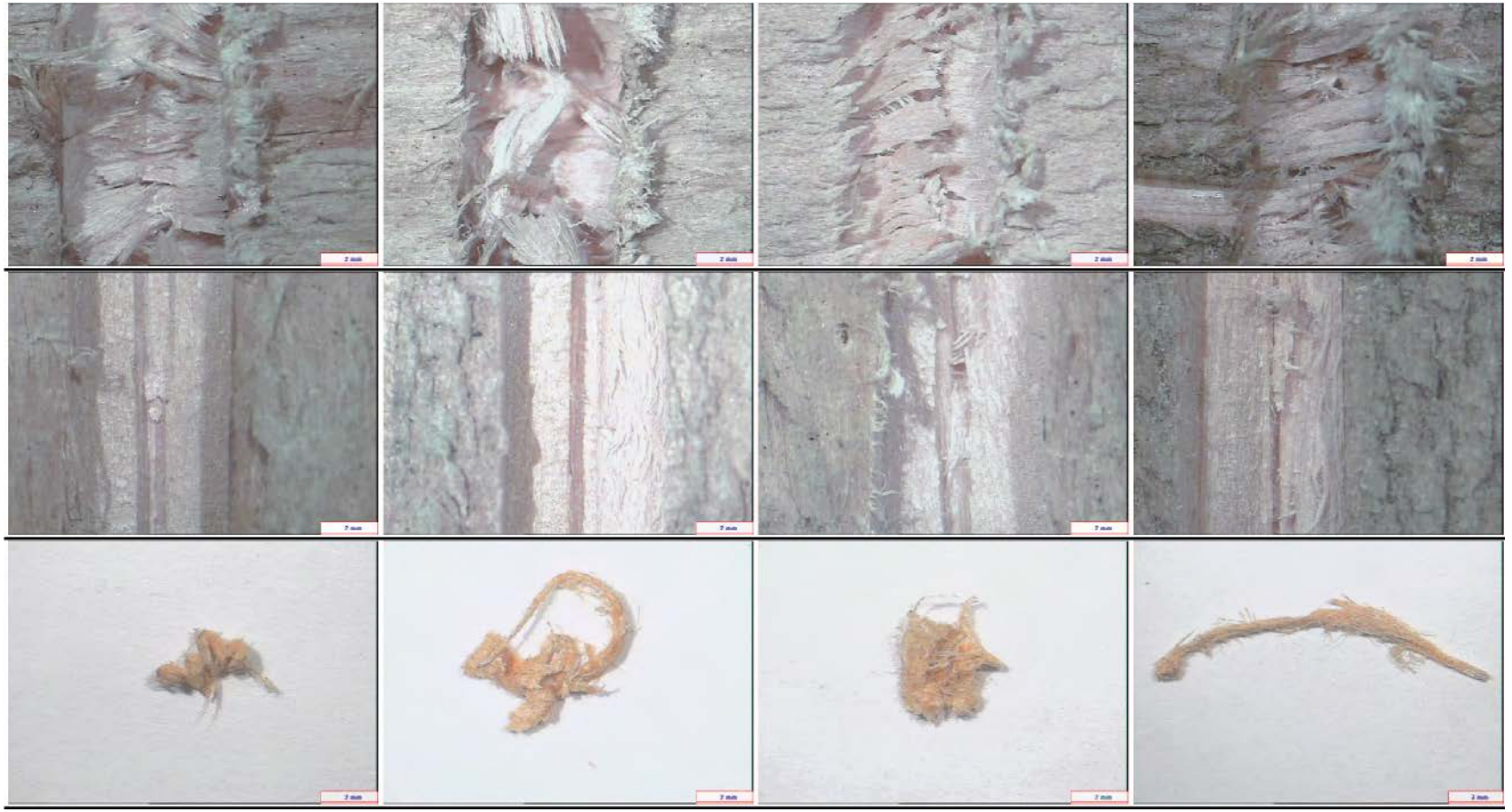

DOUGLASS FIR

1.2 mm Depth of Cut

WESTERN RED CEDAR

<u>0.4 mm Depth of Cut</u>

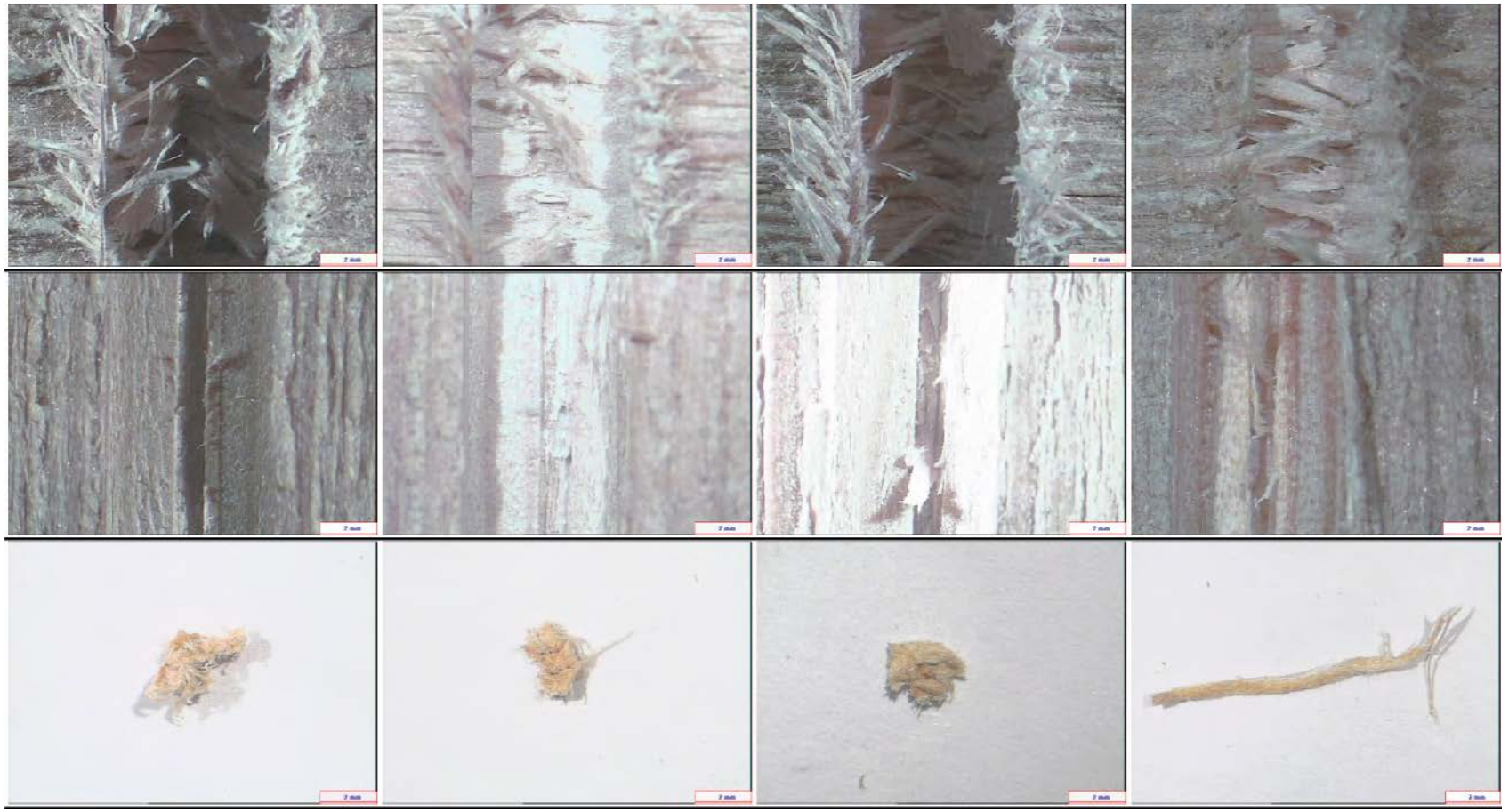

WESTERN RED CEDAR

<u>0.8 mm Depth of Cut</u>

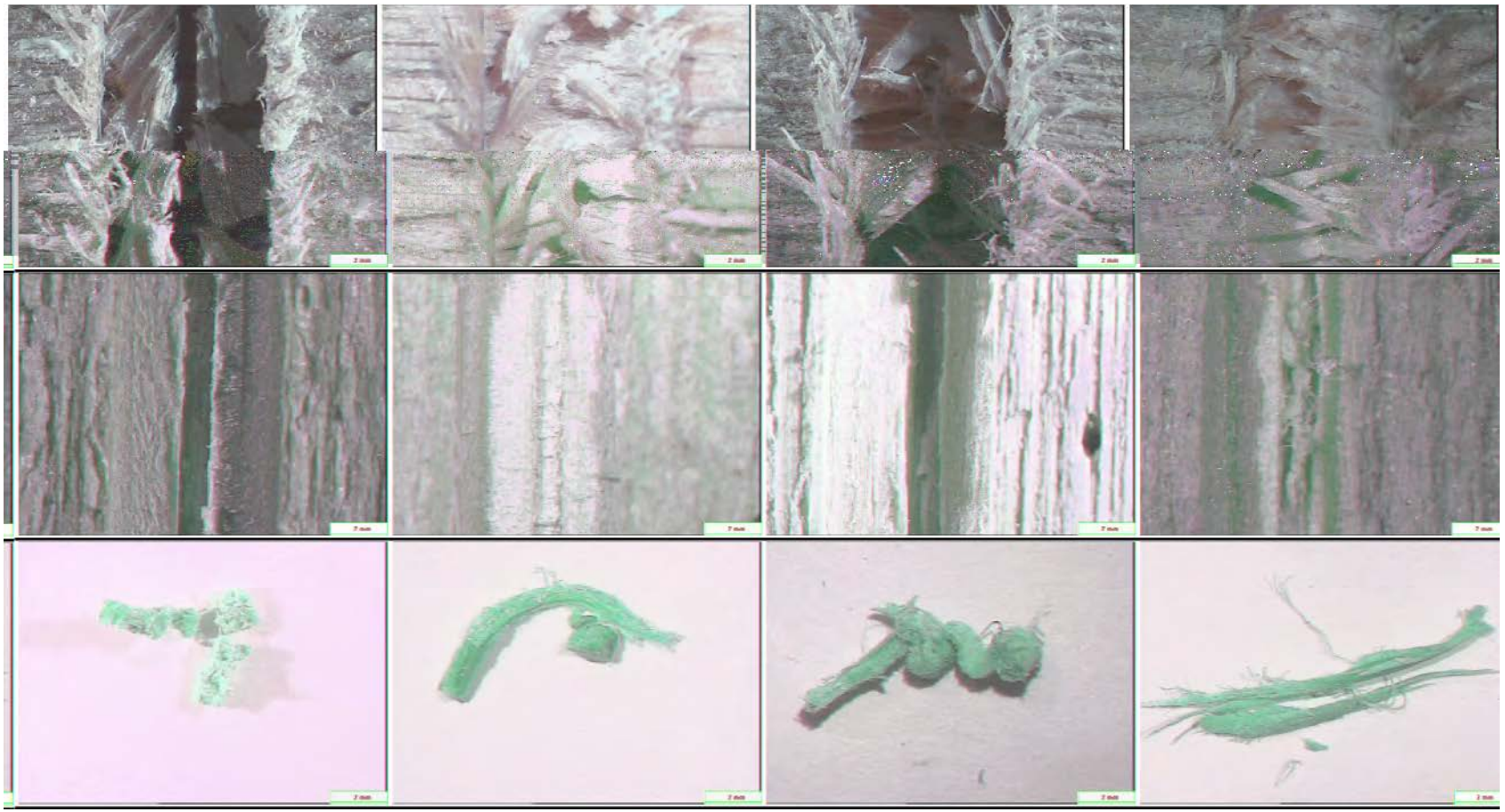

WESTERN RED CEDAR

1.2 mm Depth of Cut

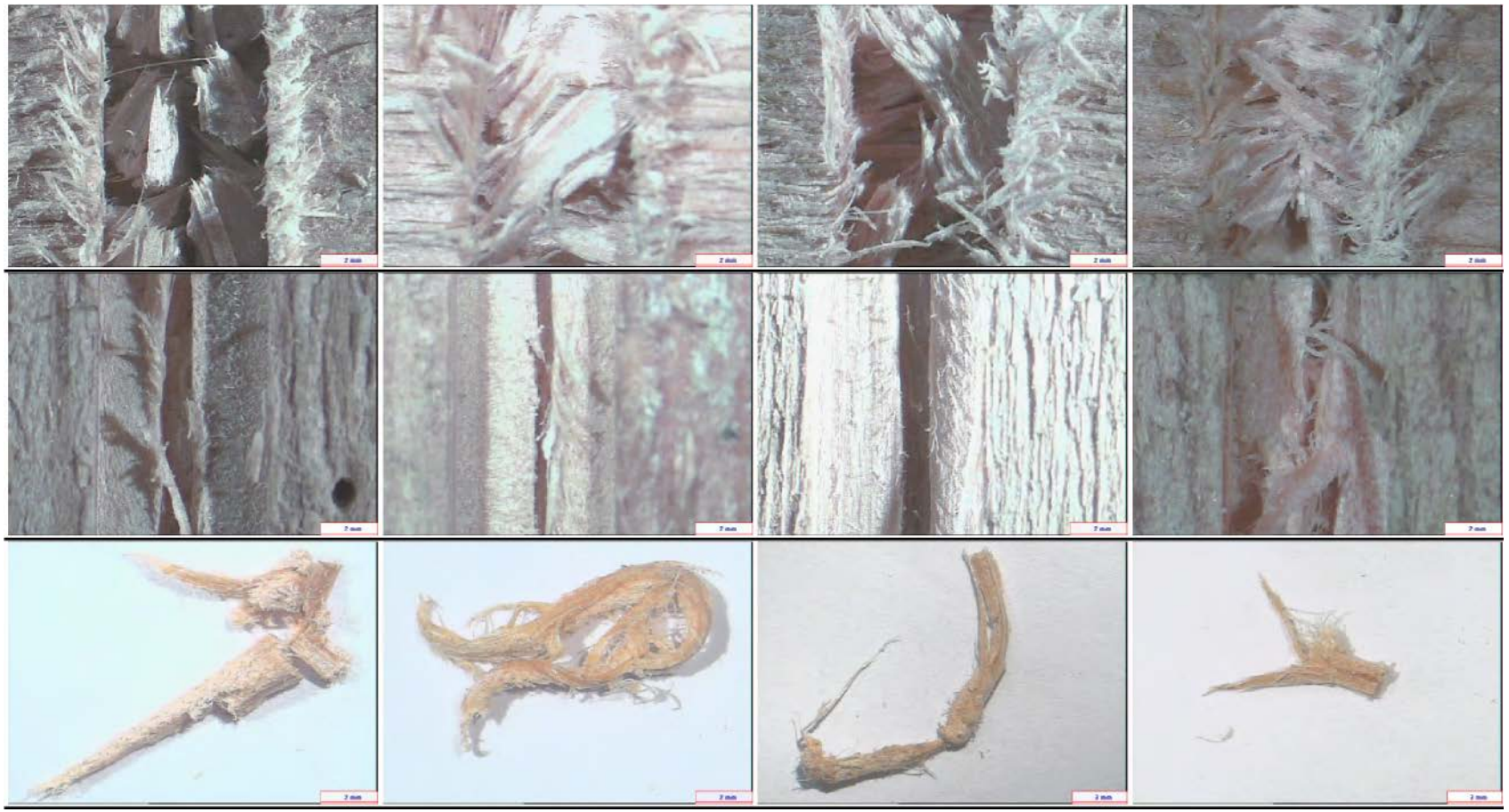

ASH

0.4mm Depth of Cut

ASH

0.8 mm Depth of Cut

ASH

1.2mm Depth of Cut

BEECH

0.4mm Depth of Cut

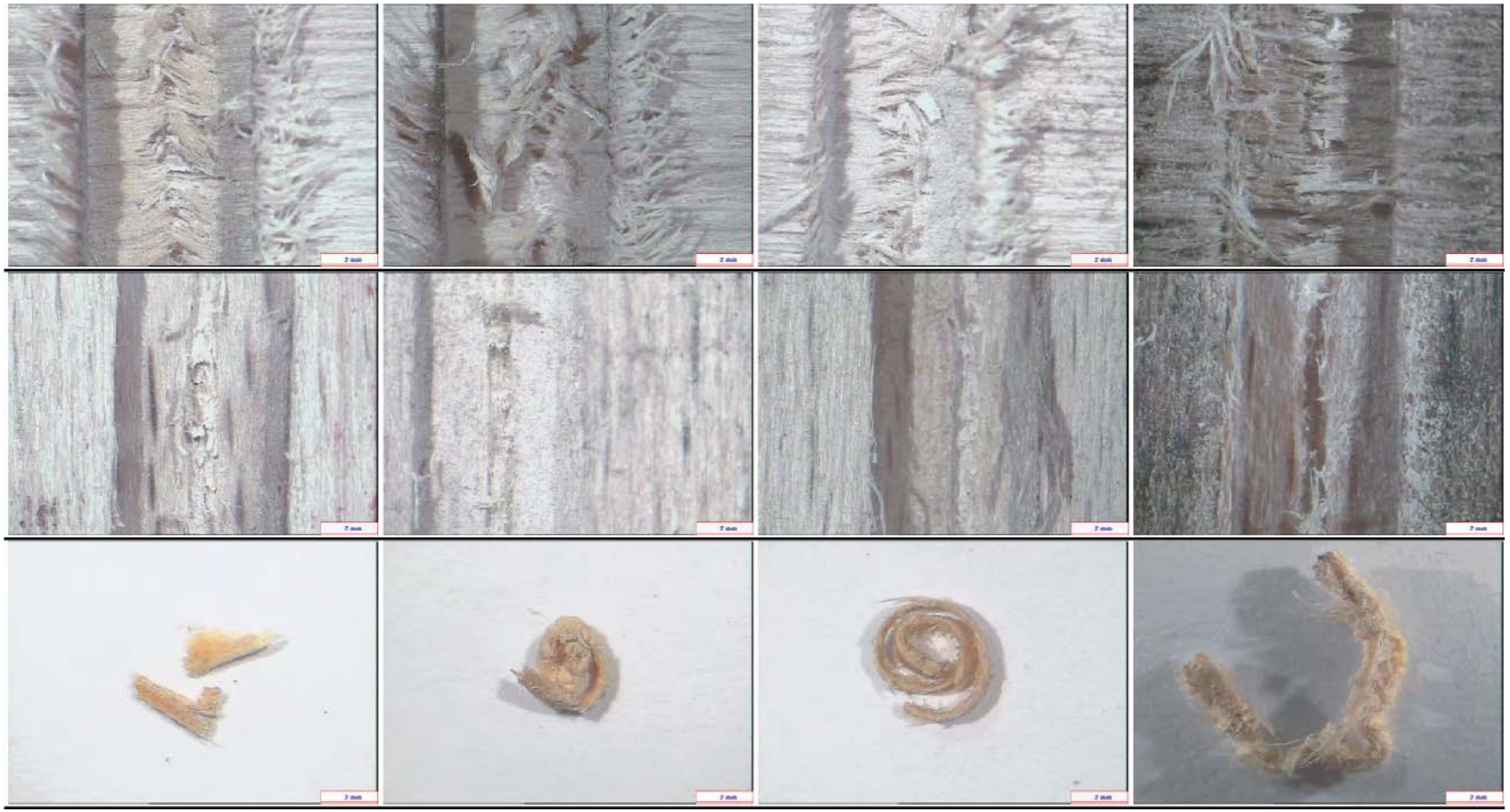

BEECH

0.8mm Depth of Cut

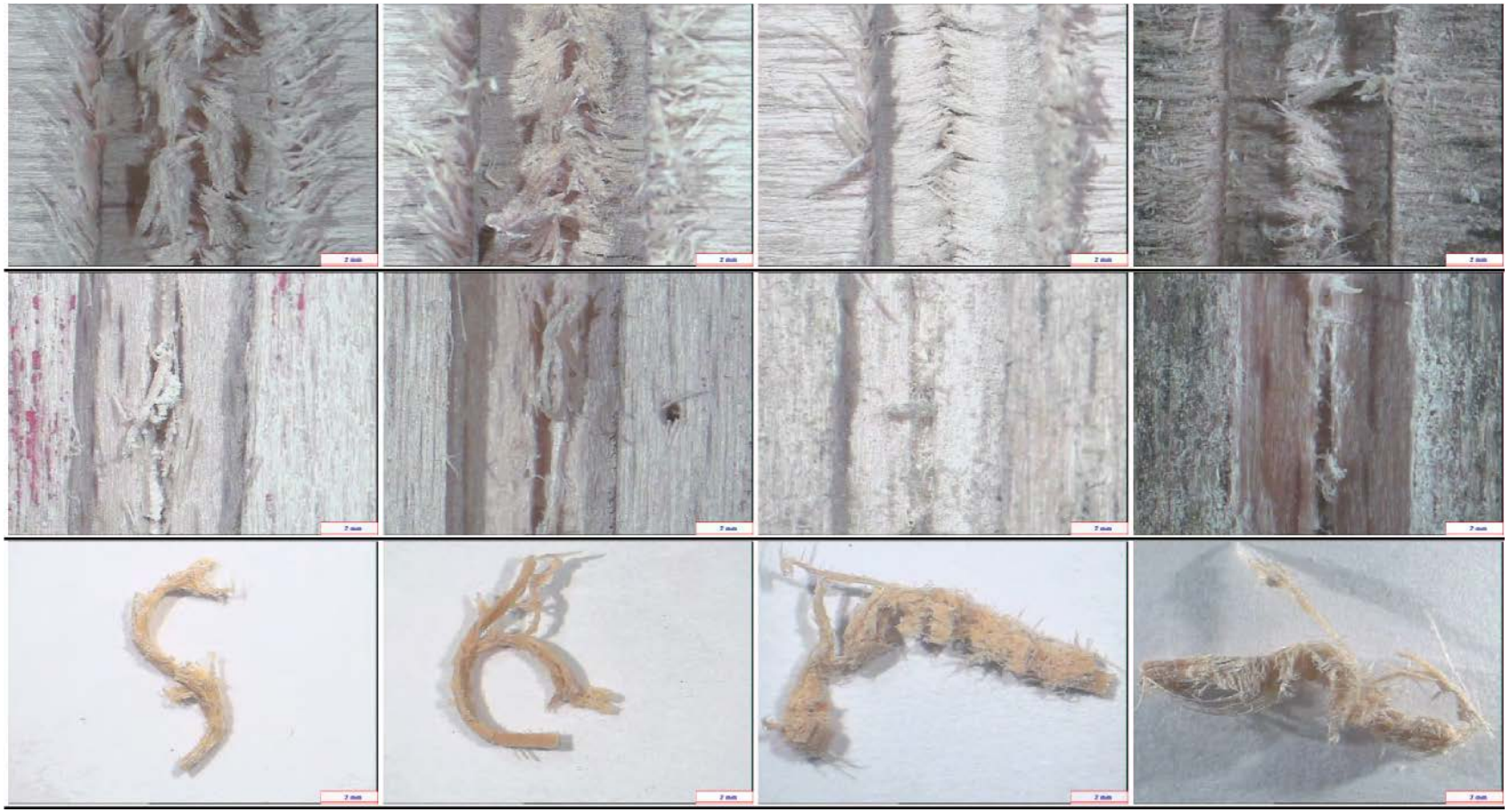

BEECH

1.2mm Depth of Cut

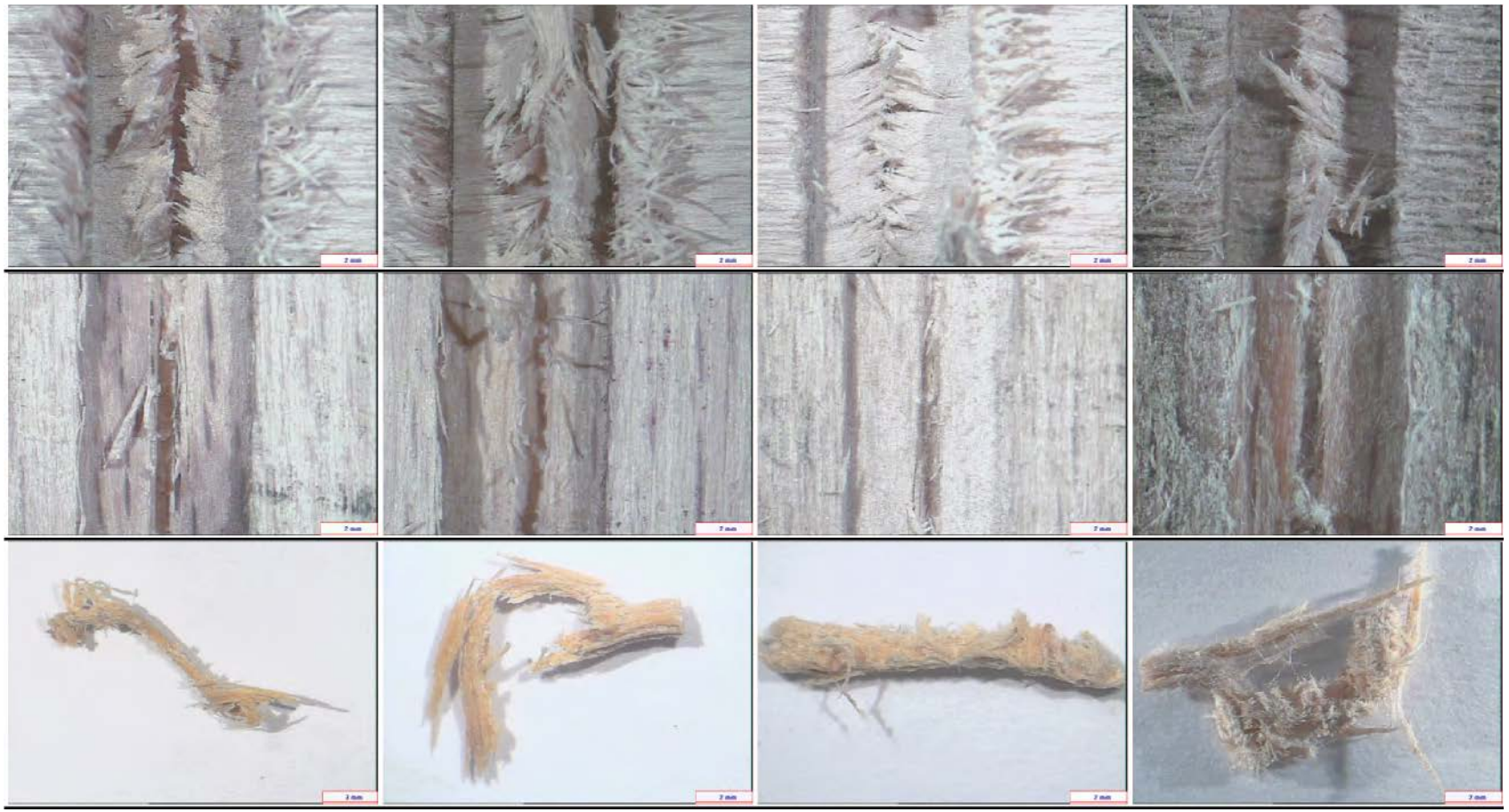

SAPELE

0.4 mm Depth of Cut

SAPELE

0.8 mm Depth of Cut

SAPELE

1.2mm Depth of Cut

APPENDIX 8 - AVERAGE DEPTHS OF CUT AND CUTTING SPEEDS FROM ENTIRE SAW TESTSING

Table of Results (Manual Tests)

	GT					U28°					U0°				
User	**L**	**T**	**N**	**t**	**δ**	**L**	**T**	**N**	**t**	**δ**	**L**	**T**	**N**	**t**	**δ**
	25	35				22	37				24	54			
1	8	6	5	0.511	0.127	9	9	6	0.378	0.119	8	7	8	0.478	0.082
	27	37				23	38				25	56			
2	3	6	5	0.374	0.120	1	2	6	0.645	0.118	7	7	8	0.798	0.079
	27	37				23	39				26	50			
3	5	9	5	0.326	0.119	8	4	6	0.365	0.114	1	4	7	0.682	0.089
	27	30				25	34				26	58			
4	6	4	4	0.491	0.148	2	7	5	0.485	0.130	5	4	8	0.686	0.077
	28	31				25	49				27	60			
5	3	2	4	0.358	0.144	5	2	7	0.492	0.091	2	0	8	0.507	0.075
	28	39				26	43				28	54			
6	9	8	5	0.574	0.113	2	3	6	0.401	0.104	2	4	7	0.474	0.083
	29	24				26	50				28	62			
7	9	7	3	0.506	0.182	3	7	7	0.415	0.089	5	8	8	0.442	0.072
	30	25				26	36				29	56			
8	6	3	3	0.311	0.178	6	7	5	0.504	0.123	1	1	7	0.757	0.080
	32	35				27	45				29	57			
9	3	6	4	0.337	0.126	2	0	6	0.555	0.100	9	7	7	0.548	0.078
	32	26				27	37				32	53			
10	4	8	3	0.515	0.168	2	5	5	0.606	0.120	2	2	6	0.503	0.085
MEAN δ	0.142438216					0.110751671					0.080018123				
STDEV δ	0.025748463					0.013881105					0.005044345				
MEAN Vc	0.675342784					0.524143624					0.473531915				
STDEV Vc	0.225270427					0.167978769					0.170516504				

Table of Results (Controlled Tests)*

GT						U28°					
L	**T**	**N**	**t**	**δ**	**Vc**	**L**	**T**	**N**	**t**	**δ**	**Vc**
105	434	15	16.7	0.1	94.31	105	405	14	15.9	0.11	92.45

Where: **L** = Average Stroke Length (mm)
T = Total number of teeth used to perform the cut
N = Number of Strokes
t = Time taken (s)
δ = Depth of per tooth (mm)
Vc = Cutting speed (m/s)

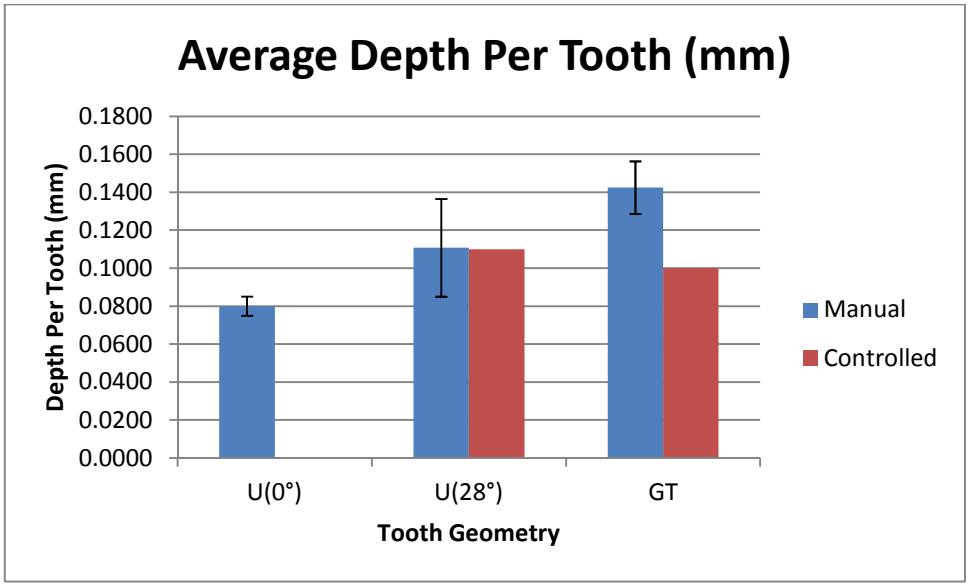

Average depth of cut per tooth for each of the selected geometries

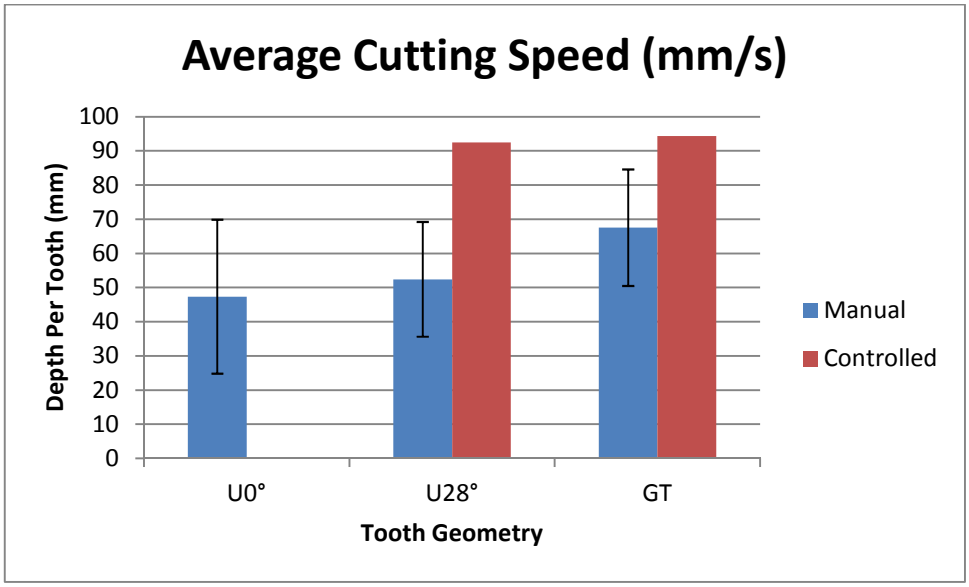

Average cutting speed for each of the selected geometries (including error bars)

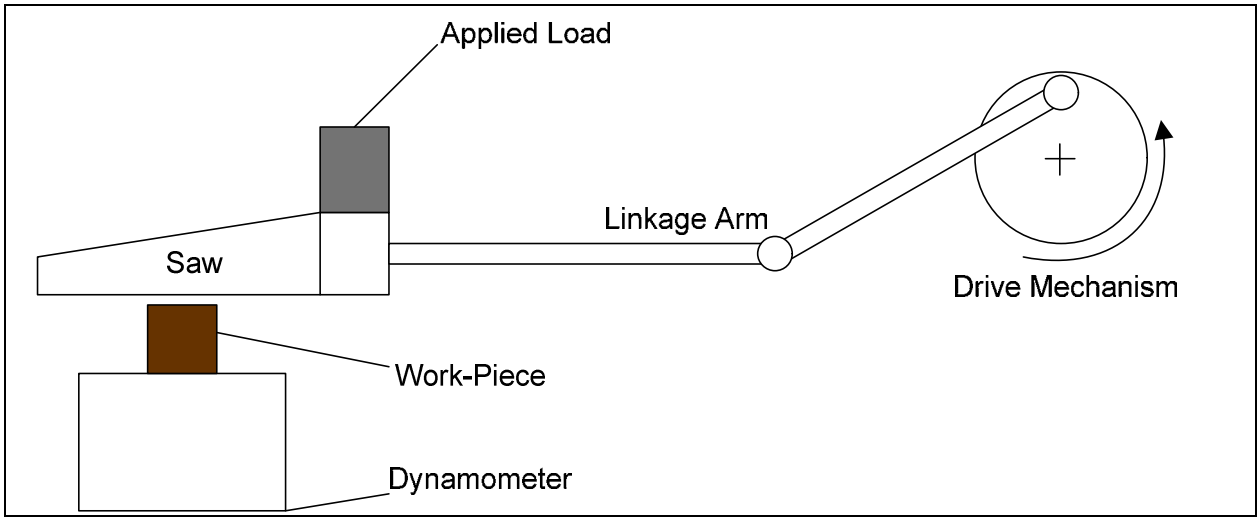

Simplified schematic diagram

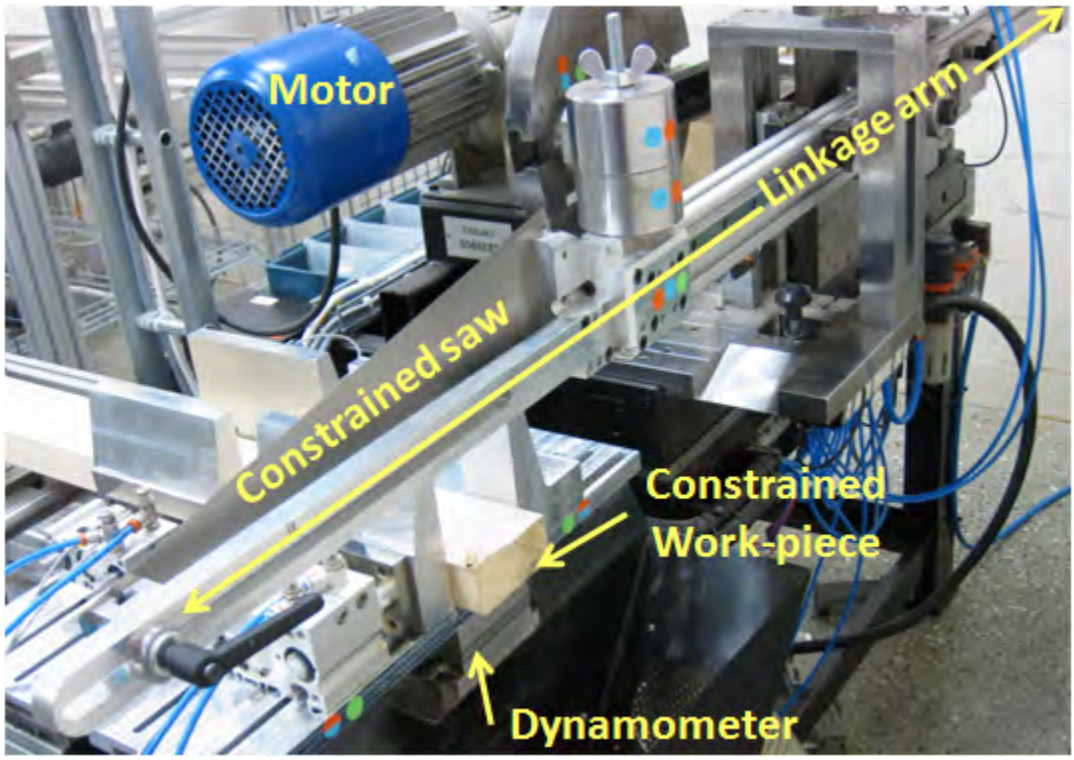

Test-rig photograph*

*Table of data and photograph provided my Mr. Emil Clahr of SNA Europe, Wood-Working Research and Development, Bollnäs, Sweden.

APPENDIX 9 – SHAPER TEST RIG: APPARATUS AND ERROR EVALUATION

KISTLER
Type 9257B

Multicomponent Dynamometer

–5 ... 10 kN, Top Plate 100x170 mm

Quartz three-component dynamometer for measuring the three orthogonal components of a force. The dynamometer has a great rigidity and consequently a high natural frequency. Its high resolution enables the smallest dynamic changes in large forces to be measured.

- Universal applicable
- For cutting force measurements
- Stable and reliable

Description

The dynamometer consists of four three-component force sensors fitted under high preload between a baseplate and a top plate. Each sensor contains three pairs of quartz plates, one sensitive to pressure in the z direction and the other two responding to shear in the x and y directions respectively. The force components are measured practically without displacement.

The outputs of the four built-in force sensors are connected inside the dynamometer in a way to allow multicomponent measurements of forces and moments to be performed. The eight output signals are available at the 9-conductor flange socket.

The four sensors are mounted ground-insulated. Therefore ground loop problems are largely eliminated.

The dynamometer is rustproof and protected against penetration of splashwater and cooling agents. Together with the connecting cable Type 1687B5/1689B5 and Type 1677A5/1679A5 it corresponds to the protection class IP67.

A special thermal isolation coating is integrated in the top plate which renders the dynamometer largely insensitive to temperature influences.

Application Examples

- Dynamic and quasistatic measurement of the three orthogonal components of a force
- Measuring cutting force when turning, milling, grinding etc. In conjunction with the calibrated partial ranges the high sensitivity and low threshold allow exact measurements on small tools and when grinding.
- Measurements on scale models in wind channels

Technical Data

Range	F_x, F_y, F_z	kN	–5 ... 5 [1]
F_z for F_x and $F_y \leq 0{,}5\ F_z$	F_z	kN	–5 ... 10 [2]
Calibrated partial range 1	F_x, F_y	N	0 ... 500
	F_z	N	0 ... 1 000
Calibrated partial range 2	F_x, F_y	N	0 ... 50
	F_z	N	0 ... 100
Overload	F_x, F_y, F_z	kN	–7,5/7,5
F_z for F_x and $F_y \leq 0{,}5\ F_z$	F_z	kN	–7,5/15
Threshold		N	<0,01
Sensitivity	F_x, F_y	pC/N	≈–7,5
	F_z	pC/N	≈–3,7
Linearity, all ranges		%FSO	≤±1
Hysteresis, all ranges		%FSO	≤0,5
Cross talk		%	≤±2
Rigidity	c_x, c_y	kN/µm	>1
	c_z	kN/µm	>2
Natural frequency	$f_n(x, y, z)$	kHz	≈3,5 [4]
Natural frequency	$f_n(x, y)$	kHz	≈2,3 [4]
(mounted on flanges)	$f_n(z)$	kHz	≈3,5 [4]
Operating temperature range		°C	0 ... 70
Capacitance	F_x, F_y, F_z	pF	≈220
Insulation resistance (20 °C)		Ω	$>10^{13}$
Ground insulation		Ω	$>10^{8}$
Protection class EN60529		–	IP67 [3]
Weight		kg	7,3
Clamping area	mm	100x170	
Connection		Fischer flange, 9 pol. neg.	

[1] Application of force inside and max. 25 mm above top plate area
[2] Range for turning, application of force at point A
[3] With connecting cable Types 1687B5, 1689B5, 1677A5, 1679A5
[4] Without tool holder Type 9403

Kistler dynamometer type K9257B technical specifications

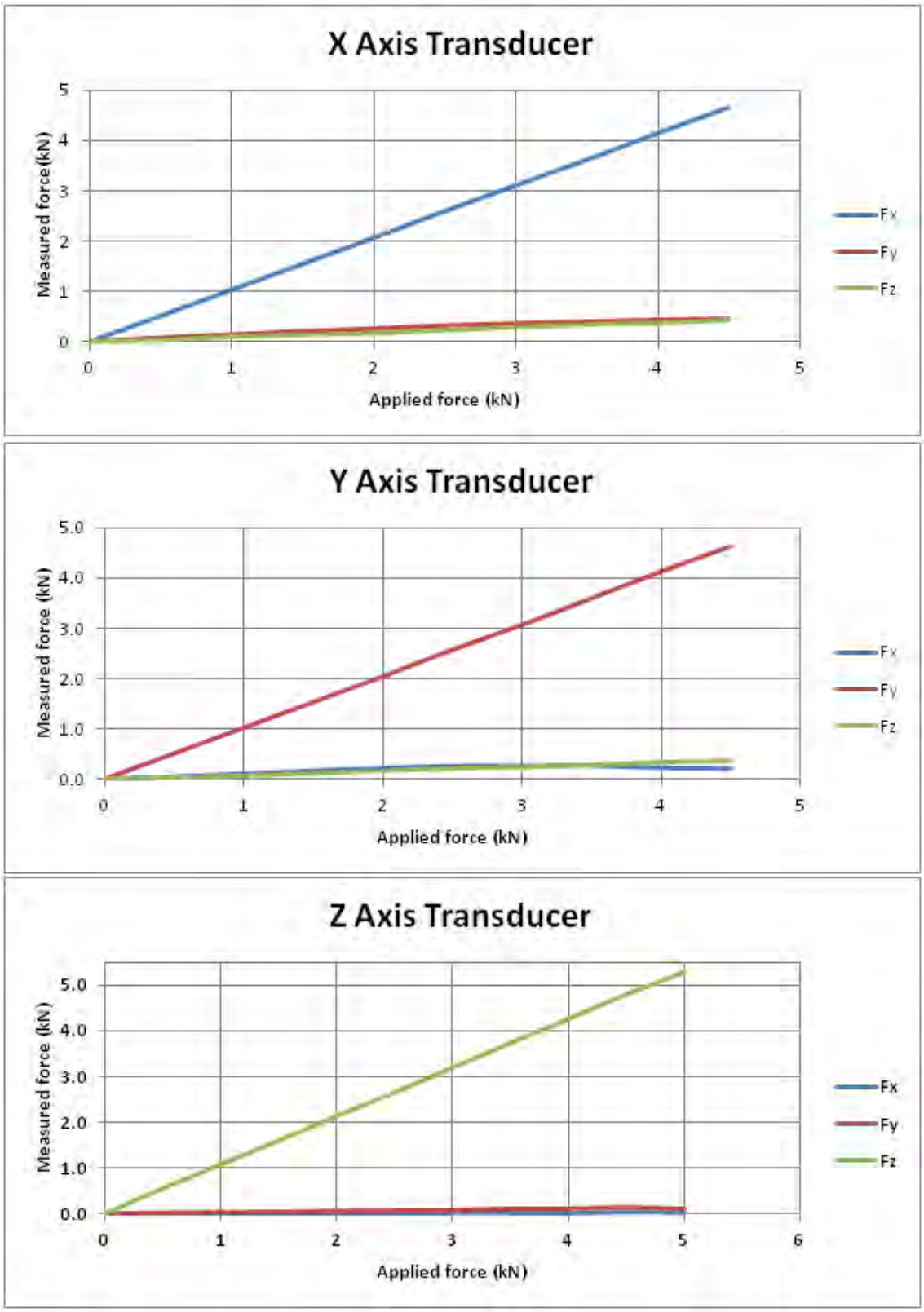

Loading of the K9257B dynamometer in the universal testing machine (with cross interference in un-tested directions)

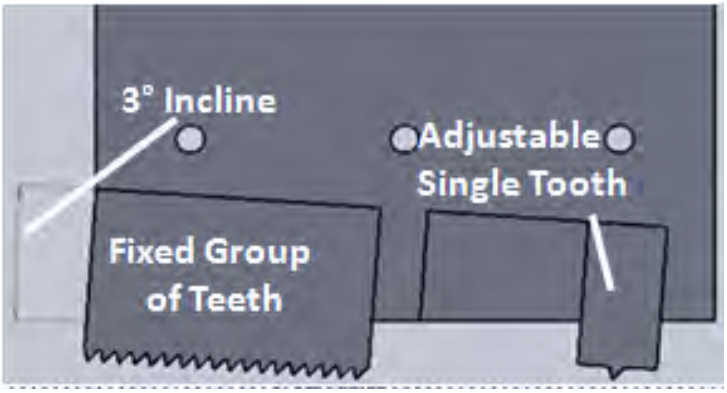

CAD drawing showing a section view of the tool holder constraining both the fixed group and single tooth

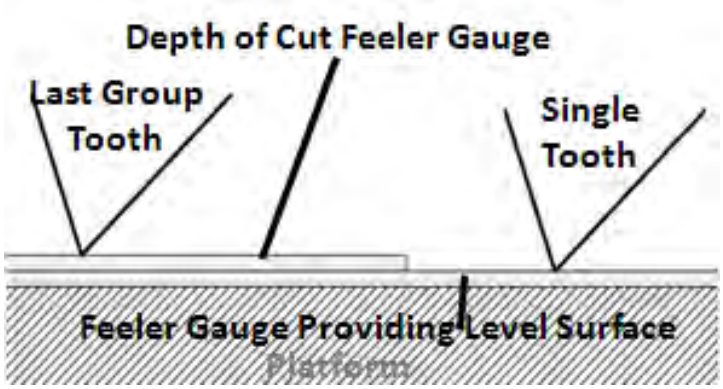

Feeler gauge method used to set depth of cut offset between single tooth and group of teeth

Feeler (thickness) gauges used

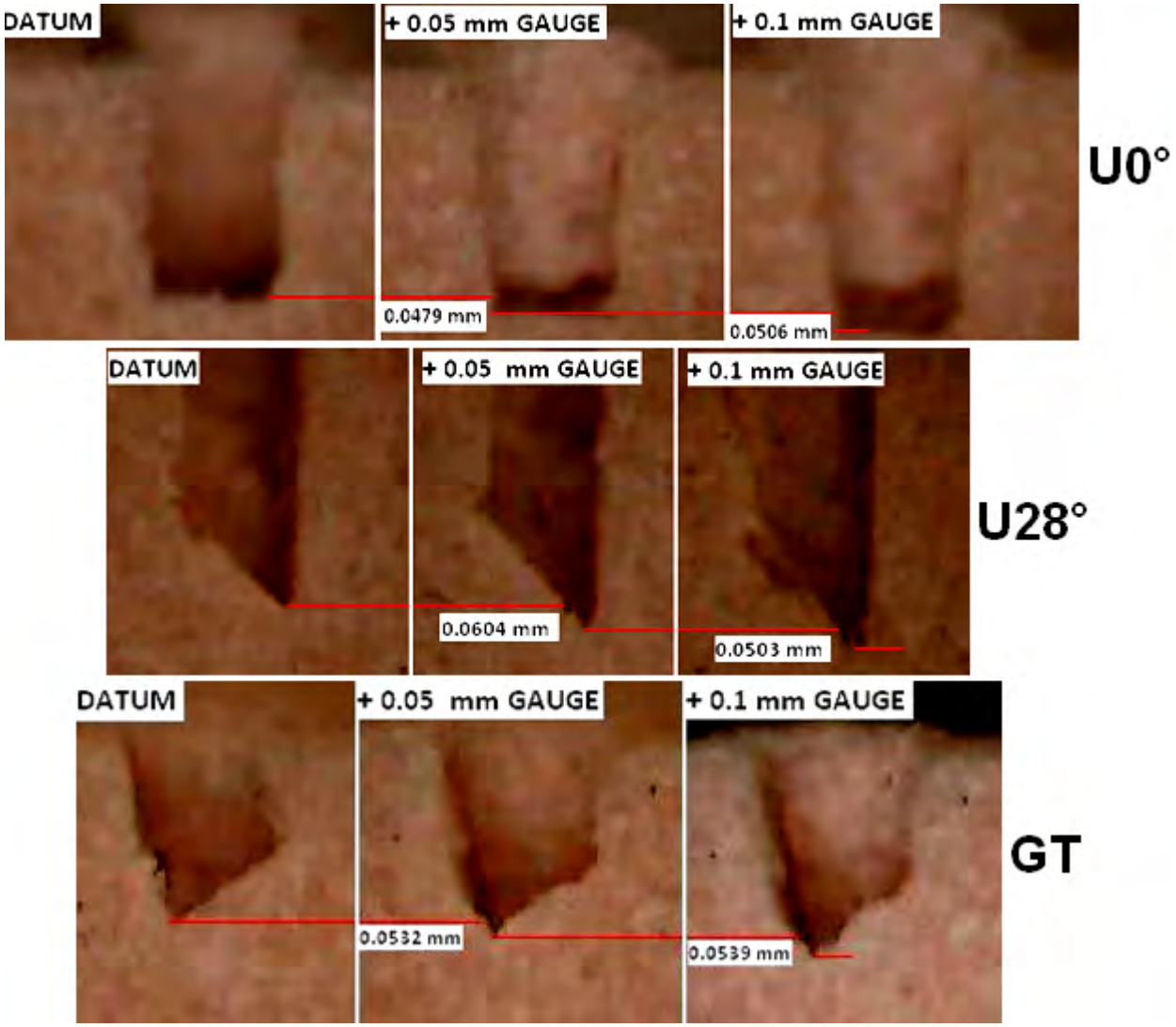

Nominal and measured depth of cut for the three saw tooth geometries. Work-piece material used is Obomodulan

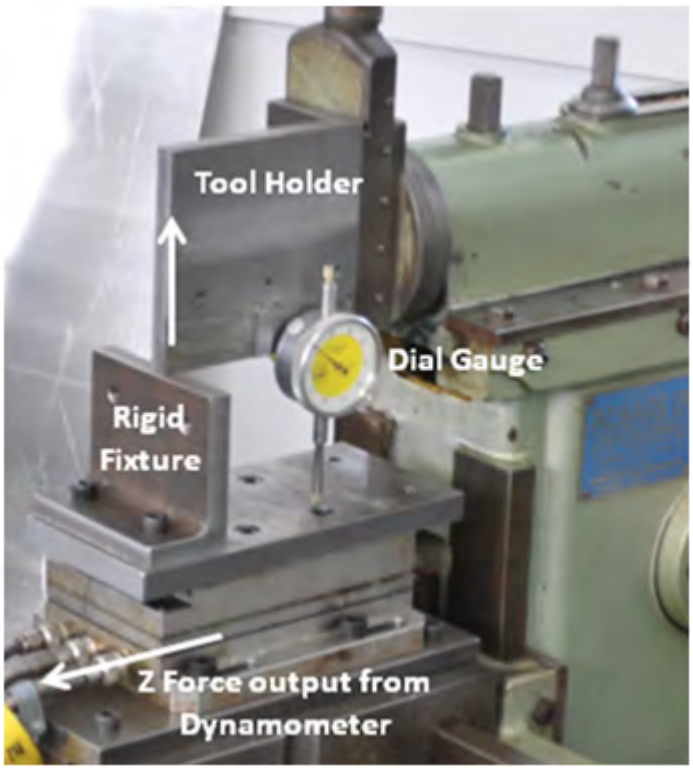

Vertical stiffness set-up (dial gauge constrained at single tooth position)

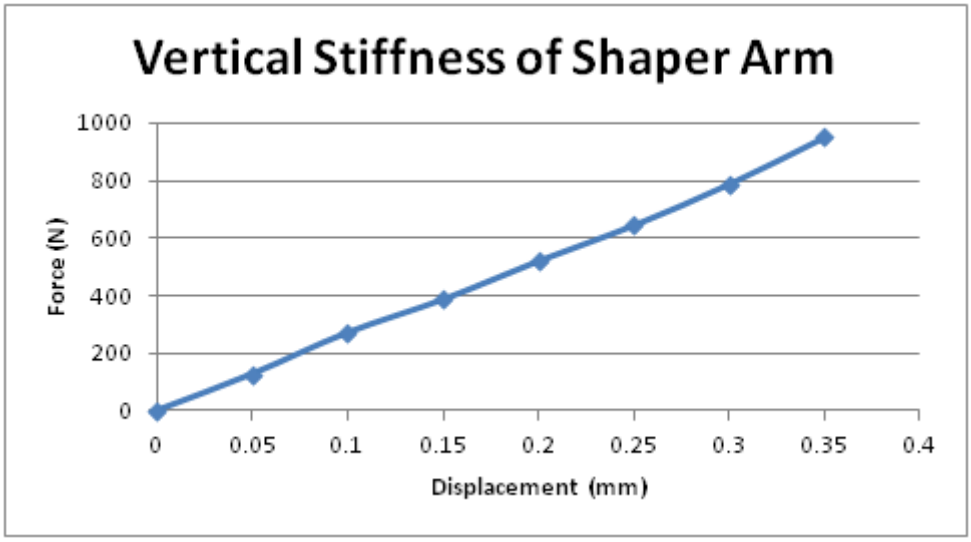

Force vs. displacement plot up to 1000 N for vertical loading

$$k = \frac{F}{\delta} = \frac{952}{0.00035} = 2.72\ MNm^{-1}$$

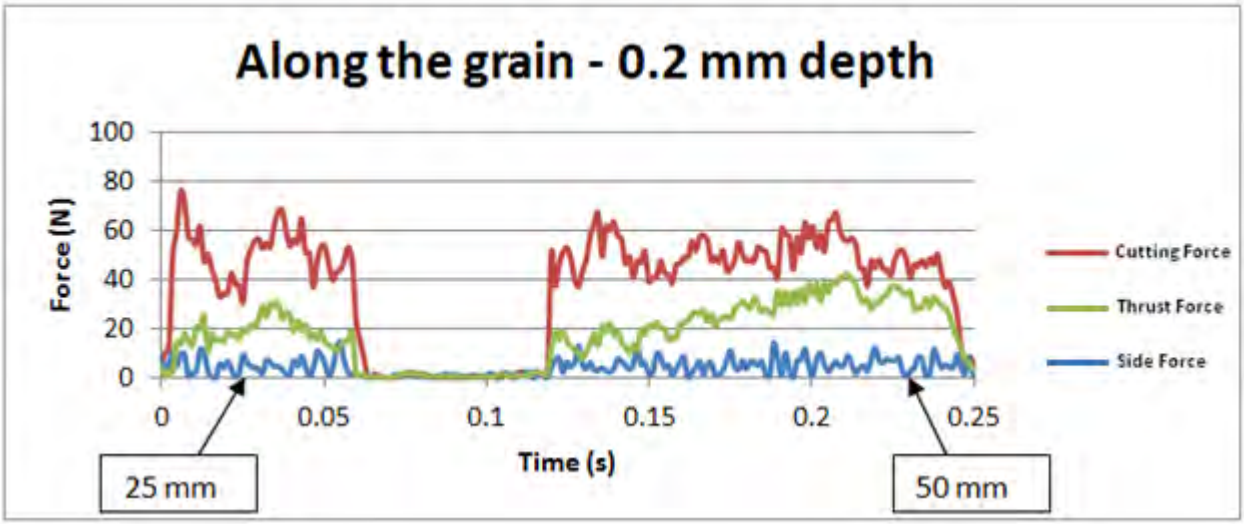

Comparison of tool forces for two different widths of timber (along the grain)

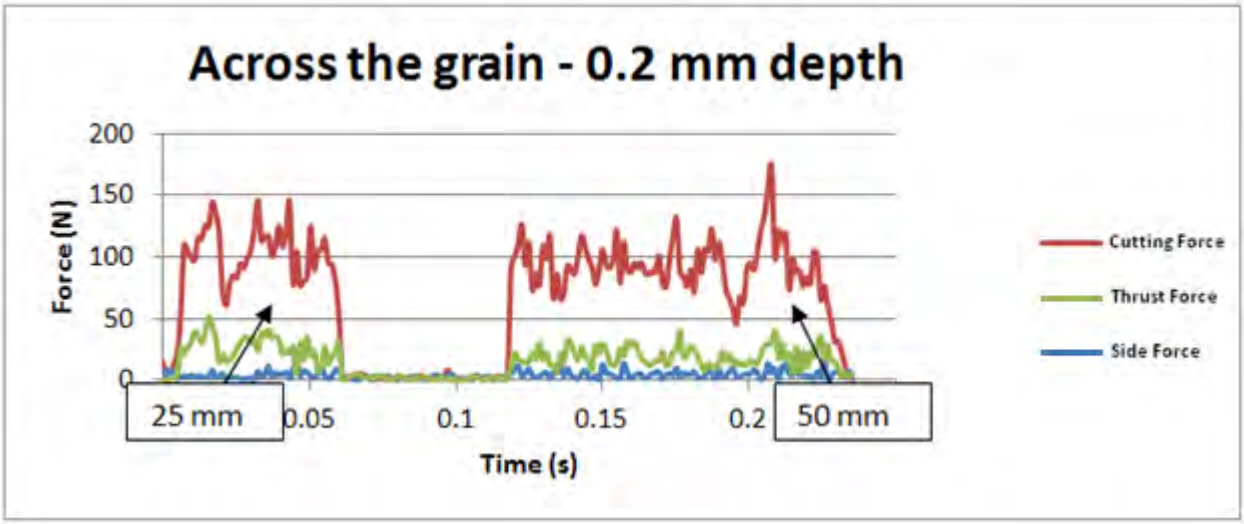

Comparison of tool forces for two different widths of timber (across the grain)

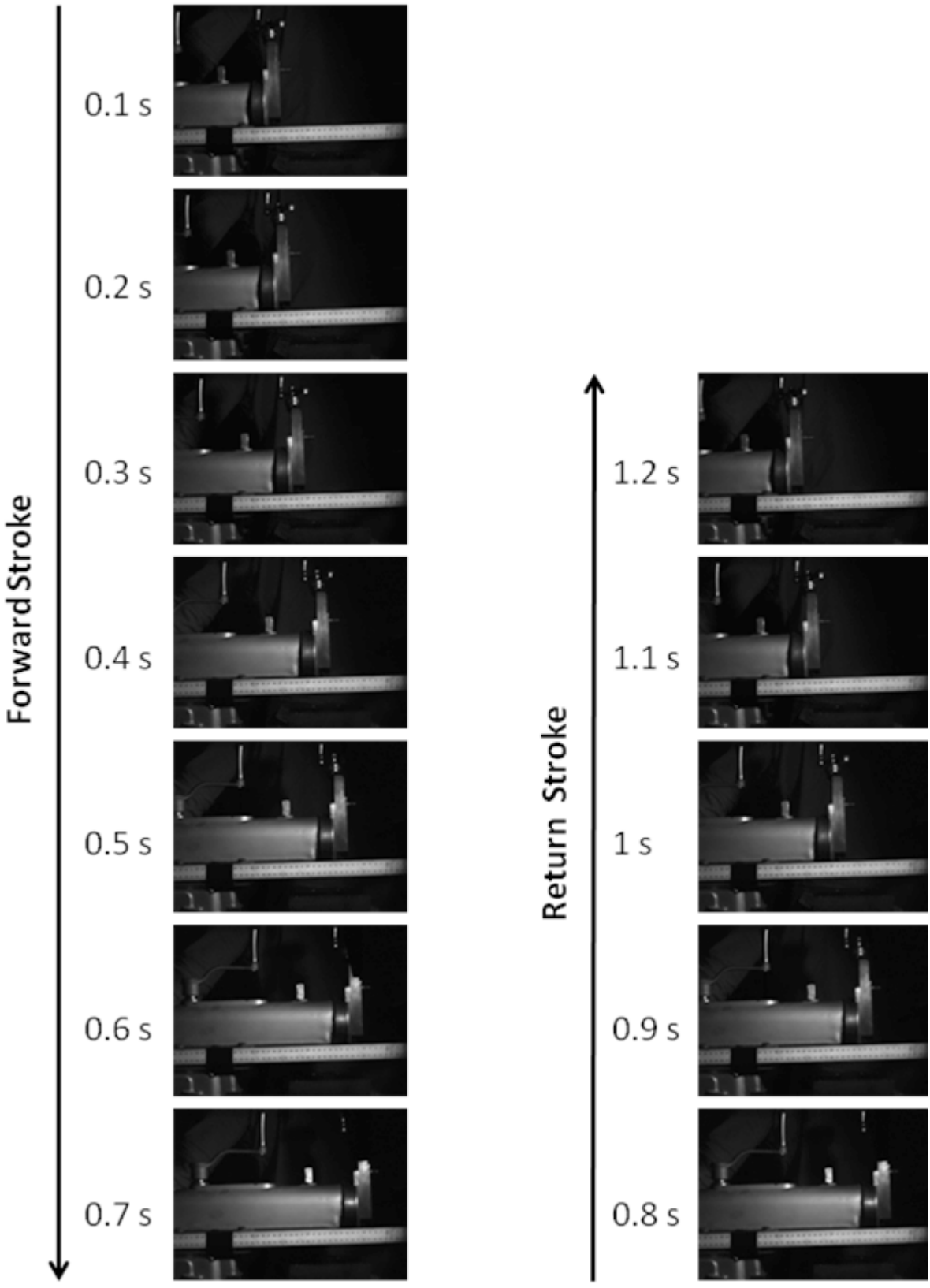

High speed video frames measuring the displacement of the shaper arm at 100 millisecond intervals (both forward and return strokes)

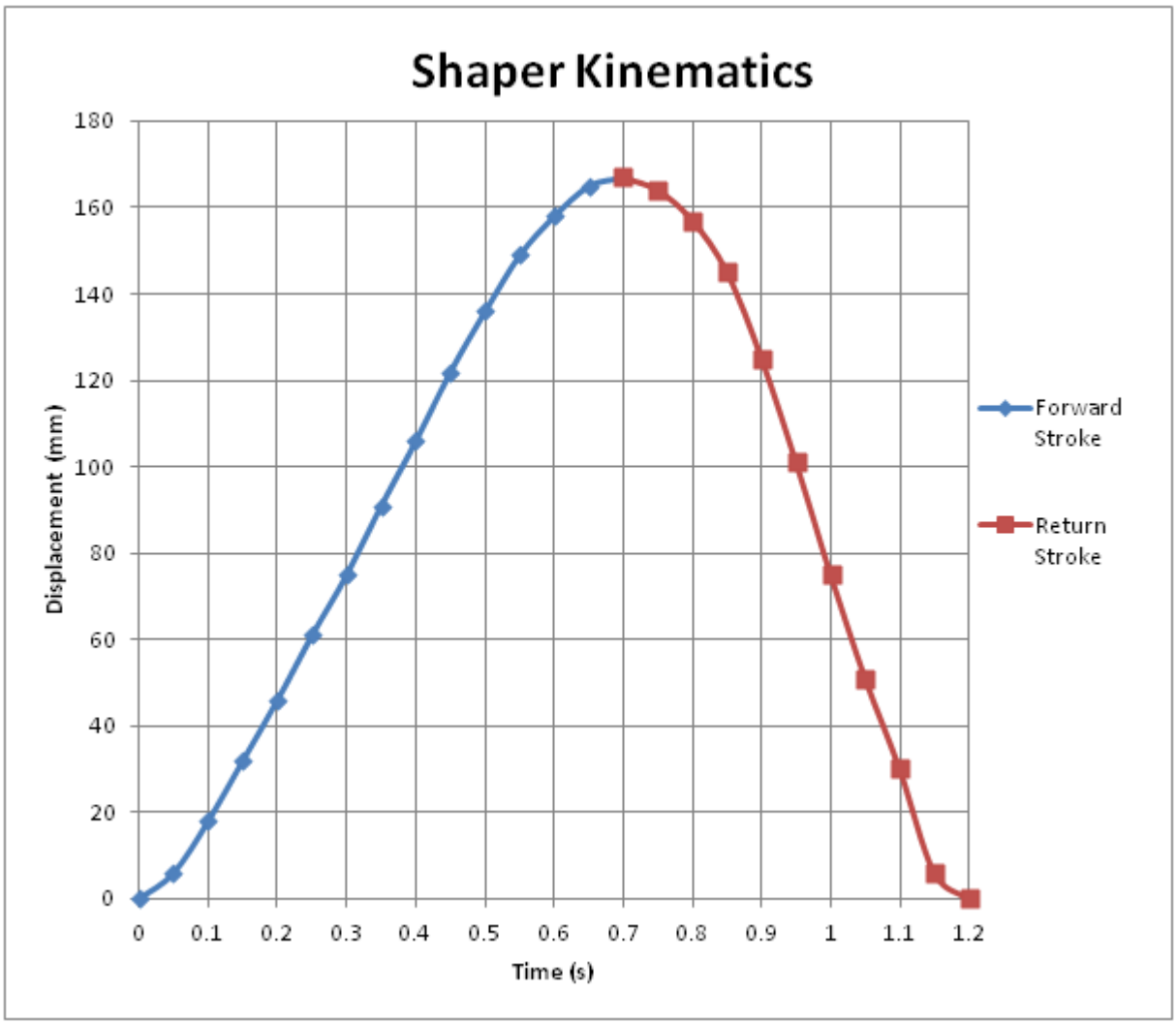

Displacement vs. time plot for one entire stroke of the shaper arm

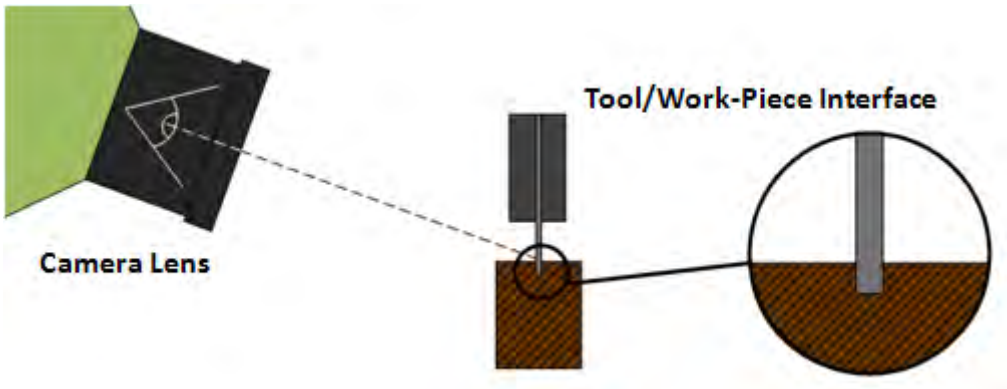

High speed camera set-up

APPENDIX 10 – STATISTICAL SUMMARY OF DATA FROM CUTTING TESTS PERFORMED IN SHAPER MACHINE

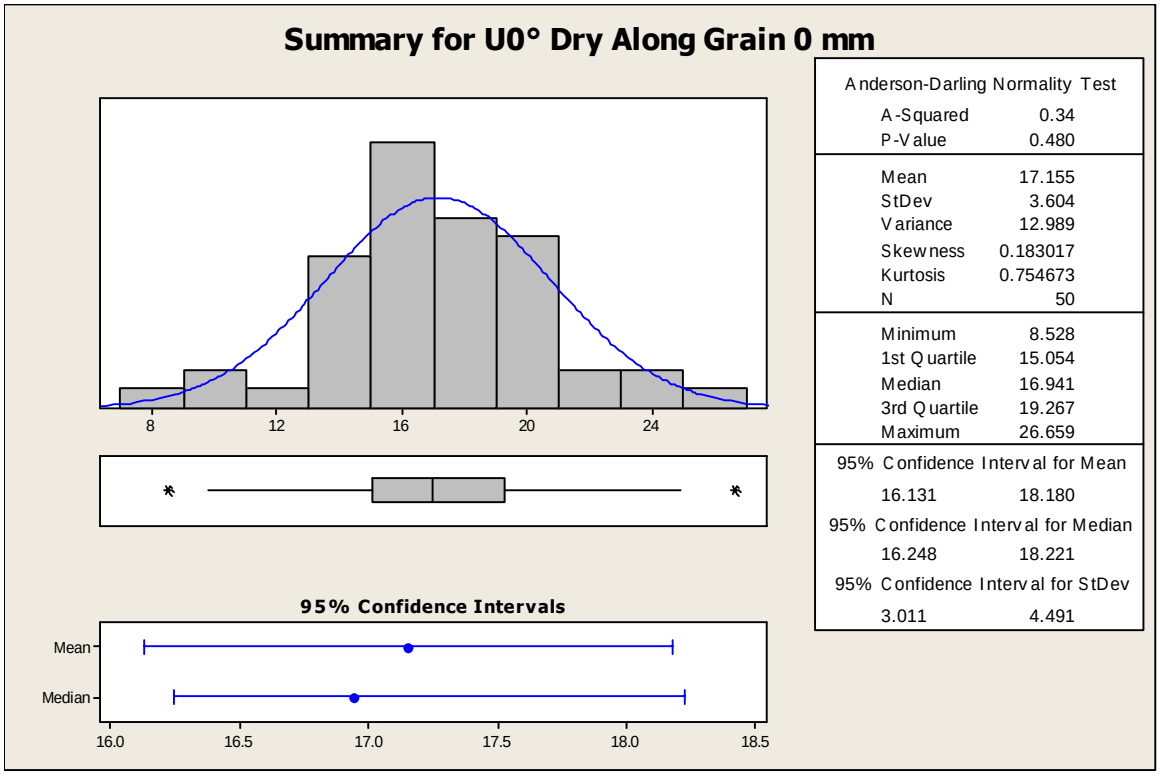

Anderson-Darling Normality Test	
A-Squared	0.34
P-Value	0.480
Mean	17.155
StDev	3.604
Variance	12.989
Skewness	0.183017
Kurtosis	0.754673
N	50
Minimum	8.528
1st Quartile	15.054
Median	16.941
3rd Quartile	19.267
Maximum	26.659
95% Confidence Interval for Mean	
16.131	18.180
95% Confidence Interval for Median	
16.248	18.221
95% Confidence Interval for StDev	
3.011	4.491

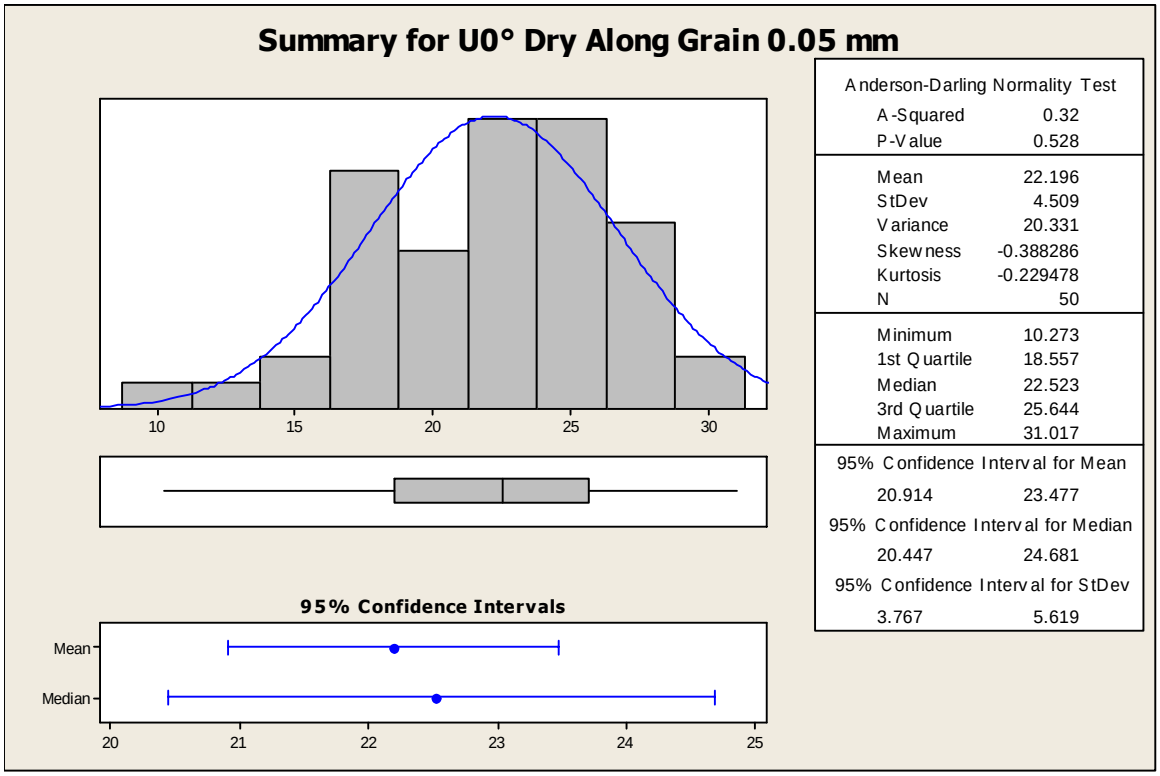

Anderson-Darling Normality Test	
A-Squared	0.32
P-Value	0.528
Mean	22.196
StDev	4.509
Variance	20.331
Skewness	-0.388286
Kurtosis	-0.229478
N	50
Minimum	10.273
1st Quartile	18.557
Median	22.523
3rd Quartile	25.644
Maximum	31.017
95% Confidence Interval for Mean	
20.914	23.477
95% Confidence Interval for Median	
20.447	24.681
95% Confidence Interval for StDev	
3.767	5.619

Summary for U0° Dry Along Grain 0.1 mm

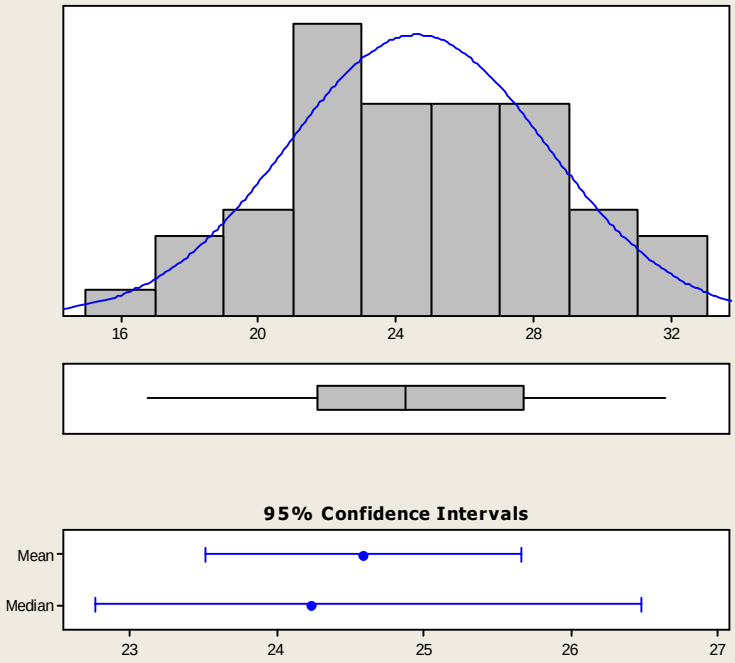

Anderson-Darling Normality Test	
A-Squared	0.31
P-Value	0.554
Mean	24.592
StDev	3.773
Variance	14.233
Skewness	0.004431
Kurtosis	-0.821571
N	50
Minimum	16.751
1st Quartile	21.702
Median	24.240
3rd Quartile	27.663
Maximum	31.804
95% Confidence Interval for Mean	
23.520	25.664
95% Confidence Interval for Median	
22.770	26.473
95% Confidence Interval for StDev	
3.151	4.701

Summary for U0° Dry Along Grain 0.15 mm

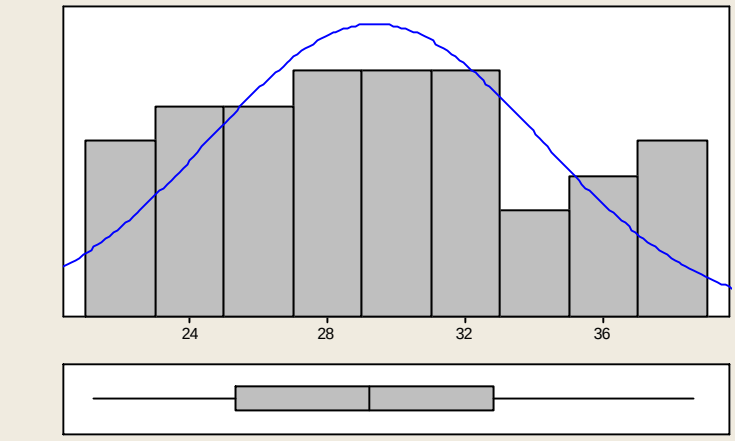

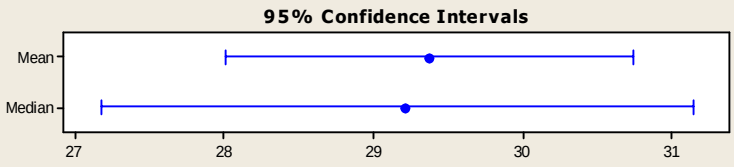

Anderson-Darling Normality Test	
A-Squared	0.54
P-Value	0.156
Mean	29.374
StDev	4.796
Variance	23.000
Skewness	0.209516
Kurtosis	-0.979446
N	50
Minimum	21.209
1st Quartile	25.313
Median	29.210
3rd Quartile	32.815
Maximum	38.636
95% Confidence Interval for Mean	
28.011	30.737
95% Confidence Interval for Median	
27.176	31.143
95% Confidence Interval for StDev	
4.006	5.976

Summary for U0° Dry Along Grain 0.2 mm

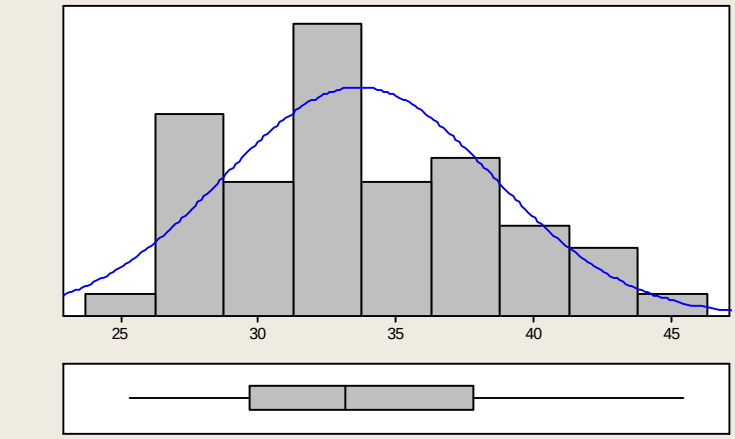

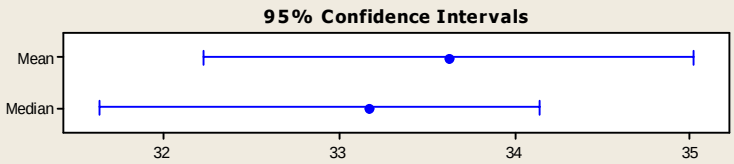

Anderson-Darling Normality Test	
A-Squared	0.44
P-Value	0.289
Mean	33.623
StDev	4.907
Variance	24.075
Skewness	0.421786
Kurtosis	-0.490345
N	50
Minimum	25.287
1st Quartile	29.662
Median	33.172
3rd Quartile	37.766
Maximum	45.389
95% Confidence Interval for Mean	
32.229	35.018
95% Confidence Interval for Median	
31.633	34.135
95% Confidence Interval for StDev	
4.099	6.114

Summary for U0° Dry Along Grain 0.25 mm

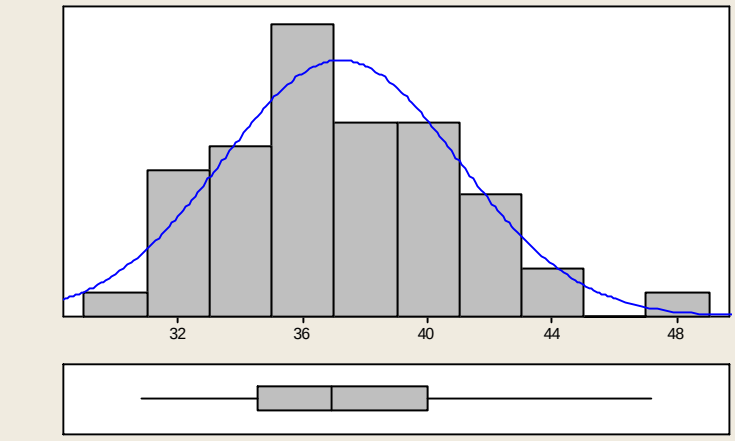

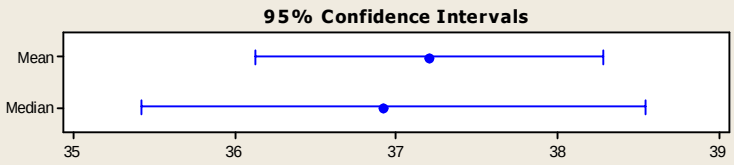

Anderson-Darling Normality Test	
A-Squared	0.20
P-Value	0.871
Mean	37.209
StDev	3.796
Variance	14.408
Skewness	0.334226
Kurtosis	-0.289639
N	50
Minimum	30.856
1st Quartile	34.554
Median	36.914
3rd Quartile	40.000
Maximum	47.157
95% Confidence Interval for Mean	
36.131	38.288
95% Confidence Interval for Median	
35.423	38.544
95% Confidence Interval for StDev	
3.171	4.730

Summary for U0° Dry Along Grain 0.3 mm

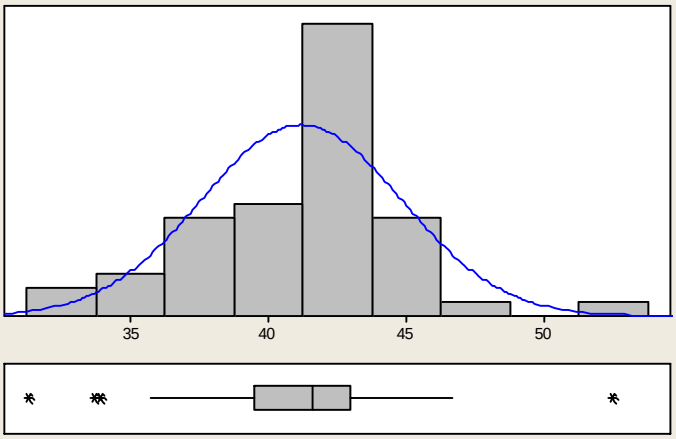

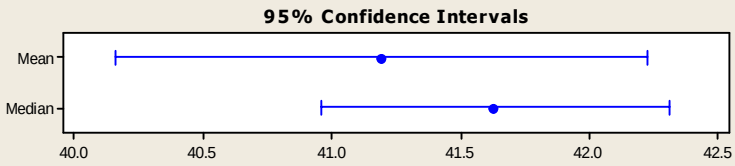

Anderson-Darling Normality Test	
A-Squared	0.97
P-Value	0.013
Mean	41.191
StDev	3.636
Variance	13.218
Skewness	-0.16049
Kurtosis	1.77646
N	50
Minimum	31.260
1st Quartile	39.479
Median	41.623
3rd Quartile	42.948
Maximum	52.504
95% Confidence Interval for Mean	
40.158	42.224
95% Confidence Interval for Median	
40.959	42.310
95% Confidence Interval for StDev	
3.037	4.530

Summary for U0° Dry Along Grain 0.35 mm

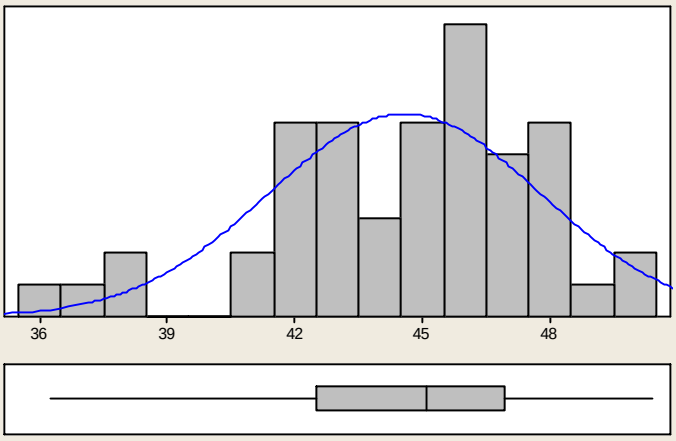

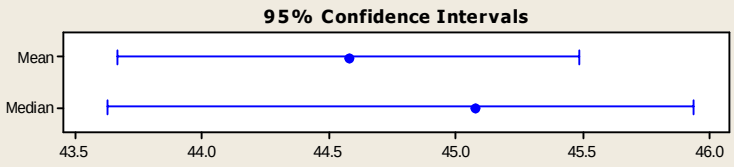

Anderson-Darling Normality Test	
A-Squared	0.59
P-Value	0.117
Mean	44.578
StDev	3.198
Variance	10.225
Skewness	-0.714026
Kurtosis	0.502571
N	50
Minimum	36.229
1st Quartile	42.519
Median	45.073
3rd Quartile	46.930
Maximum	50.425
95% Confidence Interval for Mean	
43.670	45.487
95% Confidence Interval for Median	
43.624	45.935
95% Confidence Interval for StDev	
2.671	3.985

Summary for U0° Dry Across Grain 0 mm

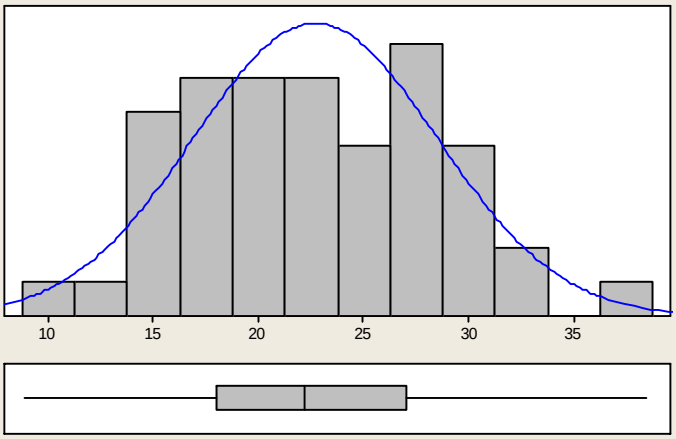

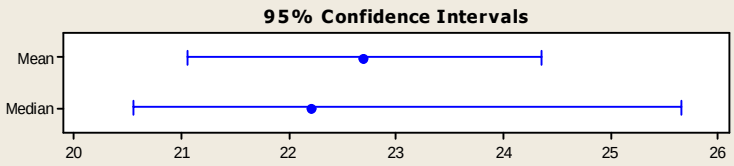

Anderson-Darling Normality Test	
A-Squared	0.30
P-Value	0.574
Mean	22.700
StDev	5.812
Variance	33.777
Skewness	0.145144
Kurtosis	-0.014309
N	50
Minimum	8.831
1st Quartile	17.991
Median	22.204
3rd Quartile	27.028
Maximum	38.407
95% Confidence Interval for Mean	
21.048	24.352
95% Confidence Interval for Median	
20.559	25.647
95% Confidence Interval for StDev	
4.855	7.242

Summary for U0° Dry Across Grain 0.05 mm

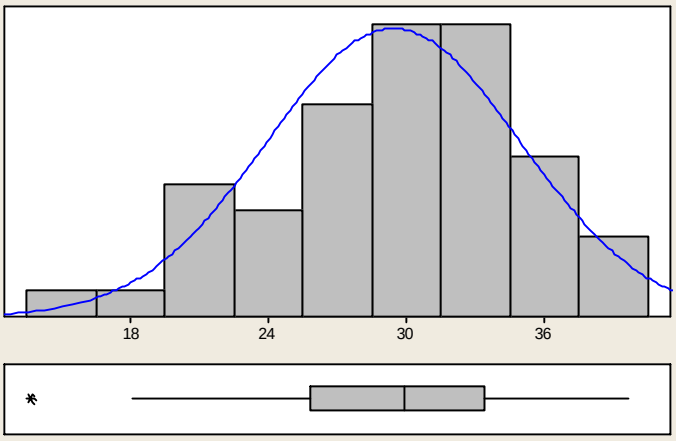

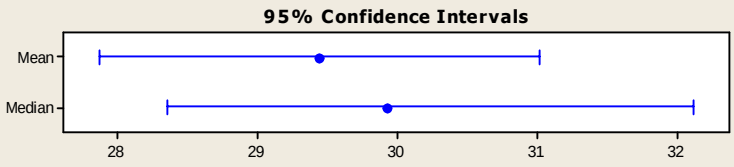

Anderson-Darling Normality Test	
A-Squared	0.34
P-Value	0.493
Mean	29.442
StDev	5.526
Variance	30.532
Skewness	-0.531991
Kurtosis	0.237707
N	50
Minimum	13.660
1st Quartile	25.783
Median	29.927
3rd Quartile	33.408
Maximum	39.709
95% Confidence Interval for Mean	
27.872	31.012
95% Confidence Interval for Median	
28.356	32.120
95% Confidence Interval for StDev	
4.616	6.886

Summary for U0° Dry Across Grain 0.1 mm

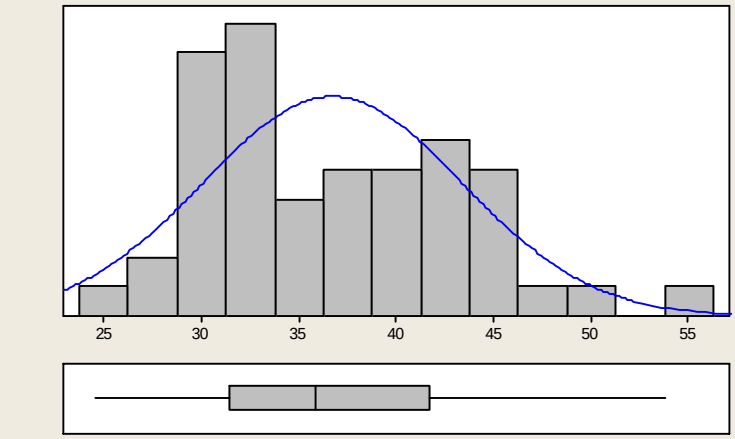

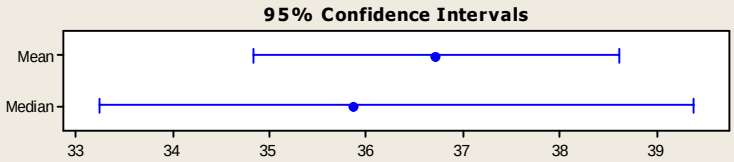

Anderson-Darling Normality Test	
A-Squared	0.61
P-Value	0.107
Mean	36.717
StDev	6.652
Variance	44.243
Skewness	0.414204
Kurtosis	-0.512212
N	50
Minimum	24.542
1st Quartile	31.426
Median	35.864
3rd Quartile	41.661
Maximum	53.754
95% Confidence Interval for Mean	
34.827	38.608
95% Confidence Interval for Median	
33.240	39.381
95% Confidence Interval for StDev	
5.556	8.289

Summary for U0° Dry Across Grain 0.15 mm

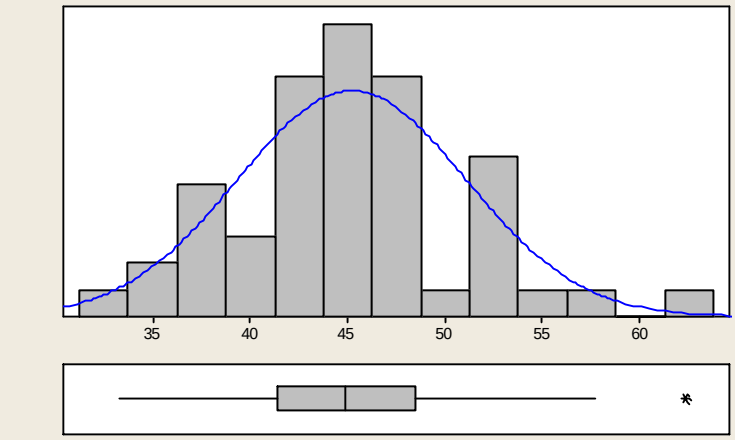

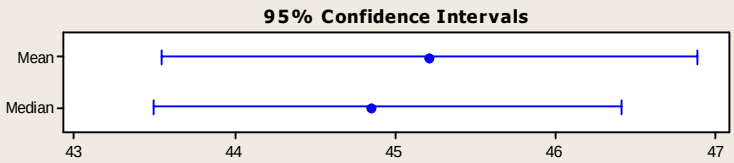

Anderson-Darling Normality Test	
A-Squared	0.34
P-Value	0.473
Mean	45.211
StDev	5.874
Variance	34.503
Skewness	0.512985
Kurtosis	0.584093
N	50
Minimum	33.327
1st Quartile	41.368
Median	44.847
3rd Quartile	48.451
Maximum	62.325
95% Confidence Interval for Mean	
43.542	46.881
95% Confidence Interval for Median	
43.491	46.412
95% Confidence Interval for StDev	
4.907	7.320

Summary for U0° Dry Across Grain 0.2 mm

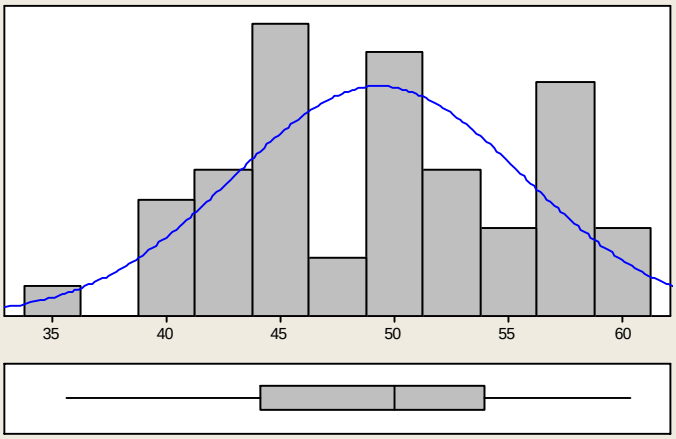

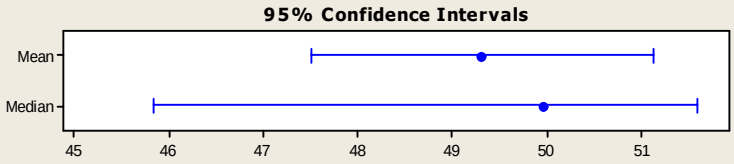

Anderson-Darling Normality Test	
A-Squared	0.52
P-Value	0.175
Mean	49.308
StDev	6.351
Variance	40.340
Skewness	-0.021058
Kurtosis	-0.967312
N	50
Minimum	35.606
1st Quartile	44.135
Median	49.961
3rd Quartile	53.921
Maximum	60.331
95% Confidence Interval for Mean	
47.503	51.113
95% Confidence Interval for Median	
45.846	51.581
95% Confidence Interval for StDev	
5.305	7.915

Summary for U0° Dry Across Grain 0.25 mm

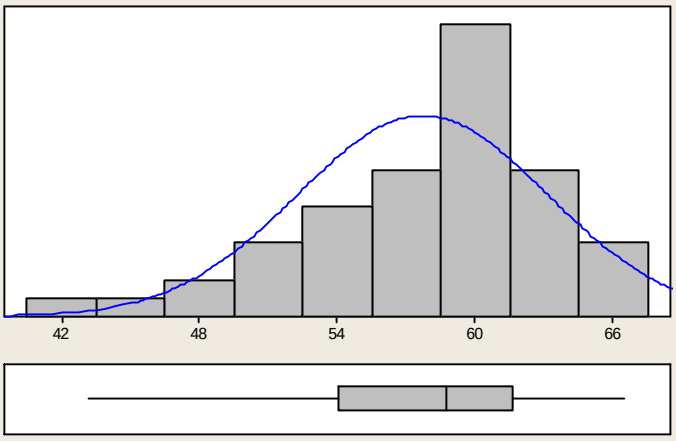

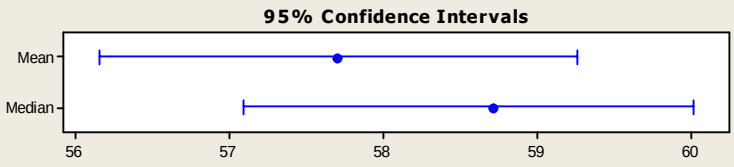

Anderson-Darling Normality Test	
A-Squared	0.76
P-Value	0.044
Mean	57.706
StDev	5.445
Variance	29.647
Skewness	-0.696599
Kurtosis	-0.003156
N	50
Minimum	43.186
1st Quartile	54.006
Median	58.708
3rd Quartile	61.604
Maximum	66.461
95% Confidence Interval for Mean	
56.159	59.253
95% Confidence Interval for Median	
57.093	60.014
95% Confidence Interval for StDev	
4.548	6.785

Summary for U0° Dry Across Grain 0.3 mm

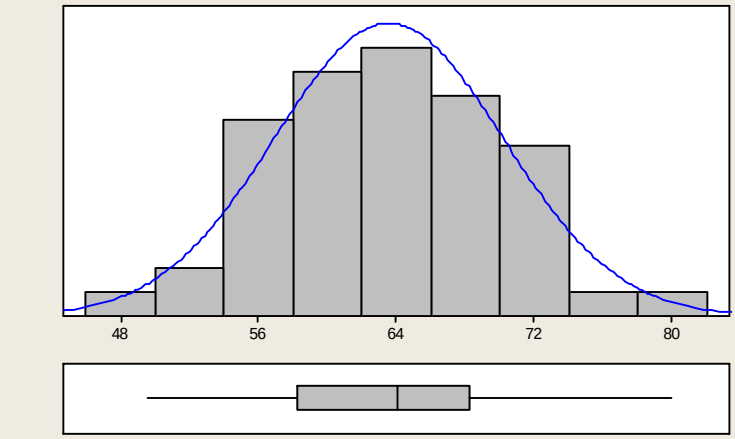

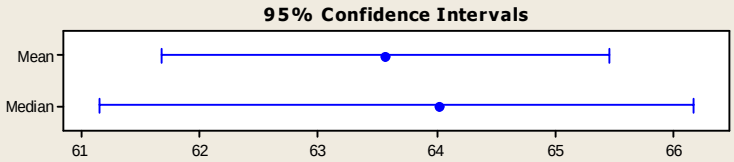

Anderson-Darling Normality Test	
A-Squared	0.23
P-Value	0.801
Mean	63.564
StDev	6.655
Variance	44.287
Skewness	0.094055
Kurtosis	-0.490915
N	50
Minimum	49.507
1st Quartile	58.291
Median	64.020
3rd Quartile	68.275
Maximum	79.993
95% Confidence Interval for Mean	
61.673	65.455
95% Confidence Interval for Median	
61.151	66.161
95% Confidence Interval for StDev	
5.559	8.293

Summary for U0° Dry Across Grain 0.35 mm

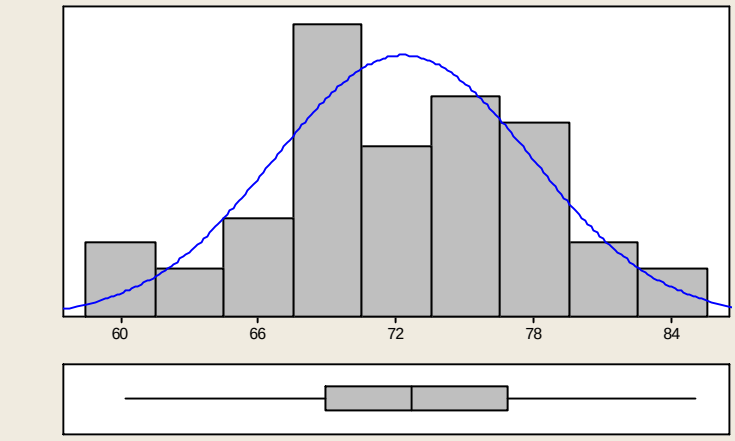

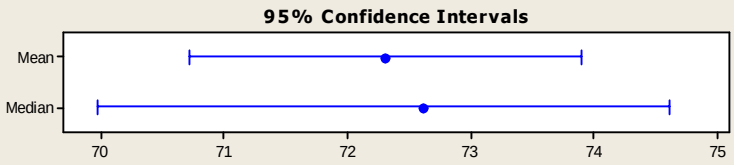

Anderson-Darling Normality Test	
A-Squared	0.21
P-Value	0.843
Mean	72.300
StDev	5.583
Variance	31.169
Skewness	-0.173981
Kurtosis	-0.161368
N	50
Minimum	60.220
1st Quartile	68.888
Median	72.621
3rd Quartile	76.844
Maximum	85.025
95% Confidence Interval for Mean	
70.713	73.887
95% Confidence Interval for Median	
69.975	74.614
95% Confidence Interval for StDev	
4.664	6.957

Summary for U0° Sat Along Grain 0 mm

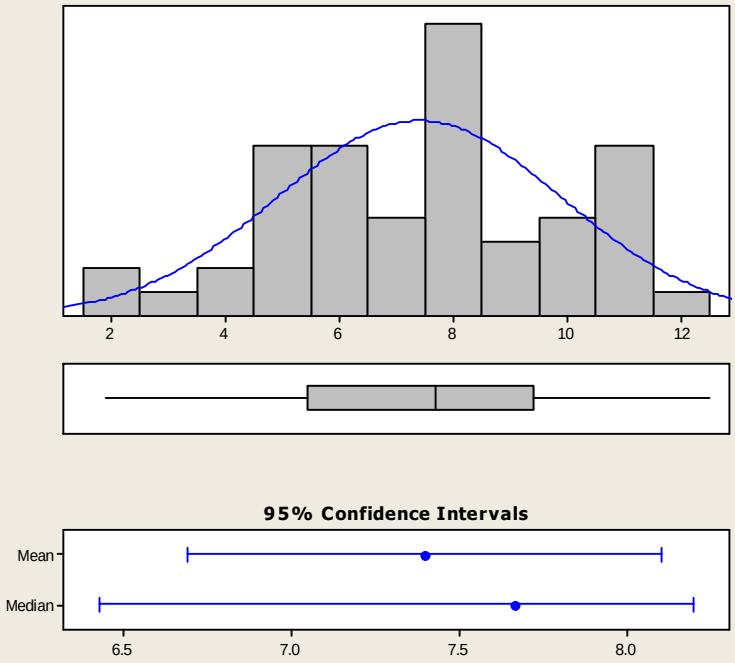

Anderson-Darling Normality Test	
A-Squared	0.31
P-Value	0.548
Mean	7.3982
StDev	2.4892
Variance	6.1963
Skewness	-0.084523
Kurtosis	-0.606693
N	50
Minimum	1.9046
1st Quartile	5.4476
Median	7.6658
3rd Quartile	9.3847
Maximum	12.4763
95% Confidence Interval for Mean	
6.6908	8.1056
95% Confidence Interval for Median	
6.4290	8.1991
95% Confidence Interval for StDev	
2.0793	3.1019

Summary for U0° Sat Along Grain 0.05 mm

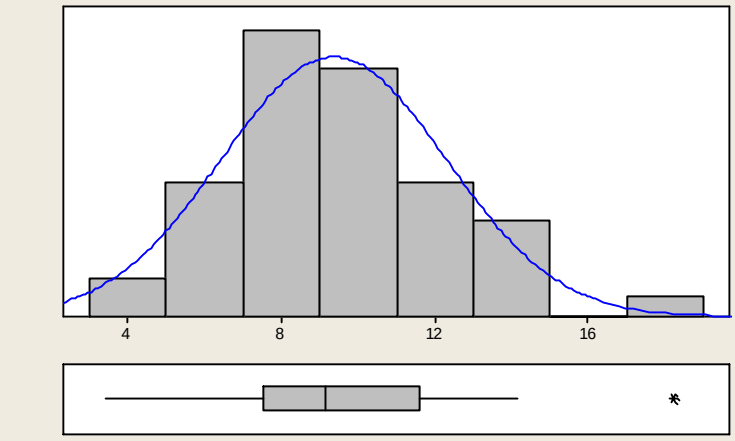

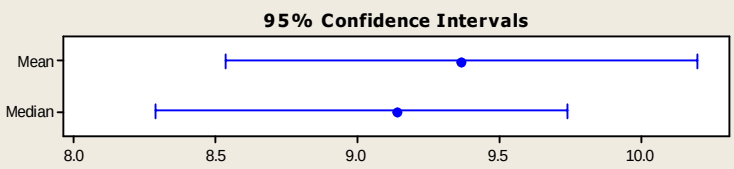

Anderson-Darling Normality Test	
A-Squared	0.40
P-Value	0.346
Mean	9.3668
StDev	2.9245
Variance	8.5528
Skewness	0.427194
Kurtosis	0.551013
N	50
Minimum	3.4037
1st Quartile	7.5629
Median	9.1407
3rd Quartile	11.5823
Maximum	18.2049
95% Confidence Interval for Mean	
8.5357	10.1980
95% Confidence Interval for Median	
8.2842	9.7418
95% Confidence Interval for StDev	
2.4430	3.6443

Summary for U0° Sat Along Grain 0.1 mm

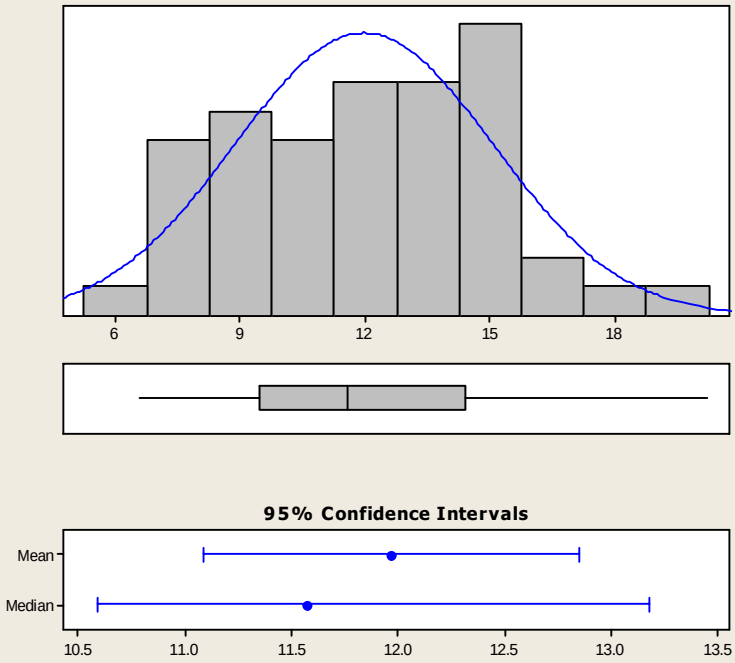

Summary for U0° Sat Along Grain 0.2 mm

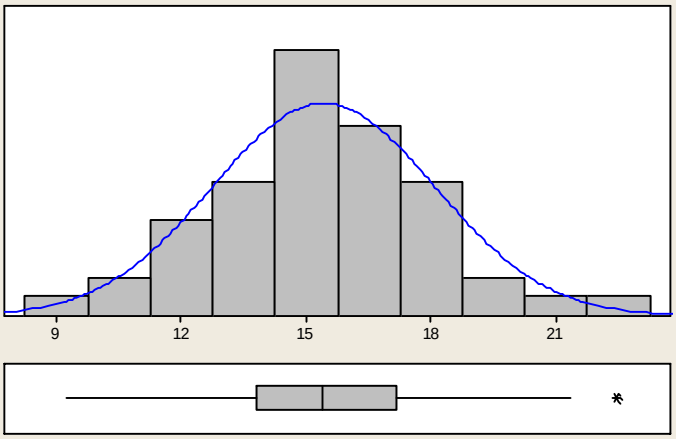

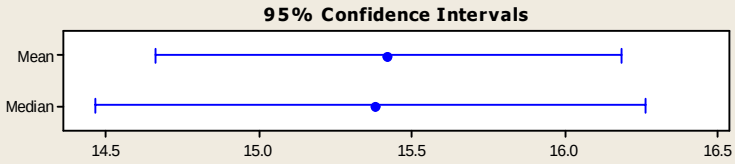

Anderson-Darling Normality Test	
A-Squared	0.13
P-Value	0.980
Mean	15.419
StDev	2.681
Variance	7.188
Skewness	0.208987
Kurtosis	0.244620
N	50
Minimum	9.249
1st Quartile	13.788
Median	15.380
3rd Quartile	17.148
Maximum	22.473
95% Confidence Interval for Mean	
14.657	16.181
95% Confidence Interval for Median	
14.467	16.261
95% Confidence Interval for StDev	
2.240	3.341

Summary for U0° Sat Along Grain 0.25 mm

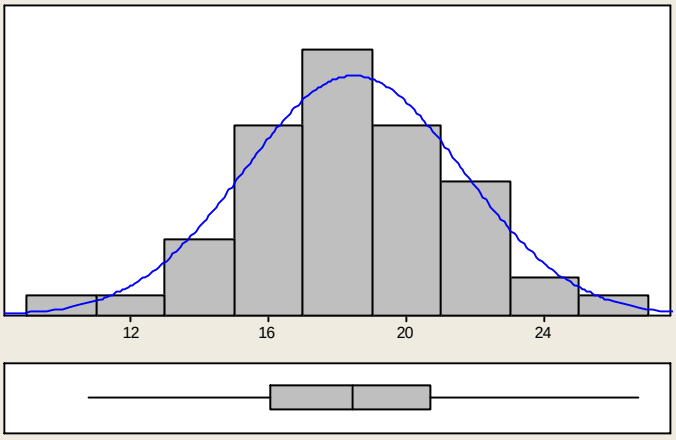

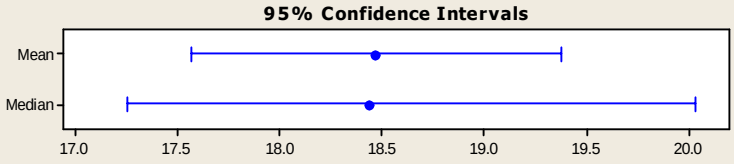

Anderson-Darling Normality Test	
A-Squared	0.18
P-Value	0.913
Mean	18.470
StDev	3.170
Variance	10.048
Skewness	0.0857621
Kurtosis	0.0892687
N	50
Minimum	10.756
1st Quartile	16.048
Median	18.440
3rd Quartile	20.685
Maximum	26.718
95% Confidence Interval for Mean	
17.569	19.371
95% Confidence Interval for Median	
17.253	20.027
95% Confidence Interval for StDev	
2.648	3.950

Summary for U0° Sat Along Grain 0.3 mm

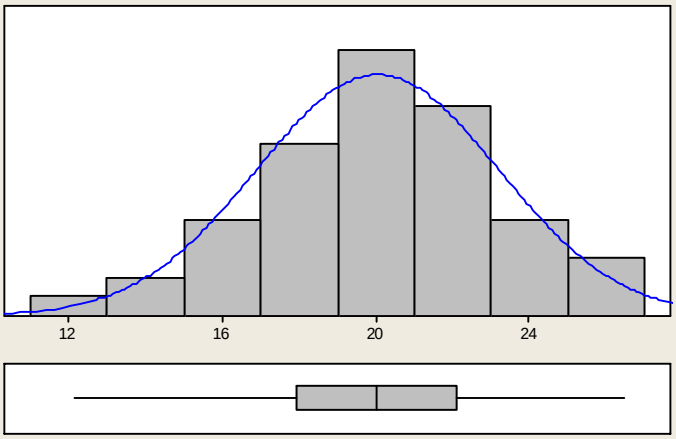

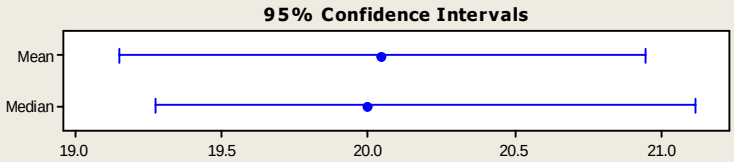

Anderson-Darling Normality Test	
A-Squared	0.19
P-Value	0.893
Mean	20.047
StDev	3.148
Variance	9.908
Skewness	-0.200702
Kurtosis	0.226046
N	50
Minimum	12.129
1st Quartile	17.929
Median	19.995
3rd Quartile	22.071
Maximum	26.476
95% Confidence Interval for Mean	
19.153	20.942
95% Confidence Interval for Median	
19.277	21.111
95% Confidence Interval for StDev	
2.629	3.922

Summary for U0° Sat Along Grain 0.35 mm

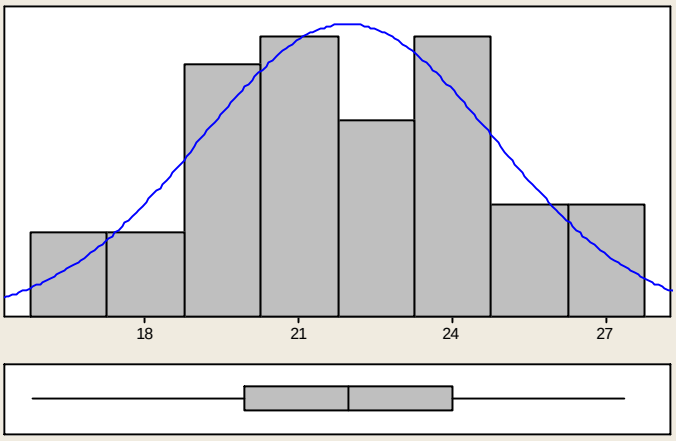

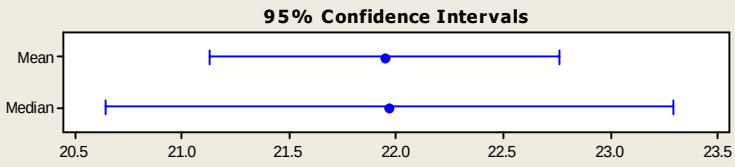

Anderson-Darling Normality Test	
A-Squared	0.25
P-Value	0.736
Mean	21.946
StDev	2.867
Variance	8.222
Skewness	-0.118152
Kurtosis	-0.469639
N	50
Minimum	15.778
1st Quartile	19.929
Median	21.965
3rd Quartile	23.998
Maximum	27.367
95% Confidence Interval for Mean	
21.132	22.761
95% Confidence Interval for Median	
20.641	23.290
95% Confidence Interval for StDev	
2.395	3.573

Summary for U0° Sat Across Grain 0 mm

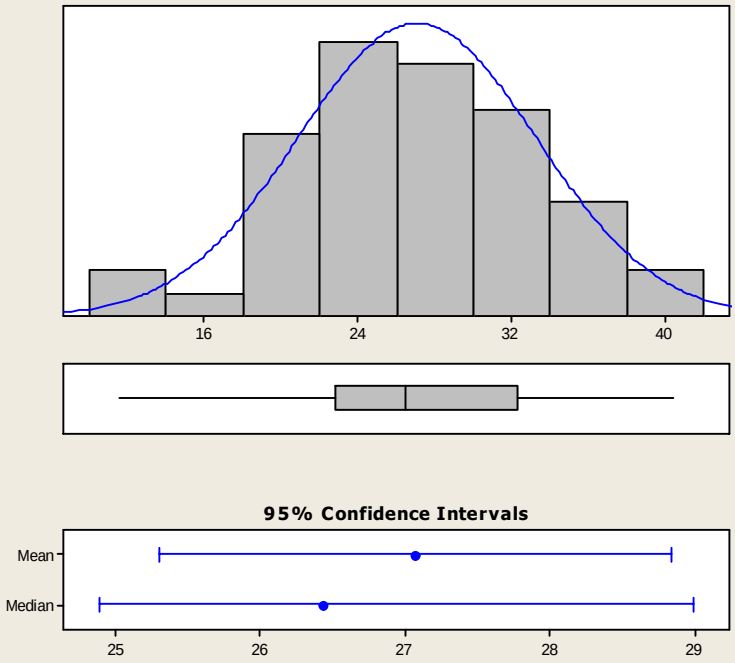

Anderson-Darling Normality Test	
A-Squared	0.31
P-Value	0.534
Mean	27.070
StDev	6.228
Variance	38.786
Skewness	-0.136140
Kurtosis	0.008230
N	50
Minimum	11.559
1st Quartile	22.861
Median	26.434
3rd Quartile	32.312
Maximum	40.408
95% Confidence Interval for Mean	
25.300	28.840
95% Confidence Interval for Median	
24.886	28.989
95% Confidence Interval for StDev	
5.202	7.761

Summary for U0° Sat Across Grain 0.05 mm

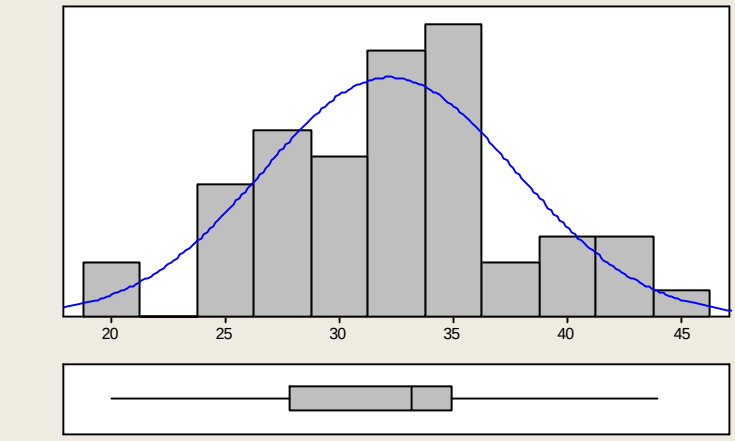

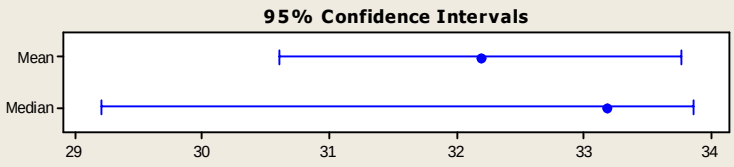

Anderson-Darling Normality Test	
A-Squared	0.53
P-Value	0.163
Mean	32.187
StDev	5.546
Variance	30.756
Skewness	-0.012486
Kurtosis	-0.364500
N	50
Minimum	20.023
1st Quartile	27.812
Median	33.186
3rd Quartile	34.905
Maximum	43.964
95% Confidence Interval for Mean	
30.611	33.763
95% Confidence Interval for Median	
29.200	33.864
95% Confidence Interval for StDev	
4.633	6.911

Summary for U0° Sat Across Grain 0.1 mm

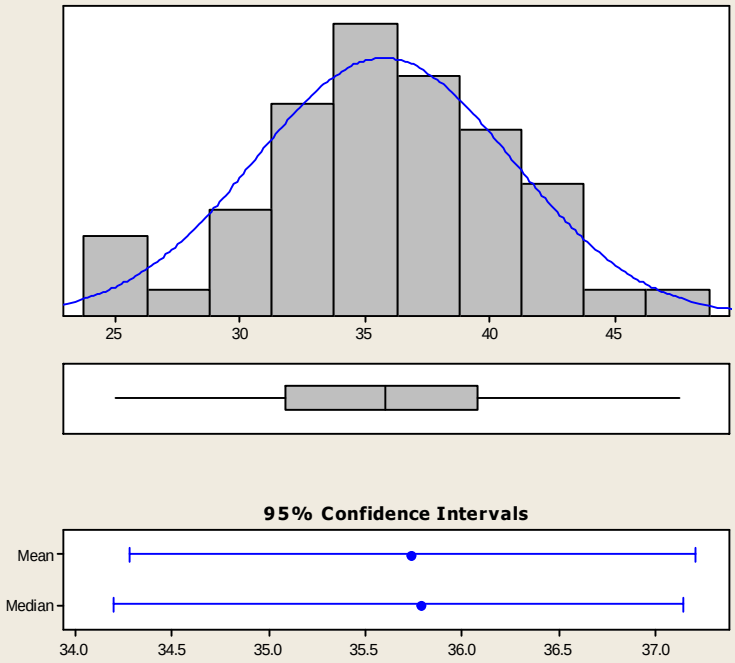

Anderson-Darling Normality Test	
A-Squared	0.27
P-Value	0.652
Mean	35.737
StDev	5.137
Variance	26.385
Skewness	-0.0409137
Kurtosis	-0.0769797
N	50
Minimum	25.036
1st Quartile	31.786
Median	35.788
3rd Quartile	39.500
Maximum	47.608
95% Confidence Interval for Mean	
34.278	37.197
95% Confidence Interval for Median	
34.203	37.144
95% Confidence Interval for StDev	
4.291	6.401

Summary for U0° Sat Across Grain 0.15 mm

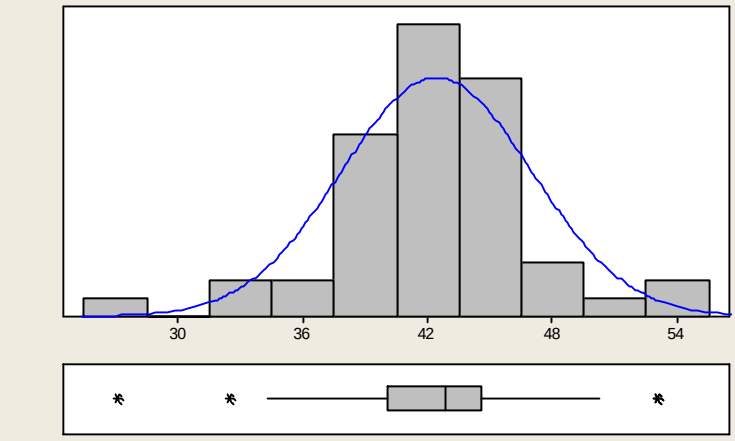

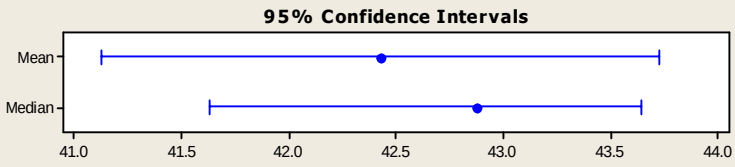

Anderson-Darling Normality Test	
A-Squared	0.78
P-Value	0.041
Mean	42.427
StDev	4.579
Variance	20.968
Skewness	-0.46683
Kurtosis	2.38188
N	50
Minimum	27.060
1st Quartile	40.115
Median	42.880
3rd Quartile	44.632
Maximum	53.081
95% Confidence Interval for Mean	
41.126	43.728
95% Confidence Interval for Median	
41.627	43.646
95% Confidence Interval for StDev	
3.825	5.706

Summary for U0° Sat Across Grain 0.2 mm

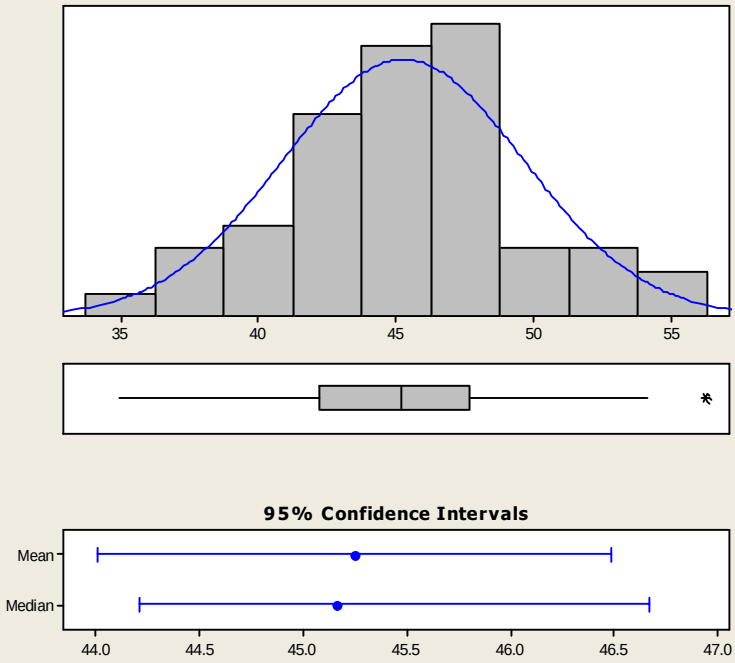

Anderson-Darling Normality Test	
A-Squared	0.27
P-Value	0.663
Mean	45.246
StDev	4.376
Variance	19.146
Skewness	0.000162
Kurtosis	0.387014
N	50
Minimum	34.919
1st Quartile	42.172
Median	45.167
3rd Quartile	47.670
Maximum	56.201
95% Confidence Interval for Mean	
44.002	46.489
95% Confidence Interval for Median	
44.212	46.670
95% Confidence Interval for StDev	
3.655	5.453

Summary for U0° Sat Across Grain 0.25 mm

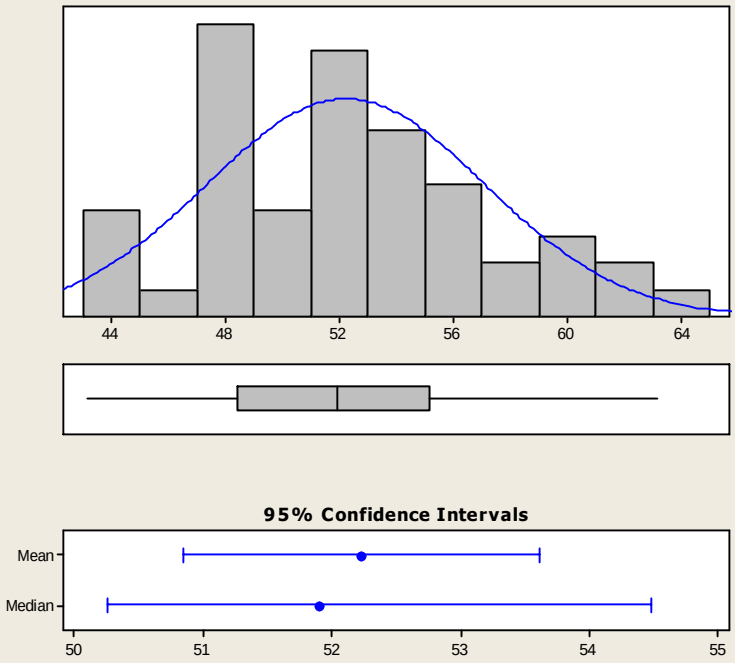

Anderson-Darling Normality Test	
A-Squared	0.31
P-Value	0.549
Mean	52.225
StDev	4.870
Variance	23.719
Skewness	0.197458
Kurtosis	-0.422232
N	50
Minimum	43.166
1st Quartile	48.433
Median	51.899
3rd Quartile	55.150
Maximum	63.135
95% Confidence Interval for Mean	
50.841	53.610
95% Confidence Interval for Median	
50.256	54.472
95% Confidence Interval for StDev	
4.068	6.069

Summary for U0° Sat Across Grain 0.3 mm

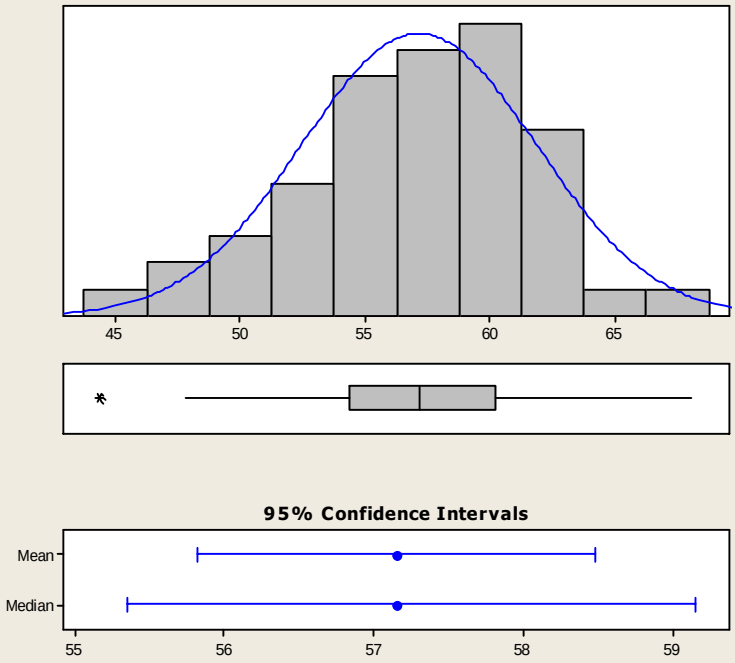

Anderson-Darling Normality Test	
A-Squared	0.18
P-Value	0.910
Mean	57.152
StDev	4.696
Variance	22.057
Skewness	-0.270685
Kurtosis	0.353478
N	50
Minimum	44.342
1st Quartile	54.406
Median	57.158
3rd Quartile	60.227
Maximum	68.077
95% Confidence Interval for Mean	
55.818	58.487
95% Confidence Interval for Median	
55.353	59.150
95% Confidence Interval for StDev	
3.923	5.852

Summary for U0° Sat Across Grain 0.35 mm

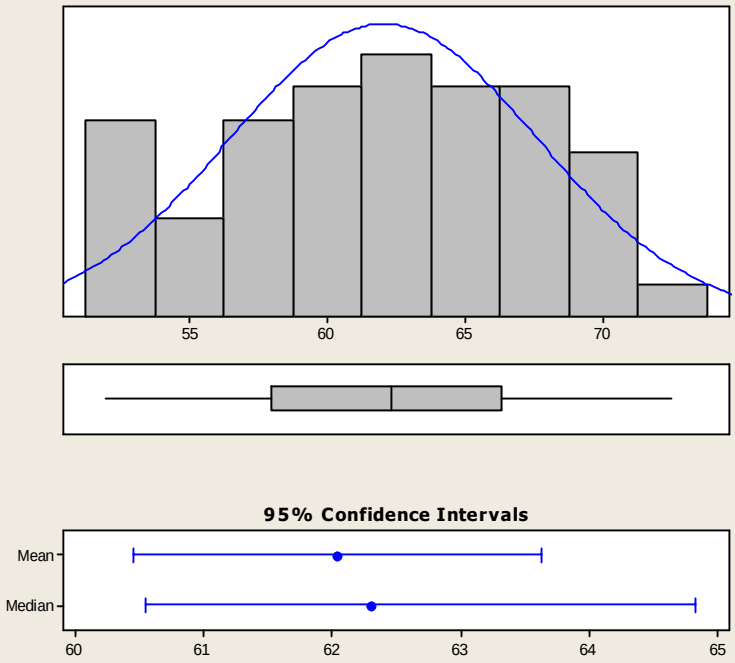

Anderson-Darling Normality Test	
A-Squared	0.43
P-Value	0.300
Mean	62.039
StDev	5.591
Variance	31.258
Skewness	-0.200139
Kurtosis	-0.859090
N	50
Minimum	51.967
1st Quartile	57.989
Median	62.302
3rd Quartile	66.342
Maximum	72.460
95% Confidence Interval for Mean	
60.450	63.628
95% Confidence Interval for Median	
60.544	64.821
95% Confidence Interval for StDev	
4.670	6.967

Summary for U28° Dry Along Grain 0 mm

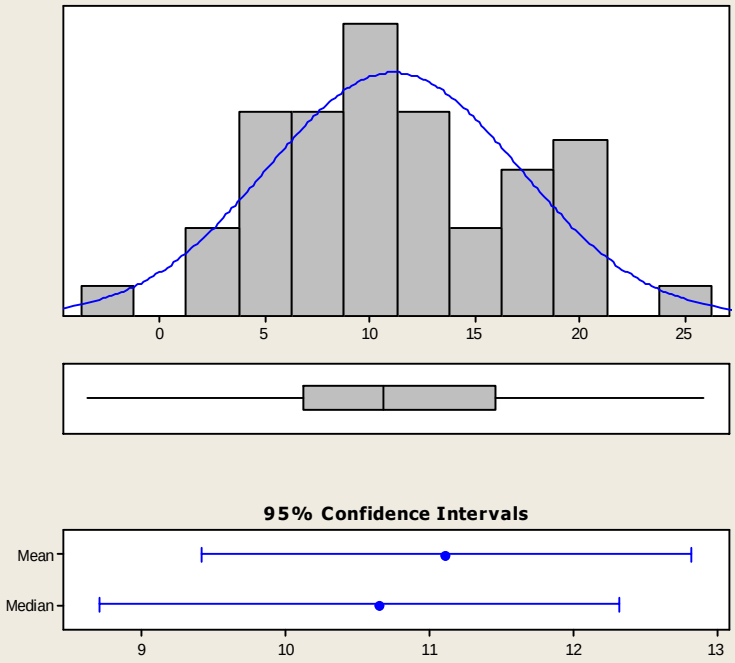

Anderson-Darling Normality Test	
A-Squared	0.45
P-Value	0.267
Mean	11.108
StDev	5.994
Variance	35.923
Skewness	0.182047
Kurtosis	-0.252746
N	50
Minimum	-3.413
1st Quartile	6.827
Median	10.641
3rd Quartile	15.996
Maximum	25.882
95% Confidence Interval for Mean	
9.405	12.811
95% Confidence Interval for Median	
8.696	12.319
95% Confidence Interval for StDev	
5.007	7.469

Summary for U28° Dry Along Grain 0.05 mm

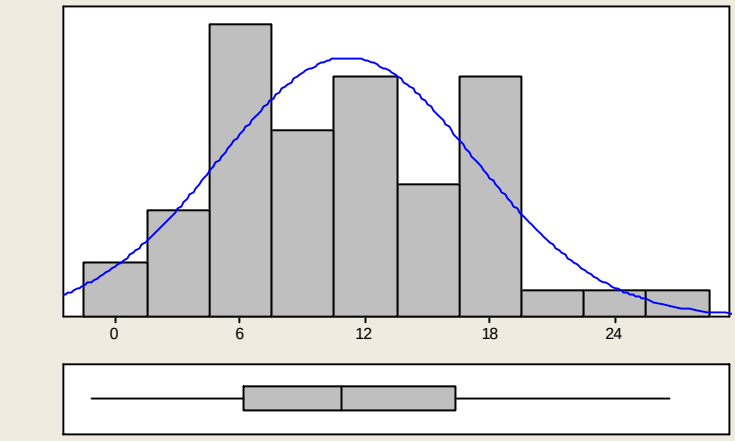

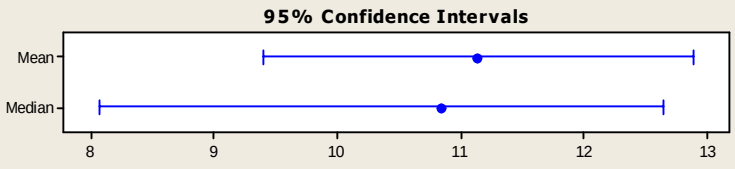

Anderson-Darling Normality Test	
A-Squared	0.45
P-Value	0.262
Mean	11.138
StDev	6.147
Variance	37.783
Skewness	0.358413
Kurtosis	-0.411844
N	50
Minimum	-1.116
1st Quartile	6.168
Median	10.844
3rd Quartile	16.345
Maximum	26.651
95% Confidence Interval for Mean	
9.391	12.885
95% Confidence Interval for Median	
8.067	12.636
95% Confidence Interval for StDev	
5.135	7.660

Summary for U28° Dry Along Grain 0.1 mm

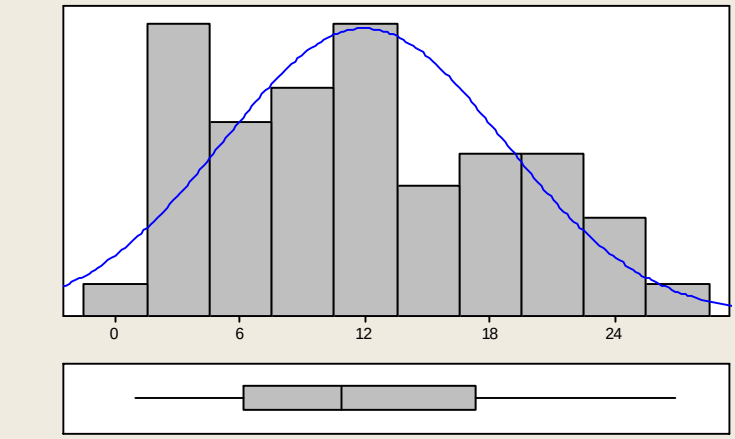

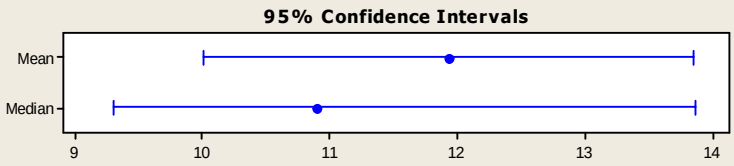

Anderson-Darling Normality Test	
A-Squared	0.62
P-Value	0.102
Mean	11.929
StDev	6.768
Variance	45.807
Skewness	0.369287
Kurtosis	-0.844815
N	50
Minimum	0.973
1st Quartile	6.115
Median	10.896
3rd Quartile	17.254
Maximum	26.915
95% Confidence Interval for Mean	
10.006	13.852
95% Confidence Interval for Median	
9.301	13.856
95% Confidence Interval for StDev	
5.654	8.434

Summary for U28° Dry Along Grain 0.15 mm

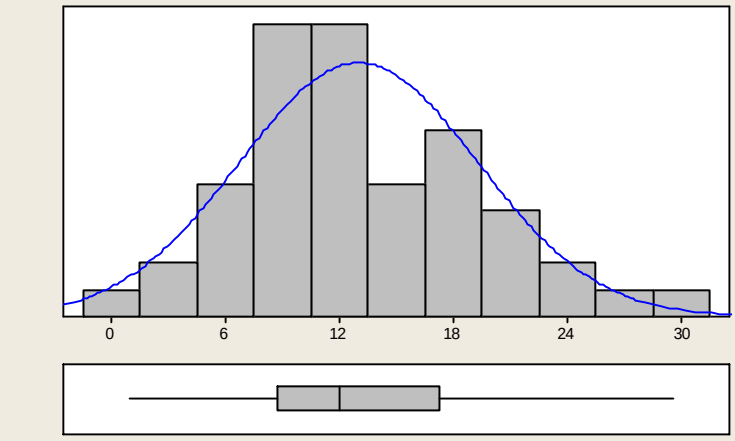

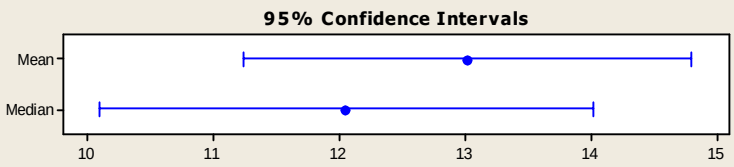

Anderson-Darling Normality Test	
A-Squared	0.44
P-Value	0.280
Mean	13.017
StDev	6.274
Variance	39.359
Skewness	0.493024
Kurtosis	0.200949
N	50
Minimum	0.998
1st Quartile	8.730
Median	12.049
3rd Quartile	17.234
Maximum	29.554
95% Confidence Interval for Mean	
11.234	14.800
95% Confidence Interval for Median	
10.096	14.021
95% Confidence Interval for StDev	
5.241	7.818

Summary for U28° Dry Along Grain 0.2 mm

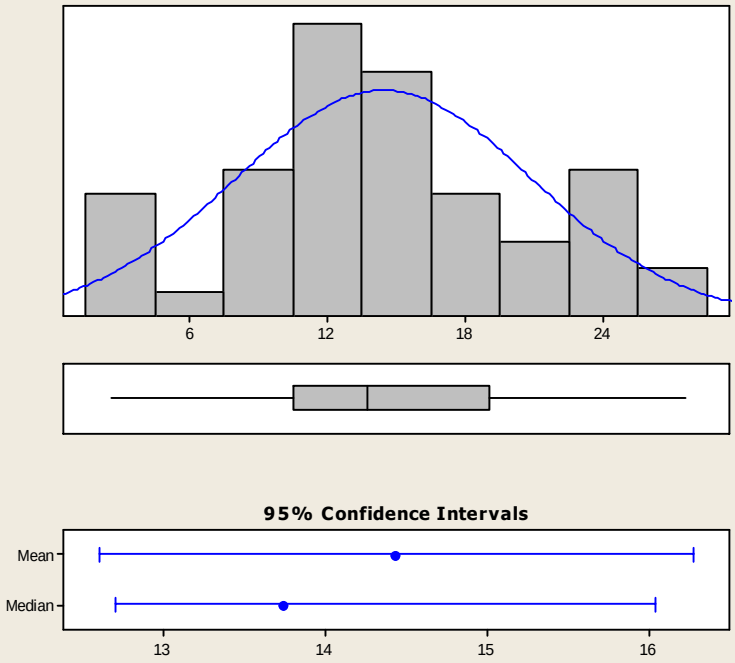

Anderson-Darling Normality Test	
A-Squared	0.39
P-Value	0.369
Mean	14.439
StDev	6.457
Variance	41.690
Skewness	0.080372
Kurtosis	-0.400202
N	50
Minimum	2.611
1st Quartile	10.513
Median	13.737
3rd Quartile	19.076
Maximum	27.591
95% Confidence Interval for Mean	
12.604	16.274
95% Confidence Interval for Median	
12.699	16.041
95% Confidence Interval for StDev	
5.394	8.046

Summary for U28° Dry Along Grain 0.25 mm

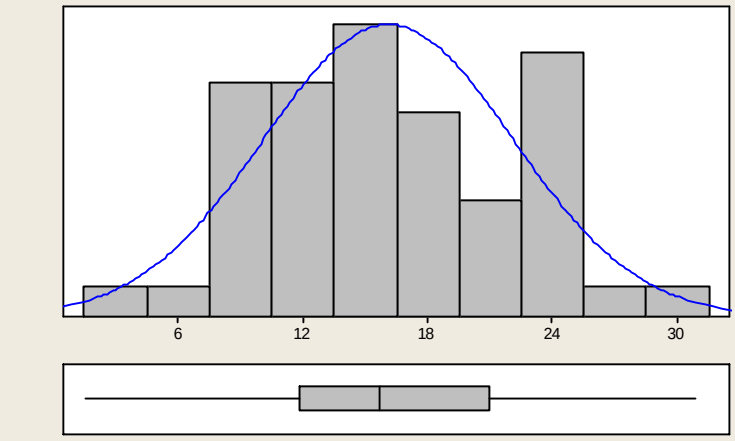

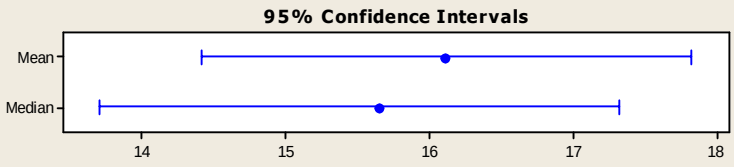

Anderson-Darling Normality Test	
A-Squared	0.45
P-Value	0.267
Mean	16.108
StDev	5.994
Variance	35.923
Skewness	0.182047
Kurtosis	-0.252746
N	50
Minimum	1.587
1st Quartile	11.827
Median	15.641
3rd Quartile	20.996
Maximum	30.882
95% Confidence Interval for Mean	
14.405	17.811
95% Confidence Interval for Median	
13.696	17.319
95% Confidence Interval for StDev	
5.007	7.469

Summary for U28° Dry Along Grain 0.3 mm

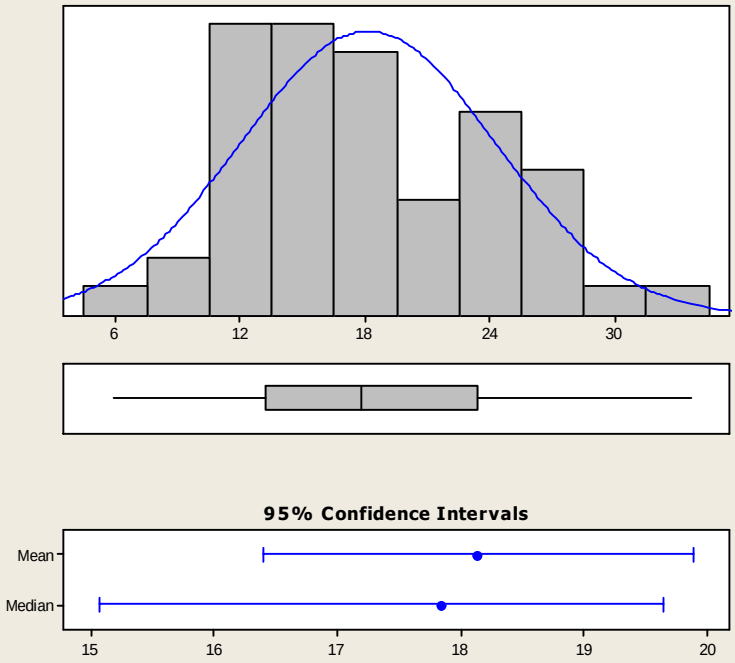

Anderson-Darling Normality Test	
A-Squared	0.45
P-Value	0.262

Mean	18.138
StDev	6.147
Variance	37.783
Skewness	0.358413
Kurtosis	-0.411844
N	50

Minimum	5.884
1st Quartile	13.168
Median	17.844
3rd Quartile	23.345
Maximum	33.651

95% Confidence Interval for Mean	
16.391	19.885
95% Confidence Interval for Median	
15.067	19.636
95% Confidence Interval for StDev	
5.135	7.660

Summary for U28° Dry Along Grain 0.35 mm

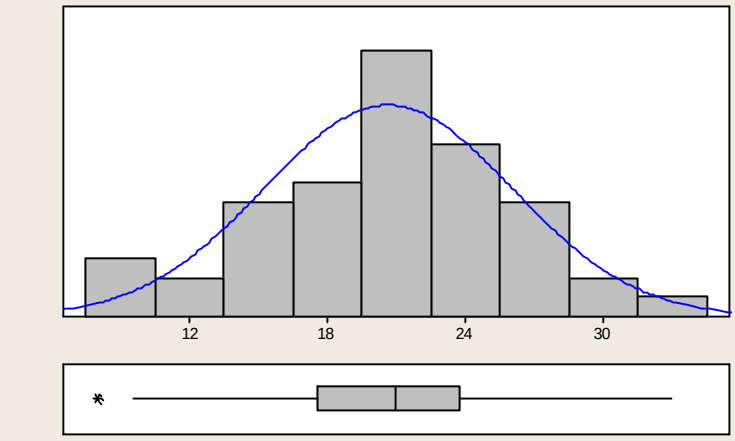

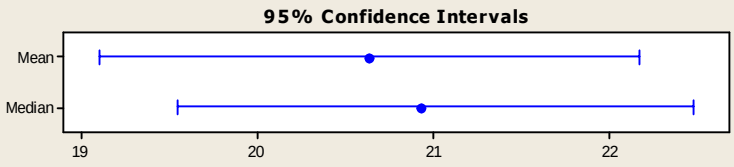

Anderson-Darling Normality Test	
A-Squared	0.27
P-Value	0.653

Mean	20.634
StDev	5.388
Variance	29.036
Skewness	-0.191018
Kurtosis	0.207232
N	50

Minimum	7.958
1st Quartile	17.570
Median	20.930
3rd Quartile	23.772
Maximum	32.941

95% Confidence Interval for Mean	
19.102	22.165
95% Confidence Interval for Median	
19.549	22.471
95% Confidence Interval for StDev	
4.501	6.715

Summary for U28° Dry Across Grain 0 mm

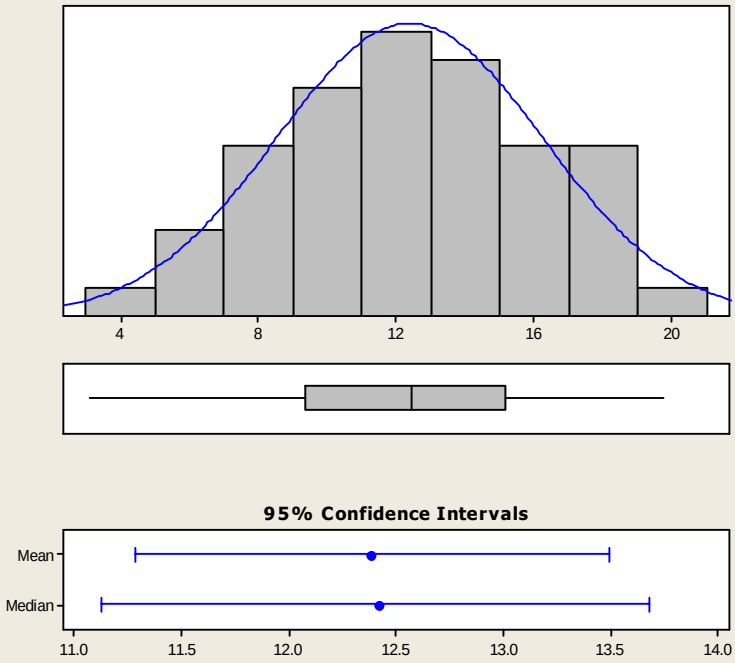

Anderson-Darling Normality Test	
A-Squared	0.15
P-Value	0.962
Mean	12.387
StDev	3.876
Variance	15.020
Skewness	-0.121116
Kurtosis	-0.522596
N	50
Minimum	3.079
1st Quartile	9.382
Median	12.423
3rd Quartile	15.167
Maximum	19.760
95% Confidence Interval for Mean	
11.285	13.488
95% Confidence Interval for Median	
11.122	13.675
95% Confidence Interval for StDev	
3.237	4.829

Summary for U28° Dry Across Grain 0.05 mm

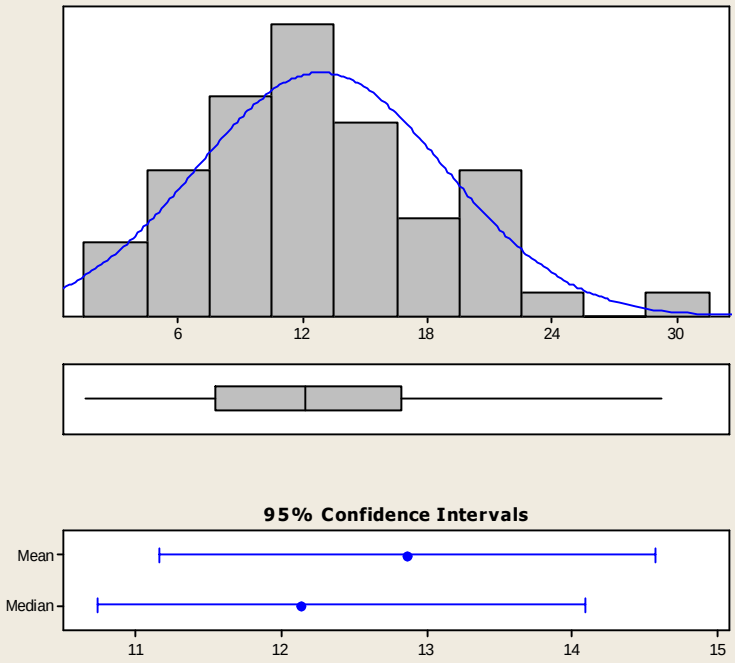

Anderson-Darling Normality Test	
A-Squared	0.36
P-Value	0.433
Mean	12.863
StDev	5.979
Variance	35.748
Skewness	0.489110
Kurtosis	0.060552
N	50
Minimum	1.570
1st Quartile	7.821
Median	12.134
3rd Quartile	16.736
Maximum	29.275
95% Confidence Interval for Mean	
11.164	14.563
95% Confidence Interval for Median	
10.730	14.086
95% Confidence Interval for StDev	
4.994	7.451

Summary for U28° Dry Across Grain 0.1 mm

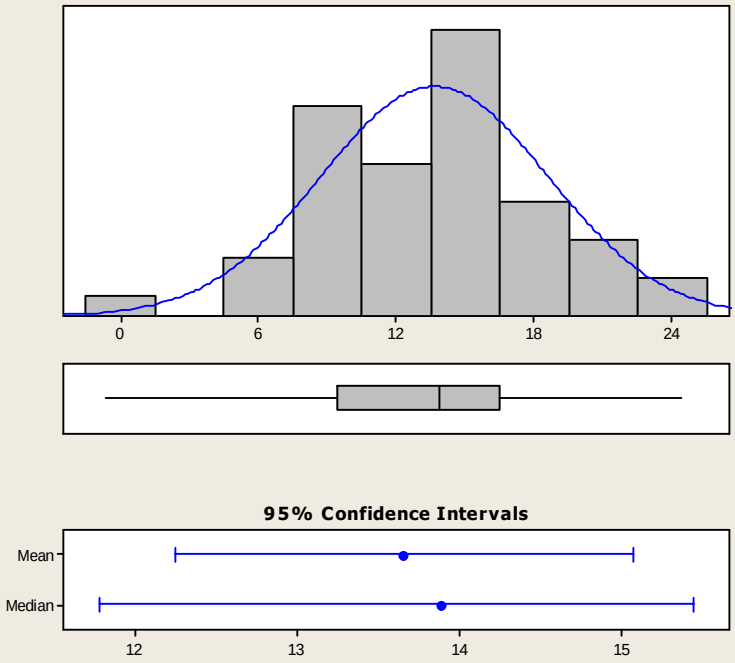

Anderson-Darling Normality Test	
A-Squared	0.28
P-Value	0.644
Mean	13.653
StDev	4.961
Variance	24.608
Skewness	-0.105990
Kurtosis	0.414029
N	50
Minimum	-0.694
1st Quartile	9.463
Median	13.891
3rd Quartile	16.442
Maximum	24.438
95% Confidence Interval for Mean	
12.243	15.063
95% Confidence Interval for Median	
11.779	15.439
95% Confidence Interval for StDev	
4.144	6.182

Summary for U28° Dry Across Grain 0.15 mm

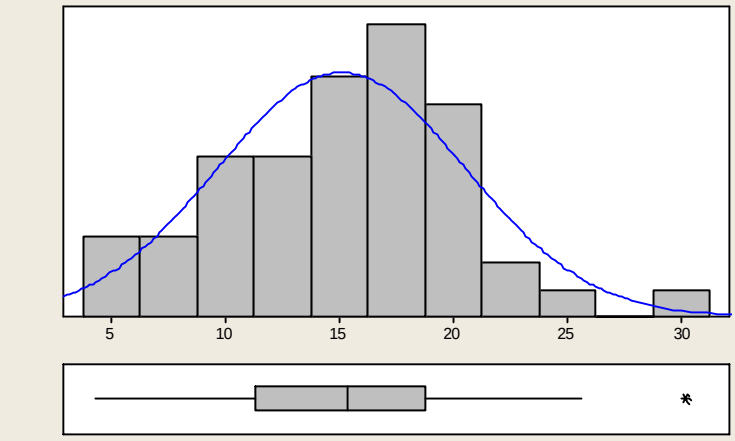

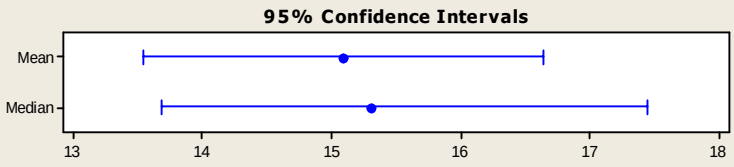

Anderson-Darling Normality Test	
A-Squared	0.28
P-Value	0.630
Mean	15.092
StDev	5.440
Variance	29.594
Skewness	0.121828
Kurtosis	0.181148
N	50
Minimum	4.277
1st Quartile	11.323
Median	15.312
3rd Quartile	18.801
Maximum	30.115
95% Confidence Interval for Mean	
13.546	16.638
95% Confidence Interval for Median	
13.679	17.439
95% Confidence Interval for StDev	
4.544	6.779

Summary for U28° Dry Across Grain 0.2 mm

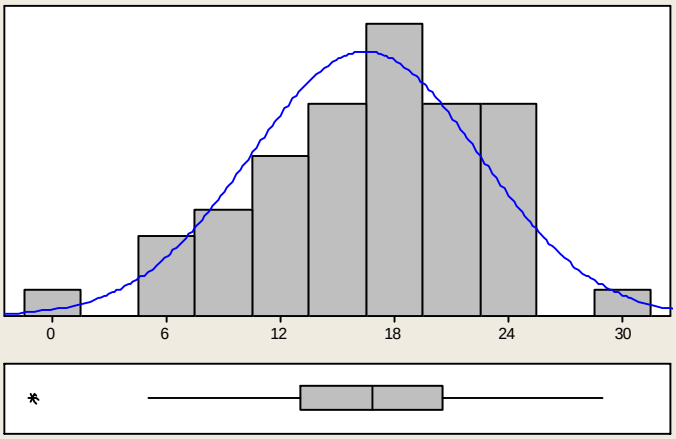

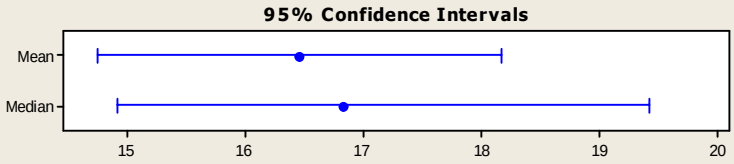

Anderson-Darling Normality Test	
A-Squared	0.31
P-Value	0.553
Mean	16.450
StDev	6.016
Variance	36.195
Skewness	-0.516011
Kurtosis	0.351236
N	50
Minimum	-1.056
1st Quartile	13.024
Median	16.832
3rd Quartile	20.570
Maximum	28.944
95% Confidence Interval for Mean	
14.741	18.160
95% Confidence Interval for Median	
14.915	19.413
95% Confidence Interval for StDev	
5.026	7.497

Summary for U28° Dry Across Grain 0.25 mm

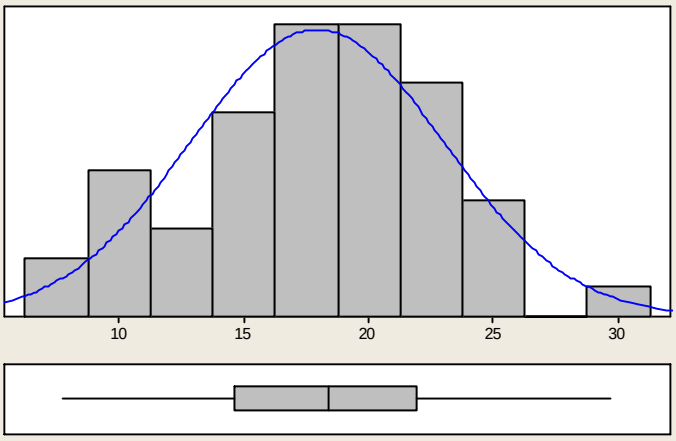

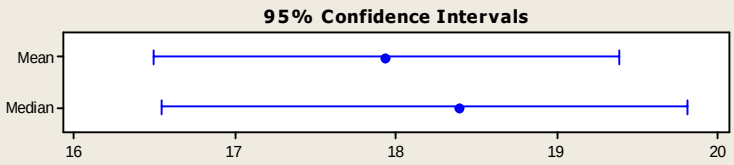

Anderson-Darling Normality Test	
A-Squared	0.25
P-Value	0.721
Mean	17.934
StDev	5.083
Variance	25.838
Skewness	-0.164338
Kurtosis	-0.451655
N	50
Minimum	7.769
1st Quartile	14.643
Median	18.396
3rd Quartile	21.922
Maximum	29.644
95% Confidence Interval for Mean	
16.489	19.379
95% Confidence Interval for Median	
16.539	19.803
95% Confidence Interval for StDev	
4.246	6.334

Summary for U28° Dry Across Grain 0.3 mm

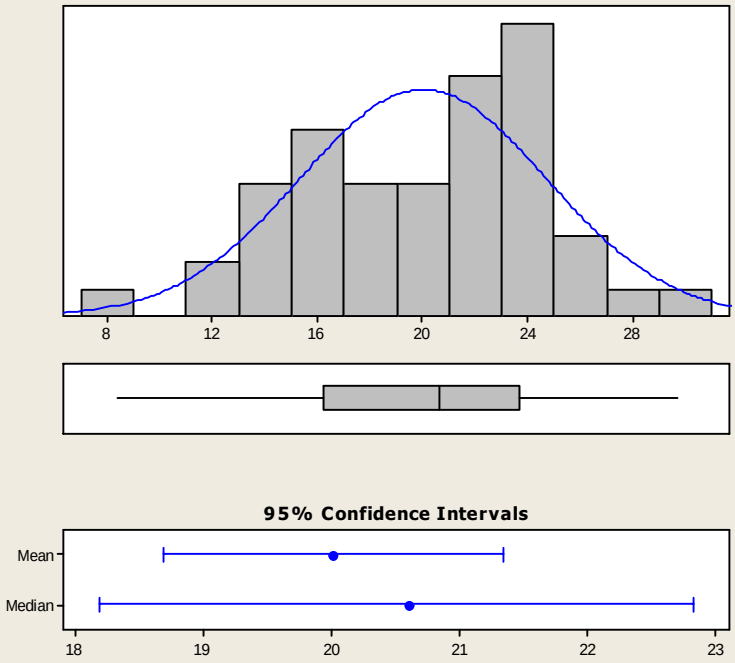

Anderson-Darling Normality Test	
A-Squared	0.52
P-Value	0.177
Mean	20.013
StDev	4.684
Variance	21.940
Skewness	-0.271802
Kurtosis	-0.530778
N	50
Minimum	8.414
1st Quartile	16.191
Median	20.609
3rd Quartile	23.707
Maximum	29.695
95% Confidence Interval for Mean	
18.682	21.344
95% Confidence Interval for Median	
18.186	22.824
95% Confidence Interval for StDev	
3.913	5.837

Summary for U28° Dry Across Grain 0.35 mm

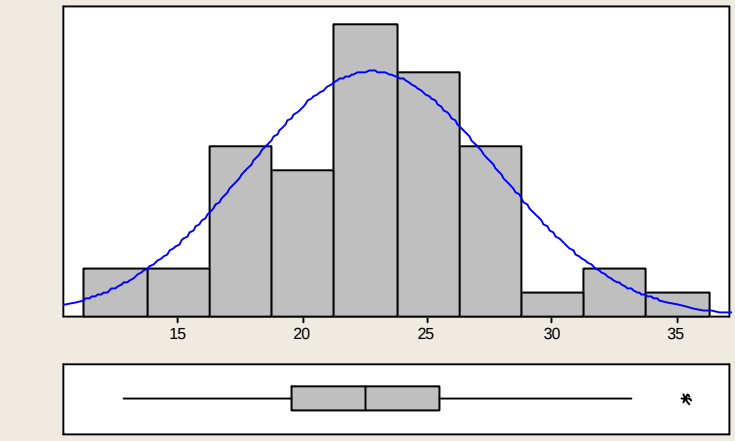

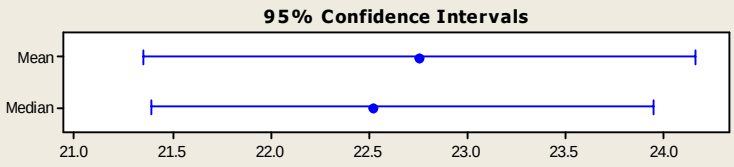

Anderson-Darling Normality Test	
A-Squared	0.30
P-Value	0.566
Mean	22.755
StDev	4.958
Variance	24.583
Skewness	0.261723
Kurtosis	0.102599
N	50
Minimum	12.825
1st Quartile	19.533
Median	22.522
3rd Quartile	25.476
Maximum	35.327
95% Confidence Interval for Mean	
21.346	24.164
95% Confidence Interval for Median	
21.390	23.949
95% Confidence Interval for StDev	
4.142	6.179

Summary for U28° Sat Along Grain 0 mm

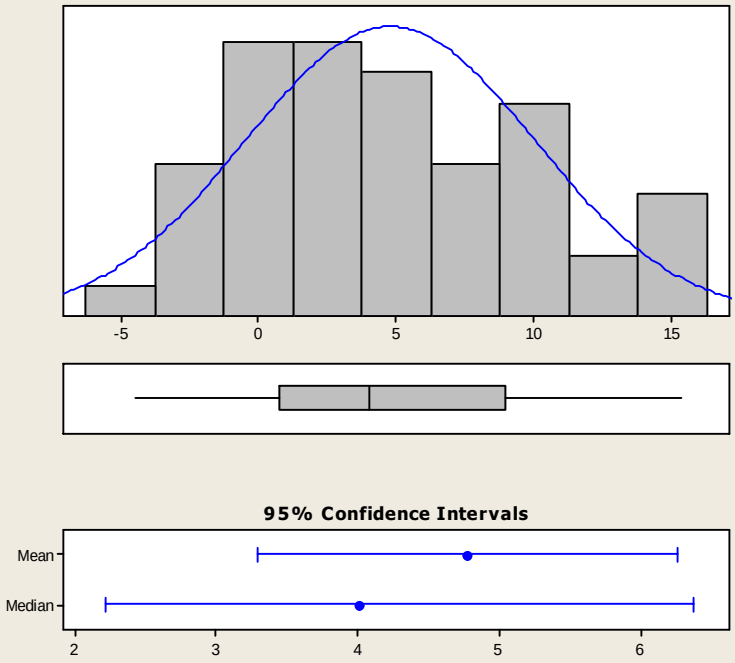

Summary for U28° Sat Along Grain 0.1 mm

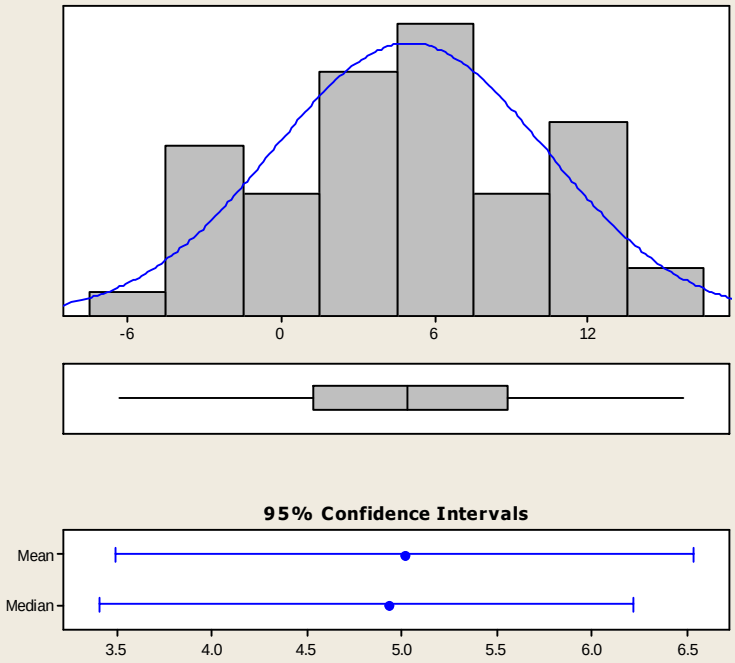

Anderson-Darling Normality Test	
A-Squared	0.36
P-Value	0.437
Mean	5.0122
StDev	5.3444
Variance	28.5629
Skewness	0.080143
Kurtosis	-0.633987
N	50
Minimum	-6.2866
1st Quartile	1.2725
Median	4.9304
3rd Quartile	8.8550
Maximum	15.7041
95% Confidence Interval for Mean	
3.4934	6.5311
95% Confidence Interval for Median	
3.4076	6.2163
95% Confidence Interval for StDev	
4.4644	6.6599

Summary for U28° Sat Along Grain 0.15 mm

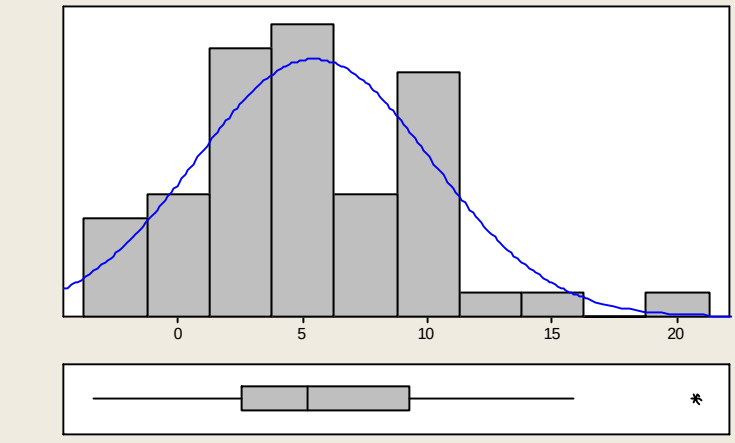

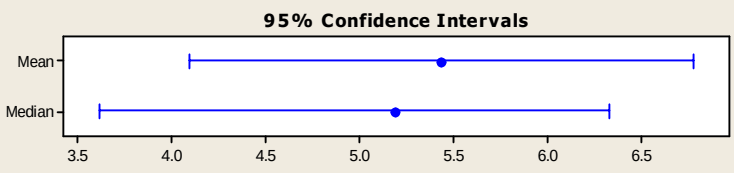

Anderson-Darling Normality Test	
A-Squared	0.36
P-Value	0.434
Mean	5.4341
StDev	4.7210
Variance	22.2883
Skewness	0.62174
Kurtosis	1.14605
N	50
Minimum	-3.3685
1st Quartile	2.5211
Median	5.1879
3rd Quartile	9.3018
Maximum	20.7300
95% Confidence Interval for Mean	
4.0924	6.7758
95% Confidence Interval for Median	
3.6117	6.3318
95% Confidence Interval for StDev	
3.9437	5.8831

Summary for U28° Sat Along Grain 0.2 mm

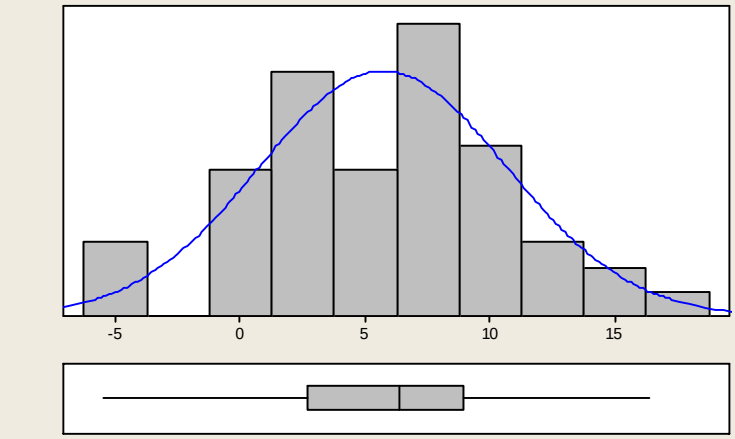

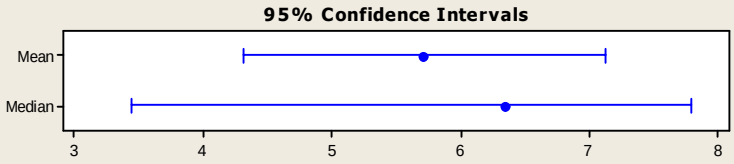

Anderson-Darling Normality Test	
A-Squared	0.20
P-Value	0.887
Mean	5.7140
StDev	4.9622
Variance	24.6235
Skewness	-0.127964
Kurtosis	-0.232608
N	50
Minimum	-5.4595
1st Quartile	2.7074
Median	6.3529
3rd Quartile	8.9136
Maximum	16.3597
95% Confidence Interval for Mean	
4.3038	7.1243
95% Confidence Interval for Median	
3.4435	7.7952
95% Confidence Interval for StDev	
4.1451	6.1836

Summary for U28° Sat Along Grain 0.25 mm

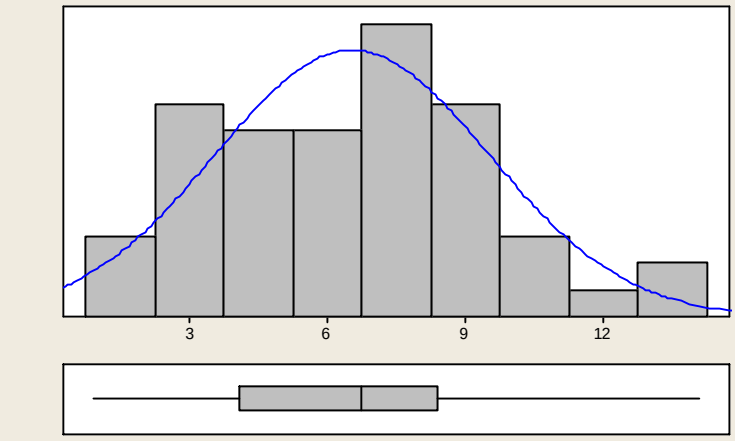

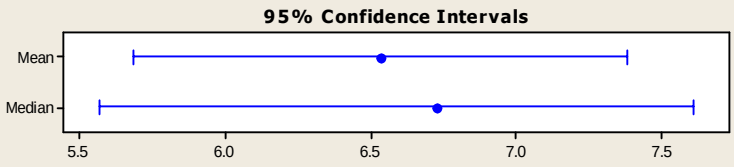

Anderson-Darling Normality Test	
A-Squared	0.22
P-Value	0.830
Mean	6.5328
StDev	2.9880
Variance	8.9284
Skewness	0.287712
Kurtosis	-0.145254
N	50
Minimum	0.9237
1st Quartile	4.0968
Median	6.7271
3rd Quartile	8.3980
Maximum	14.0863
95% Confidence Interval for Mean	
5.6836	7.3820
95% Confidence Interval for Median	
5.5682	7.6071
95% Confidence Interval for StDev	
2.4960	3.7235

Summary for U28° Sat Along Grain 0.3 mm

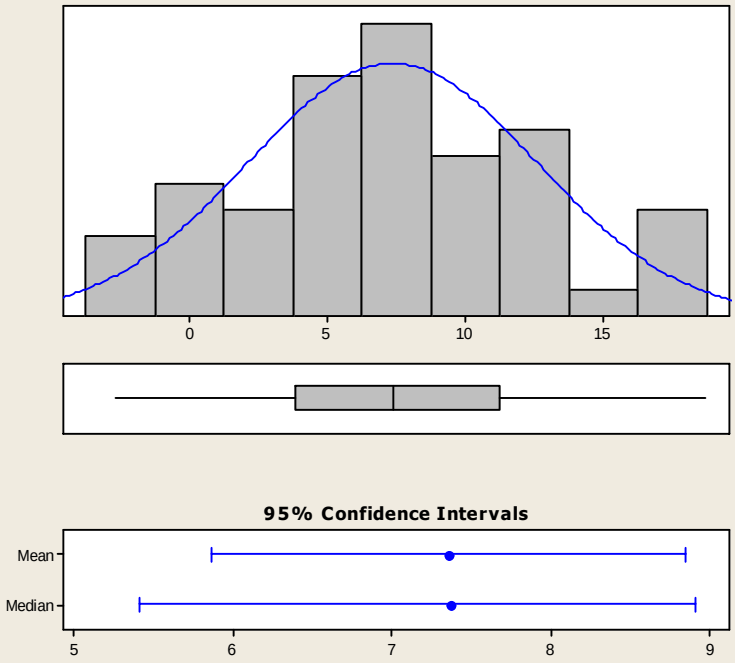

Summary for U28° Sat Across Grain 0 mm

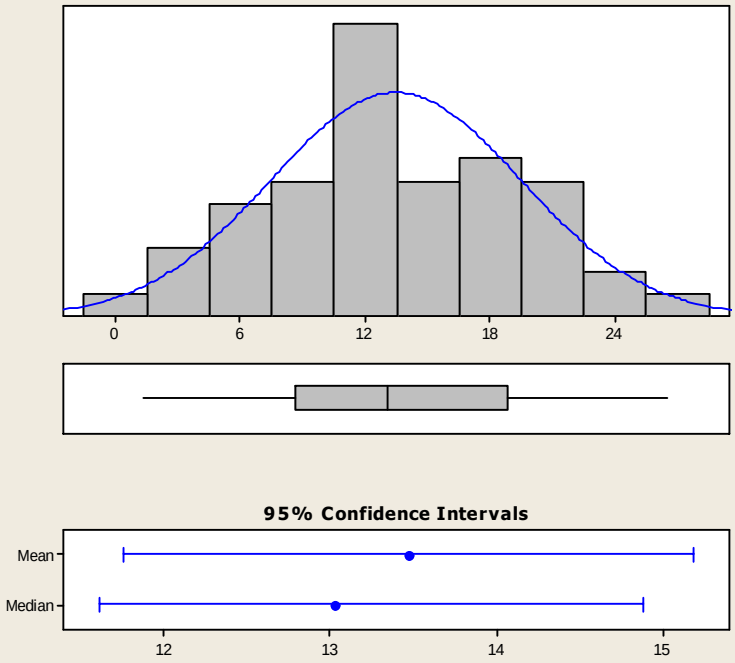

Anderson-Darling Normality Test	
A-Squared	0.30
P-Value	0.580
Mean	13.471
StDev	6.022
Variance	36.267
Skewness	0.016540
Kurtosis	-0.597600
N	50
Minimum	1.323
1st Quartile	8.673
Median	13.031
3rd Quartile	18.791
Maximum	26.486
95% Confidence Interval for Mean	
11.759	15.182
95% Confidence Interval for Median	
11.608	14.884
95% Confidence Interval for StDev	
5.031	7.505

Summary for U28° Sat Across Grain 0.05 mm

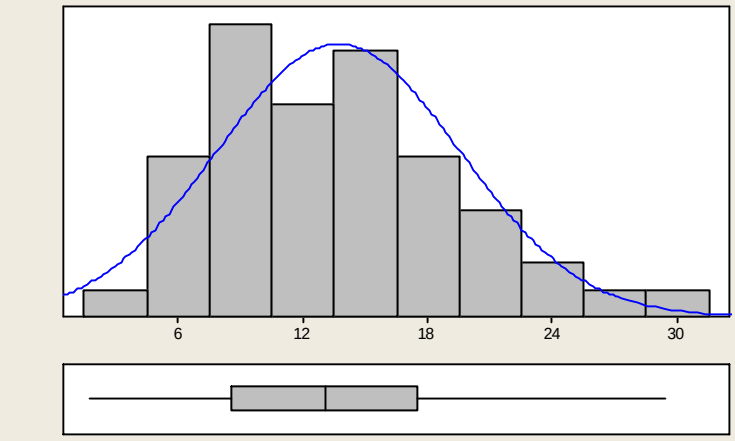

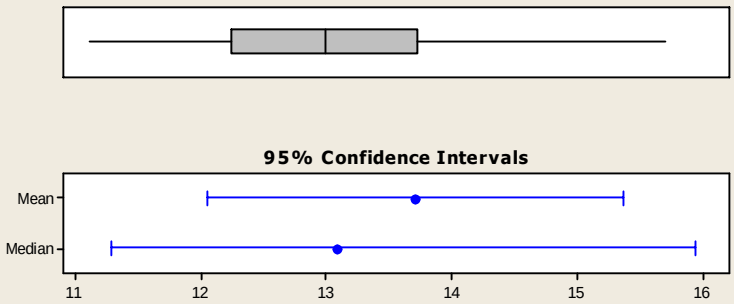

Anderson-Darling Normality Test	
A-Squared	0.44
P-Value	0.275
Mean	13.711
StDev	5.841
Variance	34.119
Skewness	0.412606
Kurtosis	-0.062144
N	50
Minimum	1.702
1st Quartile	8.600
Median	13.089
3rd Quartile	17.462
Maximum	29.444
95% Confidence Interval for Mean	
12.051	15.371
95% Confidence Interval for Median	
11.288	15.930
95% Confidence Interval for StDev	
4.879	7.279

Summary for U28° Sat Across Grain 0.1 mm

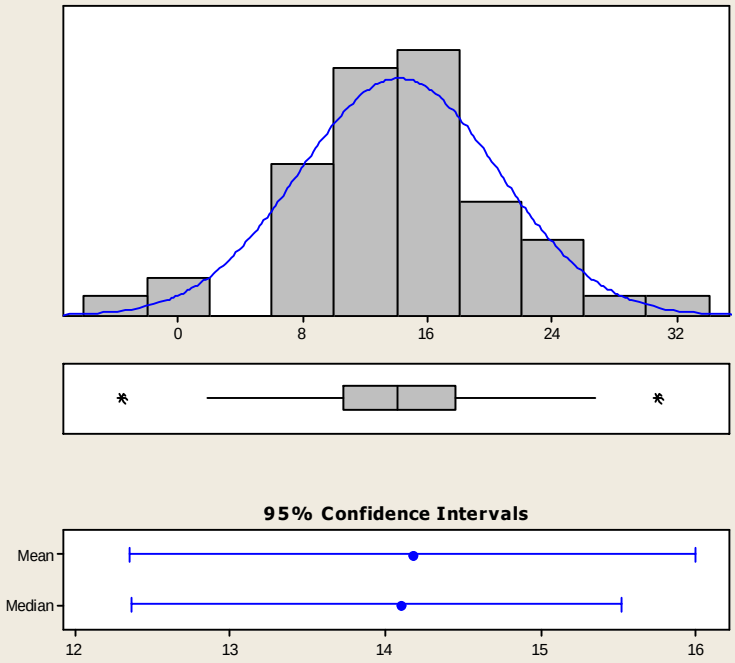

Anderson-Darling Normality Test	
A-Squared	0.42
P-Value	0.311
Mean	14.173
StDev	6.401
Variance	40.977
Skewness	0.007721
Kurtosis	0.939536
N	50
Minimum	-3.583
1st Quartile	10.606
Median	14.106
3rd Quartile	17.806
Maximum	30.665
95% Confidence Interval for Mean	
12.354	15.992
95% Confidence Interval for Median	
12.371	15.512
95% Confidence Interval for StDev	
5.347	7.977

Summary for U28° Sat Across Grain 0.15 mm

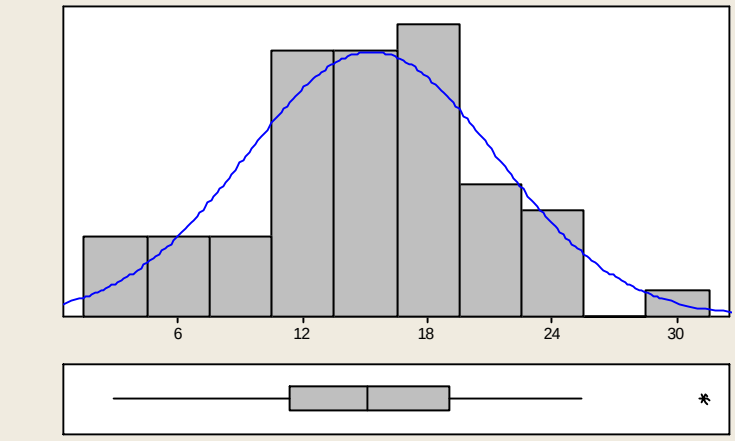

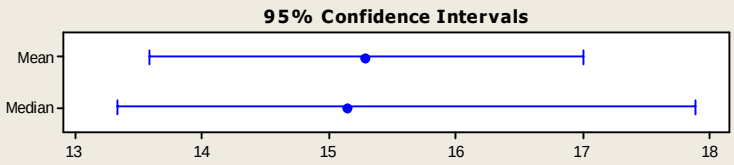

Anderson-Darling Normality Test	
A-Squared	0.19
P-Value	0.888
Mean	15.290
StDev	6.011
Variance	36.130
Skewness	0.009450
Kurtosis	0.135884
N	50
Minimum	2.869
1st Quartile	11.337
Median	15.142
3rd Quartile	19.029
Maximum	31.207
95% Confidence Interval for Mean	
13.581	16.998
95% Confidence Interval for Median	
13.333	17.879
95% Confidence Interval for StDev	
5.021	7.490

Summary for U28° Sat Across Grain 0.2 mm

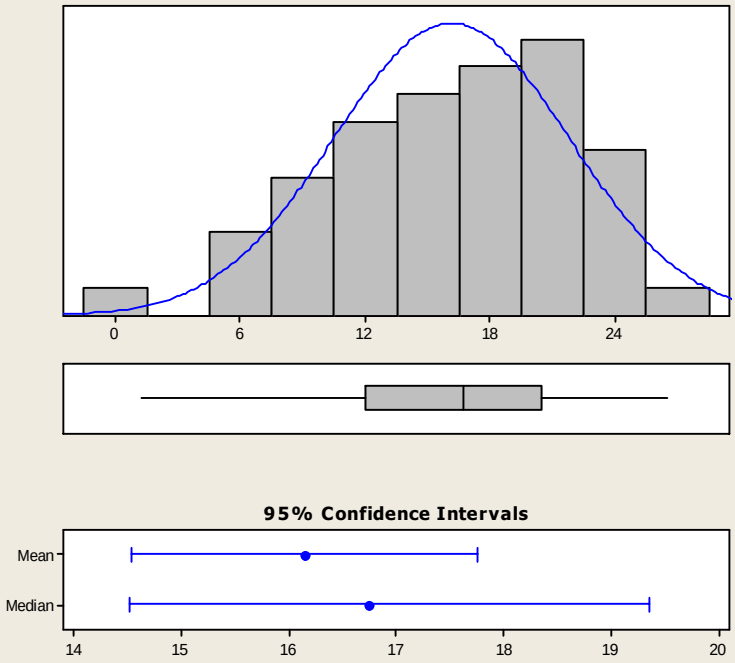

Anderson-Darling Normality Test	
A-Squared	0.44
P-Value	0.289
Mean	16.146
StDev	5.664
Variance	32.078
Skewness	-0.410432
Kurtosis	-0.422391
N	50
Minimum	1.279
1st Quartile	12.035
Median	16.740
3rd Quartile	20.452
Maximum	26.489
95% Confidence Interval for Mean	
14.536	17.756
95% Confidence Interval for Median	
14.520	19.356
95% Confidence Interval for StDev	
4.731	7.058

Summary for U28° Sat Across Grain 0.25 mm

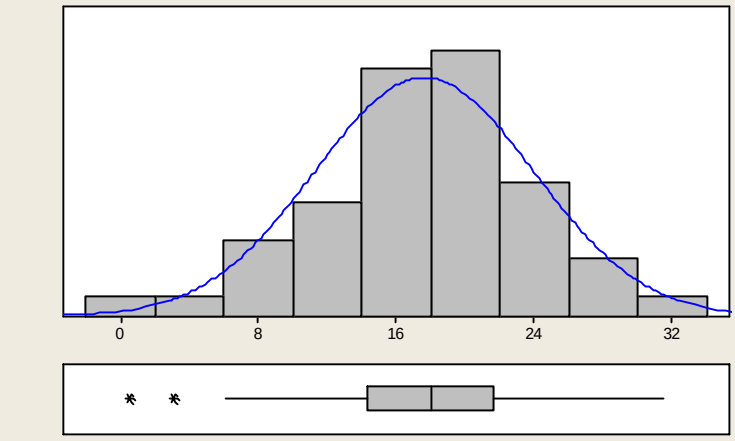

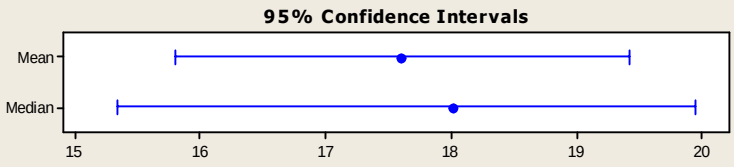

Anderson-Darling Normality Test	
A-Squared	0.33
P-Value	0.504
Mean	17.607
StDev	6.365
Variance	40.511
Skewness	-0.377976
Kurtosis	0.534263
N	50
Minimum	0.501
1st Quartile	14.347
Median	18.011
3rd Quartile	21.603
Maximum	31.497
95% Confidence Interval for Mean	
15.798	19.416
95% Confidence Interval for Median	
15.343	19.938
95% Confidence Interval for StDev	
5.317	7.931

Summary for U28° Sat Across Grain 0.3 mm

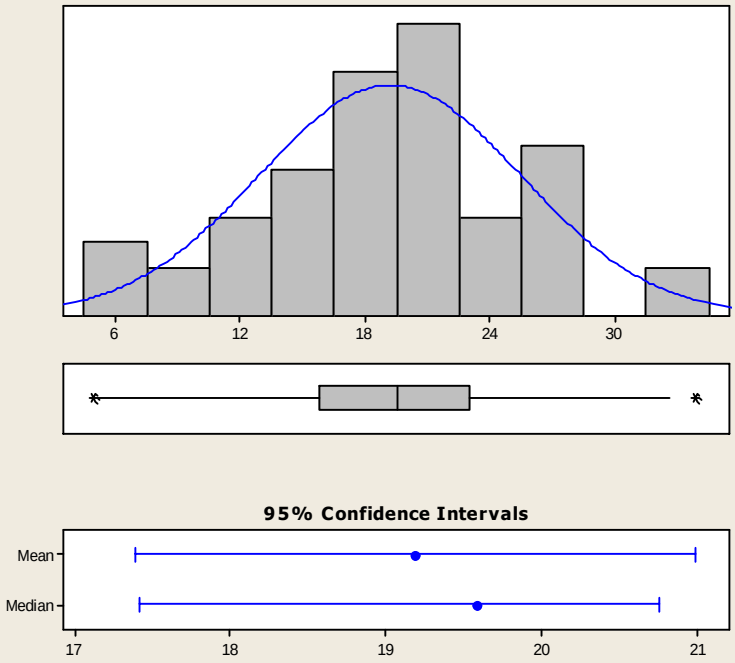

Anderson-Darling Normality Test	
A-Squared	0.33
P-Value	0.503
Mean	19.189
StDev	6.321
Variance	39.959
Skewness	-0.164191
Kurtosis	0.312424
N	50
Minimum	4.960
1st Quartile	15.824
Median	19.590
3rd Quartile	22.989
Maximum	33.853
95% Confidence Interval for Mean	
17.393	20.986
95% Confidence Interval for Median	
17.420	20.747
95% Confidence Interval for StDev	
5.280	7.877

Summary for U28° Sat Across Grain 0.35 mm

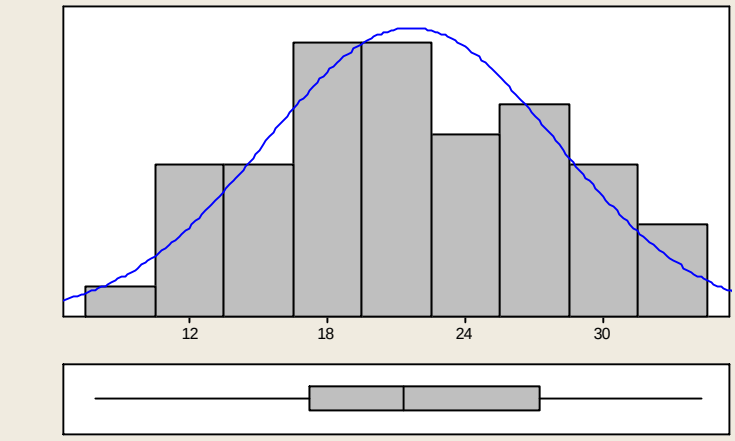

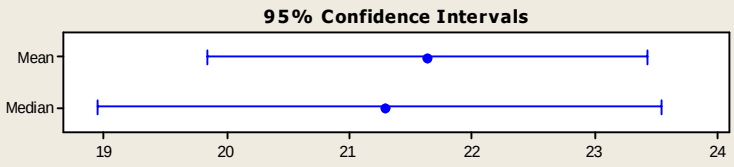

Anderson-Darling Normality Test	
A-Squared	0.24
P-Value	0.754
Mean	21.638
StDev	6.304
Variance	39.738
Skewness	0.035368
Kurtosis	-0.680035
N	50
Minimum	7.896
1st Quartile	17.237
Median	21.287
3rd Quartile	27.217
Maximum	34.320
95% Confidence Interval for Mean	
19.846	23.429
95% Confidence Interval for Median	
18.946	23.542
95% Confidence Interval for StDev	
5.266	7.855

Summary for GT Dry Along Grain 0 mm

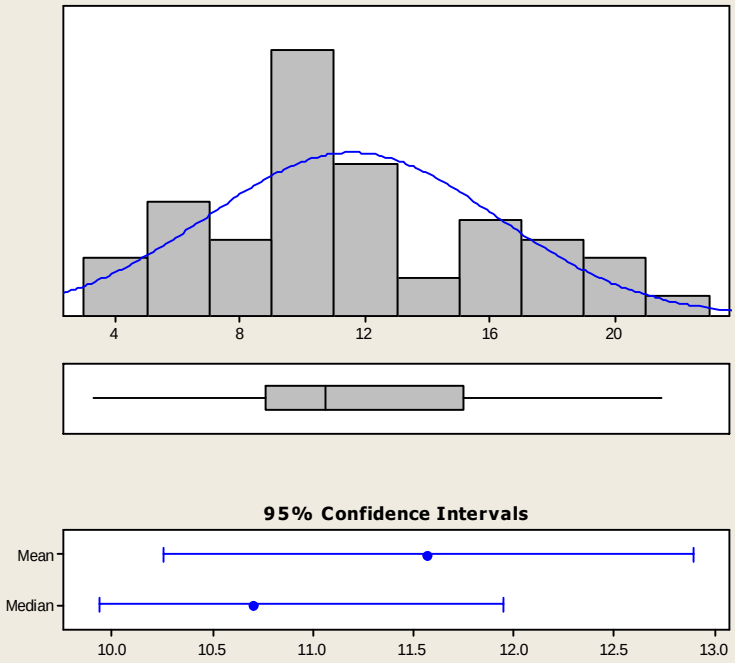

Anderson-Darling Normality Test	
A-Squared	0.60
P-Value	0.110
Mean	11.572
StDev	4.654
Variance	21.656
Skewness	0.342900
Kurtosis	-0.508072
N	50
Minimum	3.266
1st Quartile	8.832
Median	10.701
3rd Quartile	15.139
Maximum	21.503
95% Confidence Interval for Mean	
10.249	12.895
95% Confidence Interval for Median	
9.933	11.950
95% Confidence Interval for StDev	
3.887	5.799

Summary for GT Dry Along Grain 0.05 mm

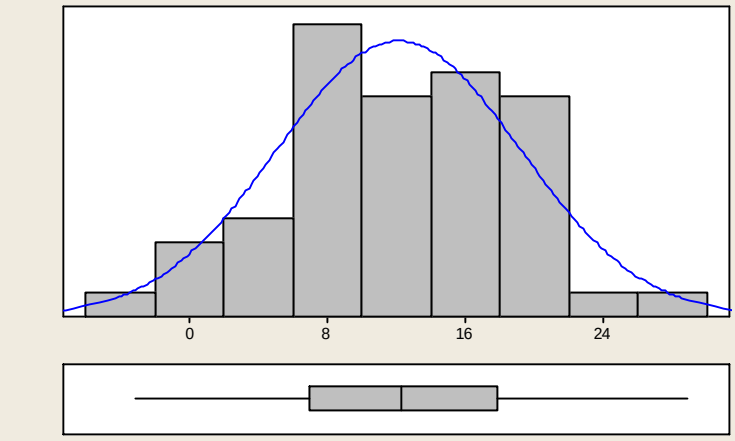

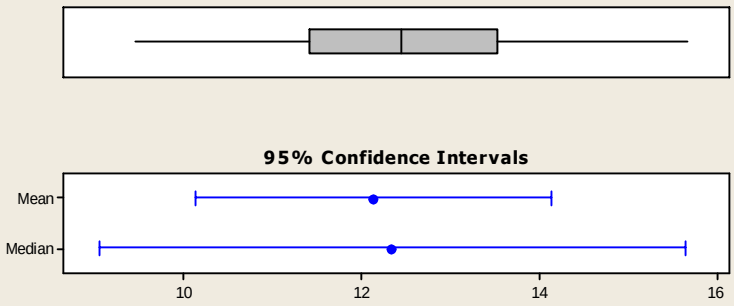

Anderson-Darling Normality Test	
A-Squared	0.27
P-Value	0.650
Mean	12.131
StDev	7.060
Variance	49.845
Skewness	-0.121637
Kurtosis	-0.350622
N	50
Minimum	-3.097
1st Quartile	6.905
Median	12.334
3rd Quartile	17.850
Maximum	28.850
95% Confidence Interval for Mean	
10.125	14.138
95% Confidence Interval for Median	
9.041	15.638
95% Confidence Interval for StDev	
5.898	8.798

Summary for GT Dry Along Grain 0.1 mm

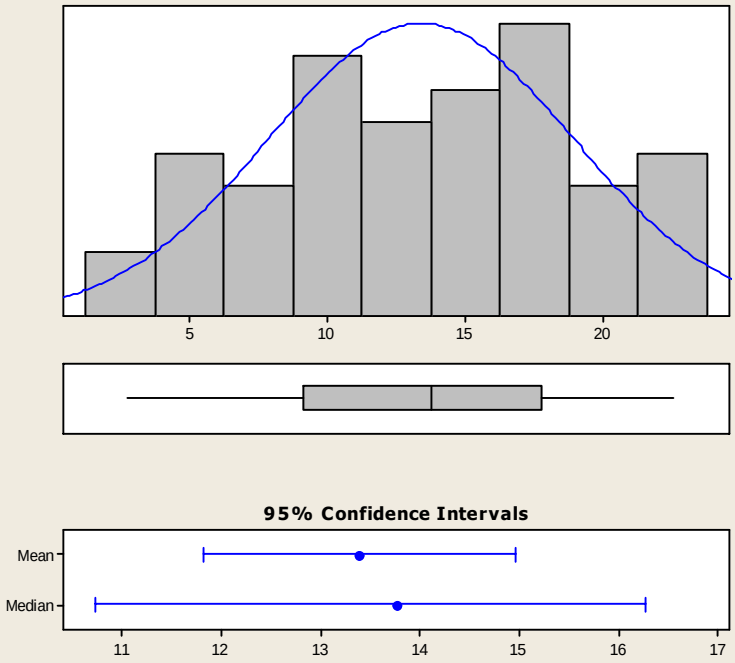

Anderson-Darling Normality Test	
A-Squared	0.71
P-Value	0.060
Mean	13.391
StDev	5.528
Variance	30.562
Skewness	-0.18761
Kurtosis	-1.07386
N	50
Minimum	2.718
1st Quartile	9.093
Median	13.770
3rd Quartile	17.748
Maximum	22.523
95% Confidence Interval for Mean	
11.819	14.962
95% Confidence Interval for Median	
10.743	16.264
95% Confidence Interval for StDev	
4.618	6.889

Summary for GT Dry Along Grain 0.15 mm

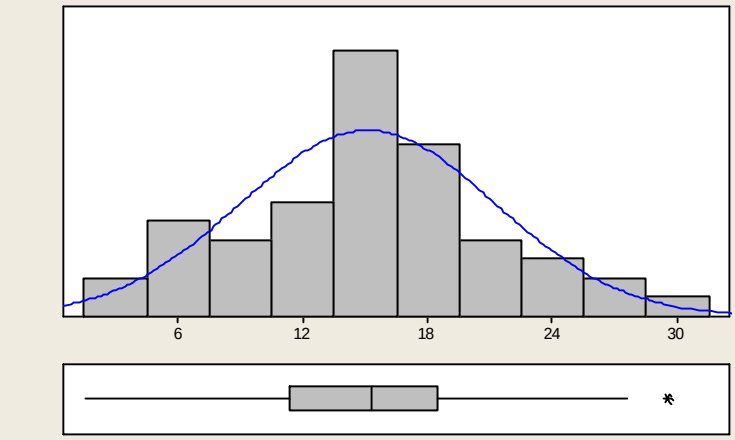

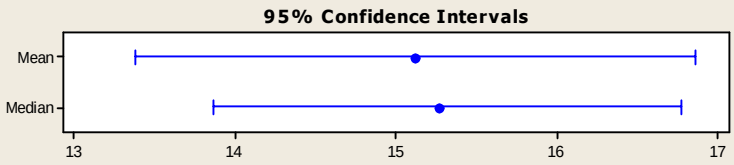

Anderson-Darling Normality Test	
A-Squared	0.33
P-Value	0.504
Mean	15.119
StDev	6.126
Variance	37.528
Skewness	0.0866621
Kurtosis	0.0746316
N	50
Minimum	1.604
1st Quartile	11.359
Median	15.272
3rd Quartile	18.454
Maximum	29.548
95% Confidence Interval for Mean	
13.378	16.860
95% Confidence Interval for Median	
13.862	16.768
95% Confidence Interval for StDev	
5.117	7.634

Summary for GT Dry Along Grain 0.2mm

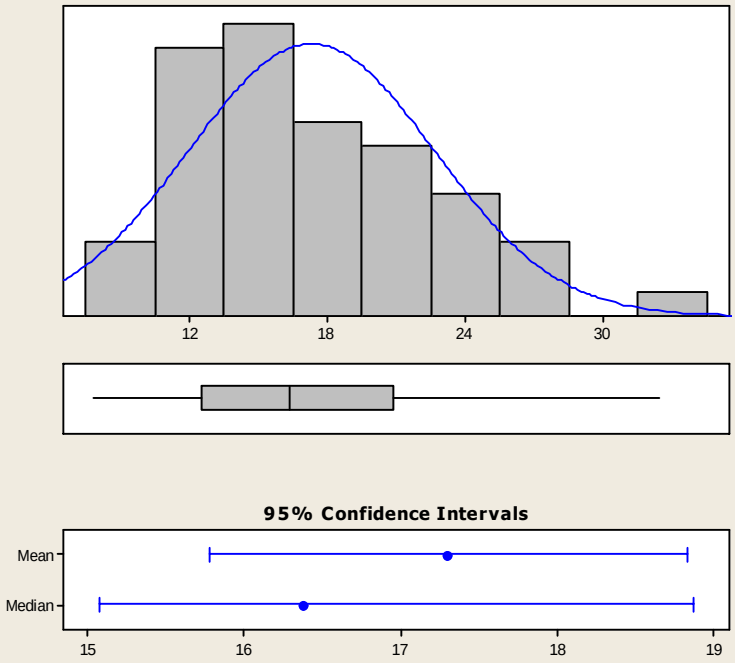

Anderson-Darling Normality Test	
A-Squared	0.43
P-Value	0.291
Mean	17.299
StDev	5.363
Variance	28.765
Skewness	0.591459
Kurtosis	0.042870
N	50
Minimum	7.841
1st Quartile	12.548
Median	16.381
3rd Quartile	20.866
Maximum	32.453
95% Confidence Interval for Mean	
15.775	18.824
95% Confidence Interval for Median	
15.071	18.867
95% Confidence Interval for StDev	
4.480	6.683

Summary for GT Dry Along Grain 0.25 mm

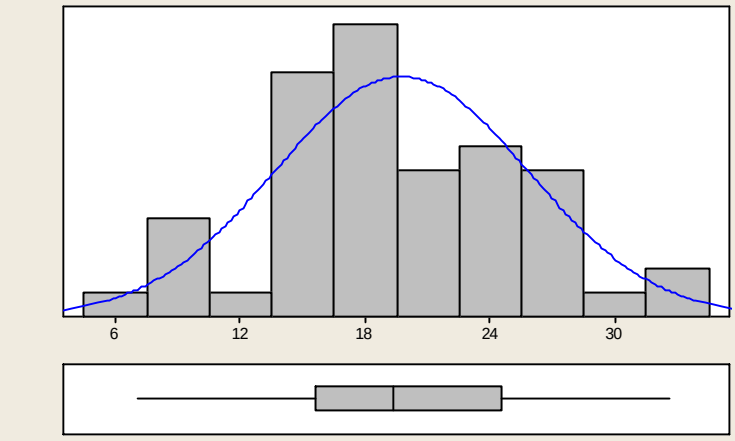

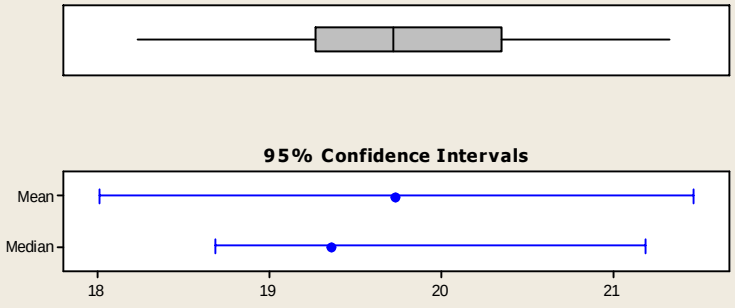

Anderson-Darling Normality Test	
A-Squared	0.29
P-Value	0.609
Mean	19.741
StDev	6.080
Variance	36.971
Skewness	0.033445
Kurtosis	-0.226834
N	50
Minimum	7.039
1st Quartile	15.617
Median	19.368
3rd Quartile	24.547
Maximum	32.614
95% Confidence Interval for Mean	
18.013	21.469
95% Confidence Interval for Median	
18.695	21.187
95% Confidence Interval for StDev	
5.079	7.577

Summary for GT Dry Along Grain 0.3 mm

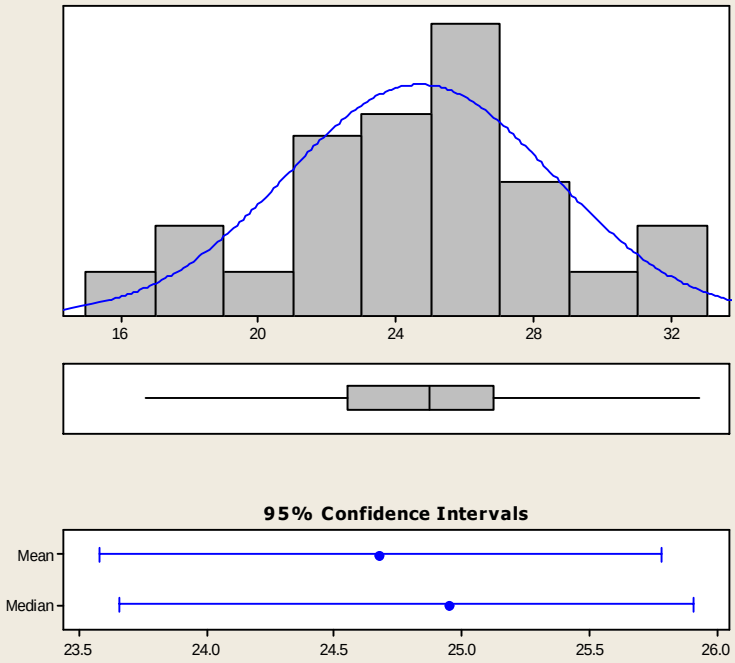

Anderson-Darling Normality Test	
A-Squared	0.25
P-Value	0.727
Mean	24.680
StDev	3.877
Variance	15.030
Skewness	-0.048077
Kurtosis	-0.225258
N	50
Minimum	16.698
1st Quartile	22.564
Median	24.949
3rd Quartile	26.796
Maximum	32.777
95% Confidence Interval for Mean	
23.578	25.781
95% Confidence Interval for Median	
23.656	25.903
95% Confidence Interval for StDev	
3.238	4.831

Summary for GT Dry Along Grain 0.35 mm

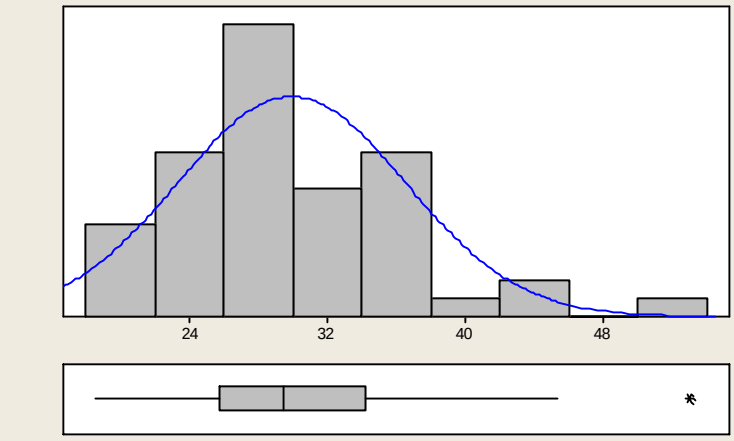

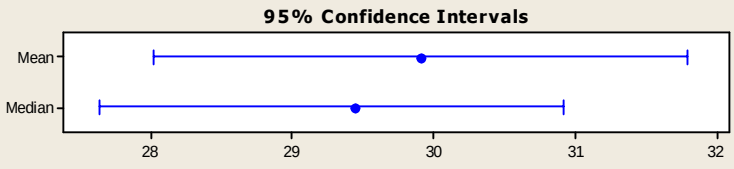

Anderson-Darling Normality Test	
A-Squared	0.62
P-Value	0.102
Mean	29.908
StDev	6.632
Variance	43.982
Skewness	1.03666
Kurtosis	2.14126
N	50
Minimum	18.547
1st Quartile	25.764
Median	29.438
3rd Quartile	34.144
Maximum	53.050
95% Confidence Interval for Mean	
28.023	31.793
95% Confidence Interval for Median	
27.631	30.907
95% Confidence Interval for StDev	
5.540	8.264

Summary for GT Dry Across Grain 0 mm

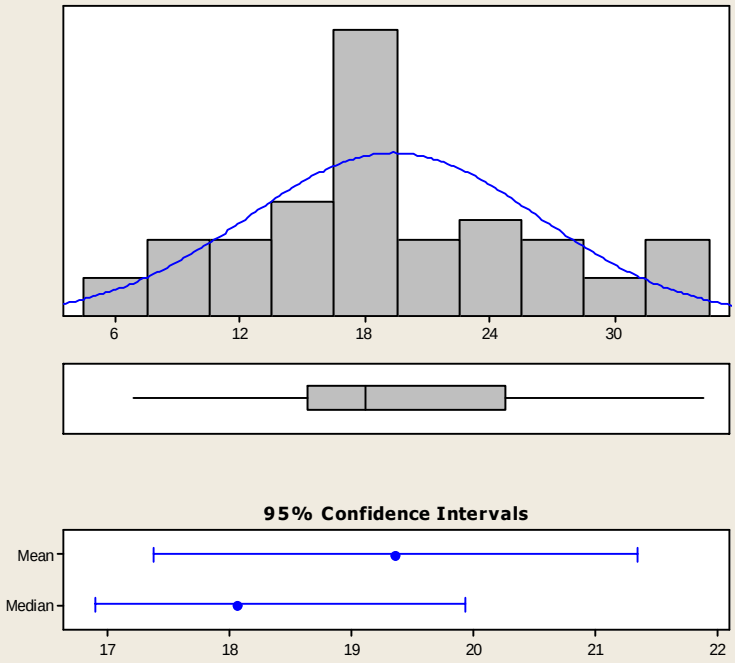

Anderson-Darling Normality Test	
A-Squared	0.60
P-Value	0.110
Mean	19.358
StDev	6.980
Variance	48.727
Skewness	0.342900
Kurtosis	-0.508072
N	50
Minimum	6.898
1st Quartile	15.248
Median	18.051
3rd Quartile	24.708
Maximum	34.254
95% Confidence Interval for Mean	
17.374	21.342
95% Confidence Interval for Median	
16.900	19.924
95% Confidence Interval for StDev	
5.831	8.699

Summary for GT Dry Across Grain 0.05 mm

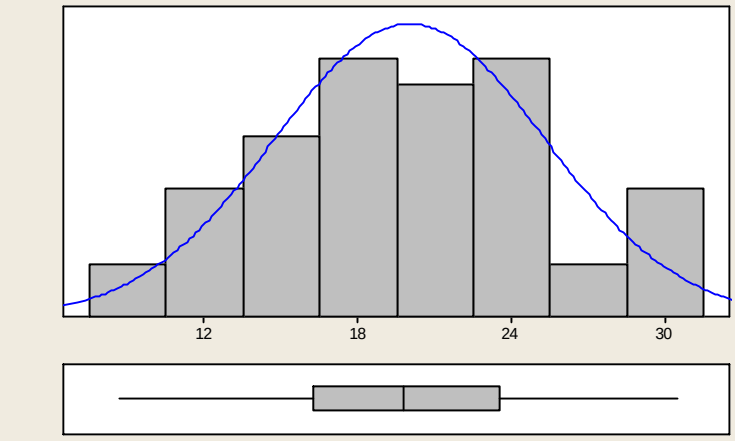

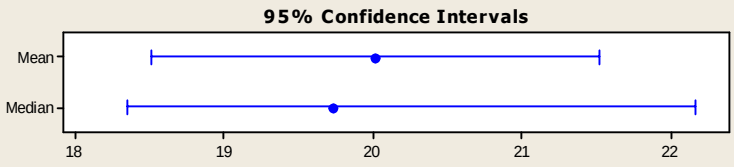

Anderson-Darling Normality Test	
A-Squared	0.15
P-Value	0.956
Mean	20.016
StDev	5.274
Variance	27.816
Skewness	-0.051330
Kurtosis	-0.312734
N	50
Minimum	8.688
1st Quartile	16.296
Median	19.735
3rd Quartile	23.485
Maximum	30.489
95% Confidence Interval for Mean	
18.517	21.515
95% Confidence Interval for Median	
18.352	22.162
95% Confidence Interval for StDev	
4.406	6.572

Summary for GT Dry Across Grain 0.1 mm

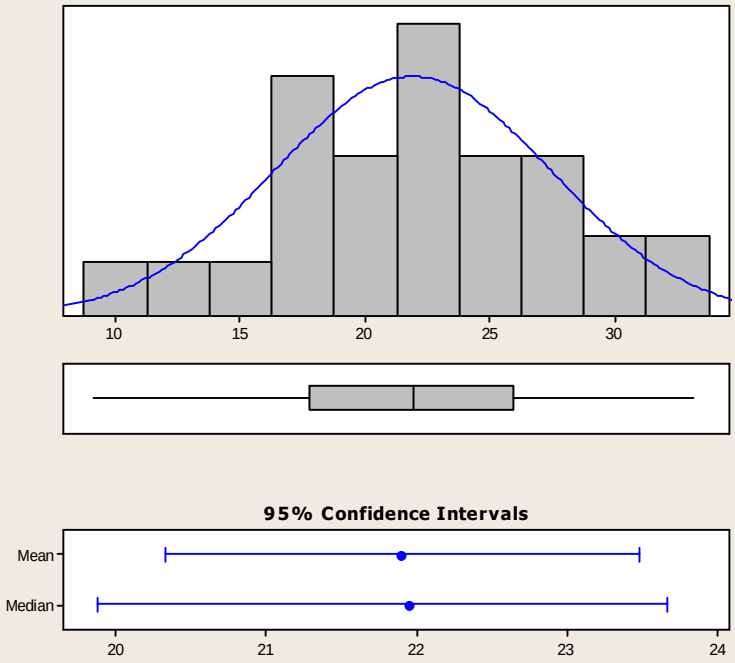

Anderson-Darling Normality Test	
A-Squared	0.15
P-Value	0.956
Mean	21.900
StDev	5.538
Variance	30.668
Skewness	-0.085373
Kurtosis	-0.180009
N	50
Minimum	9.141
1st Quartile	17.736
Median	21.950
3rd Quartile	25.959
Maximum	33.120
95% Confidence Interval for Mean	
20.326	23.474
95% Confidence Interval for Median	
19.877	23.670
95% Confidence Interval for StDev	
4.626	6.901

Summary for GT Dry Across Grain 0.15 mm

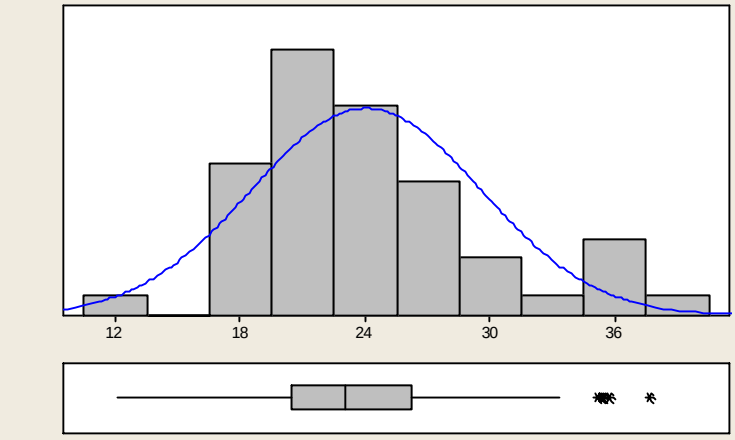

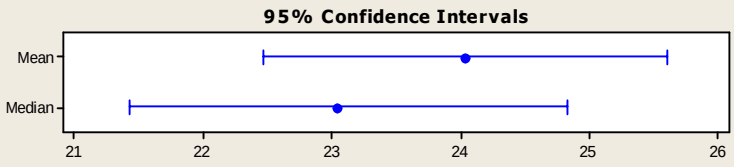

Anderson-Darling Normality Test	
A-Squared	1.17
P-Value <	0.005
Mean	24.037
StDev	5.500
Variance	30.254
Skewness	0.753414
Kurtosis	0.453090
N	50
Minimum	12.056
1st Quartile	20.436
Median	23.045
3rd Quartile	26.257
Maximum	37.676
95% Confidence Interval for Mean	
22.474	25.600
95% Confidence Interval for Median	
21.428	24.828
95% Confidence Interval for StDev	
4.595	6.854

Summary for GT Dry Across Grain 0.2 mm

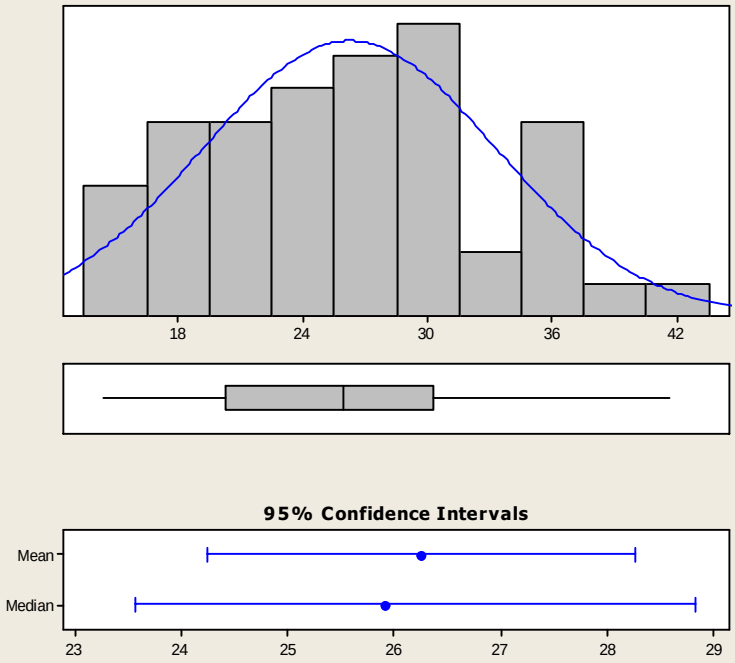

Summary for GT Dry Across Grain 0.3 mm

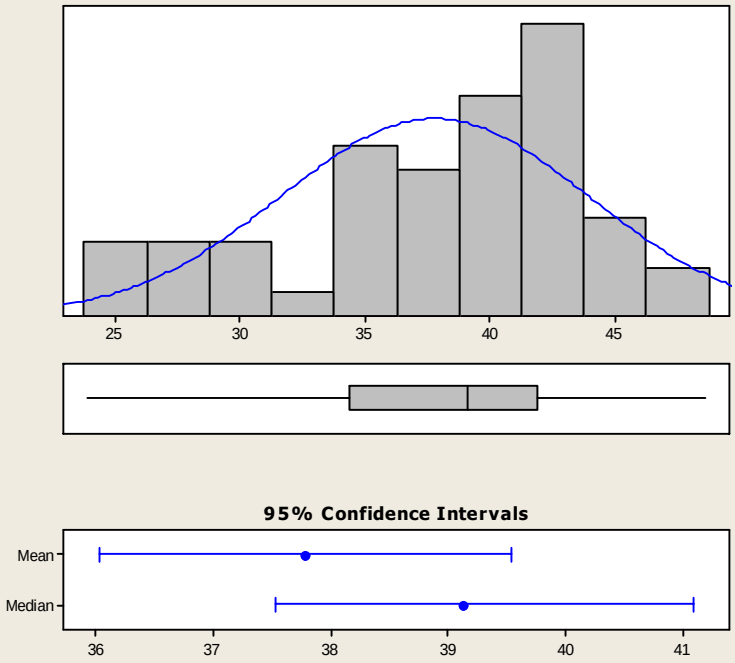

Anderson-Darling Normality Test	
A-Squared	0.98
P-Value	0.012
Mean	37.779
StDev	6.158
Variance	37.926
Skewness	-0.690742
Kurtosis	-0.212920
N	50
Minimum	23.874
1st Quartile	34.333
Median	39.128
3rd Quartile	41.926
Maximum	48.658
95% Confidence Interval for Mean	
36.029	39.529
95% Confidence Interval for Median	
37.536	41.087
95% Confidence Interval for StDev	
5.144	7.674

Summary for GT Dry Across Grain 0.35 mm

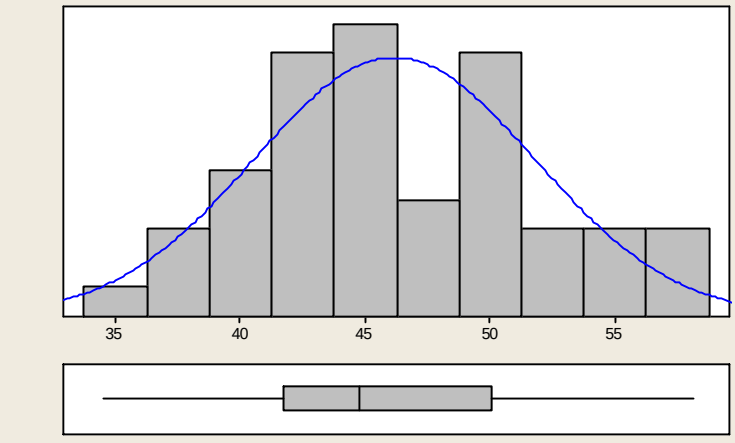

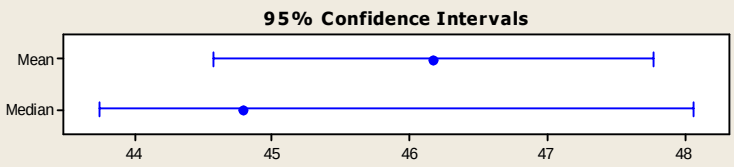

Anderson-Darling Normality Test	
A-Squared	0.40
P-Value	0.349
Mean	46.165
StDev	5.632
Variance	31.725
Skewness	0.271119
Kurtosis	-0.495668
N	50
Minimum	34.524
1st Quartile	41.752
Median	44.792
3rd Quartile	50.024
Maximum	58.137
95% Confidence Interval for Mean	
44.564	47.765
95% Confidence Interval for Median	
43.738	48.062
95% Confidence Interval for StDev	
4.705	7.019

Summary for GT Sat Along Grain 0 mm

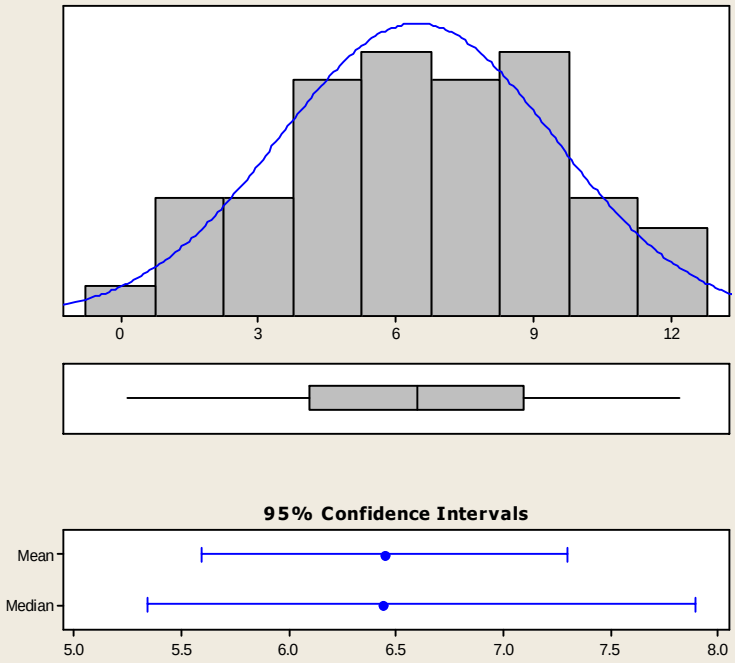

Anderson-Darling Normality Test	
A-Squared	0.24
P-Value	0.779
Mean	6.4464
StDev	3.0068
Variance	9.0409
Skewness	-0.069479
Kurtosis	-0.729310
N	50
Minimum	0.1385
1st Quartile	4.0865
Median	6.4406
3rd Quartile	8.7772
Maximum	12.1543
95% Confidence Interval for Mean	
5.5918	7.3009
95% Confidence Interval for Median	
5.3363	7.8903
95% Confidence Interval for StDev	
2.5117	3.7469

Summary for GT Sat Along Grain 0.05 mm

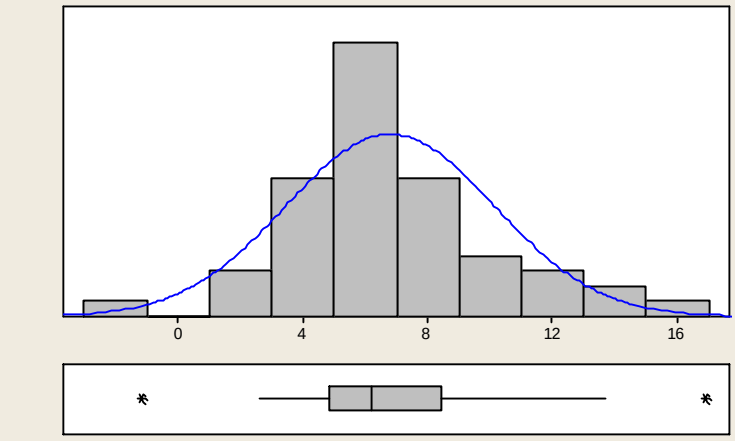

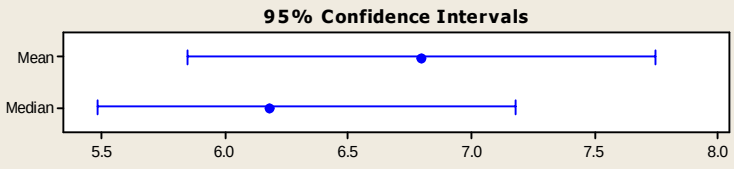

Anderson-Darling Normality Test	
A-Squared	0.79
P-Value	0.038
Mean	6.7945
StDev	3.3336
Variance	11.1127
Skewness	0.71339
Kurtosis	1.11867
N	50
Minimum	-1.1604
1st Quartile	4.8335
Median	6.1777
3rd Quartile	8.4217
Maximum	16.9032
95% Confidence Interval for Mean	
5.8471	7.7419
95% Confidence Interval for Median	
5.4780	7.1735
95% Confidence Interval for StDev	
2.7846	4.1541

Summary for GT Sat Along Grain 0.1 mm

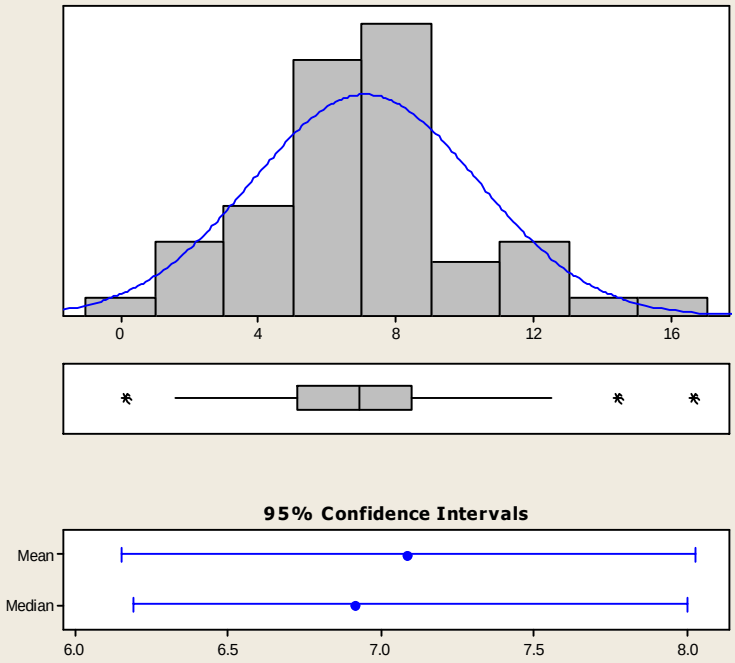

Anderson-Darling Normality Test	
A-Squared	0.47
P-Value	0.231
Mean	7.0867
StDev	3.2945
Variance	10.8537
Skewness	0.476483
Kurtosis	0.690367
N	50
Minimum	0.1130
1st Quartile	5.1128
Median	6.9141
3rd Quartile	8.4392
Maximum	16.6344
95% Confidence Interval for Mean	
6.1504	8.0230
95% Confidence Interval for Median	
6.1905	8.0016
95% Confidence Interval for StDev	
2.7520	4.1054

Summary for GT Sat Along Grain 0.15 mm

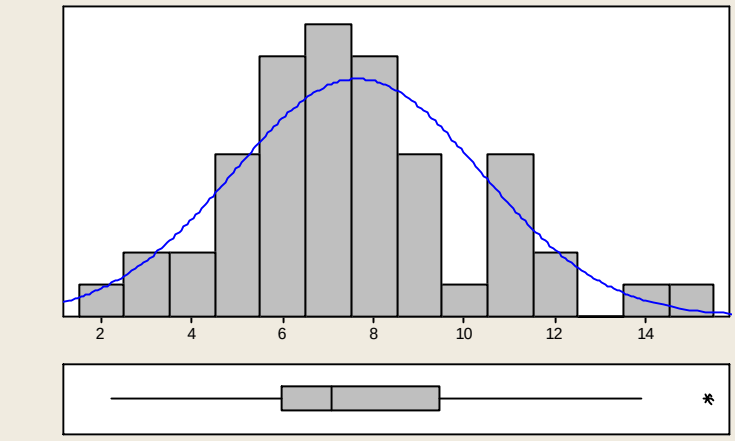

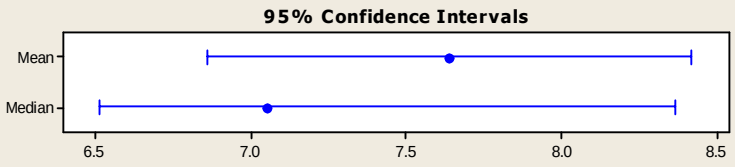

Anderson-Darling Normality Test	
A-Squared	0.38
P-Value	0.387
Mean	7.6373
StDev	2.7288
Variance	7.4463
Skewness	0.543347
Kurtosis	0.492727
N	50
Minimum	2.2054
1st Quartile	5.9767
Median	7.0552
3rd Quartile	9.4311
Maximum	15.3366
95% Confidence Interval for Mean	
6.8618	8.4128
95% Confidence Interval for Median	
6.5111	8.3616
95% Confidence Interval for StDev	
2.2795	3.4004

Summary for GT Sat Along Grain 0.2 mm

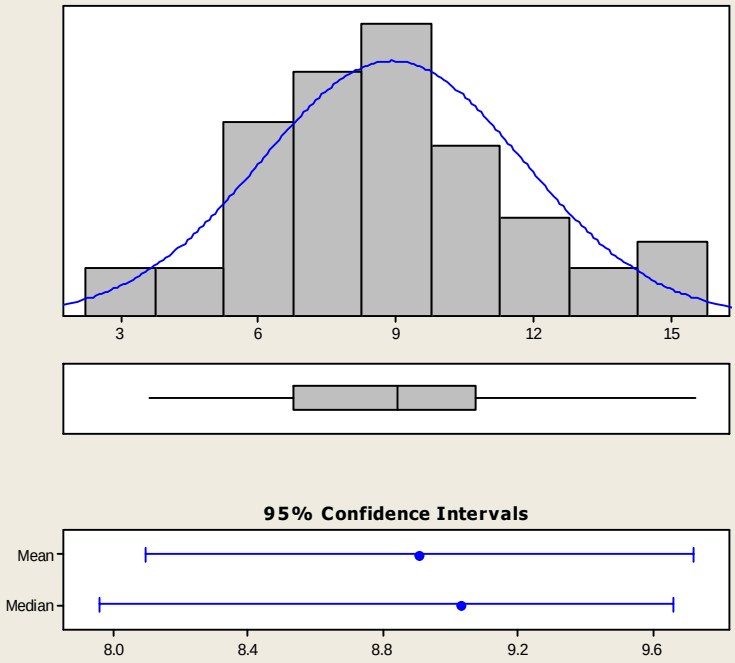

Anderson-Darling Normality Test	
A-Squared	0.17
P-Value	0.936
Mean	8.9076
StDev	2.8589
Variance	8.1733
Skewness	0.238827
Kurtosis	-0.178452
N	50
Minimum	3.6108
1st Quartile	6.7643
Median	9.0309
3rd Quartile	10.7057
Maximum	15.5273
95% Confidence Interval for Mean	
8.0951	9.7201
95% Confidence Interval for Median	
7.9565	9.6603
95% Confidence Interval for StDev	
2.3881	3.5626

Summary for GT Sat Along Grain 0.25 mm

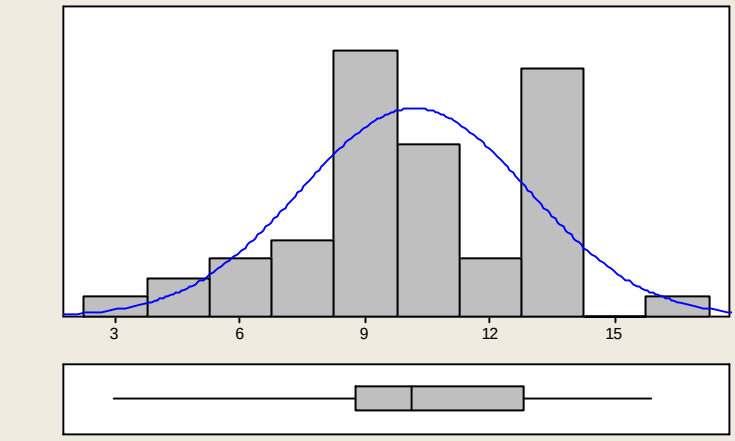

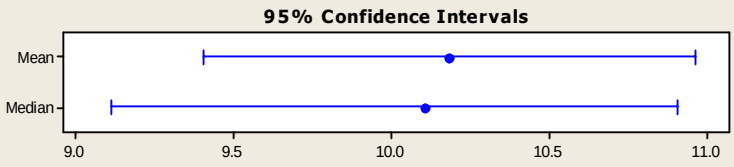

Anderson-Darling Normality Test	
A-Squared	0.48
P-Value	0.225
Mean	10.182
StDev	2.736
Variance	7.484
Skewness	-0.366906
Kurtosis	0.045232
N	50
Minimum	2.941
1st Quartile	8.768
Median	10.106
3rd Quartile	12.798
Maximum	15.899
95% Confidence Interval for Mean	
9.404	10.959
95% Confidence Interval for Median	
9.116	10.904
95% Confidence Interval for StDev	
2.285	3.409

Summary for GT Sat Along Grain 0.3 mm

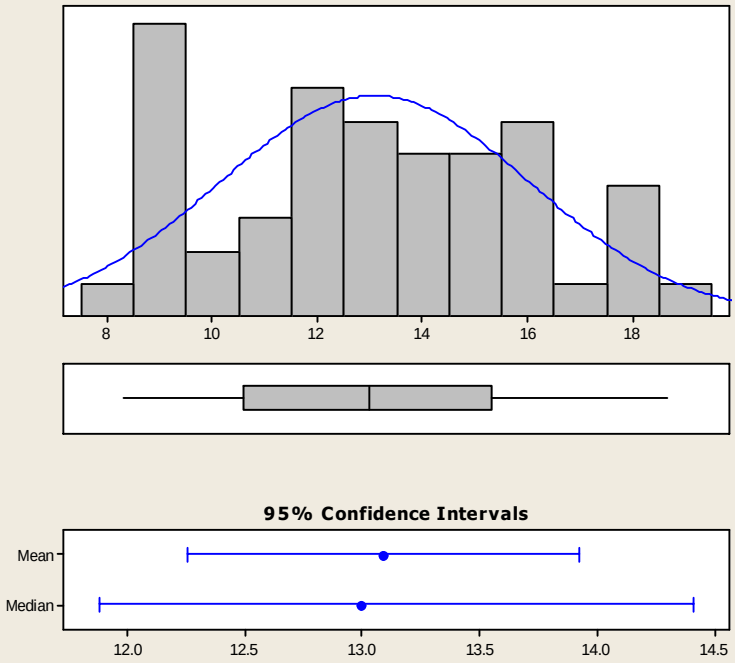

Anderson-Darling Normality Test	
A-Squared	0.50
P-Value	0.202
Mean	13.087
StDev	2.943
Variance	8.661
Skewness	0.128581
Kurtosis	-0.899241
N	50
Minimum	8.305
1st Quartile	10.572
Median	12.992
3rd Quartile	15.296
Maximum	18.636
95% Confidence Interval for Mean	
12.250	13.923
95% Confidence Interval for Median	
11.879	14.409
95% Confidence Interval for StDev	
2.458	3.667

Summary for GT Sat Along Grain 0.35 mm

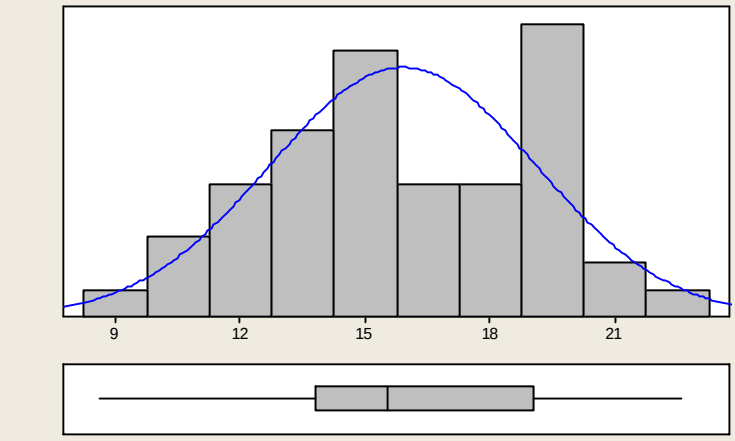

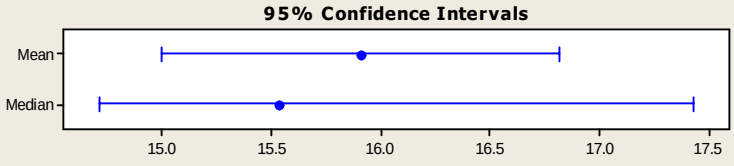

Anderson-Darling Normality Test	
A-Squared	0.42
P-Value	0.319
Mean	15.905
StDev	3.192
Variance	10.191
Skewness	-0.135580
Kurtosis	-0.633341
N	50
Minimum	8.608
1st Quartile	13.783
Median	15.531
3rd Quartile	19.037
Maximum	22.612
95% Confidence Interval for Mean	
14.998	16.812
95% Confidence Interval for Median	
14.710	17.428
95% Confidence Interval for StDev	
2.667	3.978

Summary for GT Sat Across Grain 0 mm

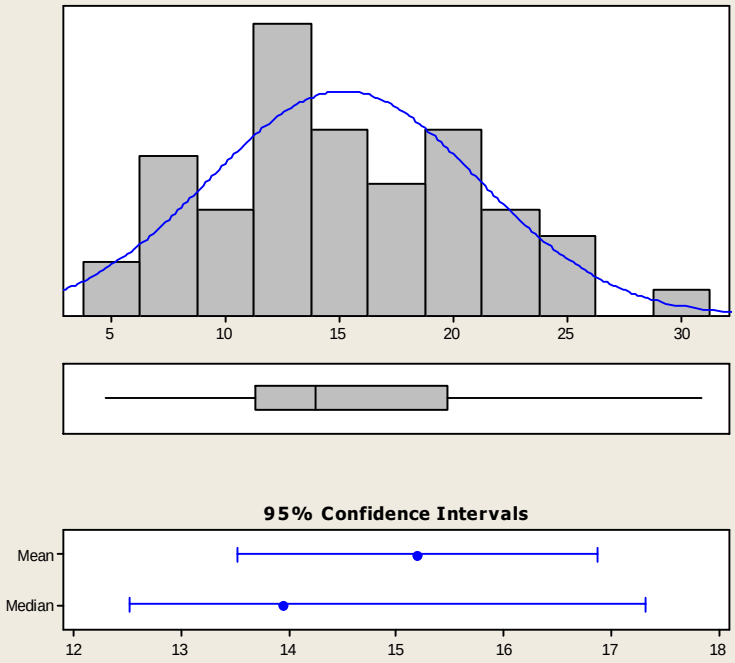

Anderson-Darling Normality Test	
A-Squared	0.36
P-Value	0.424
Mean	15.197
StDev	5.895
Variance	34.750
Skewness	0.397850
Kurtosis	-0.359096
N	50
Minimum	4.726
1st Quartile	11.290
Median	13.949
3rd Quartile	19.760
Maximum	30.843
95% Confidence Interval for Mean	
13.522	16.872
95% Confidence Interval for Median	
12.509	17.314
95% Confidence Interval for StDev	
4.924	7.346

Summary for GT Sat Across Grain 0.05 mm

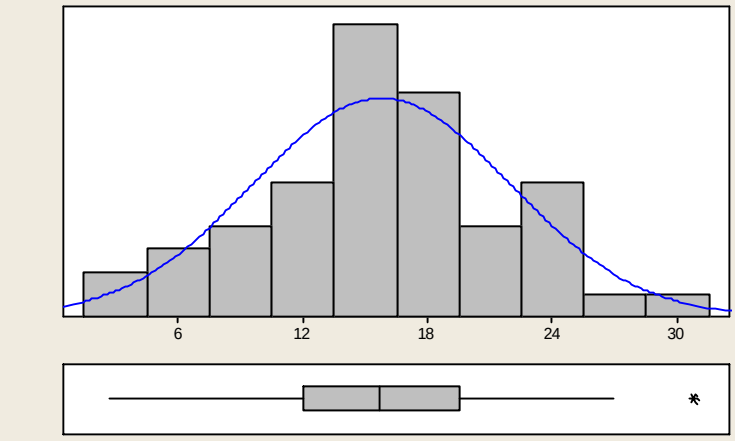

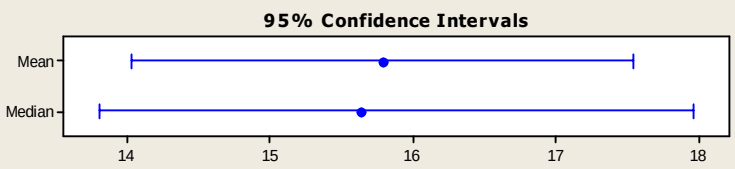

Anderson-Darling Normality Test	
A-Squared	0.19
P-Value	0.892
Mean	15.786
StDev	6.165
Variance	38.013
Skewness	0.044198
Kurtosis	-0.121190
N	50
Minimum	2.688
1st Quartile	12.037
Median	15.641
3rd Quartile	19.479
Maximum	30.793
95% Confidence Interval for Mean	
14.034	17.538
95% Confidence Interval for Median	
13.803	17.959
95% Confidence Interval for StDev	
5.150	7.683

Summary for GT Sat Across Grain 0.1 mm

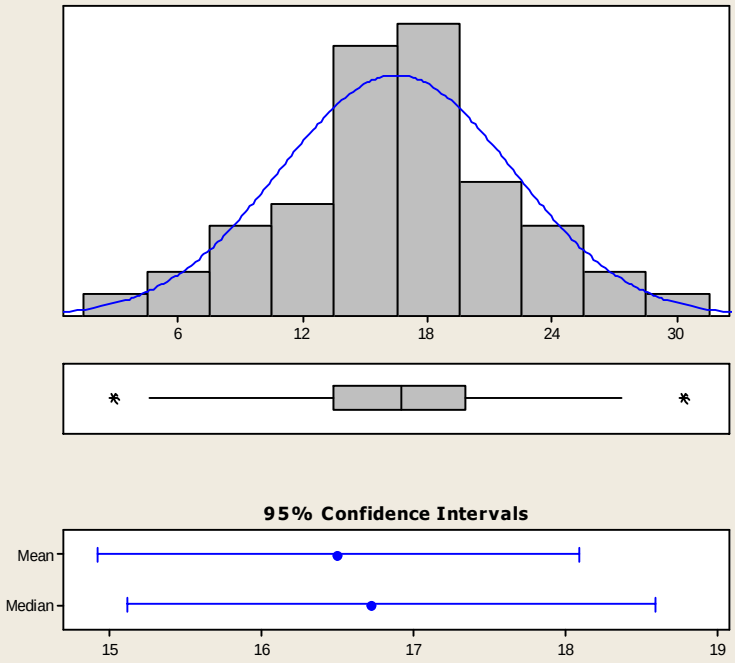

Anderson-Darling Normality Test	
A-Squared	0.22
P-Value	0.839
Mean	16.498
StDev	5.587
Variance	31.210
Skewness	-0.055694
Kurtosis	0.349508
N	50
Minimum	2.943
1st Quartile	13.512
Median	16.712
3rd Quartile	19.805
Maximum	30.324
95% Confidence Interval for Mean	
14.910	18.086
95% Confidence Interval for Median	
15.105	18.586
95% Confidence Interval for StDev	
4.667	6.962

Summary for GT Sat Across Grain 0.15 mm

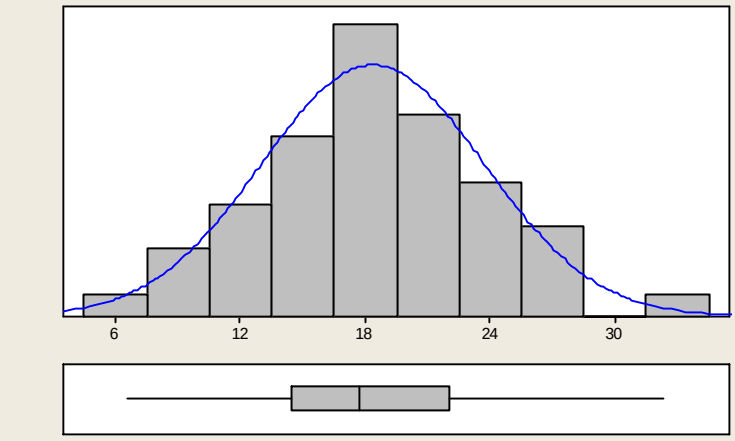

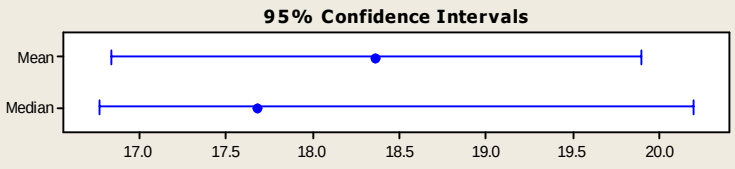

Anderson-Darling Normality Test	
A-Squared	0.13
P-Value	0.984
Mean	18.364
StDev	5.354
Variance	28.664
Skewness	0.188716
Kurtosis	-0.092307
N	50
Minimum	6.572
1st Quartile	14.482
Median	17.679
3rd Quartile	22.030
Maximum	32.357
95% Confidence Interval for Mean	
16.843	19.886
95% Confidence Interval for Median	
16.769	20.192
95% Confidence Interval for StDev	
4.472	6.672

Summary for GT Sat Across Grain 0.2 mm

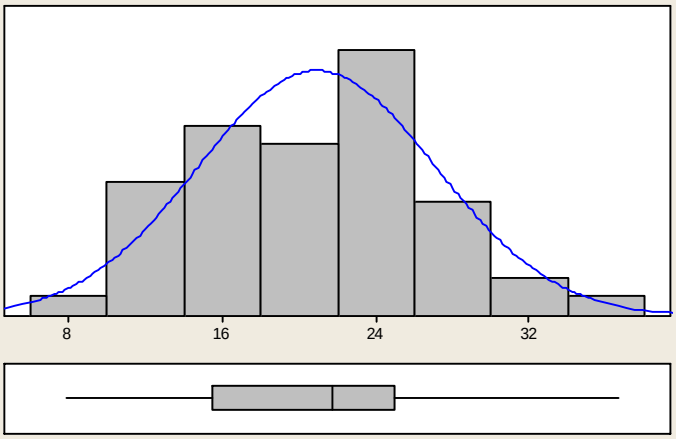

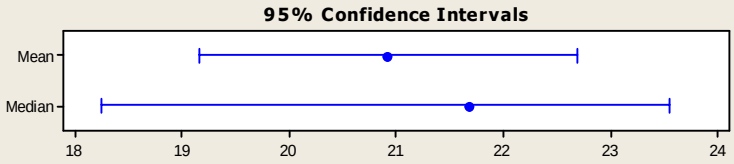

Anderson-Darling Normality Test	
A-Squared	0.23
P-Value	0.788
Mean	20.925
StDev	6.193
Variance	38.355
Skewness	0.107787
Kurtosis	-0.322846
N	50
Minimum	7.868
1st Quartile	15.462
Median	21.689
3rd Quartile	25.017
Maximum	36.596
95% Confidence Interval for Mean	
19.165	22.685
95% Confidence Interval for Median	
18.243	23.544
95% Confidence Interval for StDev	
5.173	7.717

Summary for GT Sat Across Grain 0.25 mm

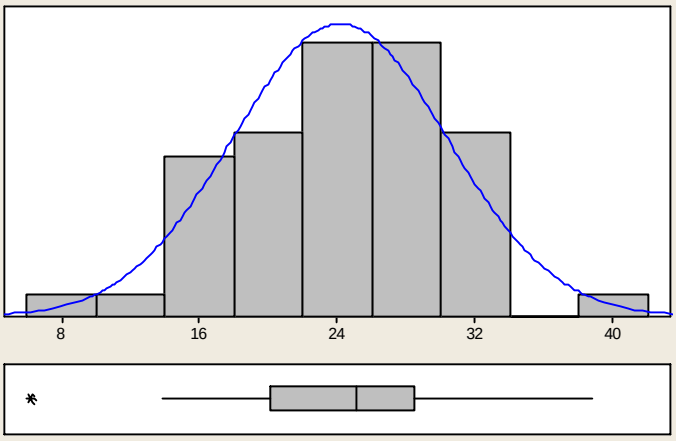

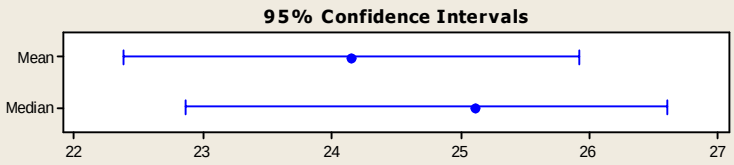

Anderson-Darling Normality Test	
A-Squared	0.45
P-Value	0.258
Mean	24.149
StDev	6.242
Variance	38.958
Skewness	-0.407433
Kurtosis	0.368252
N	50
Minimum	6.180
1st Quartile	20.072
Median	25.106
3rd Quartile	28.415
Maximum	38.835
95% Confidence Interval for Mean	
22.375	25.922
95% Confidence Interval for Median	
22.855	26.603
95% Confidence Interval for StDev	
5.214	7.778

Summary for GT Sat Across Grain 0.3 mm

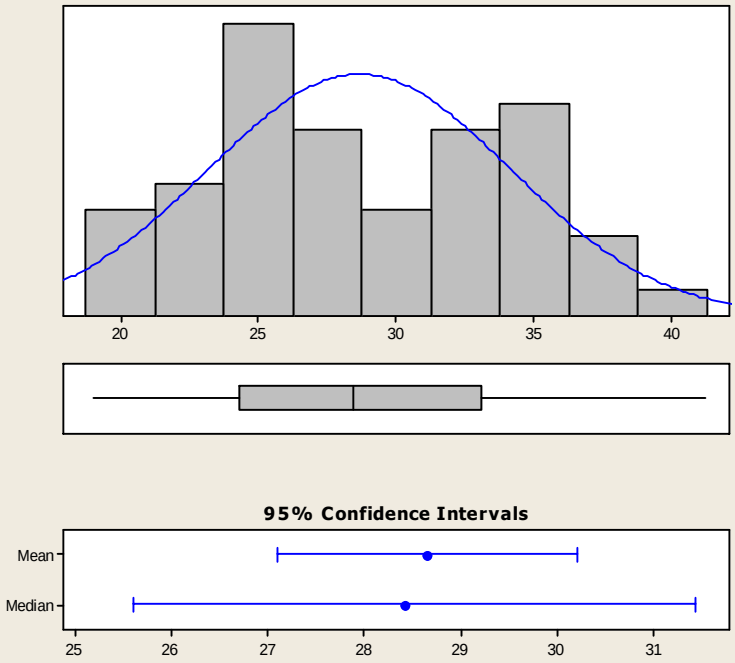

Anderson-Darling Normality Test	
A-Squared	0.38
P-Value	0.393
Mean	28.657
StDev	5.483
Variance	30.063
Skewness	0.155782
Kurtosis	-0.809431
N	50
Minimum	18.996
1st Quartile	24.287
Median	28.435
3rd Quartile	33.084
Maximum	41.210
95% Confidence Interval for Mean	
27.099	30.215
95% Confidence Interval for Median	
25.619	31.433
95% Confidence Interval for StDev	
4.580	6.833

Summary for GT Sat Across Grain 0.35 mm

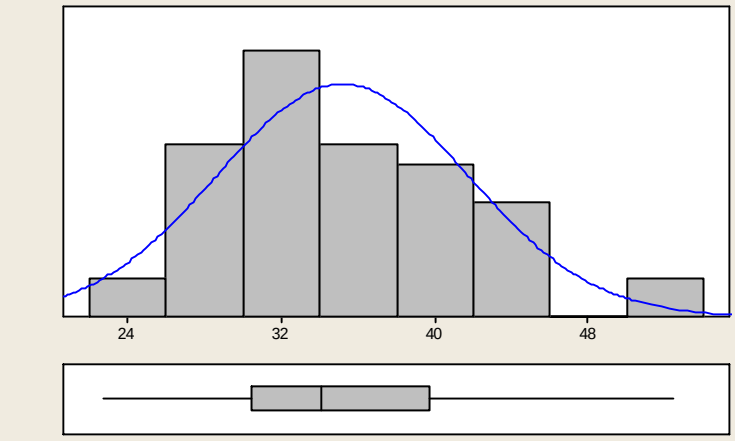

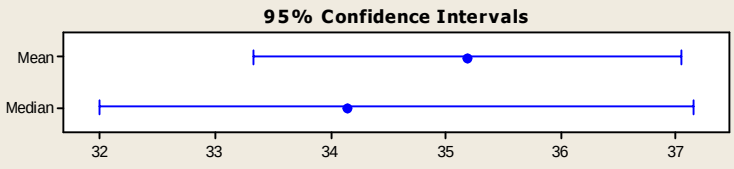

Anderson-Darling Normality Test	
A-Squared	0.44
P-Value	0.278
Mean	35.186
StDev	6.542
Variance	42.801
Skewness	0.537882
Kurtosis	0.016156
N	50
Minimum	22.762
1st Quartile	30.413
Median	34.139
3rd Quartile	39.735
Maximum	52.404
95% Confidence Interval for Mean	
33.327	37.046
95% Confidence Interval for Median	
31.991	37.147
95% Confidence Interval for StDev	
5.465	8.153